MODELOCKED VIBRONIC LASERS FOR THE 700NM - 1000NM REGION

David E. Spence

A Thesis Submitted for the Degree of PhD
at the
University of St Andrews

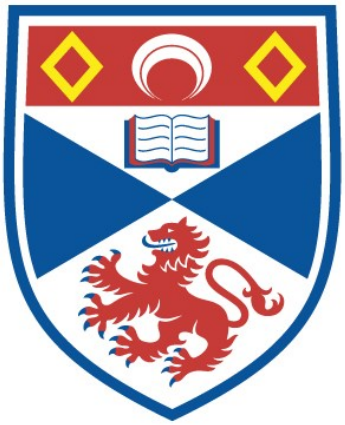

1993

Full metadata for this item is available in
St Andrews Research Repository
at:
http://research-repository.st-andrews.ac.uk/

Please use this identifier to cite or link to this item:
http://hdl.handle.net/10023/13805

This item is protected by original copyright

Modelocked Vibronic Lasers for the 700 nm - 1000 nm Region

Thesis submitted for the degree of Doctor of Philosophy to the

University of St. Andrews

by

David E. Spence, B.Sc.

The J.F. Allen Physics Research Laboratories

Department of Physics and Astronomy

University of St. Andrews

North Haugh

St. Andrews, Fife

KY16 9SS, Scotland

June 1992.

ProQuest Number: 10170657

All rights reserved

INFORMATION TO ALL USERS
The quality of this reproduction is dependent upon the quality of the copy submitted.

In the unlikely event that the author did not send a complete manuscript
and there are missing pages, these will be noted. Also, if material had to be removed,
a note will indicate the deletion.

ProQuest 10170657

Published by ProQuest LLC (2017). Copyright of the Dissertation is held by the Author.

All rights reserved.
This work is protected against unauthorized copying under Title 17, United States Code
Microform Edition © ProQuest LLC.

ProQuest LLC.
789 East Eisenhower Parkway
P.O. Box 1346
Ann Arbor, MI 48106 – 1346

TL B161

Declaration

I hereby certify that this thesis has been composed by myself, that it is a record of my own work and that it has not been accepted in partial or complete fulfilment of any other degree or professional qualification.

I was admitted to the Faculty of Science of the University of St. Andrews as a candidate for the degree of Ph.D under ordinance general no. 12 on 1st October, 1988.

Signed Date 25 June 1992

Certificate

I hereby certify that the candidate has fulfilled the conditions of the Resolution and Regulations appropriate to the degree of Ph.D.

Signature of Superviso: Date 25 June 1992.

Copyright

In submitting this thesis to the University of St. Andrews I understand that I am giving permission for it to be made available for use in accordance with the regulations of the University Library for the time being in force, subject to any copyright vested in the work not being affected thereby. I also understand that the title and abstract will be published, and that a copy of the work may be made and supplied to any bona fide library or research worker.

Dedicated to

my

mother and father

Abstract

The work in this thesis is concerned with the characterisation and development of modelocked solid-state lasers covering the 700 - 1000 nm region. Results are presented for a passively modelocked LiF:F_2^+ colour-centre laser, however, most of the work has concentrated on the Ti:sapphire (Ti:Al_2O_3) laser.

In chapter 2, the operation of a cw LiF:F_2^+ colour-centre laser is discussed. This laser was passively modelocked using the saturable absorber dye, DaQTeC and pulses as short as 170 fs were generated with average output powers of ~10 mW. Pulses as short as 127 fs were generated in a dispersion compensated, colliding-pulse modelocked geometry over a wavelength range of 925 - 950 nm. A nonlinear external cavity was added to the basic laser configuration in an attempt to extend the modelocked tuning range and the saturable absorber dye lifetime.

The technique of coupled-cavity modelocking was applied to a Ti:Al_2O_3 laser and enabled pulses as short as 1.3 ps to be generated. These pulses were frequency chirped and could be directly compressed to 290 fs outside the laser. By using the technique of intracavity dispersion compensation in both the main and coupled cavities, pulses as short as 90 fs were generated, having average powers of ~200 mW and peak powers of more than 20 kW.

The simpler technique of self-modelocking is described in chapter 5 and allowed the generation of pulses as short as 60 fs from a dispersion compensated cavity configuration. Average output powers of ~600 mW were measured, which corresponded to peak powers of 110 kW. This laser had a modelocked tuning range which spanned the 750 - 950 nm region. Using fibre/prism pulse compression techniques pulses as short as 45 fs were produced.

In chapter 6, the measurement and suppression of phase noise on the self-modelocked Ti:Al_2O_3 laser are discussed. The technique for noise reduction was also applied to two similar self-modelocked lasers in an attempt to synchronise the two laser pulse sequences.

Contents

Chapter 1
Introduction and Basic Theory

1.1 Introductory Overview

Laser action has probably existed for millions of years - amplified spontaneous emission has been observed to occur naturally in the atmosphere of Mars, which consists mainly of CO_2[1]. However, the first steps towards realising laser emission in a laboratory were not taken until 1917 when Albert Einstein first predicted stimulated emission[2]. Almost forty years passed before stimulated emission was first observed in the laboratory when in 1954 C. H. Townes et. al. at Columbia University demonstrated Microwave Amplification by Stimulated Emission of Radiation with the ammonia beam maser at 24 GHz[3]. Throughout the 1950's much theoretical and experimental work was carried out with the aim of constructing an optical frequency device. In 1956 N. Bloembergen of Harvard University proposed a continuous three level pumping scheme for obtaining a continuous population inversion at one microwave transition frequency by pumping at a different transition frequency[4]. The optical maser or LASER was finally proposed in 1958 by Schawlow and Townes[5]. Two years passed until, in 1960, T.H. Maiman of Hughes Research Laboratories demonstrated laser action for the first time using a flashlamp pumped ruby device operating at 694 nm[6]. Later in the same year, A. Javan et. al. operated the first HeNe laser at 1.15 μm and at 633 nm in the following year[7].

In the three decades since its invention, an enormous amount of other laser devices have emerged. Several hundred thousand discrete wavelengths are available from close to one thousand different materials. Up to one million distinct laser transitions have been found, ranging from wavelengths in excess of 600 μm to the 116 nm transition of the pulsed H_2 laser. In fact, the principle known as Schawlow's law states that 'almost anything will go if you hit it hard enough.' It is rumoured that Schawlow later demonstrated this fact when, after observing laser action in 'jelly' pumped with a CO_2 laser at 10.6 μm, he proceeded to eat the

gain medium[8]. Laser operation has also been observed in the far infrared from Scotch whisky fumes.

New laser materials are being developed continuously. Present day interests are directed towards new materials such as rare earth ion doped solid-state materials, including: Nd^{3+} (~0.9, 1.06, 1.3 μm), Er^{3+} (~1.6, 2.9 μm), Tm^{3+} (~2.0 μm) and Ho^{3+} (~2.1 μm). These materials have the advantage of very high efficiencies at room temperature, but they are restricted to certain wavelength regions. Of equal interest are the transition metal ion doped materials[9] using: Ti^{3+}, Cr^{3+}, Cr^{4+}, Co^{2+} and Ni^{2+}. They have broad tunability due to electron phonon interactions, however, most suffer from excited state absorption (ESA) and non-radiative transitions which often degrade their performance.

The mode of operation of a laser can be broadly categorised into two main classes. If the radiation has a relatively narrow optical bandwidth (less than 1 GHz, say) then the laser is said to be line narrowed or single frequency. If, on the other hand, the output in the time domain consists of a periodic sequence of pulses, the laser is said to be pulsed, Q-switched, or modelocked depending on the exact nature of the output. In this case the oscillating bandwidths can be relatively large.

This thesis will discuss the operation of tunable, modelocked sources based on vibronic laser materials covering the near infrared wavelength region up to ~1 μm. The emphasis is placed mostly on $Ti:Al_2O_3$, but chapter 2 begins by looking at the performance of a cw, passively modelocked $LiF:F_2^+$ colour-centre laser. At the time the work was performed, this laser represented a serious alternative to the dye laser. It had a broader tuning range than many single dyes and could often give higher output powers. Its solid state nature helped overcome many of the disadvantages associated with organic dyes. Its one drawback was the requirement that it be kept at cryogenic temperatures to slow down the gradual fading which inevitably occurred with time and which resulted in the eventual destruction of the laser active centres.

With the application of passive saturable absorber modelocking to this system, pulses as short as 130 fs were generated over a tuning range extending from 925 - 950 nm. A nonlinear external cavity was added to this basic configuration in an attempt to extend both the modelocked tuning range and the usable lifetime of the saturable absorber dye.

The remainder of the thesis is devoted to describing the construction, operation and performance of a modelocked Ti:Al_2O_3 laser. This laser material solves most, if not all, of the disadvantages of the dye and colour-centre lasers. It has a solid state construction, it is tunable over a wide wavelength region extending from 660 - 1100 nm, it does not display any reduction in performance with time and can be operated at room temperature with simple water cooling.

An acousto-optically modelocked Ti:Al_2O_3 laser is described in chapter 3, which produced pulses having durations less than 100 ps. Of more interest is the coupled-cavity modelocked Ti:Al_2O_3 laser which was able to generate pulses as short as 90 fs in a dispersion compensated configuration. The simpler technique of self-modelocking allowed pulses as short as 60 fs to be generated, again in a dispersion compensated cavity. Pulses as short as 45 fs were generated using an optical fibre and prism delay line for pulse compression outside the laser resonator. These results are presented in chapter 5.

In chapter 6, the measurement and reduction of pulse timing jitter, or phase noise, on the self-modelocked laser are described and the sources of such noise are discussed. The noise reduction technique is extended to synchronise two self-modelocked lasers. This technique can be generally applied to synchronise passively modelocked lasers to any reference oscillator.

In the remainder of this introductory chapter a summary of ultrashort pulse generation and measurement techniques is presented. Pulse propagation in nonlinear and dispersive media will be reviewed in section 1.4 together with pulse compression techniques, which have been used in the work described in chapter 5.

1.2 An Introduction to Modelocking

There are several reviews of modelocked lasers in the literature[10-19]. This section briefly describes the process of modelocking in lasers together with some of the techniques which can be used to obtain modelocked operation. The bandwidth of a continuous-wave (cw) laser is determined by the frequency range over which the gain exceeds the losses for the particular resonator configuration used. Often this frequency range will extend over many cavity modes so that the laser output will consist of a series of closely spaced frequencies corresponding to the axial, and perhaps, the transverse mode frequencies of the laser resonator. The variation of the output intensity as a function of time will depend on the amplitude, frequency and phase relationships of the oscillating modes. If there is nothing to fix these relationships they will all vary randomly due to random fluctuations in the laser gain and the resulting output will vary in an unpredictable way. If, on the other hand, the modes are forced to maintain equal frequency spacings and fixed phase relationships the output of the laser as a function of time, will vary in a well defined manner. Most commonly, the output under these conditions, consists of a train of optical pulses separated by the period $T = 2L/c$, where L is the laser cavity length. A laser operating under these conditions is said to be modelocked. Modelocking makes it possible to generate pulses having durations less than 10^{-13} s.

In the case of an ideal laser oscillating on a single longitudinal mode the signal amplitude, phase and frequency are all constant in time. If only two modes oscillate the output intensity will vary sinusoidally at a beat frequency equal to the difference between the frequencies of the two modes. The visibility of the beat is 100% if the two modes have equal amplitudes and decreases as the relative amplitudes change. For only two modes a change in the relative phase will change the time origin of the peaks but not the appearance of the modebeat. Therefore, modelocking is not a very meaningful concept for two modes.

The situation for three or more modes is more interesting. In fact just three modes which are properly in phase can result in reasonably good modelocked pulses. In the case of N oscillating modes, the optical field inside the resonator can be expressed as

$$E(t) = \sum_n E_n \exp\left\{ i \left[\omega_n \left(t - \frac{z}{c} \right) + \phi_n \right] \right\} \tag{1.1}$$

where E_n, ω_n and ϕ_n are the amplitude, frequency and phase of the n^{th} mode. If the mode frequencies are equally spaced so that $\omega_n = \omega_0 + n\Delta\omega$ then

$$E(t) = \exp\left\{ i\, \omega_0 \left(t - \frac{z}{c} \right) \right\} \sum_n E_n \exp\left\{ i \left[n\, \Delta\omega \left(t - \frac{z}{c} \right) + \phi_n \right] \right\}. \tag{1.2}$$

If the ϕ_n's are constant (which can arbitrarily be set to zero) this equation represents a carrier wave of frequency ω_0 whose amplitude envelope consists of a single pulse in the period $T = 2\pi/\Delta\omega$. The pulse width is given approximately by the reciprocal of the frequency range over which the E_n have an appreciable value, ie. $\tau_p \approx T/N$ where N is the number of oscillating modes. The field inside the resonator now no longer consists of individual modes but is expressed as a superposition of modes with fixed amplitudes, phases and frequencies, ie. a modelocked field. The exact shape of the amplitude envelope is determined by the values of the amplitudes and phases of the individual modes.

1.2.1 Active Modelocking

There are several different techniques which can be used to modelock a laser, but they can be broadly categorised into two types - active and passive modelocking. In an actively modelocked laser the mode coupling is achieved by placing an actively driven amplitude (or phase) modulator inside the laser cavity and driving it at a frequency ω_m that closely matches the resonator's round trip frequency $\Delta\omega$ or one of its harmonics. In an alternative scheme the laser gain is modulated by pumping with a modelocked pump source and the laser is said to be synchronously modelocked or synchronously pumped.

Modelocking can be modelled in either the time or frequency domain and both pictures are entirely equivalent. Historically modelocking was first analysed in the frequency domain. In this approach each oscillating cavity mode acquires sidebands at frequencies $\omega_n \pm n\,\omega_m$ as a

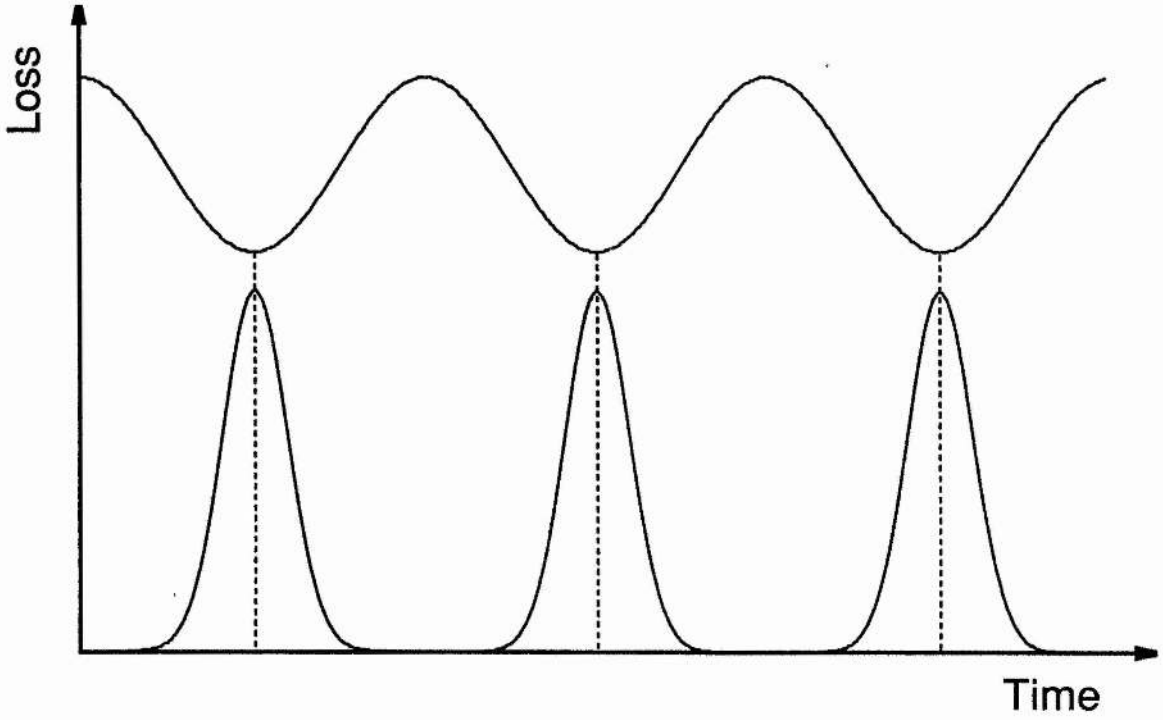

Figure 1.1. Schematic diagram illustrating the time-domain description of active modelocking.

result of the modulation, where ω_m is the modulation frequency. If $\omega_m \approx \Delta\omega$, the sidebands will fall on or near to neighbouring axial modes. Each sideband will then tend to injection lock the axial mode with which it is in resonance. Thus, the modulator will tend to couple together the axial modes to one or more of their neighbours.

If there are a large number of oscillating modes, then it becomes easier to view the modelocking process in the time-domain. If the cavity losses are modulated at c/2L or some multiple of this round trip frequency, the light incident on the modulator at a particular time always sees the same loss on each round trip. Only the light approaching the modulator when its losses are close to their minimum value will see a net gain. Pulses tend to build up in the low loss time positions. This situation is depicted in figure 1.1. As an alternative to amplitude modulators, phase modulators may also be used to achieve modelocking. In this case light passing through the modulator will be either up or down shifted in frequency except at the times when the dielectric constant of the modulator is at its maximum or minimum value. Since the modulator is again synchronised to the cavity round trip frequency most of the light

will eventually be shifted outside the gain curve of the laser. In both the am and fm case, the shorter the pulse becomes the less loss it experiences when passing through the modulator, at least until it gets very short compared to the modulator period. At the same time the necessarily wider spectrum may become so large that it approaches the amplification bandwidth of the laser medium. The limiting pulse duration is thus a compromise between the temporal narrowing in the modulator and the spectral narrowing in the gain.

The time domain approach was developed by Kuizenga and Siegman[10] for homogeneously broadened lasers with active modulation. They assumed the existence of a pulse and followed it for one round trip through all the elements within the cavity. The effect of successive round trips on the pulse parameters could then be analysed. They assumed a gaussian pulse shape for analytical simplicity and in fact this is quite an accurate description of the pulse shape in real actively modelocked lasers. The transient build up of the modelocked signal or the steady state form that the recirculating signal must take if it is to remain unchanged and self consistent from one round trip to the next can be analysed using this method. The results of the analysis will be quoted here and will be used in chapter 3 to estimate the pulse durations from an acousto-optically modelocked Ti:Al_2O_3 laser. The Kuizenga-Siegman theory states that the steady state pulse duration for a homogeneously broadened laser which has been modelocked using an amplitude modulator is given by

$$\tau_{pss} \approx \left(\frac{2\sqrt{2}\ln(2)}{\pi^2}\right)^{1/2}\left(\frac{g}{\Delta_m}\right)^{1/4}\left(\frac{1}{f_m \Delta f_a}\right)^{1/2} \qquad (1.3)$$

where g is the round trip saturated amplitude gain, Δ_m is the peak to peak voltage modulation index, f_m is the modulator frequency and Δf_a is the atomic linewidth. From this equation it can be seen that the pulse width depends primarily on $1/(f_m \Delta f_a)^{1/2}$. The modulation index is proportional to $P_m^{1/2}$ for frequency modulation and P_m for amplitude modulation, where P_m is the rf power applied to the modulator.

If the laser gain medium is inhomogeneously broadened, many longitudinal modes will

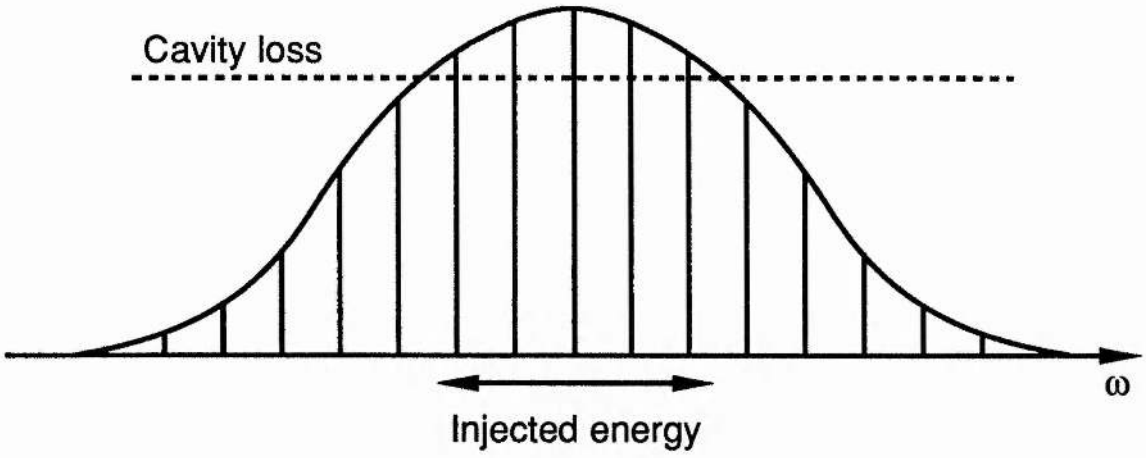

Figure 1.2. Schematic diagram illustrating the energy balance maintained by the active modulator in a modelocked, homogeneously broadened laser.

oscillate simultaneously provided the laser is far enough above threshold. In such a case the modelocking element is required to lock together the phases of modes which are already oscillating with random phases in the absence of any external modulation. The required modulation strength is therefore relatively small. On the other hand, a strongly homogeneously broadened laser will tend to oscillate on only a few axial modes so that the modulator must play a stronger role in generating additional sidebands and in causing the laser spectrum to spread out across the atomic linewidth. Now power must be continually transferred from the high gain modes with frequencies near the centre of the atomic transition to those of lower gain, ie. those that would not normally oscillate. This power is simply that of the sidebands at $\omega_0 \pm n\omega_m$ created by the modulation. The centremost modes have gains slightly greater than unity while those in the wings have gains slightly less than unity. A steady state balance is maintained by the modulator in transferring power from the stronger central modes to those in the wings. This situation is illustrated in figure 1.2. Generally, the final pulse duration in an inhomogeneously broadened laser will be of the order of the reciprocal of the gain bandwidth, ie. $\tau_p \approx 0.5/\Delta f_d$ where Δf_d is the Doppler broadened atomic linewidth. In the homogeneous case the pulses generally do not reach this limit because of the spectral narrowing in the gain medium. The final pulse width in this case (given by equation 1.3) represents a balance between the spectral broadening produced by the

modulator and the spectral narrowing in the gain which tends to push the laser towards the cw, single mode state.

Hybrid modelocking is a combination of both active and passive modelocking. A synchronously modelocked dye laser which also contains a saturable absorber is one example of a hybridly modelocked system. In this case pulse repetition rate is still determined by the active modulation but the influence of the weak saturable absorber assists with the pulse shaping.

1.2.2 Passive Modelocking

The technique of passive modelocking provides an alternative approach to the generation of ultrashort pulses. This type of operation has been observed in pulsed, Q-switched and cw lasers. It has enabled the shortest pulses yet generated to be produced in certain cw modelocked lasers. Passive modelocking can result when an element which is a purely passive saturable absorber, ie. one where the absorption is constant at low optical intensities but decreases (bleaches) at high intensities, is placed in the cavity. In passively modelocked systems the modulation is produced by the modelocked pulses themselves, which means that it is always synchronised to the circulating field within the cavity and can become stronger as the pulses become shorter. As a result the pulses generated from passively modelocked lasers tend to be shorter than those from the equivalent actively modelocked lasers. In spite of the many difficulties involved in obtaining stable and reliable operation in cw systems they are widely used in practice and have proved to be a very useful tool in many applications.

Passive modelocking is usually achieved with the use of organic dyes as the saturable absorber. When pumping is first turned on, the population inversion increases until the gain exceeds the total saturable and non-saturable losses and laser oscillation builds up from noise. The most intense noise spike will grow to an intensity where it begins to saturate the loss in the saturable absorber. As a result this noise spike then experiences less loss per round trip than the rest of the noise and it can thus grow in preference to the rest of the signal. Under the

proper conditions, which may be difficult to achieve in practice, a single noise pulse can be selected and the resulting laser output is in the form of a sequence of short pulses.

Saturable absorbers can be classified into two types: fast and slow. A fast saturable absorber is one whose absorption recovery time is much shorter than the pulse duration, in which case the absorption saturates on the instantaneous intensity. The recovery time of a slow saturable absorber is much longer than the pulse duration and so it saturates on the integrated pulse intensity or pulse energy. Pulse shortening occurs in the fast saturable absorber because the stronger central part of the pulse partially burns through the absorber and is therefore transmitted with less attenuation than the weaker front and back portions which are more strongly absorbed. Significant pulse shortening will occur only for a limited range of pulse intensities. If the intensity is too weak, no saturation will occur, while if it is too strong the whole pulse may burn through the absorption and in either case the pulse shortening mechanism will be weakened. Passive modelocking with a slow saturable absorber can be visualised in the following way. As in the case of the fast absorber the leading edge of the pulse is attenuated in the medium. But once the absorber is bleached, which usually happens before the back has been transmitted, the trailing edge of the pulse is passed virtually unchanged. Thus, pulses generated with a slow saturable absorber should be asymmetrically shaped with steeper leading edges.

In reality, slow saturable absorber modelocking does produce very short pulses which are often approximately symmetric in shape. This happens because of the effects of dynamic gain saturation on the evolution and maintenance of modelocked pulses. Although it will have some effect in all modelocked lasers, its role is particularly important in the case of modelocking using a slow saturable absorber. Initially the cavity losses are greater than the gain so that the pulse sees a net loss and is attenuated. For stable modelocked operation, the pulses must have sufficient energy to saturate the absorber down below the gain sometime during their leading edge. At a slightly later time the pulse must also saturate the gain down below the losses so that the trailing edge is also attenuated. This is depicted in figure 1.3.

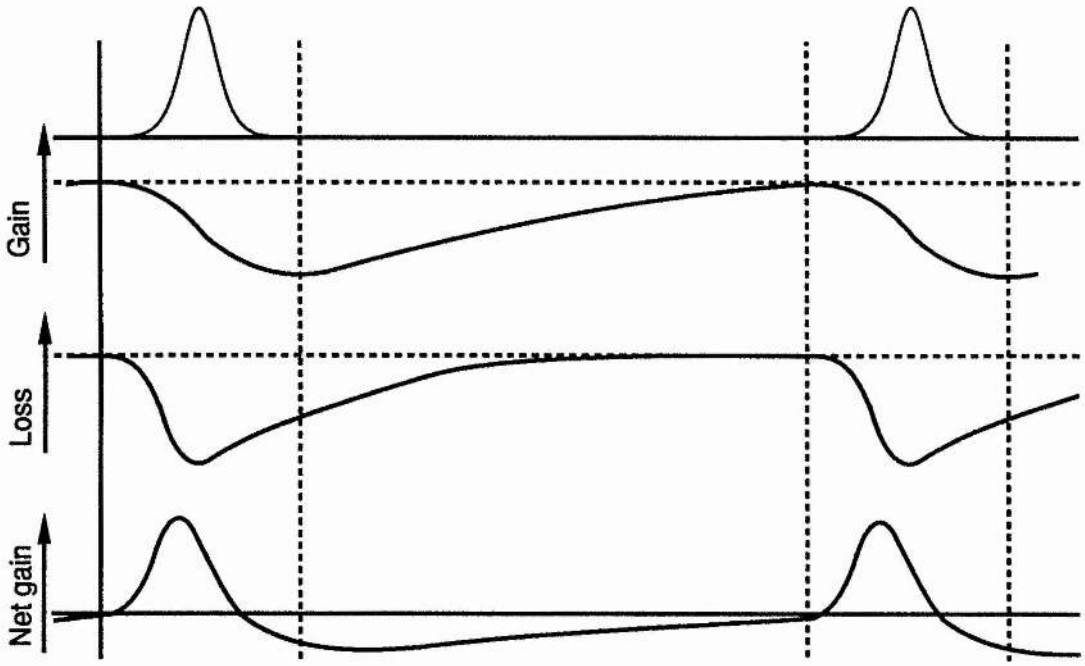

Figure 1.3. Schematic diagram showing the dynamic gain and absorber saturation during a cavity period in a passively modelocked laser.

Partial saturation on both the leading and trailing edges of the pulse is thus highly desirable for stable cw modelocking. The recovery of the absorber on each round trip to its initial pre-pulse value is obviously necessary for stability so that there will not be a net gain prior to the arrival of each pulse. For this same reason the gain must not completely recover between pulses. The parameter ranges for stable passive modelocking are summarised in Table 1.1.

Passive modelocking in cw lasers, therefore, depends on a delicate interplay between the laser parameters, particularly the pulse energy, the gain and absorber recovery times and their saturation energies. Experiments and theory suggest[14] that the pulse intensity profiles from passively modelocked lasers are approximately sech^2. For successful passive modelocking, the laser must be able to sustain pulses in the steady-state which are stable against slow, large scale relaxation oscillations and which are capable of self-starting from noise or initial fluctuations when the laser is switched on. The technique of slow saturable absorber modelocking will be demonstrated experimentally in chapter 2.

1.2.3 Coupled-cavity Modelocking.

More recently, a class of modelocked lasers which utilise nonlinear effects in an external cavity have been developed. These are called coupled-cavity or additive-pulse modelocked lasers. The first demonstration of this technique was the soliton laser discovered by Mollenauer and Stolen[20]. In this laser the formation of N=2 solitons in an external cavity was thought to provided the pulse shortening mechanism, although it was later discovered that this was not the case. Theory later suggested[21,22] and experiments verified[22-24] that neither soliton formation nor even anomalous dispersion were necessary to achieve pulse shortening. In the generalised coupled-cavity laser a suitable nonlinear element is placed in the control cavity, whose length is interferometrically matched to the main cavity so that interference occurs between the pulses in both cavities. For a suitably chosen phase bias between both resonators, the nonlinear phase shift which occurs in the external cavity can lead to pulse shortening in the laser. The laser sees the external cavity as a termination which returns shorter pulses than those incident upon it. This technique will be discussed further in

Fast saturable absorber	Slow saturable absorber
$\frac{P_L}{P_A} < 1$	$\frac{T_L}{T_R} \gtrsim 1$
$T_L \geq T_R$	$s = \frac{E_L}{E_A} = k \frac{A_L \sigma_A}{A_A \sigma_L} > 1$
$\frac{T_C}{T_L} \gtrsim 1$	$\frac{T_A}{T_R} < 1$

Table 1.1. Parameter ranges for stable passive modelocking. ($P_{L(A)}$ ($E_{L(A)}$): saturation power (energy) of gain (absorber) medium; $T_{L(A)}$: relaxation time of laser (absorber) transition; T_C: cavity relaxation time and T_R: resonator round trip time.)

chapter 4. It has been suggested that the external cavity produces an effect similar to the fast saturable absorber modelocking discussed above[25]. Coupled-cavity modelocking has the advantage of being applicable to many types of laser for which no suitable conventional saturable absorbers can be found.

1.2.4 Self-modelocking

Recently it was discovered that a cw Ti:sapphire laser would self-modelock in the sense that a modelocked output could be obtained with no obvious modelocking elements present inside or outside the cavity[26]. This is an obviously attractive scheme because of its relative simplicity and unrestricted tunability. Initial observations showed that picosecond pulses could be generated from the basic laser configuration. With the inclusion of intracavity dispersion compensation pulses as short as 60 fs could be obtained. In these lasers, the high intracavity power and long gain medium imply that self-focusing effects must be considered in the modelocked regime. This effect, in the presence of a suitably located intracavity aperture, which may be provided by the spatial profile of the gain, can lead to an intensity dependent transmission which again simulates the action of a fast saturable absorber. This modelocking technique will be discussed more fully in chapter 5. In both the coupled-cavity and self-modelocked Ti:Al_2O_3 lasers, the interaction between the SPM and GVD within the laser cavity must also be considered and provides additional pulse shaping. These effects will be discussed further in chapters 4 and 5.

1.3 Ultrashort Pulse Measurement

With the advent of passively modelocked lasers the direct combination of a photodiode and oscilloscope was no longer adequate to temporally resolve the pulses generated. The fastest optical detectors have response times ~10^{-11} s and so it is not possible to use them to measure pulses shorter than a few tens of picoseconds. There are two important methods for determining the duration of pulses shorter than ~10^{-11} s. Electron-optical streak cameras can be used to measure pulses having duration ~10^{-12} s while autocorrelation techniques using

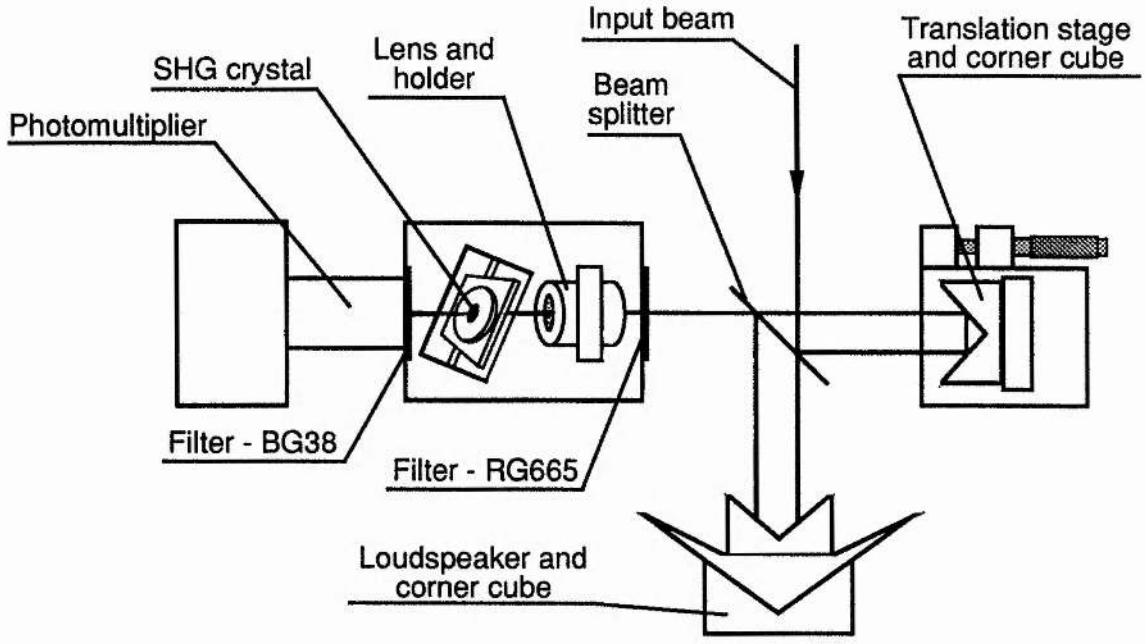

Figure 1.4. Schematic diagram showing the construction of the collinear autocorrelator.

some nonlinear material are used to measure pulses having durations $\leq 10^{-12}$ s. This latter method uses some nonlinear property to obtain a spatial autocorrelation trace of the optical intensity, rather than the actual pulse shape.

1.3.1 Autocorrelation Measurements

Pulsewidth measurement by autocorrelation is now most common using second-harmonic generation (SHG) in a suitable nonlinear crystal. This method was first reported by Mirer et. al.[27] and immediately afterwards by Armstrong[28] and Weber[29]. Its success depends on the instantaneous electronic mechanism underlying the SHG process together with the ability to accurately measure length, so that the problem of measuring $\tau_p \lesssim 10^{-12}$ s is transformed into the relatively simple task of measuring the spatial extent of an autocorrelation trace of the order of $c\tau_p \lesssim 0.3$ mm.

A practical arrangement for a real time autocorrelator is illustrated schematically in figure 1.4. (This design was used for the work described throughout this thesis.) The incoming pulses pass through a Michelson interferometer before being focused in the SHG

crystal. Suitable filters are used to prevent unwanted ambient lighting and unconverted fundamental from entering the detector, which is usually a photomultiplier tube. One arm of the interferometer has a delay, τ, relative to the other. The second harmonic generated in the crystal is incident on the slow detector (relative to the pulse duration) so that the output current is integrated over a time long compared to the pulse duration. The optical delay in the interferometer is varied by translating one of the retroreflecting mirrors about the point of coincidence. This can easily be accomplished in real time by mounting the mirror on an audio loudspeaker which scans at ~25 Hz. The resulting second harmonic signal consists of a background level due to the separate signals from each arm of the Michelson, plus an enhancement due to the spatial overlap of the pulse in the crystal. This enhancement, as a function of the relative delay between the arms of the interferometer, represents the intensity autocorrelation of the pulse.

An alternative arrangement of the autocorrelator produces background free autocorrelation traces. In this configuration the two beams at the input to the crystal are not collinear and the phase matching condition is such that second harmonic is generated only when both pulses are present in the crystal. In both of these designs type I phase matching is used. A third type of autocorrelator, which also produces background free traces, uses type II phase matching. Here, both input beams are collinear and orthogonally polarised, so that the second harmonic signal is again only generated when both beams are present.

In the absence of the SHG crystal the Michelson interferometer acts as a linear 1st order autocorrelator. This device measures the autocorrelation function of the pulse amplitude which is related to the power spectral density through its Fourier transform[30]. Thus, a Michelson interferometer measures the coherence length or coherence time of a pulse and can only provide information about the pulse duration for transform limited pulses. In this case the normalised intensity detected at the output of the interferometer for a delay of $\tau = 0$ is unity and is 0.5 for $\tau \gg \tau_p$. Hence the contrast ratio (the ratio between the peak and background level of the autocorrelation signal) is 2:1.

It is more useful to measure the second harmonic of the signal at the output of the interferometer[31]. Under phase matched conditions the SHG output is proportional to the fundamental field squared, ie.

$$E_{2\omega}(t,\tau) = \left|E_{\omega}(t) + E_{\omega}(t+\tau)\exp(-i\omega_0\tau)\right|^2 \tag{1.4}$$

The detector current is integrated and the terms with an $\omega\tau$ dependence average to zero so that

$$i_d(\tau) \propto \int_{-\infty}^{\infty} \left|E_{2\omega}(t,\tau)\right|^2 dt = W^{2\omega}\left(1 + 2G^{(2)}(\tau)\right) \tag{1.5}$$

$$\text{where} \quad W^{2\omega} = \int_{-\infty}^{\infty} E_{\omega}^4(t)\, dt \tag{1.6}$$

$$\text{and} \quad G^{(2)}(\tau) = \frac{\int_{-\infty}^{\infty} E_{\omega}^2(t)\, E_{\omega}^2(t+\tau)\, dt}{\int_{-\infty}^{\infty} E_{\omega}^4(t)\, dt} \tag{1.7}$$

In this case $i_d(\tau)/W = 3$ when $\tau = 0$ and when $\tau \gg \tau_p$, $i_d(\tau)/W = 1$, so that the contrast ratio is 3:1. Now the device measures the autocorrelation function of the pulse intensity so that $i_d(\tau)/W$ as a function of τ gives the time duration over which the energy of the pulse is distributed, ie. the pulse duration. Note that since $G^{(2)}(\tau)$ is a symmetric function all information about the pulse asymmetry is lost in the measurement.

Is is important to be able to distinguish between the different types of signal recorded by the autocorrelator so that the quality of the modelocked output can be ascertained. Random noise on top of a cw laser signal will appear as small bumps riding on an infinite background. The width of the bumps is a measure of the temporal width of the fluctuations, while the contrast ratio is a measure of the modulation depth where 100% modulation results in a contrast ratio of 2:1. A narrow spike with a peak intensity of 3 units (a coherence spike) is present in the centre of the autocorrelation function ($\tau = 0$), because even incoherent light is

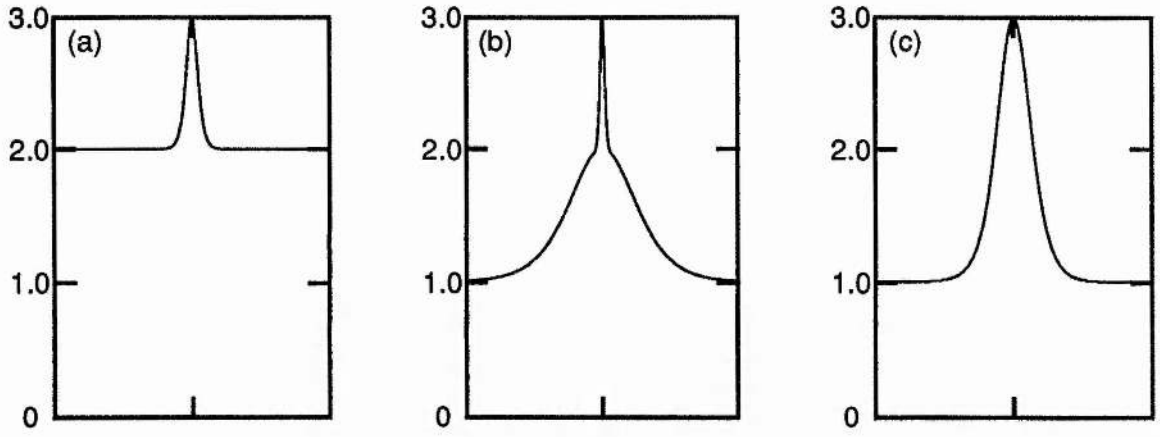

Figure 1.5. Schematic of ideal collinear SHG intensity autocorrelation traces for: (a) cw radiation, (b) partially modelocked pulses and (c) modelocked pulses.

well correlated with itself. The width of the coherence spike is a measure of the coherence time of the noise substructure. Any optical signal of finite duration results in an autocorrelation function of finite width. If some fine structure is also present within the pulse envelope, a narrow coherence spike will appear in the middle of the correlation function. Here the contrast ratio is again 3:2:1. This type of trace is typical of partially modelocked lasers. For fully modelocked pulses, the broad pedestal is shortened while the coherence spike is broadened so that the profile approaches that of a clean pulse with no pedestal or spike. In this case the contrast ratio is 3:1. These three situations are illustrated in figure 1.5.

If sufficient frequency response is available in the detection system so that the terms containing an ω dependence are not averaged, then the detected signal is again given by equation (1.5), but here the rapidly varying terms are resolved and a so called interferometric or fringe-resolved autocorrelation function is recorded. The contrast ratio in this case is 8:1 for fully modelocked pulses. The increased frequency response necessary to resolve the interference fringes can be achieved by either decreasing the scanning frequency of the loudspeaker or by impedance matching the photomultiplier tube and oscilloscope. For the results presented in the bulk of this thesis, the detector was impedance matched using a simple electronic circuit based on an AD711 operational amplifier. In this way, the recorded

autocorrelation trace could simply be switched between interferometric and intensity as required.

Interferometric autocorrelations are more sensitive to pulse shape than their intensity counterparts, but more importantly various types of frequency chirp produce distinctive patterns in the wings of the trace. Note that all information about the pulse asymmetry will still be lost. For self-phase modulation induced chirp, the frequency sweep is largest over the central part of the pulse and this is evident by a narrowing of the upper and lower envelopes in the interferometric autocorrelation. However, since the front and rear of the pulse are still fully coherent, the fringes remain visible in the wings as for unchirped pulses. In the case of linear frequency chirp there is a loss of coherence between the front and back of the pulse due to the large magnitude and opposite sign of the frequency shift in these regions. This results in a corresponding loss of fringe visibility in the wings of the interferometric autocorrelation trace and the profile approaches that of an intensity autocorrelation in the wings. Interferometric autocorrelations are self calibrating since the separation between the fringes is equal to one wavelength. But it is not trivial to infer a pulse duration from such a measurement because of the effects of chirp on the width of the trace. Only in the absence of frequency chirp can such measurements be made accurately. The intensity autocorrelation is much less sensitive to chirp and thus provides a more accurate measurement of the pulse duration.

As mentioned above, it is the autocorrelation of the pulse intensity profile which is recorded and not the actual intensity profile itself. In order to determine the true pulse duration from the autocorrelation function, a knowledge of the pulse shape is required. It can be shown that the pulse duration, $\Delta\tau_p$, is related to the intensity autocorrelation width, $\Delta\tau$, by

$$\Delta\tau_p = \frac{\Delta\tau}{k} \tag{1.8}$$

where k is a constant which depends on the pulse shape[31]. Table 1.2 shows the values of k for some ideal pulse shapes. Determination of the shape of femtosecond pulses experimentally requires the use of higher order autocorrelation or cross-correlation techniques. The former require higher powers, while the latter have, until recently, required the use of complex

computational methods to perform iterative fits to assumed pulse shapes. These techniques are sensitive to measurement errors so that neither method is trivial. In practice one assumes an ideal pulse shape which is probably quite accurate in reality. This can be cross checked from the expected duration-bandwidth product, $\Delta\tau_p\Delta\nu$, for un-chirped pulses of the assumed shape. Values of $\Delta\tau_p\Delta\nu$ for the given pulse shapes are also shown in Table 1.2. If the pulses are frequency chirped, the measured value for $\Delta\tau_p\Delta\nu$ will be larger than that expected for transform limited pulses.

Recently, a relatively simple method for directly determining the amplitude and phase of femtosecond pulses has been developed[32]. If the amplitude and phase of the pulse spectrum can be measured, then the pulse shape can be retrieved by a simple Fourier transform. In this system, the input pulse is split and one pulse is sent through a zero-dispersion pulse compressor[33] which consists of a diffraction grating, a lens and a retroreflecting mirror. In addition, a slit aperture is placed directly in front of the mirror so that only a slice of the spectrum is transmitted by the compressor. It has been shown[34], that the output from such a device is a broadened pulse which is temporally delayed by an amount equal to the phase derivative of the sampled component of the pulse spectrum. This delay can be measured by performing a simple crosscorrelation with the original, unfiltered reference pulse. Thus, the dependence of the phase derivative with wavelength can be measured by scanning the slit across the mirror. A standard monochromator and photodiode is used to determine the

Pulse intensity profile	k	$\Delta\tau_p\Delta\nu$
Symmetric exponential	2.42	0.1420
Single-sided exponential	2.00	0.1103
$Sech^2$	1.54	0.3148
Gaussian	1.41	0.4413
Square	1.00	0.8859

Table 1.2. Table showing the pulse duration correction factor, k and the transform limited duration bandwidth product for different pulse shapes.

wavelength being analysed as well as the optical power spectrum of the laser pulses. The amplitude and phase of each component in the pulse spectrum can thus be determined and the pulse shape can be calculated by performing a simple Fast Fourier Transform. This technique does not require the assumption of an initial pulse shape and can be performed with relatively little computer time. The phase of the pulse is measured in the time domain using a standard intensity crosscorrelation so that interferometric accuracy is not required. The system has already been used to analyse the modelocked pulses from a CPM dye laser and should also prove useful for studying the modelocked pulses produced from femtosecond solid-state lasers such as Ti:Al_2O_3.

The temporal resolution of SHG autocorrelators is determined primarily by the phase-matching bandwidth of the SHG crystal used. This is the difference in the phase velocities between the fundamental and second harmonic signals resulting from the dispersion of the nonlinear material and causes the two waves to walk away from one another as they travel through the crystal. The effect is known as group-velocity mismatch (GVM) and means that phase matching may not be achievable over the entire pulse bandwidth. The phase-matching bandwidth for negative uniaxial crystals of length ℓ, can be calculated from equation (1.9) which was first derived by Miller[35].

$$\Delta\lambda = \frac{1.39\,\lambda}{2\,\pi\,\ell}\left[\frac{1}{2}\frac{dn_{e(2\omega)}(\theta)}{d\lambda} - \frac{dn_{o(\omega)}}{d\lambda}\right]^{-1} \qquad (1.9)$$

where λ is the fundamental wavelength and the terms involving $dn/d\lambda$ are the relevant values of dispersion for the ordinary and extraordinary waves at the appropriate wavelengths and phase matching angle in the crystal. The GVM causes an effective frequency filter for the second harmonic signal and leads to a broadening of the second harmonic pulse. The effects of group velocity dispersion on the fundamental and second harmonic pulses are generally much smaller and can be neglected. It has been shown that GVM does not significantly effect the measured pulse durations provided the pulses are free from frequency chirp. If the pulses are frequency chirped, the measured pulse durations may vary significantly from the true

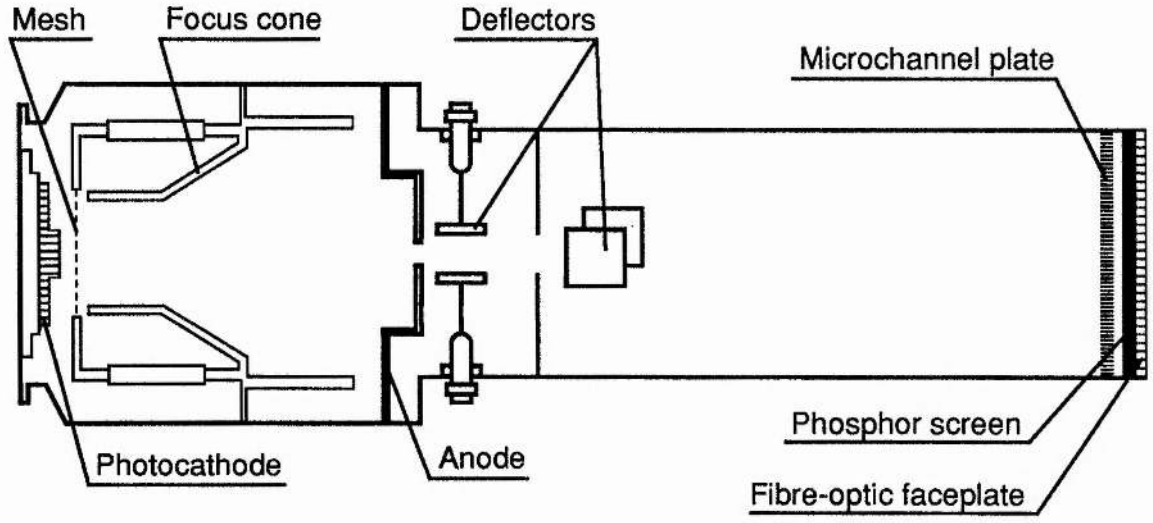

Figure 1.6. Schematic diagram of the Photochron IIC electron-optical streak camera.

intensity autocorrelation width if the GVM is large and if the phase-matching is tuned away from the peak of the pulse spectrum[36].

Equation (1.9) can be used to ensure that the chosen nonlinear crystal has a sufficient phase-matching bandwidth for the expected pulse durations. In the work described throughout this thesis, a 350 μm thick ADP crystal was used in the autocorrelator. This had a phase-matching bandwidth of approximately 50 nm, which corresponded to a pulse duration of ~15 fs at 850 nm, assuming a sech^2 pulse shape. The shortest pulse durations measured in the work described in this thesis were $\gtrsim$ 40 fs, so that this effect could be neglected.

1.3.2 The Electron-optical Streak Camera

Electron-optical streak cameras can be used to measure events (pulses) which occur on a picosecond timescale. A streak camera consists of six main parts: the photocathode, mesh electrode, focusing electrodes, deflection electrodes, constant field drift region and phosphor screen. The Photochron IIC streak camera[37], which was used for most of the work described in this thesis, is illustrated schematically in figure 1.6. In a practical arrangement, light is imaged onto the photocathode by a 10 - 20 μm slit and the liberated photo-electrons are accelerated to 5 - 10 keV by the mesh electrode. An inverting electrostatic lens structure

images the photoelectrons onto the phosphor screen. The deflection structure allows the electron beam to be 'streaked' across the phosphor so that the imaged intensity, which is proportional to the incident electron number density and hence the incident light intensity, provides a record of the pulse intensity at the photocathode as a function of time. Provided the resolution is adequate, the streak camera can record the shape and duration of the event.

The temporal resolution of a streak camera is ultimately determined by the spread in photoelectron energies liberated from the photocathode. This results in a spread in the transit times and hence the arrival times of the photoelectrons at the deflection system and is referred to as transit time dispersion. This effect can be reduced by the insertion of a mesh electrode which enables a large field to be present at the photocathode surface resulting in rapid electron acceleration. Operating close to the long wavelength end of the photocathode response also reduces the transit time dispersion. The final resolution, therefore, depends on both the photocathode material as well as the extraction field. Another factor governing the resolution is microlensing in the photocathode due to the high localised photocurrents. This results in a surface potential perturbation which causes defocusing. Microlensing is also caused by the mesh apertures. The electron packet may become distorted in space due to the mutual Coulomb repulsion between the individual electrons, which also leads to a reduction in the final achievable resolution.

Streak cameras can be operated in two ways - single shot and synchronously scanned. Synchronous operation is most useful for monitoring the pulses from cw modelocked lasers which have a repetitive output. In this mode of operation, the deflection plates are driven with a sinusoidal voltage which has a constant phase relationship with the periodic events to be recorded. If only the central part of the sinusoid is used good streak linearity can be achieved. For example, the central 1/6 of a sinusoid period is linear to within 5% so that a streak linearity which is better than 5% over 1/10 of the deflection period can be obtained[38]. There are two popular methods of deriving the deflection voltages necessary for the streak camera. These are described as active and passive drives and are illustrated schematically in

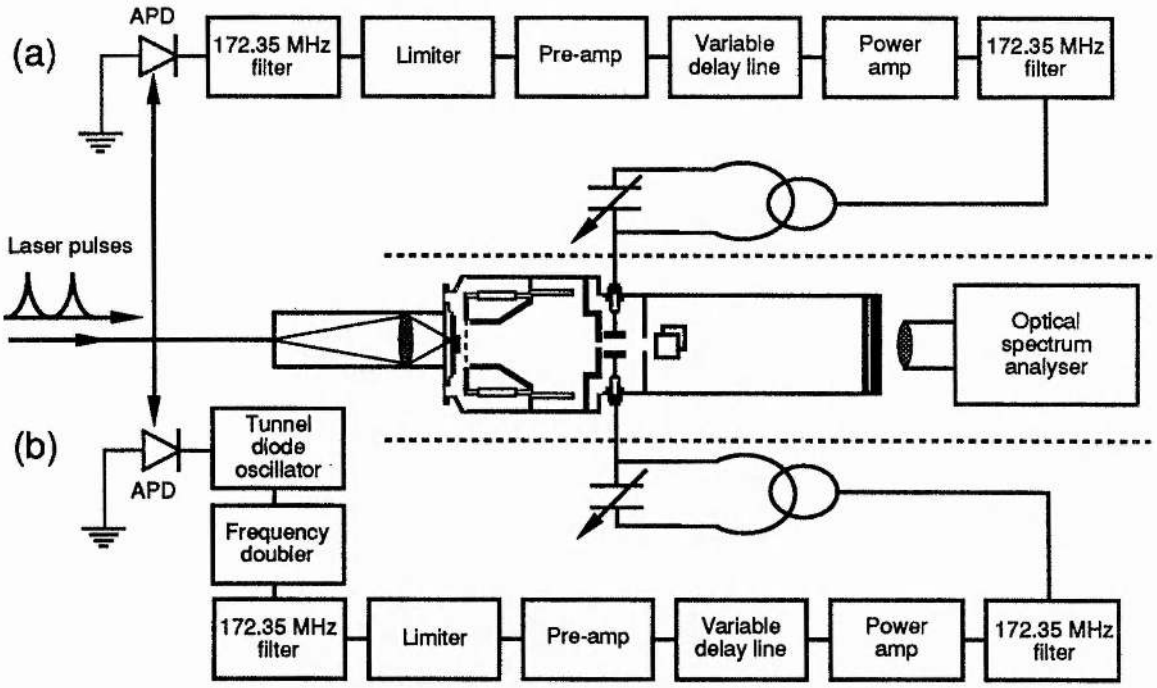

Figure 1.7. Diagram illustrating the two most common synchronisation schemes for synchronous operation of an electron-optical streak camera: (a) passive synchronisation and (b) active synchronisation.

figure 1.7. In the active scheme a tunnel diode circuit is designed to oscillate for a few periods when triggered. Its oscillation frequency is adjusted to be an exact harmonic of the laser output so that a photodiode repeatedly triggers the device into operation. A rf resonant circuit is used to generate the large deflection voltage (~160 V per cm of deflection) required, with modest rf powers. A third method is to drive the streak camera from a reference oscillator to which the laser repetition frequency is locked. This method is discussed in more detail in chapter 6.

Synchronous operation has a number of advantages associated with it. Synchronisation between the deflection waveform and optical signal is always ensured. There is inherent signal gain and signal averaging due to integration of many streaks on the phosphor screen, resulting in improved signal to noise ratios and often, no image intensification is necessary. This also results in high sensitivities and dynamic range (the useful input intensity range before deterioration in temporal resolution becomes too large). The relatively low photocurrents

required mean that space charge effects are minimised and hence optimum camera performance can be achieved. Finally, the synchronous mode of operation provides a realtime monitor and is therefore very attractive for following repetitive events. However, this mode of operation is very sensitive to relative phase fluctuations between the rf voltage driving the deflection system and the laser output, because the resulting streak smearing can seriously degrade the achievable temporal resolution. Amplitude noise can be reduced using a limiter and is less important because the image corresponds to the zero crossover point of the sinusoid. In chapter 6, an experiment will be described which used a synchronously operating streak camera to estimate the relative pulse timing jitter between two (synchronised) self-modelocked Ti:Al_2O_3 lasers.

The readout device used with the streak camera is most commonly photographic film or an optical multi-channel analyser. The resolution of this device should be better than that of the camera/intensifier so as not to cause any image degradation. The final instrument resolution, τ_r, is given by

$$\tau_r = \sqrt{(\Delta t_s)^2 + (\Delta t_d)^2 + (\Delta \tau_p)^2} \tag{1.10}$$

where Δt_s is the technical limiting resolution given by

$$\Delta t_s = \frac{\Delta s}{v_s} = \frac{\text{minimum spatial width of image}}{\text{streak speed}} \tag{1.11}$$

The transit time dispersion is Δt_d and the actual pulse duration is $\Delta \tau_p$. A measured synchroscan resolution of 0.93 ps has been achieved from a Photochron IV streak camera[38]. The Photochron IIC tube used in this thesis had a measured synchroscan resolution of 1.8 ps.

1.3.3 Spectral Measurements

Thus far techniques for measuring the durations of modelocked pulses have been discussed. Of equal importance is the measurement of the modelocked pulse spectrum. A

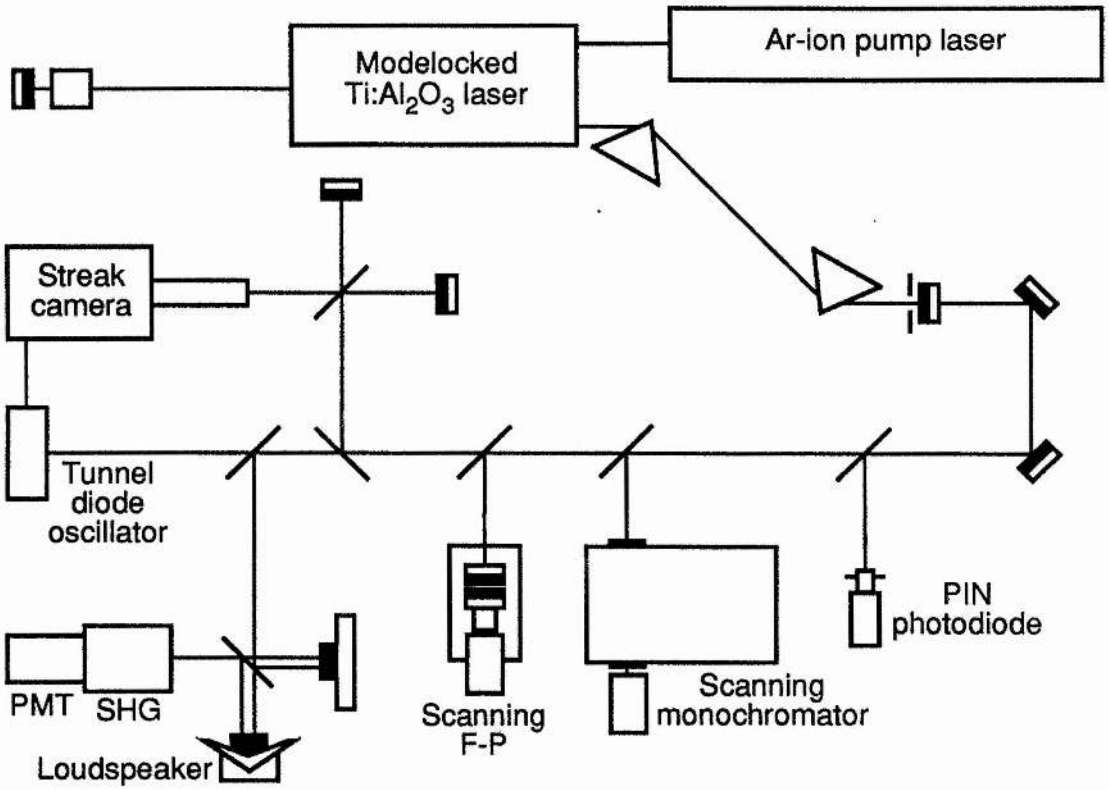

Figure 1.8. Schematic diagram showing the diagnostic equipment used to monitor the modelocked laser pulses.

knowledge of the pulse bandwidth enables one to estimate the accuracy of the assumed pulse shape used in the intensity autocorrelation measurement of the pulse duration. This is done by comparing the measured duration-bandwidth product with the theoretically expected value. Alternatively, the presence of frequency chirp on the pulses can be confirmed if the measured duration-bandwidth product is larger than that expected.

The optical power spectrum can also give information about the quality of the modelocked pulses from the laser. For example, the presence of narrow spikes superimposed on the broad modelocked spectrum usually indicates the presence of a cw component within the laser output. A modulation on the modelocked spectrum can indicate the presence of multipulsing. Often these features are not evident from the autocorrelation or pulse sequence measurements so that the frequency domain measurements provide essential additional information. Specific examples of such states will be discussed in chapter 4.

For the work described in this thesis, the spectrum of the laser was recorded using a scanning monochromator (Applied Photophysics Model. f/3.4) which had a resolution of approximately 1 nm. The laser spectrum was also monitored in realtime using a scanning Fabry-Perot interferometer constructed using two plane-parallel 96% reflecting laser output couplers and scanned by a sine wave generator and transformer. Alternatively, a linear CCD array was placed at the back of the monochromator with the output slit fully open. Due to the difficulty in accurately calibrating these real time devices they were only used as monitors and not for measurement purposes.

The application of all these diagnostic systems in a modelocked laser experiment is illustrated schematically in figure 1.8.

1.4 Pulse Propagation

In this section the effects of dispersion and nonlinearity on the propagation of short pulses will be discussed. The concept of dispersion is introduced first and its effect on pulse propagation in the absence of nonlinear effects is outlined. A scheme which can be used to provide variable group-velocity dispersion (GVD) using a sequence of prisms is also introduced. Pulse propagation in nonlinear media is discussed and the effects of self-focusing and self-phase modulation (SPM) are outlined. The combined influence of GVD and SPM on pulse propagation is discussed qualitatively. Finally, pulse compression is outlined, with particular emphasis on techniques which operate in the normal dispersion region of optical fibres. Simple conditions, which allow the optimisation of such pulse compressors are quoted.

1.4.1 Pulse Propagation in Dispersive Media

The concept of dispersion describes how the speed of light in a substance varies with the wavelength. When electromagnetic waves interact with a material, the medium's response is a function of the optical frequency. This phenomena is referred to as chromatic dispersion and manifests itself in the frequency dependence of the refractive index, $n = n(\omega)$. For most

glasses in the visible region of the spectrum, $n(\lambda)$ and $dn/d\lambda$ increase as λ decreases and this behaviour has been referred to as normal dispersion, so that blue light travels more slowly and bends more on refraction than red light. However, in the region of a resonance in the material, $n(\lambda)$ and $dn/d\lambda$ can increase as λ increases and the dispersion in this region is said to be anomalous.The first successful attempt to represent $n(\lambda)$ mathematically was the Cauchy equation

$$n(\lambda) = A + \frac{B}{\lambda^2} + \frac{C}{\lambda^4} + \ldots\ldots \qquad (1.12)$$

where A, B, C, etc. are characteristic constants of the material. The Cauchy equation is an empirical formula. This equation provides reasonably accurate values for the refractive index of many optical glasses at wavelengths below 1 μm.

In the region beyond 1 μm, the measured values of $n(\lambda)$ deviate from those predicted by the Cauchy equation. As the wavelength approaches a resonance the values of $n(\lambda)$ decrease more rapidly than those predicted by equations of this form. Further more, on the long wavelength side of the absorption $n(\lambda)$ is large and decreases with increasing wavelength. Further away from the resonance, the Cauchy equation is again satisfied with different characteristic constants. A more successful mathematical representation was provided by the Sellmeier equation, which has the form

$$n^2(\lambda) = 1 + \frac{A_0 \lambda^2}{\lambda^2 - \lambda_0^2} + \frac{A_1 \lambda^2}{\lambda^2 - \lambda_1^2} + \ldots\ldots = 1 + \sum_i^m \frac{A_i \lambda^2}{\lambda^2 - \lambda_i^2} \qquad (1.13)$$

where the λ_i are the wavelengths of the materials resonances and the A_i are dependent on the strengths of these resonances. The sum is performed over all the resonances near the frequency range of interest. The Sellmeier equation provides a good approximation of $n(\lambda)$ provided λ is not too near a resonance. Equations of this form have been used throughout the work described in this thesis to estimate the refractive index and its derivatives for many of the materials used.

The magnitude and nature of the dispersion plays a critical role in the propagation of ultrashort pulses through dispersive media because the different spectral components of the pulse will travel at different speeds given by $c/n(\lambda)$ and pulse broadening (or pulse shortening) may occur. Soliton propagation is a well known process in optical fibres where a positive index nonlinearity ($n = n_0 + n_2 I$: $n_2 > 0$) together with anomalous dispersion ($d^2n/d\lambda^2 < 0$) leads to pulse shapes which are periodic functions of distance in the absence of attenuation. Similar conditions, ie. the presence of nonlinearities and/or dispersion, exist in laser cavities and so the quality of the modelocked output will depend on these effects.

It is important to be able to carefully design laser resonators in which the effects of dispersion are known and/or controlled. This can be achieved relatively easily by including a prism sequence such as that shown in figure 1.9, in the cavity. This can provide easily adjustable dispersion with a relatively low insertion loss. Mathematically, the effects of dispersion are taken into account by expanding the propagation constant, β, in a Taylor series about the centre frequency, ω_0.

$$\beta(\omega) = \frac{\omega}{c} n(\omega) = \beta_0 + \beta_1 (\omega - \omega_0) + \frac{1}{2}\beta_2 (\omega - \omega_0)^2 + \frac{1}{3}\beta_3 (\omega - \omega_0)^3 + \ldots\ldots \quad (1.14)$$

$$\text{where } \beta_n = \left.\frac{d^n\beta}{d\omega^n}\right|_{\omega = \omega_0} \quad (1.15)$$

For most purposes the terms in β_3 and higher are small and can be neglected.

Recall that the phase velocity, v_ϕ, is the velocity of propagation of a region of constant phase (eg. a wave crest). In dispersive media the phase velocity varies with wavelength so that the individual frequency components within an optical pulse travel at different speeds. The wave packet will progress at the group velocity, $v_g = d\omega/d\beta$ and will, therefore, change its form as it propagates. The terms in equation (1.14) can be identified as follows[39]. The phase velocity v_ϕ is related to β_0 by

$$\beta_0 = \beta(\omega_0) = \frac{\omega_0}{v_\phi} \quad (1.16)$$

The group velocity is related to β_1 and is given by

$$\beta_1 = \frac{1}{v_g} \tag{1.17}$$

$$\text{where } \beta_1 = \frac{d\beta}{d\omega} = \frac{1}{c}\left(n + \omega \frac{dn}{d\omega}\right) = \frac{1}{c}\left(n - \lambda \frac{d\,n}{d\lambda}\right) = \frac{n_g}{c} \tag{1.18}$$

and n_g is the group index. The terms in β_2 and higher are responsible for pulse broadening. In particular, β_2 represents the group velocity dispersion (GVD) and is given by

$$\beta_2 = \frac{d}{d\omega}\left(\frac{1}{v_g(\omega)}\right) \tag{1.19}$$

$$= \frac{d^2\beta}{d\omega^2} = \frac{1}{c}\left(2 \frac{dn}{d\omega} + \omega \frac{d^2n}{d\omega^2}\right) = \frac{\lambda^3}{2\pi c^2}\frac{d^2n}{d\lambda^2} \tag{1.20}$$

The quantity β_2 is often used as a measure of the dispersion of an optical system. For fused silica, the term $\beta_2 = 0$ at a wavelength of approximately 1.27 μm. This wavelength is often referred to as the 'zero dispersion wavelength', λ_D. The dispersion is not really zero, even when $\lambda = \lambda_D$, because the higher order terms in equation (1.14) then become significant and must be taken into account. The term β_3 is given by

$$\beta_3 = \frac{d^2}{d\omega^2}\left(\frac{1}{v_g}\right) = \frac{1}{c}\left(3 \frac{d^2n}{d\omega^2} + \omega \frac{d^3n}{d\omega^3}\right) = -\frac{\lambda^4}{4\,\pi^2\,c^3}\left(3 \frac{d^2n}{d\lambda^2} + \lambda \frac{d^3n}{d\lambda^3}\right) \tag{1.21}$$

An alternative quantity, which is often used in engineering literature to measure dispersion, is the dispersion parameter D, which is related to β_2 by

$$D = \frac{d\beta_1}{d\lambda} = -\frac{2\pi c}{\lambda^2}\beta_2 = -\frac{\lambda}{c}\frac{d^2n}{d\lambda^2} \tag{1.22}$$

In the normal dispersion region $\beta_2 > 0$ ($D < 0$), while $\beta_2 < 0$ ($D > 0$) for anomalous dispersion. GVD for which $\beta_2 > 0$ is also referred to as positive GVD and similarly, GVD for which $\beta_2 < 0$ is referred to as negative GVD. The parameter, D, is sometimes referred to as the group delay dispersion (GDD).

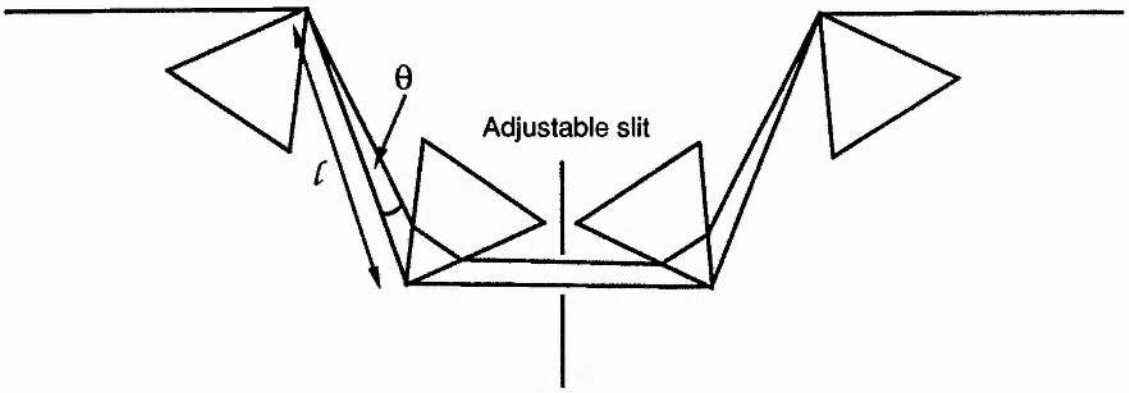

Figure 1.9. Schematic diagram illustrating the four prism sequence used to provide variable intra or extracavity group-velocity dispersion.

When calculating the dispersion in optical fibres one must also take account of the waveguiding nature of the structure, which results in an additional waveguide contribution to the total dispersion. This results from the fact that the effective mode-index is slightly lower than the material index $n(\omega)$, with the reduction being ω dependent also. The total dispersion is the sum of the material contribution and the waveguide contribution. Generally, the waveguide contribution shifts λ_D to a slightly longer wavelength. Provided one is far enough away from λ_D the waveguide dispersion can be ignored. Because the waveguide dispersion depends on the design parameters of the fibre, such as the core radius and the core-cladding index difference, it is possible to shift λ_D in the fibre to wavelengths in the vicinity of 1.55 μm where the fibre loss is also at a minimum. Such dispersion shifted fibres have obvious applications in optical communications.

The prism sequence shown in figure 1.9 can be used to provide variable dispersion which is easily adjustable from negative, through zero, to positive values. It has reasonably low insertion loss because all the prisms are oriented at the Brewster angle and can, therefore, be easily incorporated into a laser cavity to provide tunable intracavity GVD.

If the optical path length through the prism sequence is $P(\omega) = \int n(x)\,dx$, the dispersion constant in the medium is given by

$$D = \frac{1}{L}\frac{dT}{d\lambda} = -\frac{\lambda}{cL}\frac{d^2P}{d\lambda^2} \qquad (1.23)$$

where T is the time taken for the light to travel a length L corresponding to the physical length of the light path P. For a single pass of the prism sequence illustrated in figure 1.9, it can be shown that[40]

$$\frac{d^2P}{d\lambda^2} = 4\ell\left\{\left[\frac{d^2n}{d\lambda^2} + \left(2n - \frac{1}{n^3}\right)\left(\frac{dn}{d\lambda}\right)^2\right]\sin\theta - 2\left(\frac{dn}{d\lambda}\right)^2\cos\theta\right\} \qquad (1.24)$$

$$\text{ie. } \frac{d^2P}{d\lambda^2} = 4\left[\frac{d^2n}{d\lambda^2} + \left(2n - \frac{1}{n^3}\right)\left(\frac{dn}{d\lambda}\right)^2\right]\ell\sin\theta - 8\left(\frac{dn}{d\lambda}\right)^2\ell\cos\theta \qquad (1.25)$$

If, as is often the case, θ is of the order of the angular deviation of the ray bundle, then $\cos\theta \approx 1$ and $\ell\sin\theta \sim$ the spot size ≈ 2 mm. Although the material dispersion of the prisms is positive (red travels faster than blue), for sufficiently large ℓ, equation (1.25) shows that $d^2P/d\lambda^2$ will be negative and the shorter wavelength components will traverse the prism sequence more quickly than the longer ones, so that the effect is to provide overall negative GVD.

By using equations (1.22) and (1.23), the total value of $d^2P/d\lambda^2$ for the material dispersion of the prisms and other elements in the optical path can be calculated. Then, using equation (1.25), the required value of ℓ can be chosen to provide the optimum dispersion for the laser. Such calculations have been used throughout this thesis in chapters 2, 4 and 5 to estimate values of β_2 for various laser configurations having either intracavity or extracavity prism sequences.

The effect of dispersion on an optical pulse depends on the sign of the GVD and on whether or not the pulse has an initial frequency chirp[41]. The simplest case occurs when the initial pulse is bandwidth-limited. As a result of the GVD, the different frequency components of the pulse travel at slightly different speeds, with the longer wavelength components travelling faster than the shorter ones if $\beta_2 > 0$. Since the pulse can maintain its width only if all the spectral components arrive together, pulse broadening will occur if $\beta_2 \neq 0$, as a result of the time delay in the arrival of the different frequencies. The broadened pulse also develops a linear frequency chirp as a result of the redistribution of the different frequency components

within the pulse envelope. In the case where $\beta_2 > 0$, the instantaneous frequency increases linearly from the front to the back of the pulse and this is referred to as positive or up-chirp.

A pulse which is initially unchirped will broaden with increased propagation distance irrespective of the sign of β_2. However, if the pulse has an initial frequency chirp then it may broaden or shorten with distance depending on the type of dispersion and chirp. The frequency chirp can be characterised by the chirp parameter C, where $C > 0$ for up-chirp and $C < 0$ for down-chirp. The behaviour of the pulse is then determined by whether $\beta_2 C$ is positive or negative. If $\beta_2 C > 0$ then the pulse will broaden monotonically with distance, but if $\beta_2 C < 0$ the pulse will initially narrow before broadening again. This is because in this case, the initial chirp is of the opposite sign to the dispersion induced chirp so that the two initially cancel. After some distance, a minimum pulse duration is reached when the chirp cancellation is complete. With further propagation, the dispersion induced chirp begins to dominate so that the pulse broadens again as before.

This behaviour can be understood as follows. For example, in the presence of normal dispersion, the longer wavelength components travel faster than the shorter wavelength ones. If the pulse is initially down-chirped, then the faster red shifted components will be at the rear of the pulse while the slower blue shifted components are at the front. Thus, the trailing edge of the pulse can catch up with the leading edge and the pulse gets shorter as it propagates along in the dispersive medium. The shortest pulse is obtained when the front of the pulse is delayed by just the right amount so that the back has almost caught up. Further propagation causes pulse broadening again, as the faster travelling red shifted spectral components over take the slower blue shifted ones and move towards the leading edge of the pulse.

For linear dispersive systems, a useful parameter is the so called dispersion length, L_D, which is given by

$$L_D = \frac{k^2 \tau_p^2}{|\beta_2|} \tag{1.26}$$

where τ_p is the FWHM pulse duration and k is a parameter which equals 0.601 for gaussian pulses and 0.567 for $sech^2$ pulses. L_D is the length after which an initially unchirped gaussian pulse has broadened by a factor of $\sqrt{2}$.

In summary, pulse propagation through a dispersive system will either cause an increase or a decrease in the initial pulse duration depending on the sign of the dispersion, the initial frequency chirp of the pulse and the propagation distance. The pulse acquires a linear frequency chirp, but the spectral width remains unchanged.

1.4.2 Pulse Propagation in Nonlinear Media

So far the effects of the nonlinear response of the medium through which the pulse travels have been ignored. These will briefly be considered here in isolation, before discussing pulse propagation in nonlinear and dispersive media. The discussion will be restricted to the optical Kerr effect as this is by far the most important nonlinear effect for ultrashort pulse propagation in low-loss dielectric materials.

The response of any dielectric material to light becomes nonlinear for sufficiently intense electromagnetic fields. This is due to the anharmonic motion of the bound electrons under the influence of the intense applied field. The induced macroscopic polarisation, p, is no longer a linear function of the applied field and can be expressed in a somewhat simplified, but general form, as

$$p = \sum_n \varepsilon_0 \chi_{(n)} E^n \tag{1.27}$$

The linear term $\chi_{(1)}$, is related to the material refractive index in the usual manner so that $n = \mathrm{Re}\left[\sqrt{1 + \chi_{(1)}}\right]$. The $\chi_{(2)}$ term is responsible for processes such as second harmonic generation, but is non-zero only in materials which have noncentrosymmetric crystal structures. In contrast, the $\chi_{(3)}$ term is present in all materials. For consistency, the effect of the $\chi_{(3)}$ term can be expressed as a nonlinear refractive index so that the total refractive index of the material is given by

$$n = n_0 + n_2 I \tag{1.28}$$

ie. the material refractive index is intensity dependent. This effect is commonly referred to as the optical Kerr effect. In silica the nonlinear index has a value $n_2 \sim 3\times10^{-16}$ cm^2W^{-1}.

This effect is responsible for the so called self-focusing of optical beams[42]. If the beam has a smooth intensity profile which increases towards the centre, then it will induce a higher value of refractive index in the centre than at the edges provided $n_2 > 0$. The medium will thus behave as a positive lens. If the focusing effect of this induced lens is sufficiently strong, so that diffraction effects can be overcome, the beam will begin to be focused within the material. The decrease in the spot size will cause a corresponding increase in the intensity and also in the strength of the self-focusing. It can be shown that if the beam power exceeds a certain critical value, the beam will continue to be focused in a runaway fashion. This critical power level represents the power at which the self-focusing effects just balance the diffraction spreading. Propagation at the critical power leads to the self-trapping effect when the spot size does not change with distance.

Real laser beams do not have perfectly smooth spatial intensity profiles. Self-focusing can lead to the exponential growth with distance, of any small intensity fluctuations in the transverse beam profile. The spatial variation in intensity produces a corresponding variation in the transverse refractive index profile, ie. a refractive index grating is induced. The resulting diffraction of the beam by this grating occurs in exactly such a way as to enhance the initial intensity fluctuations with propagation distance.

These effects can cause catastrophic damage and must be considered whenever high power optical beams propagate through materials. At the very least, the beam profile will be severely distorted. Self-focusing will be discussed further in chapter 5 with reference to pulse propagation within the gain medium of a self-modelocked Ti:Al_2O_3 laser. In this case dynamic self-focusing effects can be exploited to provide fast temporal amplitude modulation which can assist in the formation and maintenance of the modelocked pulses.

Another important effect resulting from the optical Kerr effect is known as self-phase modulation (SPM)[43,44] and is the time domain equivalent of the spatial effects just described. The phase of an optical signal will change by an amount $\phi = 2\pi nL/\lambda$ after it has travelled a distance L in a medium of refractive index, n. The intensity varies with time during a pulse so that the instantaneous refractive index and hence, the phase shift which the pulse experiences, will also vary with time. The resulting intensity dependent phase shift is given by

$$\phi_{NL} = \frac{2\pi n_2 L I}{\lambda} \tag{1.29}$$

Since ϕ_{NL} is a function of time, the instantaneous optical frequency shift is given by

$$\delta\omega = -\frac{\partial\phi_{NL}}{\partial t} = -\frac{2\pi n_2 L}{\lambda}\frac{dI}{dt} \tag{1.30}$$

If $n_2 > 0$, this SPM will cause a decrease in the instantaneous optical frequency during the leading edge of the pulse and an increase during the trailing edge. For gaussian or $sech^2$ pulses the chirp is linear and positive over the central region of the pulse. In general, since $\delta\omega$ is proportional to dI/dt, the extent and shape of the frequency chirp will depend on the exact pulse shape. In the absence of dispersion, the pulse shape will remain unchanged but the pulse spectrum will broaden and the pulse will become frequency chirped in the way just described.

The equivalent length scale to L_D for nonlinear pulse propagation is the nonlinear length, L_{NL}, defined as follows

$$L_{NL} = \frac{c A}{n_2 \omega_0 P_0} = \frac{1}{\gamma P_0} \tag{1.31}$$

where P_0 is the peak pulse power, A is the beam cross-sectional area and γ is a nonlinearity coefficient. Thus, L_{NL} is the propagation distance at which $\phi_{max} = \gamma P_0 z = 1$. If pulse propagation in optical fibres is being considered, the mode field radius should be used to calculate the area, A, in equation (1.31). If the propagation medium is lossy then the

propagation distance, z, is replaced by an effective propagation distance which is reduced by an amount depending on the magnitude of the attenuation.

Dispersive and nonlinear effects both cause frequency chirping of the propagating pulses and so it is evident that the combined effects of SPM and GVD must be taken into account when considering pulse evolution in nonlinear and dispersive media. The ratio, L_D/L_{NL} provides a useful parameter to classify the propagation regime in terms of which effect, if any, will dominate and is given by

$$N^2 = \frac{L_D}{L_{NL}} = \frac{\gamma P_0 (k \tau_p)^2}{|\beta_2|} \tag{1.32}$$

The interaction is quite complicated and must be expressed in terms of the wave equation describing the propagation of electromagnetic waves in dielectrics. The effects of GVD, SPM and attenuation are included through the expression for the induced macroscopic polarisation in the medium. The resulting nonlinear partial differential equation must, in general, be solved numerically for the particular case under study. While the exact solutions depend on the particular situation, some general trends can be identified.

The effect of SPM is to generate new frequency components which are red shifted at the leading edge and blue shifted at the trailing edge of the pulse (for $n_2 > 0$). In the normal dispersion regime ($\beta_2 > 0$), the addition of SPM leads to enhanced pulse broadening because the red shifted spectral components at the leading edge of the pulse travel more quickly than the blue shifted frequencies in the rear of the pulse. In contrast, the broader pulse means that the SPM is reduced and ϕ_{NL} is less than that which would occur in the absence of GVD. Even if $L_D/L_{NL} \gg 1$, the GVD cannot be neglected because the SPM induced frequency chirp means that even a small amount of dispersion can lead to considerable pulse shaping. Numerical simulations show that for normal dispersion, the pulses become nearly rectangular in shape and have an almost linear frequency chirp over their entire width[45]. This behaviour has important consequences for pulse compression which will be discussed in section 1.4.3.

In the anomalous dispersion region ($\beta_2 < 0$), the situation is quite different. Now the frequency chirp contributions from SPM and GVD oppose one another. In optical fibres, this leads to the evolution and propagation of solitons[46] when the pulse shape adjusts itself to make the chirp cancellation as complete as possible and the GVD and SPM cooperate to maintain a chirp-free pulse.

Pulse propagation in optical fibres, when the fibre loss is ignored, can be described by the nonlinear Schrödinger equation (NLSE)[47]. This equation has a special set of solutions in the anomalous dispersion region, which correspond to optical solitons. In general, solitons are waves that can propagate over long distances without distortion. Solving the NLSE shows that optical solitons have a sech^2 intensity profile. Pulses of this form can propagate for arbitrarily long distances either without change in shape for the fundamental soliton, or with periodic shape changes for higher order solitons.

This behaviour can be understood qualitatively by considering the interplay between SPM and GVD with distance along the fibre. The effect of SPM is to generate a positive frequency chirp over the pulse with corresponding spectral broadening. However, since the dispersion is anomalous, its effect is to decrease the duration of the positively chirped pulse, at least over the central linearly chirped section. In the case of the fundamental soliton, where $N = \sqrt{L_D/L_{NL}} = 1$, the GVD and SPM balance each other so that neither the pulse spectrum nor the shape changes with distance. For higher order solitons, where $N > 1$, the effect of SPM dominates at first but GVD becomes increasingly important as the propagation distance increases. In the light of the periodic evolution of higher order solitons, a useful parameter is the soliton period z_0, which is defined as follows

$$z_0 = \frac{\pi}{2} L_D = \frac{\pi}{2} \frac{(k\,\tau_p)^2}{|\beta_2|} \tag{1.33}$$

This is the distance after which a higher order soliton will have recovered its original shape.

Soliton propagation in optical fibres has not been studied in this thesis because the operating wavelengths of the lasers were $\lesssim 1\ \mu m$ so that pulse propagation always occurred

in the normal dispersion region. However similar conditions to those necessary for soliton propagation (negative GVD and SPM) can occur at these wavelengths inside laser cavities which have net negative GVD produced by a prism sequence such as that discussed earlier. In such lasers, soliton-like pulse shaping can occur with the interaction of intracavity negative GVD and SPM. These processes are particularly important for sub-100 fs pulses. The nonlinear propagation of pulses in dispersive media are important in solid-state modelocked lasers such as Ti:Al_2O_3, where the relatively long gain medium and high intracavity powers lead to significant amounts of SPM. This will be demonstrated for a modelocked Ti:Al_2O_3 laser in chapters 4 and 5 where it it is ultimately these effects that determine the final pulse durations generated.

1.4.3 Pulse Compression

Pulse compression techniques are an important application of nonlinear and dispersive effects in optical fibres. They have enabled pulses as short as 6 fs to be generated[48] - the shortest optical pulses ever reported which were only six optical cycles in length. There are two possible schemes for pulse compression depending on the wavelength region of interest - fibre-grating/prism pulse compressors which use fibres in the normal dispersion region followed by a grating or prism sequence providing negative GVD and soliton effect compressors which use higher order solitons supported in the anomalous dispersion region of optical fibres.

The basic idea for pulse compression was borrowed from chirp radar where microwave pulses having an initial frequency chirp were passed through a dispersive delay line. As outlined above, a linear dispersive medium will impose a linear frequency chirp on pulses propagating through it. If the product of the chirp parameter and the GVD parameter, $\beta_2 C < 0$, then the dispersion induced chirp will tend to cancel the initial chirp and a shorter pulse can be obtained at the output of the delay line. For maximum effect the input pulse

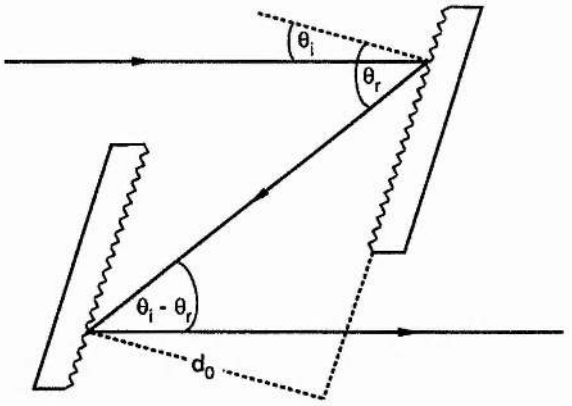

Figure 1.10. Schematic diagram of the diffraction-grating pair used for extracavity pulse compression.

should be linearly chirped so that the GVD (which also produces a linear chirp) can provide complete cancellation. The delay line must be constructed so that this cancellation occurs at its output.

The first experiments, which involved compression of inherently chirped pulses, used the dispersion provided by liquids or solids or by a grating pair[49,50]. In 1969 it was suggested that the nonlinear process of SPM could be used for pulse compression[51], but the idea was not demonstrated[52] until single mode optical fibres became available in the 1980's. In the fibre grating compressor the combined action of SPM and GVD in the fibre provides a nearly linear positive frequency chirp on the pulse and a grating pair then provides the required negative GVD. In soliton compression schemes only a single length of fibre is used. The pulse propagates in the anomalous dispersion regime and is compressed through the interplay of SPM and GVD which leads to soliton formation and pulse compression under the proper conditions. The compression results from the initial narrowing phase through which all higher order solitons go before the initial shape is restored after one soliton period. It is the peak power that determines the soliton order and hence the final compression factor.

Soliton effect compressors are only effective in the anomalous dispersion region where solitons can be propagated. Fibre grating compressors can be used in the normal dispersion region and will now be considered in more detail. The different spectral components of a

pulse incident on a diffraction grating will be diffracted at slightly different angles and as a result will experience different time delays during their passage through a grating pair. The blue shifted components arrive before the red ones and so the trailing edge of a positively chirped pulse can catch up with the leading edge as it travels through the grating pair.

Referring to figure 1.10, it can be shown that for first order diffraction, the angle of diffraction from the normal to the grating is given by

$$\sin\theta_r = \frac{2\pi c}{\omega\Lambda} - \sin\theta_i \tag{1.34}$$

where Λ is the grating period, ie. the line spacing and θ_i is the angle of incidence. The time delay for propagation through the gratings is

$$t_d(\omega) = \frac{l(\omega)}{c} = \frac{d\phi_c}{d\omega} \tag{1.35}$$

where $l(\omega)$ is the optical path length and $\phi(\omega)$ is the phase shift acquired by light of frequency ω. This phase shift can be expanded as a Taylor series about ω_0. The second order coefficient in this expansion is given by[41]

$$a_c = \frac{4\pi^2 c b_0}{\omega_0^3 \Lambda^2 \cos\theta_{r0}} \tag{1.36}$$

where θ_{r0} is given by equation (1.34) with $\omega = \omega_0$ and where $b_0 = d_0 \sec\theta_{r0}$ is the centre-to-centre grating spacing. The grating pair produces a negative phase shift which corresponds to an anomalous dispersion with an effective GVD parameter given by

$$\beta_2^{eff} = -\frac{2a_c}{b_0} \tag{1.37}$$

Grating pairs have a few disadvantages associated with them. The output pulses are spatially dispersed so that the output beam is elliptical in shape, however, a double pass configuration can be used to remedy this problem and double the available GVD. Also, because most gratings are only 60 - 80% reflective in the first order there is a factor of two reduction in the energy throughput of a grating pair and a factor of four for a double pass

configuration. Alternatively, a Gires-Tournois interferometer or a prism sequence can be used which generally have much smaller losses. The GVD provided by a prism sequences is, however, much smaller so that larger separations are required - often by two orders of magnitude. High dispersion materials such as TeO_2[53] or ZnSe[54] and high dispersion configurations may be used to make the separation more convenient, but these have correspondingly higher third order dispersion.

To get the best performance from a compressor it is important to be able to estimate the optimum fibre length and grating separation required to produce high quality output pulses with maximum compression for a given set of input pulse parameters. The fibre grating compressor can be modelled by numerically solving the wave equation governing pulse propagation in the fibre in the presence of GVD and SPM. The output pulse obtained from this analysis is then used as the input to the grating pair. The parameter a_c given by equation (1.36) can be adjusted to obtain the optimum pulse compression, ie. the peak power at the output is maximised.

The results show that the SPM induced frequency chirp in the absence of GVD, is linear only over the central portion of the pulse so that only this part can be properly compressed. A significant amount of energy remains in the wings so that the resulting pulses are not of a high quality. Fortunately SPM in the presence of GVD, broadens and reshapes the pulse to become nearly rectangular with a nearly linear frequency sweep across its entire width. The gratings or prisms can therefore compress most of the energy into a short pulse, but the benefits of improved quality are only achieved at the expense of reduced compression at a given value of input peak power.

The results of the simulations suggest some simple design rules for optimising the performance of the pulse compressor[55]. These can be expressed mathematically as follows

$$\frac{z_{opt}}{z_0} \approx \frac{1.6}{N} \tag{1.38}$$

$$\frac{a_c}{\tau_i^2} \approx \frac{1.6}{N} \tag{1.39}$$

$$\frac{1}{F_c} = \frac{\tau_c}{\tau_i} \approx \frac{1.6}{N} \tag{1.40}$$

where z_{opt} is the optimum fibre length to just linearise the SPM induced chirp, τ_i and τ_c are the full widths at half maximum intensity of the input and compressed pulses respectively and F_c is the compression factor. The parameters, z_0 and N, are those already identified for soliton propagation. The soliton period, z_0, also has an useful interpretation in the normal dispersion region - it is the length at which the initial pulse width has nearly doubled in the absence of SPM[55].

The factor of 1.6 is dependent on the input pulse shape being $sech^2$ and is slightly different for other pulse shapes, however if $N \gtrsim 10$ this slight difference can be ignored. These equations also assume unchirped input pulses, but again provided $N > 10$, the effects of chirp are typically less than 10% on the final pulse shapes. The effects of higher-order nonlinearity and dispersion have also been neglected, which provides an accurate approximation provided $\Delta\omega \ll \omega_0$. The results have been shown to be fairly accurate for $\tau_p \gtrsim 200$ fs. Further, if $\tau_p \lesssim 100$ fs, the gratings no longer act as quadratic compressors and the cubic phase terms become important[56]. It is also worth noting that the pulse energies in the fibre should be kept below the Raman threshold[57].

1.5 Conclusions

This chapter has presented a brief historical introduction to lasers and has summarised the work to be presented in the remainder of this thesis. An overview of the most important modelocking techniques has also been given. The methods for pulse width measurement used throughout the work to be described have also been outlined and their advantages and limitations have been pointed out. A brief discussion of pulse propagation in nonlinear and dispersive media has been presented along with an introduction to pulse compression techniques. The relatively high peak intensities and short durations of the modelocked pulses generated in the laser systems to be described, require that these effects be considered if a

complete understanding of the modelocked operation is to be reached and if optimised performance is to be achieved.

1.6 References

1. M.J. Mumma, Science **212**, 45, (1981).

2. A. Einstein, Physikalische Zeitschrift **18**, 121, (1917).

3. J.P. Gordon, H.J. Zeiger and C.H. Townes, Phys. Rev. **18**,1264, (1955).

4. N. Bloembergen, Phys. Rev. **104**, 324, (1956).

5. A.L. Schawlow and C.H. Townes, Phys. Rev. **112**, 1940, (1958).

6. T.H. Maimam, Nature **187**, 87, (1960).

7. A. Javan, W.R. Bennett, Jr. and D.R. Herriott, Phys. Rev. Lett. **6**, 106, (1961).

8. T.W. Hänsch, M. Pernier and A.L. Schawlow, IEEE J. Quant. Electron. **QE-7**, 45, (1961).

9. G. Huber, Conference on Lasers and Electro-Optics, CLEO Tech. Digest Series **10**, paper CTuU1, (1991).

10. D.J. Kuizenga and A.E. Siegman, IEEE J. Quant. Electron. **QE-6**, 694, (1970).

11. A.E. Siegman and D.J. Kuizenga, Appl. Phys. Lett. **14**, 181, (1969).

12. G.C.H. New, IEEE J. Quant. Electron. **QE-10**, 115, (1974).

13. H.A. Haus, J. Appl. Phys. **46**, 3049, (1975).

14. H.A. Haus, IEEE J. Quant. Electron. **QE-11**, 736, (1975).

15. H.A. Haus, IEEE J. Quant. Electron. **QE-12**, 169, (1976).

16. P.W. Smith, Proc. IEEE **58**, 1342, (1970).

17. D. von der Linde, Appl. Phys. **2**, 281, (1973).

18. A. Miller and W. Sibbett, J. Mod. Optics. **35**, 1879, (1988).

19. H.A. Haus, IEEE J. Quant. Electron. **QE-11**, 323, (1975).

20. L.F. Mollenauer and R.H. Stolen, Opt. Lett. **9**, 13, (1984).

21. K.J. Blow and D. Wood, J. Opt. Soc. Am. B **5**, 629, (1988).

22. J. Mark, L.Y. Liu, K.L. Hall, H.A. Haus and E.P. Ippen, Opt. Lett. **14**, 48, (1989).

23. K.J. Blow and B.P. Nelson, Opt. Lett. **13**, 1026, (1988).

24. P.N. Kean, X. Zhu, D.W. Crust, R.S. Grant, N. Langford and W. Sibbett, Opt. Lett. **14**, 39, (1989).

25. E.P. Ippen, L.Y. Liu and H.A. Haus, Opt. Lett. **15**, 183, (1990).

26. D.E. Spence, P.N. Kean and W. Sibbett, Opt. Lett. **16**, 42, (1991).

27. M. Maier, W. Kaiser and J.A. Giordmaine, Phys. Rev. Lett. **17**, 1275, (1966).

28. J.A. Armstrong, Appl. Phys. Lett. **10**, 16, (1967).

29. H.P. Weber, J. Appl. Phys. **38**, 2231, (1967).

30. W.B. Davenport, Jr. and W.L. Root, in 'An Introduction to the Theory of Random Signals and Noise', McGraw-Hill, New York, (1958).

31. K.L. Sala, G.A. Kenney-Wallace and G.E. Hall, IEEE J. Quant. Electron. **QE-16**, 990, (1980).

32. J.L.A. Chilla and O.E. Martinez, Opt. Lett. **16**, 39, (1991).

33. A.M. Weiner, J.P. Heritage and E.M. Kirschner, J. Opt. Soc. Am. B **5**, 1563, (1988).

34. J.L.A. Chilla and O.E. Martinez, IEEE J. Quant. Electron. **QE-27**, 1228, (1991).

35. R.C. Miller, Phys. Lett. **26A**, 166, (1968).

36. A.M. Weiner, IEEE J. Quant. Electron. **QE-19**, 1276, (1983).

37. W. Sibbett, W.E. Sleat and W. Krause, Proceedings of the European Space Agency Workshop on Laser Applications and Technology (Les Diablerets, Switz) **ESA SP-20**, 171, (1984).

38. A. Finch, Ph.D. Thesis, (1989).

39. A.E. Siegman, in 'Lasers', University Science Books, Mill Valley, California, (1986), Ch. 9.

40. R.L. Fork, O.E. Martinez and J.P. Gordon, Opt. Lett. **9**, 150, (1984).

41. G.P. Agrawal, in 'Nonlinear Fibre Optics', Academic Press, London, (1989).

42. W. Koechner, in 'Solid-State Laser Engineering', Springer-Verlag, New York, (1973), ch. 12.

43. F. Shimizu, Phys. Rev. Lett. **19**, 1097, (1967).

44. R.H. Stolen and C. Lin, Phys. Rev. A **17**, 1448, (1978).

45. D. Grischkowsky and A.C. Balant, Appl. Phys. Lett. **41**, 1, (1982).

46. L.F. Mollenauer, R.H. Stolen and J.P. Gordon, Phys. Rev. Lett. **45**, 1095, (1980).

47. G.L. Lamb, Jr., in 'Elements of Soliton Theory', Wiley, New York, (1980).

48. R.L. Fork, C.H. Bristo Cruz,P.C. Becker and C.V. Shank, Opt. Lett. **12**, 483, (1987).

49. J.A. Gordmaine, M.A. Duguay and J.W. Hansen, IEEE J. Quant. Electron. **QE-4**, 252, (1968).

50. E.B. Treacy, Phys. Lett. **28A**, 34, (1968).

51. R.A. Fisher, P.L. Kelley and T.K. Gustafson, Appl. Phys. Lett. **14**, 140, (1969).

52. H. Nakatsuka, D. Grischkowsky and A.C. Balant, Phys. Rev. Lett. **47**, 910, (1981).

53. M. Nakazawa, T. Nakashima, H. Kubota and S. Scikai, J. Opt. Soc. Am. B **5**, 215, (1988).

54. F.J. Duarte, Opt. and Quant. Electron. **19**, 223, (1987).

55. W.J. Tomlinson, R.H. Stolen and C.V. Shank, J. Opt. Soc. Am. B **1**, 139, (1984)

56. W.J. Tomlinson and W.H. Knox, J. Opt. Soc. Am. B **4**, 1404, (1987).

57. M. Kuckartz, R. Schulz and H. Harde, J. Opt. Soc. Am. B **5**, 1353, (1988).

Chapter 2
The LiF:F_2^+ Colour-centre Laser

2.1 Introduction

Colour-centre defects in various alkali-halide compounds provide the basis for a very useful class of laser - the so-called colour-centre laser. These lasers cover the very important wavelength range extending from 0.8 μm to 4.0 μm by utilising various colour centres in about a dozen different hosts. The applications of such lasers are, therefore, numerous, spanning many areas of science and technology such as molecular spectroscopy, chemical dynamics, pollution detection, fibre-optic communications and narrow band-gap semiconductor spectroscopy. Colour-centre lasers are most often optically pumped by a krypton-ion or Nd:YAG laser and can provide a few Watts of output power. Their solid-state nature, together with a homogeneously broadened linewidth, mean that they can be operated either as a single frequency or an ultrashort pulse source. In the former case the laser linewidth can be of the order of a few kHz, while in the latter the pulse durations can be of the order of 100 fs.

This chapter begins with a brief summary of some of the relevant physics of colour centres, together with laser crystal production and handling methods. The design of the colour-centre laser used in this work is then described. This was based on the F_2^+ centre in lithium fluoride (LiF). It will be shown that the laser could be operated in the wavelength range extending from 820 nm to 1000 nm, with average output powers as high as 400 mW. With adequate cryogenic cooling at liquid nitrogen temperature (77 K), a useful operating lifetime of approximately 200 hrs could be obtained from a single crystal. In the absence of this low temperature operation, the crystal lifetime was reduced to just over 2 hrs. The technique of passive modelocking using a slow saturable absorber dye will also be discussed and results will be presented showing how this scheme was applied to the laser operating in the 925 - 950 nm wavelength range. Pulses having durations of 170 fs were generated with

average powers of approximately 10 mW and peak powers of ~700 W. The technique of intracavity dispersion compensation was applied in a colliding pulse modelocked geometry, resulting in pulses having durations as short as 127 fs with an average power of approximately 7 mW per output beam. Finally, the application of a coupled-cavity scheme to the passively modelocked laser will be described. This enabled the tuning range of the modelocked laser to be extended to ~900 nm and also permitted extended operating intervals between saturable absorber dye changes.

2.2 The Physics of Colour Centres

Colour centres are point defects in a crystal lattice. The most important types, as far as laser physics is concerned, are electronic defects, which consist of one or more electrons trapped at an ionic vacancy, or a combination of an ionic vacancy and an adjacent impurity ion in the lattice[1]. They are present in many crystalline solids including the alkali-halides, where their presence results in the otherwise transparent crystal becoming coloured, hence the term 'colour centre'[2]. It is in some of these alkali-halide hosts that the laser active colour centres are found, although there have also been reports of laser oscillation from colour centres in diamond[3] and calcium oxide[4]. The alkali-halides have a large forbidden energy gap of the order of 10 eV between conduction and valence band so that they are transparent in the absence of colour-centre defects. Melting points of less than 1000°C enable large, single crystals of high optical quality to be grown relatively easily[1]. Nearly all alkali-halides have a face-centred-cubic lattice structure where each ion is surrounded by six nearest neighbours of opposite charge[1].

The simplest colour centre is the F-centre which consists of a single electron bound to the effective positive charge of an anion vacancy. Although not laser active itself, the F-centre provides a useful starting point for understanding the spectroscopy of colour centres in general, and in particular, the physics of the more complicated laser active colour centres. The F-centre can be modelled in terms of a simple three-dimensional square well potential

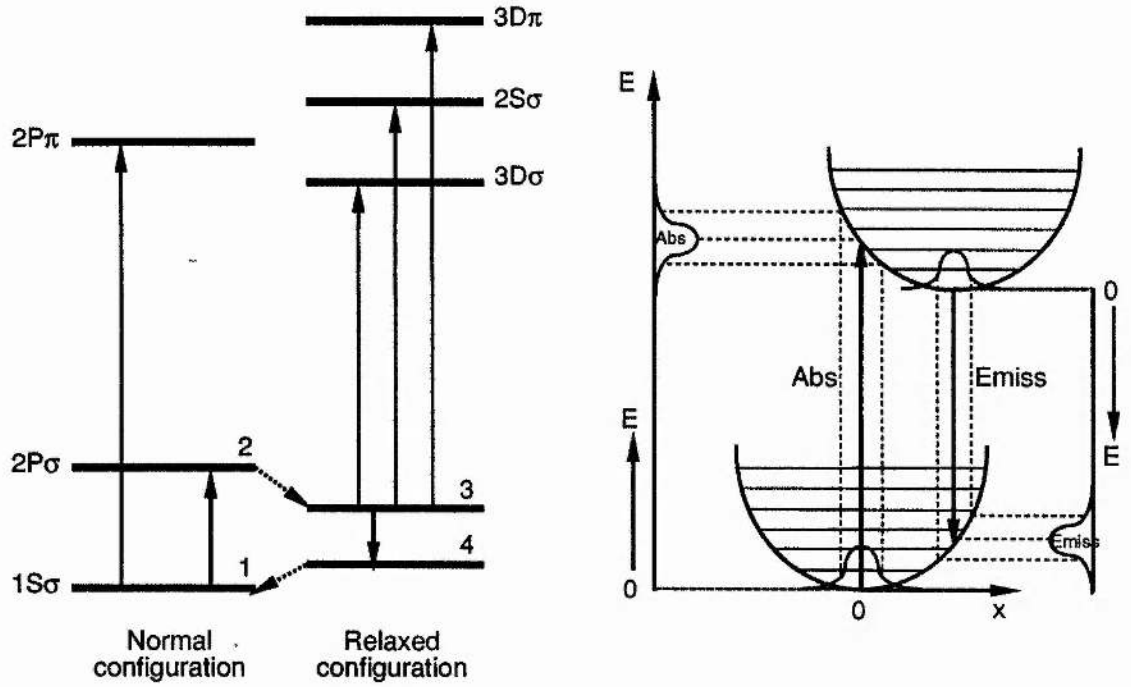

Figure 2.1. Energy level diagram and configuration-coordinate diagram for the F_2^+ colour centre in LiF.

extending over the range of the vacancy together with a connecting Coulomb potential in the region beyond, which increases towards the conduction band[6].

The colour centre responsible for laser action in the LiF laser studied in this thesis was the F_2^+ type. This consists of two adjacent anion vacancies lying along the <110> direction in the crystal lattice and sharing a single trapped electron[5]. This can be modelled as a hydrogenic molecular ion (H_2^+) embedded in an infinite dielectric medium of dielectric constant k - the dielectric constant of the host crystal[6,7]. Provided the interactions with the phonon field of the crystal lattice are taken into account, this model is quite successful in explaining the observed absorption and emission spectra. The colour centre will be influenced by the local crystal field in which it is situated and its equilibrium position will therefore be partly determined by its electronic charge distribution which is in turn dependent on the electronic energy state occupied. The result is a displacement of the equilibrium position after the centre is excited, which can be illustrated using a configuration coordinate diagram. The Stokes shift is just

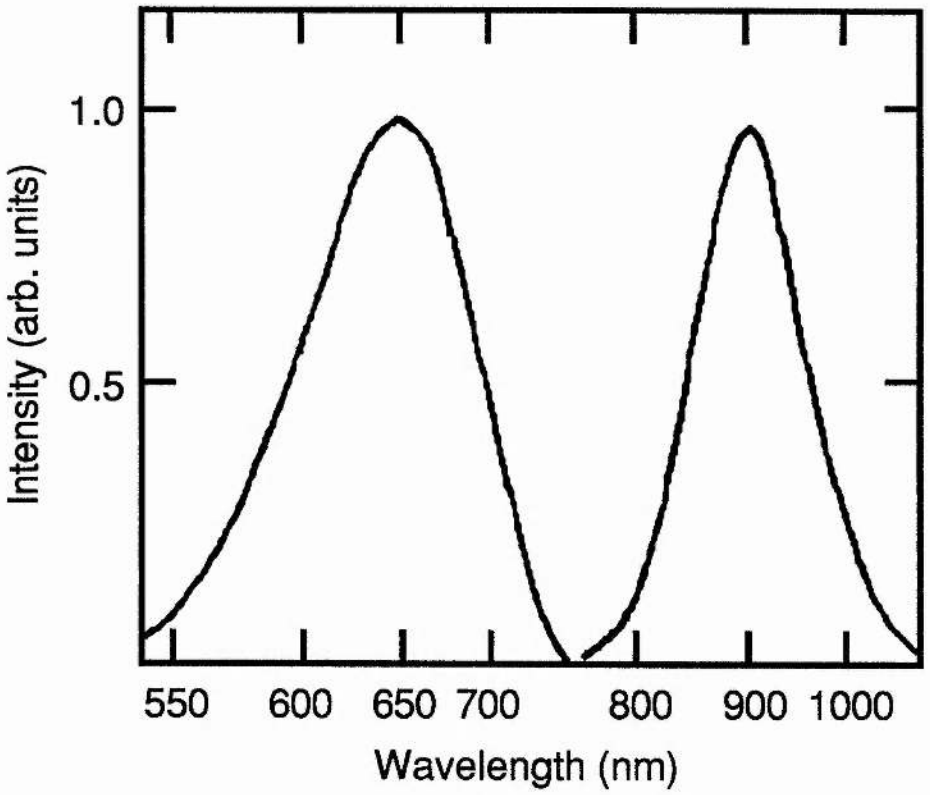

Figure 2.2. Absorption and emission spectra for the F_2^+ colour centre in LiF. (Taken from reference 8.)

large enough that the resulting broad emission and absorption bands do not overlap. The energy levels[2] and configuration-coordinate diagram[8] for the F_2^+ colour centre are shown in figure 2.1. The centre shows two strong transitions: the $1s_\sigma$ - $2p_\sigma$ in the infra-red (having an oscillator strength of ~0.2) and the $1s_\sigma$ - $2p_\pi$ transition in the visible (with an oscillator strength of ~0.5). The visible transition is not useful for laser action as it is strongly quenched by non-radiative transitions to the $2p_\sigma$ level at temperatures above 50 K. Figure 2.2 illustrates the absorption and emission spectra associated with the infra-red transition of the F_2^+ centre in LiF[8]. Note that the absorption is well suited to optical pumping with the 647 and 676 nm lines of a krypton-ion laser. Generally, there is a strong scaling of the transition energies in these colour centres with the dielectric constant of the host, and as a result the wavelength range of lasers based on F_2^+ centres covers 0.8 - 2.2 μm.

The laser cycle can be described as follows. Firstly, absorption of the pump radiation excites the colour centres into the excited state as illustrated by transition 1 in figure 2.1. Configurational relaxation to the upper laser level follows with the emission of phonons to the crystal lattice on a timescale of ~10^{-13} s. This is represented by transition 2 in the figure. Optical emission follows, ideally by stimulated emission in the presence of the laser field, back to the lower electronic state, as shown in the diagram by transition 3. Finally, configurational relaxation again occurs back to the ground state with a further emission of phonons. The configurational relaxations occur so fast, relative to the optical absorption/emission processes, that virtually all the excited centres end up in the upper laser level where they can contribute to laser action. Also, following photon emission, the lower laser level is de-populated quickly so that the population inversion is not reduced. Thus, an almost ideal four-level laser transition results. Some of the relevant properties of the F_2^+ centre in LiF are given in Table 2.1.

The F_2^+ centre has a number of properties that make it a potentially excellent laser material[2]. The absorption and emission cross-sections are relatively large with σ ~10^{-16} cm^2, allowing efficient absorption of the pump radiation and large single-pass gains in millimetre thick crystals having only modest centre concentrations (~3×10^{17} cm^{-3}). The quantum

Property	Value
λ_{abs} (pk)	645 nm
λ_{emis} (pk)	910 nm
$\Delta\lambda_{emis}$	0.2 eV
centre orientation	<110>
τ_{rad}	29 ns
σ	1×10^{-16} cm^2
n	1.39
η	~1

Table 2.1. Some properties of the F_2^+ centre in LiF.

efficiency of the transition is 100% and is independent of the temperature allowing for low laser thresholds. Higher lying excited states are sufficiently distant that there is little possibility of self-absorption within the laser tuning band. The absorption and emission bands are homogeneously broadened so that all the centres can contribute energy to a given laser mode and will be equally well excited by the given pump laser wavelength within the absorption band. Since the absorption and emission bands do not overlap the laser light is not reabsorbed by centres in the ground state.

In summary, the F_2^+ centre can be characterised as follows: the absorption and emission process is homogeneous (phonon broadened). A Stokes shift results due to the energy lost to the phonon field, so that the absorption band is at shorter wavelengths than the emission band and the two do not overlap. Finally, the configurational relaxation occurs so fast that an almost ideal four-level laser transition results.

2.3 Production of Colour-centre Crystals

Colour centres are most frequently created in alkali-halide crystals using one of three techniques. Additive colouration[9] occurs when the alkali-halide is heated to a temperature which is 50 - 100°C below its melting point, in the metal (or halogen vapour) atmosphere of its constituent atoms. This leads to a change of stoichiometry of the crystal where the opposite constituent to that in the vapour atmosphere diffuses out of the crystal leaving an excess of the other. The resulting anion vacancies form F-centres. This method of colouration is preferred because it produces long-lived colour centres - to destroy them would require the removal of the excess ions created during the colouration.

Electrolytic colouration[10] occurs when the alkali-halide crystal is subjected to an electric field of several hundred volts per centimetre at a temperature which is again just below its melting point. The temperature must be high enough so that sufficient thermal vacancies are created to permit electrolytic conduction. During this process, an F-centre cloud appears at the pointed cathode and slowly spreads through the crystal.

Colouration by radiation damage[11] is by far the most versatile method of creating colour centres in alkali-halides. It is also the most practical method for producing F_2^+ colour centres. High energy electron beams are the preferred form of ionizing radiation because the available intensities allow short exposure times and the penetration depth is large enough to permit millimetre thick crystals to be processed. The incident electrons can produce a large number of defects of various kinds, the stability of which depends on the purity of the crystal, the temperature, the radiation dose and the optical conditions prevalent at the time. Under the conditions used in colour-centre crystal production, the radiation pulse leads to the formation of F-centres and empty anion vacancies. The crystals also contain a high concentration of deep electron traps, formed as a result of radiation products, or which were already present in the form of intentional dopants. Upon warming the crystal up to room temperature, the vacancies become highly mobile and are eventually trapped by F-centres to complete the F_2^+ centre formation process. In practice, suitably polished alkali-halide crystals are placed in a sealed aluminium foil wrapping and irradiated with an electron beam having an energy in the 1 - 1.5 MeV range. The crystals are cooled to <-100°C in a stream of dry nitrogen gas or liquid nitrogen during the irradiation process. Typically electron currents of 2 - 10 $\mu A\ cm^{-2}$ are used and exposure times range from 5 - 20 minutes.

A laser medium based on the F_2^+ colour centre suffers from two serious drawbacks. Firstly, it exhibits a slow fading with extended operation and secondly, the crystal must always be maintained at cryogenic temperatures. The fading occurs because the intense optical fields of the pump laser can cause a multiphoton excitation into the $2p_\pi$ state from where the colour centre decays via a non-radiative transition and accompanying reorientation into one of five other possible directions in the lattice. This reduces the efficiency of excitation of the centres by the polarised pump source, but more importantly, after many such reorientations the centre has taken a random walk through the crystal lattice. If, during this walk, the centre encounters another colour centre or impurity ion, it may react with it to form another non-laser active complex. Migration of the colour centre can also result if there is sufficient optical or

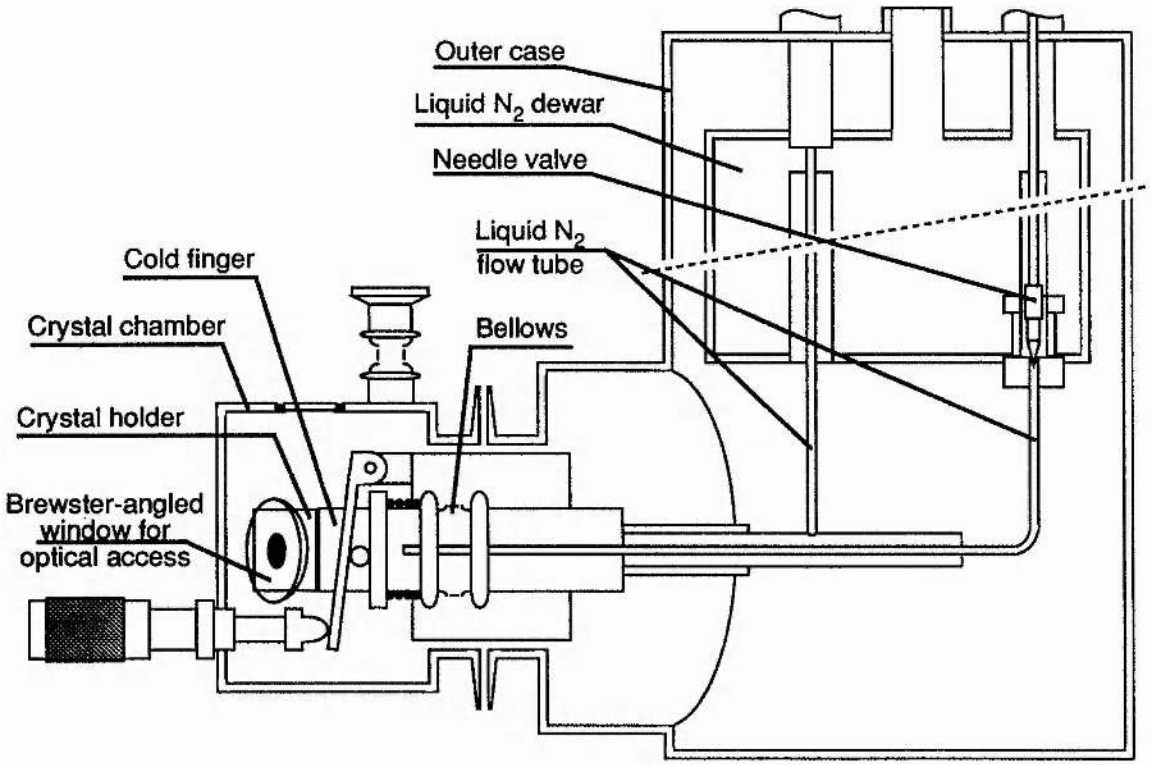

Figure 2.3. Schematic diagram of the colour-centre laser cryostat.

thermal excitation to cause a neighbouring anion to tunnel into one of the vacancies. Similarly, an electron may tunnel into the F_2^+ centre from a neighbouring electron trap transforming it into an F_2 centre.

Cold storage can minimise the occurrences of these detrimental processes. It also minimises the annihilation of the colour centres with other radiation by-products such as interstitials, which also take place at elevated temperatures through thermal motion. Provided care is taken to prevent these thermal and optical instabilities, lasers based on the F_2^+ colour centre can be a practical reality.

2.4 Design Considerations for Colour-centre Lasers

The most significant problem to be overcome when designing a colour-centre laser system is the requirement that the crystal be kept at cryogenic temperatures. This can only be achieved by enclosing the laser material in a liquid nitrogen cooled cryostat. The experiments that will be described in this chapter were performed using the laser cryostat shown schematically in

figure 2.3. This design allowed maximum flexibility for cavity configuration because only the colour centre crystal was housed within the evacuated chamber. This was in contrast to commercially available systems in which the focusing optics were also housed within the cryostat[12,13], so that only one cavity configuration was available and which provided only limited adjustment to the cavity alignment once the crystal was loaded.

The cryostat shown in the figure had a number of important features. Liquid nitrogen flowed directly to the back of the crystal mounting block which allowed efficient removal of heat from the colour centre crystal and provided rapid and accurate control of the crystal temperature. This temperature could be regulated by varying the flow of nitrogen to the block by means of the needle valve shown. The crystal temperature was monitored using a platinum resistance thermometer housed within the crystal holder. Liquid nitrogen was supplied from a five litre capacity dewar which sat to the rear of and above the crystal chamber. This dewar also had an internal platinum resistance thermometer which acted as a liquid nitrogen level sensor. An electrical heater was installed in the crystal mounting block which allowed rapid warm-up times to be realised once the nitrogen supply had been shut of at the needle valve. This enabled the time required for a crystal change to be cut from more than twelve hours, as was required for previous designs, to just thirty minutes. Separate vacuum chambers for the crystal and main dewar meant that the entire cryostat did not have to be warmed up to room temperature each time a crystal was changed. These two chambers could be linked once the crystal was loaded. The main dewar contained three adsorption pumps which helped to maintain the ultra-high vacuum necessary to provide good thermal isolation.

The colour-centre crystal was housed in its own evacuated chamber as described above. Optical access was provided via. two Brewster-angled windows on either side. The crystal was also mounted at the Brewster angle. A bellows assembly allowed horizontal movement of the crystal position within the cavity when the entire cryostat was under vacuum. The whole assembly was mounted on adjustable feet which allowed vertical positioning of the crystal within the laser cavity.

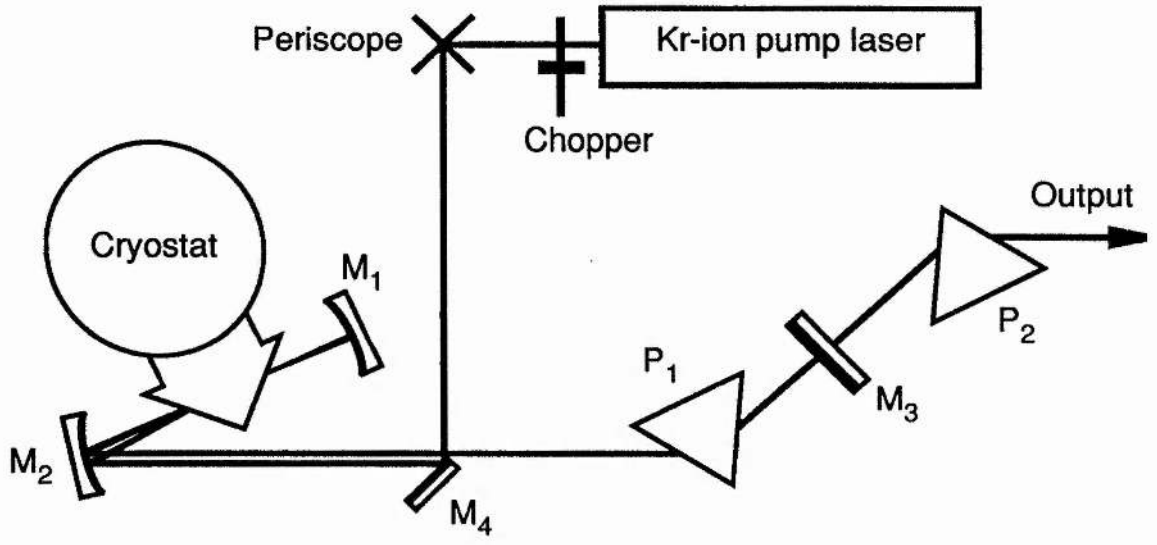

Figure 2.4. Three-mirror cavity configuration for the LiF laser.

To obtain oscillation in colour centre lasers, a population inversion of the order of 10^{16} cm^{-3}[11] is required. This condition can easily be met using optical pumping schemes. The required pump intensity (in the 1 kW cm^{-2} region[11]) can readily be achieved if a three-mirror cavity such as the type previously designed for dye lasers is used. In such a scheme, illustrated in figure 2.4, the laser gain medium is placed at the position of the cavity beam waist and the pump laser beam is also focused into the same region. However, unlike the dye laser equivalent, a separate pump focusing mirror cannot be used because even a small angle between the cavity and pump modes (as little as 5°) results in less than 20% overlap of the two beams in a 2 mm thick crystal. Rather, collinear or quasi-collinear pumping schemes are used. A typical 2 mm thick colour-centre crystal absorbs ~80% of the pump radiation. The cavity losses are minimised at the laser wavelength by orienting all the intracavity transmissive elements at the Brewster angle. In this colour-centre laser the cryostat windows and the output coupler were wedged (approximately 40') to minimise etalon effects within the cavity.

The laser cavity was astigmatically compensated as described by Kogelnik et. al.[14]. The refractive indices for LiF and for the fused quartz (Suprasil) windows were taken as 1.39 and 1.45 respectively. The window material was chosen because of its high transmission in the near-infrared spectral region. The windows and the crystal both had a thickness of 2 mm.

Using the notation of reference 14, with $R_1 = 5$ cm, $R_2 = 10$ cm and $R_3 = \infty$, the angle for astigmatic compensation was calculated to be $2\theta = 26°$.

2.5 Characterisation of the cw LiF:F_2^+ Colour-centre Laser

The three-mirror cavity used for the cw colour centre laser was similar to that illustrated in figure 2.4. This cavity had an intracavity fused silica prism, P_1, placed before the output coupler, M_3, to restrict the laser bandwidth and to provide a means of tuning the laser. A further extracavity prism, P_2, was placed on the other side of the output coupler to recollimate the spectrally dispersed output. Alternatively, a dielectric tuning wedge was used. This had the advantage of providing an output which was not spectrally dispersed, but it was not designed for the wavelength range covered by this laser and resulted in a higher intracavity loss which compromised performance.

The pump beam from the Kr-ion laser was directed into the cavity via the periscope and the steering mirror M_4. The periscope was used to rotate the plane of polarisation of the pump from vertical to horizontal in order to match the lowest loss polarisation of the colour centre cavity. It also lowered the optical height of the pump beam to 12.5 cm above the table top which matched the height of the optical axis of the LiF laser. The colour-centre cavity mirrors, M_1 and M_2, had broadband multilayer dielectric coatings and were highly reflecting over the 820 - 970 nm wavelength range, with radii of curvature of 5 cm and 10 cm respectively. The mirror M_2, was of a multistack construction so that it was also highly reflecting over the 630 - 750 nm range. In this way it could be used as a pump beam focusing mirror, providing an almost collinear pumping arrangement. Since dielectric mirrors can be a source of dispersion for ultrashort pulses, the shorter wavelength stack was deposited on the bottom. Three output couplers were available having transmissions of approximately 3%, 10% and 20% over a similar near-infrared wavelength range. The 20% transmitting mirror was concave with a radius of curvature of ~1.6 m while the other optics were plane.

The pump laser was a Spectra-Physics 171 krypton-ion system which was specified to give 4.6 W when oscillating on the 647.1 and 676.4 nm lines. However, due to an ageing

plasma tube the maximum output was restricted to 2.8 W during the course of this work. The laser construction was similar to that of the argon-ion laser, but the critical dependence of the output power on the plasma pressure required the use of a gas pressure control which could pump gas into and out of the tube to maintain its pressure at predetermined optimised values. The pump beam was chopped with a 1:10 duty cycle in order to prevent rapid crystal fading due to thermal ionization of electron traps caused by local heating.

The LiF crystals used were obtained from British Drug Houses (BDH) or Rank-Hilger (RaHi) and coloured by electron bombardment. They had dimensions of 10 x 10 x 2 mm and were cleaved and polished along the <100> crystal axis. Colouration was carried out at a temperature of 77 K, using 1.5 MeV electrons produced by a van de Graaf accelerator. The exposure time was three minutes and five seconds with a total electron current of 2.6 μA and a current density of 0.5 μA cm^{-2}. The crystals were subsequently stored at 77 K until required. Before loading into the cryostat, the crystals were brought up to room temperature. They were removed from the sealed aluminium foil packing and wrapped in indium foil, which provided a good thermal contact with the crystal holder, before being placed into the crystal chamber. Good thermal contact between the crystal holder and the cold finger was ensured by using cryogenic grease on the dove-tail mount. The chamber was then evacuated and cooled. The whole process, which took about ten minutes, allowed sufficient annealing time at room temperature for the frozen F-centres and anion vacancies to migrate within the crystal and combine to form the required F_2^+ centres. This process was accompanied by a gradual dark blue colouring of the crystal.

With the colour-centre crystal loaded, the cryostat was suitably positioned on the optical table, taking care to ensure that the folding angle was correct for astigmatic compensation. The feet were adjusted so that the cryostat was level and the centre of the aperture in the crystal holder was 12.5 cm above the table top. With the Kr^+ laser power reduced to a safe level, the periscope and steering mirror, M_4, were adjusted so that the pump beam was also level at 12.5 cm. The focusing mirror, M_2, was placed approximately in position, 5 cm from the

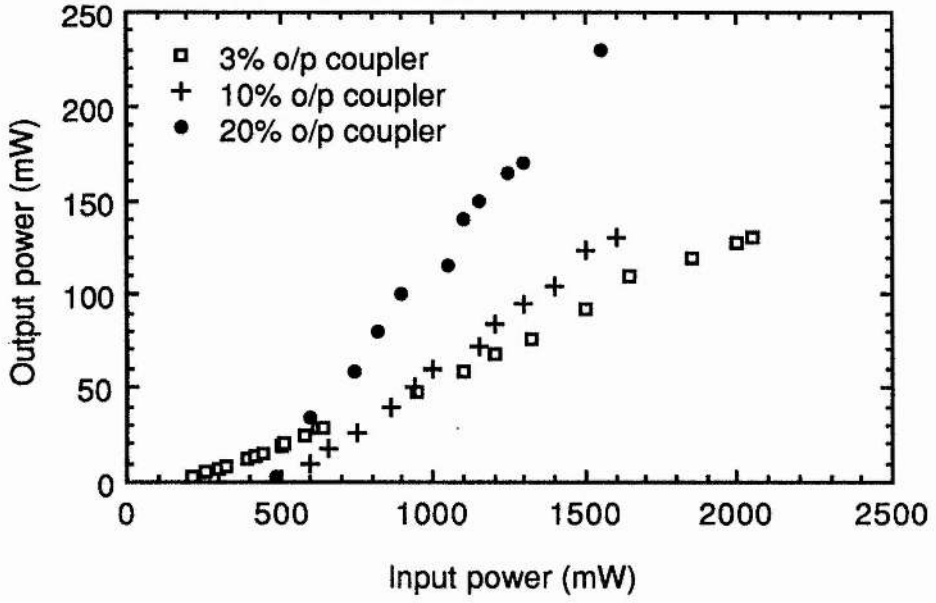

Figure 2.5. Plot showing cw LiF:F_2^+ laser performance for three different output couplers.

crystal, and the pump beam directed through the cryostat so that it also passed through the crystal. The mirror, M_1, could then be positioned using the pump as a guide. The cavity focusing then had to be optimised. The pump power was increased to maximum and with M_1 blocked using a piece of card, the fluorescence collected from the crystal by M_2 was observed at infinity (ie. the other end of the optical table), using an infra-red viewer (FJW Industries Find-r-Scope). The distance of M_2 from the crystal was adjusted to obtain a collimated beam. Next M_1 was unblocked and the procedure was repeated for the fluorescence fed back through the crystal from this mirror. With M_1 slightly misaligned the two fluorescence spots were distinctly visible. With the two spots overlapped the output coupler, M_3, was positioned on the table and oriented so that the fluorescence was reflected back along the cavity axis. By placing a piece of white card in front of the output coupler it was possible to observe the fluorescence transmitted by this mirror after one and many cavity round trips. By overlapping these spots using the output coupler and making small adjustments to the folding mirrors the laser could be aligned and threshold reached. Once laser oscillation had been achieved, the

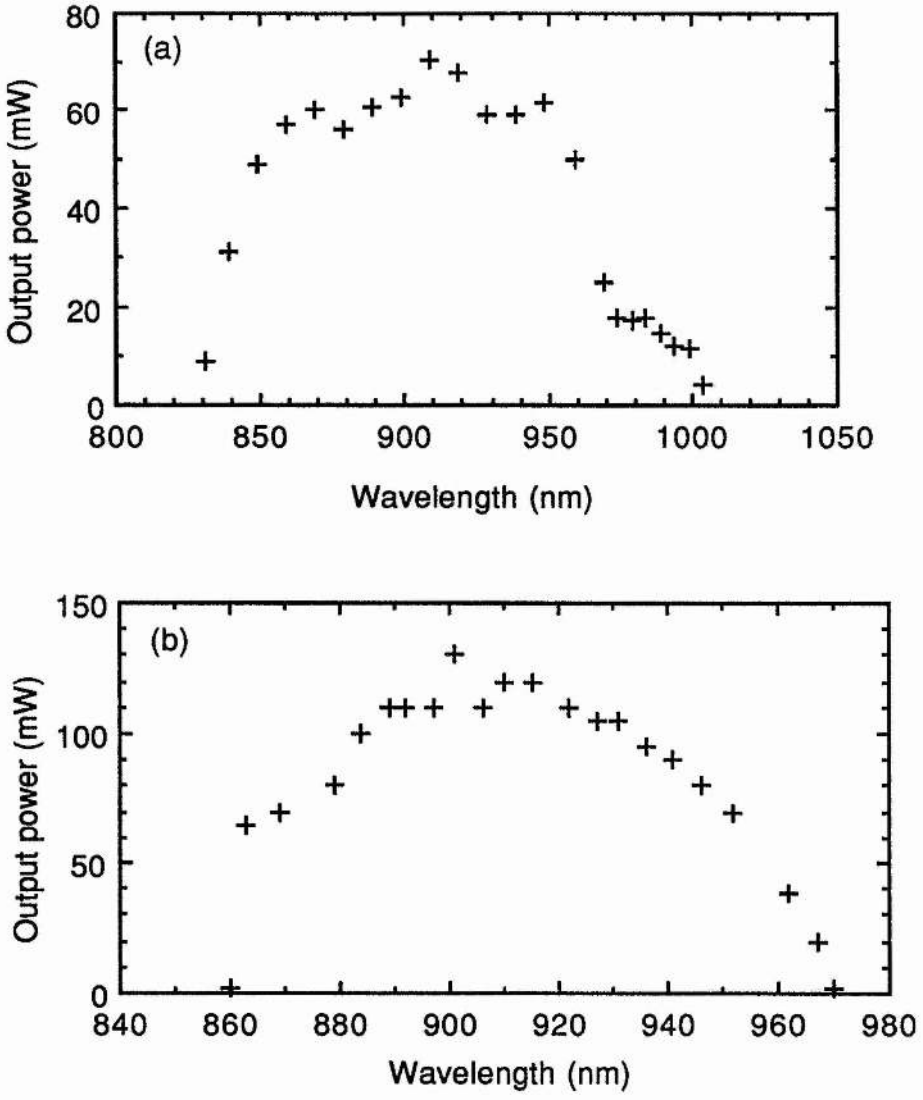

Figure 2.6. Tuning curves for the LiF:F_2^+ laser with (a) a 3% output coupler and (b) a 20% output coupler.

alignment was optimised for maximum power output using a photodiode, amplifier and oscilloscope.

With the 3% transmitting output coupler the minimum laser threshold was ~140 mW and the average output power at threshold was ~40 mW. The average output power was estimated by multiplying the measured output power by the duty cycle of the chopper - 1:10 in this case. These measurements were taken using a Photon Control Model 11A power meter. For a pump

power of 1.5 W the laser was tunable from 817 nm to 1000 nm. The upper and lower ends of this tuning range were limited by the reflectivity of the double stack focusing mirror, M_2. In figure 2.5 a graph showing more typical data for the variation of output power with input power is presented for the 3%, 10% and 20% transmitting output couplers. The graph in figure 2.6 (a) illustrates the laser's tuning range for the 3% output coupler and 1.5 W pump power, while figure 2.6 (b) shows the tuning range for the 20% transmitting mirror. In this latter case the laser tuned from 860 nm to 970 nm.

It is interesting to note that the threshold for the 20% output coupler was lower than that for the 10% mirror. This would not normally be expected, but in this case the 20% transmitting mirror was concave with R = 1.6 m which resulted in better mode matching in the gain and hence a lower threshold. It can be shown that, provided the losses are small, the output intensity of a laser oscillator is given by the following expression[18]

$$I_{out} = \left[\frac{P_p}{P_{th}} - 1\right]\frac{\delta_e I_{sat}}{2} \tag{2.1}$$

where P_p is the pump power, P_{th} is the threshold pump power, δ_e is the exponential output coupling factor ($\delta_e \approx T$ for $\delta_e \ll 1$ where T is the transmission of the output coupler) and I_{sat} is the saturation intensity of the gain medium. If we assume that the gain recovery time is approximately equal to the radiating lifetime, then we can simplify the equation and write

$$P_{out} \approx \left[P_p - P_{th}\right]\frac{\hbar\omega_a}{\hbar\omega_p}\frac{T}{T+L} \tag{2.2}$$

where T + L is the total cavity losses and ω_p and ω_a are the pump and laser frequencies respectively. If we also assume a pump wavelength of 647 nm, with 80% absorption and apply this equation to the data in figure 2.5 we can calculate L for the different laser configurations. The results suggest that L = 18% for the 3% output coupler and about 30% for the laser configurations with the 10% and 20% output couplers. These large values are probably due to the fact that the results were taken using relatively old crystals which were

also quite lossy. The predicted threshold for the 3% case was 215 mW. In fact, thresholds as low as 140 mW have been measured for new crystals.

The threshold pump power density required for laser oscillation can also be predicted using basic theory. It is given approximately by the following expression for a homogeneous laser[15]

$$\left(\frac{P_p}{V}\right)_{th} \approx \frac{8\pi^2}{\eta_p} \frac{N_{2th}}{\Delta N_{th}} \frac{\omega_p}{\omega_a} \frac{\gamma_2}{\gamma_{rad}} \frac{\hbar \Delta\omega}{\lambda^3} \frac{c\,\delta_c}{n\,p_m} \qquad (2.3)$$

where N_{2th} is the population of the upper laser level at threshold, ΔN_{th} is the population inversion at threshold, $\eta_p\gamma_{rad}/\gamma_2$ is the fluorescence quantum efficiency, $\Delta\omega$ is the gain linewidth and δ_c=T+L is the total cavity loss. If we assume a pump beam waist of ~20 μm and 80% absorption of the pump radiation, the calculated threshold pump power is ~250 mW if we use the value for δ_c calculated above. This is reasonably close to the 230 mW threshold observed experimentally. For smaller losses of $\lesssim$ 10%, say, which would be expected with a new crystal, the calculated threshold is $\lesssim$ 150 mW which also agrees reasonably well with the experimentally measured values for such crystals[11,16].

The fading behaviour of the colour-centre crystals was also studied by shutting off the nitrogen flow to the cold finger and monitoring the crystal temperature and output power as a function of time for a constant incident pump power. The results are presented graphically in figure 2.7 for a cavity having a 20% output coupler. It is evident that the output power decreased steadily from the time the nitrogen was shut off until laser oscillation ceased altogether after approximately 135 minutes. The results presented were for an unchopped pump beam, but the effect of chopping was merely to decrease the rate of decay and slow down the eventual destruction of the laser active colour centres. These effects can be explained by the thermal ionization of electron traps together with centre migration and annihilation that can occur at higher temperatures as discussed previously. Thus, as the crystal heated up, the laser active F_2^+ centres were eventually destroyed, reducing the output power until insufficient

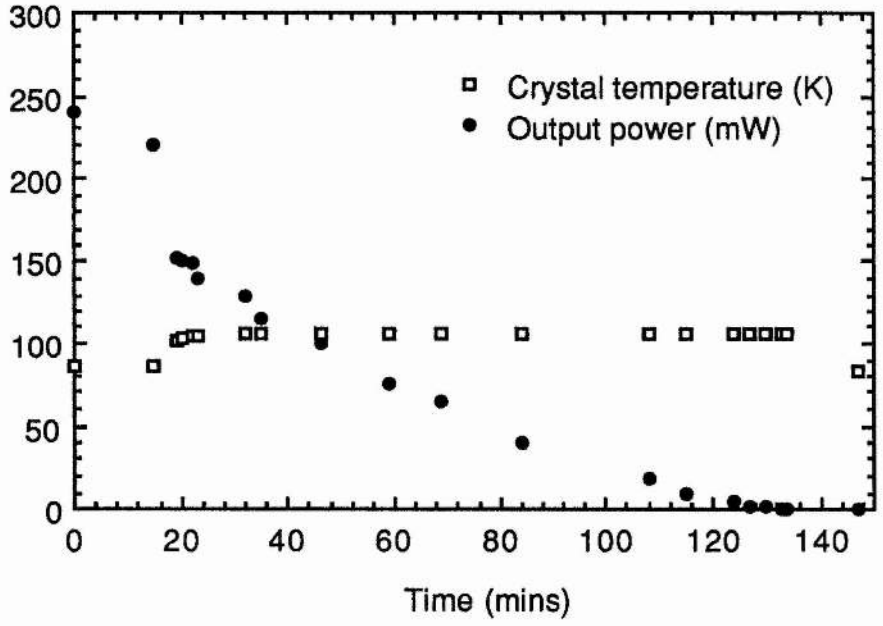

Figure 2.7. Crystal temperature (squares) and average laser output power (circles) as a function of time. (No liquid nitrogen flow to coldfinger.)

gain remained for laser oscillation. Typically, the cooled crystals had useful lifetimes of ~200 hrs, but obviously low pump powers and output coupling (higher intracavity powers and hence effectively shorter lifetimes for the relaxed excited state) would extend the crystal life.

2.6 The Passively Modelocked LiF:F_2^+ Laser

Passive modelocking[15] has been mentioned briefly in chapter 1. In this section a passively modelocked cw LiF colour-centre laser will be discussed[17]. Passive saturable absorber modelocking provides a convenient technique for the generation of ultrashort pulses and has enabled the shortest pulses to be generated from dye laser systems. In the experiments described here, the saturable absorber used was an organic dye known as 1-diethyl-2, 13-acetoxy-1, 2-quintotetracarbocyanine perchlorate, or DaQTeC for short[18]. Since dyes such as these have absorption recovery times of the order of several nanoseconds, and the

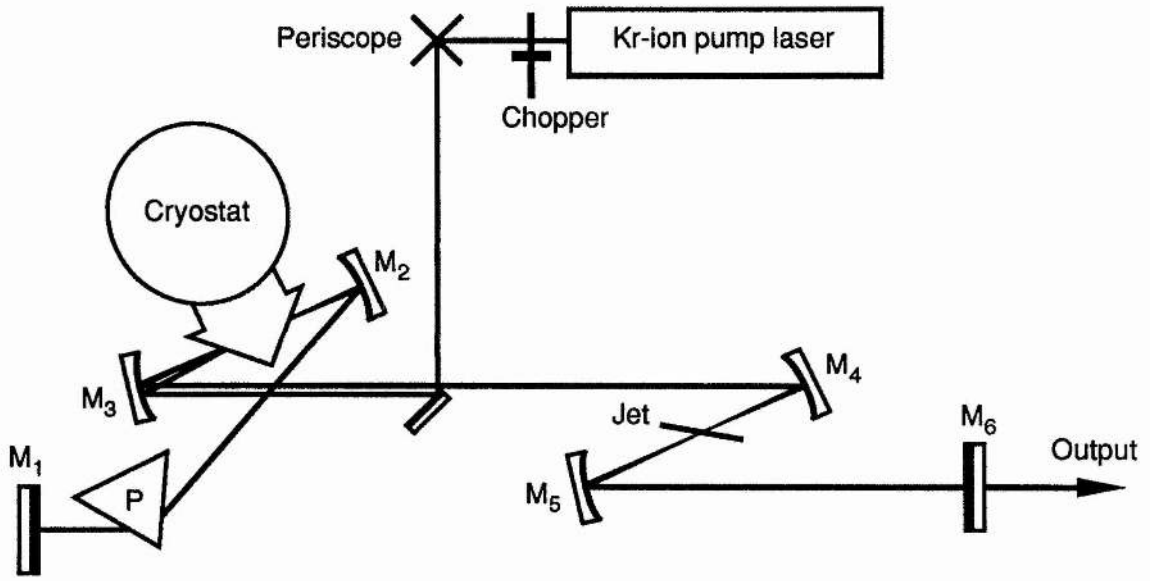

Figure 2.8. Schematic diagram of the six-mirror cavity used for the passively modelocked LiF:F_2^+ laser.

experimentally measured pulses had durations of a few hundred femtoseconds, it can be concluded that the dye was operating as a slow saturable absorber[19,20].

Initially a linear, six-mirror cavity configuration having a second folded section was used as illustrated in figure 2.8. Mirrors, M_2 and M_3, had 10 cm radii of curvature while the mirrors forming the second folded section, M_4 and M_5, both had 5 cm radii of curvature. The laser oscillating bandwidth was controlled by means of the prism, P, and the output coupler, M_6, transmitted 3% of the intracavity intensity. The cavity period was ~12 ns. A fast flowing jet of ethelyne glycol (~20 ms^{-1}) having an estimated thickness of 65 μm was positioned at the Brewster angle near the waist of the second folded section. The folding angle was kept as small as possible to minimise astigmatism. The dye was dissolved in a small quantity of ethanol before being added to the ethelyne glycol solvent in a container which was immersed in a temperature controlled water bath. Typical dye concentrations of ~10^{-5} mol/l were used. The measured dependence of the small signal absorption with wavelength for a ~10^{-5} mol/l solution of DaQTeC is presented in figure 2.9.

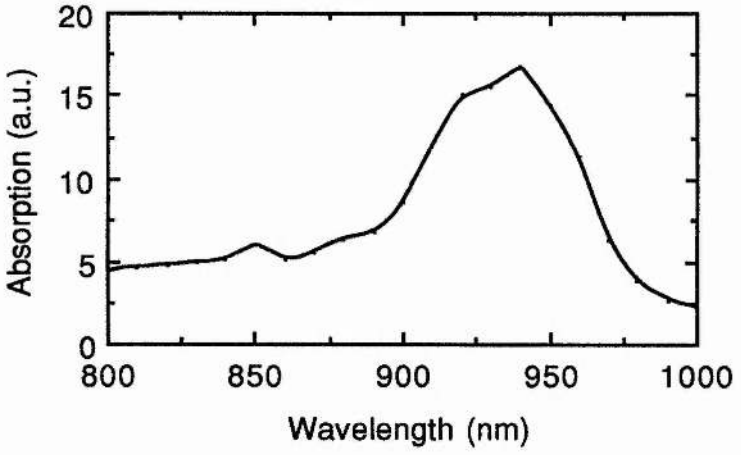

Figure 2.9. Measured small signal absorption for saturable absorber DaQTeC.

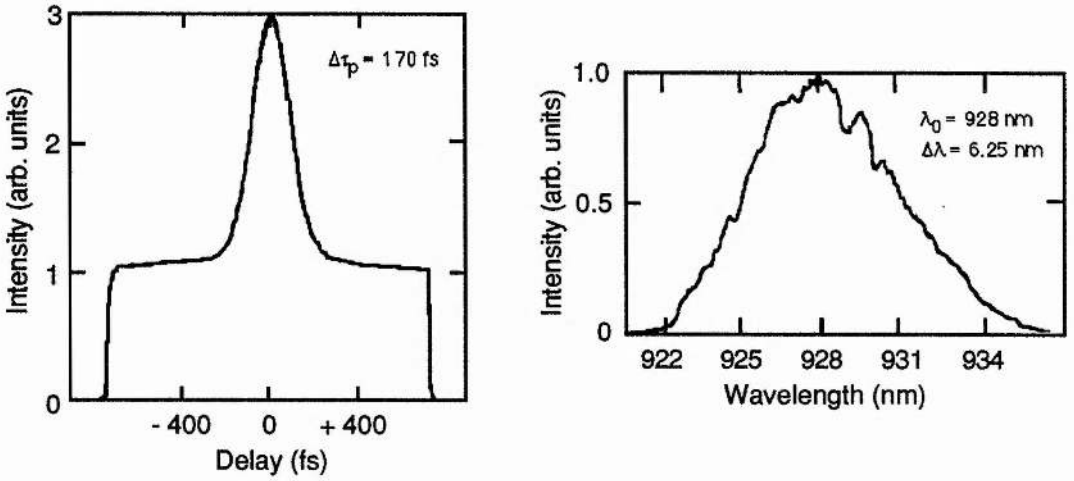

Figure 2.10. Intensity autocorrelation trace and associated pulse spectrum for the passively modelocked colour-centre laser.

In this configuration the laser threshold was approximately 2 W. The pump beam was chopped with a duty cycle of 1:10 and for a pump power of 2.8 W the average output power was ~10 mW with the saturable absorber jet flowing. Modelocked operation could be achieved for wavelengths ranging from 924 nm to 946 nm with the shortest pulses being generated around 930 nm. The pulse durations were determined using a second harmonic generation collinear autocorrelator similar to that described in chapter 1. The stability of the

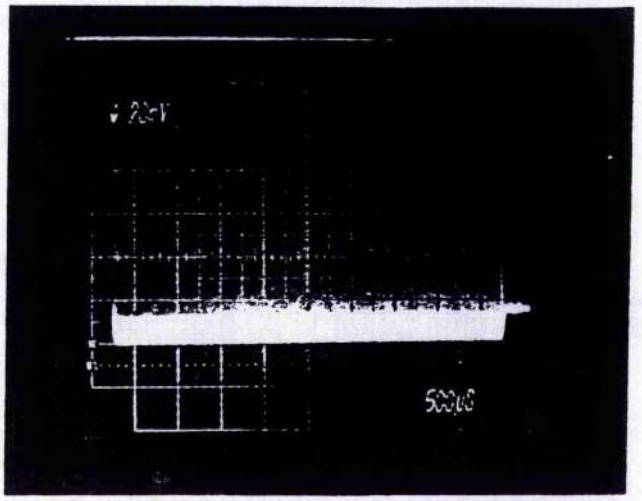

Figure 2.11. Oscillogram showing the modelocked laser output. The duration of the pulse train corresponds to the pump beam chopping window.

modelocked output was monitored using a fast photodiode (Telefunken BPW 28) and an oscilloscope having a bandwidth of 400 MHz. The modelocked spectrum was recorded with a 25 cm monochromator (Applied Photophysics f/3.4) and linear CCD array.

An intensity autocorrelation trace for the shortest pulses, having durations of 170 fs if $sech^2$ intensity profiles are assumed, is shown in figure 2.10, together with the associated pulse spectrum. The measured spectral bandwidth of 6.25 nm implied a duration-bandwidth product for the modelocked pulses of $\Delta\tau_p\Delta\nu \approx 0.38$. This was not much larger than the theoretical limit of 0.32 for transform limited pulses, but nevertheless suggested that a small amount of frequency chirp was present. The oscillogram in figure 2.11 shows the stability of the modelocked output where the pulse train lasts for the duration of the open window in the chopped pump beam. The shortest pulses were generated for dye concentrations of 6 - 10 x 10^{-5} mol/l. The plot in figure 2.12 illustrates the variation of pulse duration with dye concentration taken at ~930 nm.

It was expected that a ring cavity configuration might improve both the pulse duration and stability of the modelocked laser by exploiting the technique of colliding pulse modelocking (CPM)[21], which has been extensively used in cw modelocked dye lasers. The basic principle

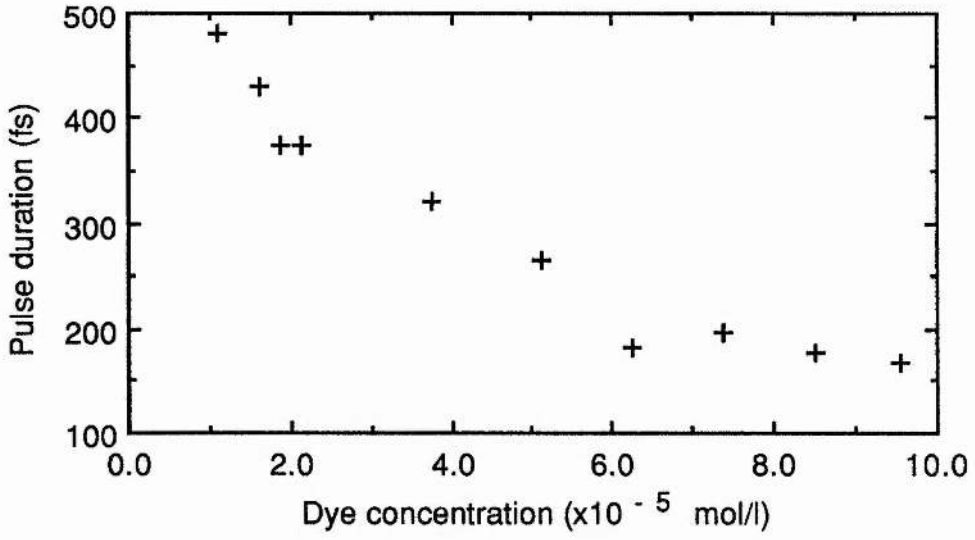

Figure 2.12. Plot showing the variation of the modelocked pulse duration with wavelength for the passively modelocked LiF laser.

involved in the CPM laser is that the modelocked pulses 'collide' with one another in the saturable absorber. These overlapping pulses interfere producing a transient standing-wave grating in the optical field, and consequently a transient grating in the population inversion of the absorber molecules. This has the effect of coupling the two pulses together - the envelope of one pulse is diminished by scattering into the oppositely travelling wave and vice versa. In general, it is the ratio of the optical field intensity which saturates the absorber to that which saturates the gain that determines the relative stability and duration of the modelocked output. This was summarised in the so called 'S'-parameter[19], where $S = E_g/E_a = k(A_g\,\sigma_a)/(A_a\,\sigma_g)$, which should be greater than about 2 in order to ensure stable modelocking[19,20]. Here k is the 'collision parameter' and has a value between 1 and 2. (Note that in all the experiments described here the choice of R = 10 cm for the gain, and R = 5 cm for the absorber focusing mirrors helped ensure that $S > 2$.) In the case of CPM, this ratio is increased because both counter-propagating pulses are present in the absorber together, while only one passes through the gain at any time and also because there is an additional enhancement due to the coherent interaction in the absorber.

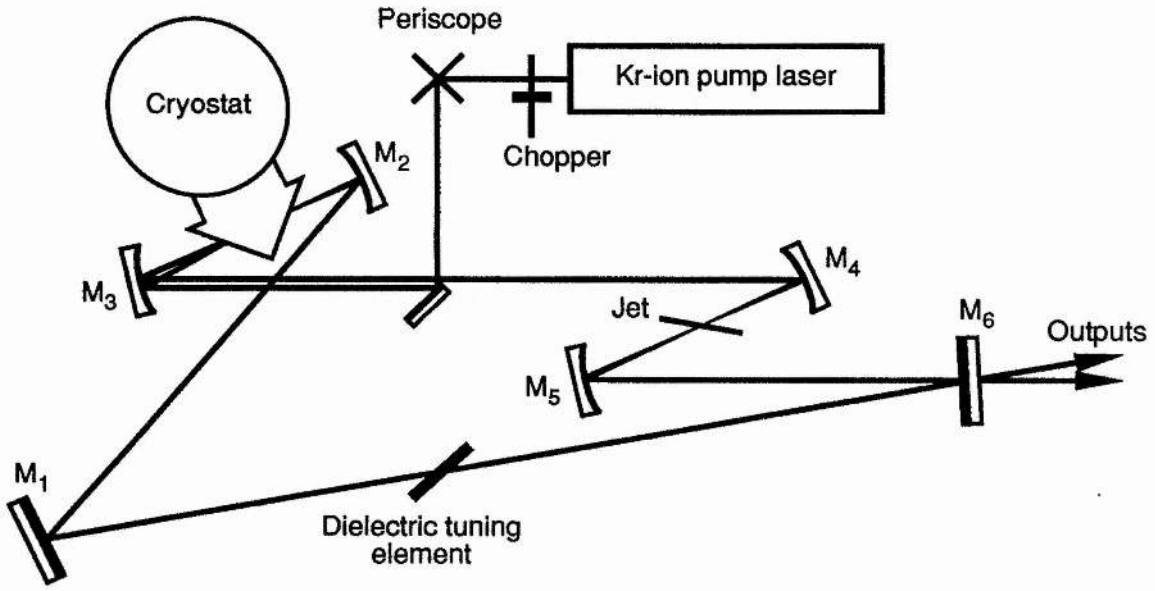

Figure 2.13. Schematic diagram showing the cavity configuration for the LiF CPM laser.

A measure of the efficiency of the modelocking process is given by the 'pulse shortening velocity' (PSV), which is defined as the percentage change in pulse duration per round trip, and is independent, to a large extent, of the pulse shape[22]. To increase the PSV one should: increase S by proper choice of dye for the wavelength range of interest, by making the ratio A_g/A_a as large as possible and by reducing the linear loss and increasing the saturable absorption. The CPM action can lead to an increase of the PSV by a factor of between 7 and 8 and can decrease the pulse duration by a factor of 2 to 3. It is theoretically equivalent to increasing the saturable absorber cross-section.

The ring cavity was constructed by suitably changing the angles of mirrors M_1 and M_6 as illustrated in figure 2.13. The gain and absorber sections were separated by approximately one quarter of the cavity length to ensure that the gain had recovered equally for each of the counter-propagating pulses. This ensured that the pulses colliding in the absorber had approximately equal amplitudes. Pulse synchronism in the absorber is assured because this results in minimum energy loss to the absorber. This is because the maxima of the optical field standing-wave pattern coincides with the minima of the grating induced in the population of

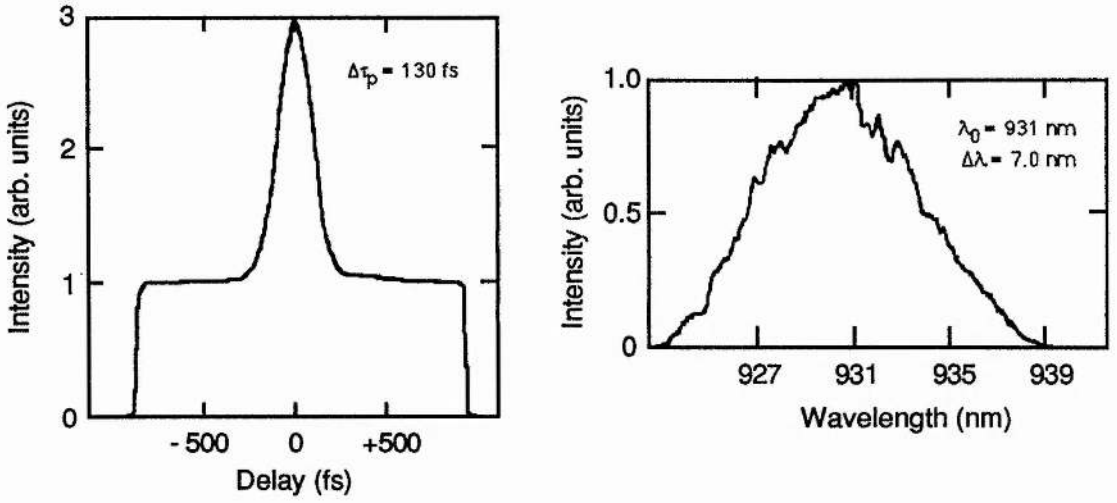

Figure 2.14. Intensity autocorrelation trace and associated pulse spectrum for the CPM colour-centre laser.

the absorber molecules and vice versa. In this configuration the cavity period was increased slightly to ~13 ns. The dye concentration which produced the shortest pulses was between 8 and 10 x 10^{-4} mol/l. The pump power was approximately 2.5 W (chopped with a duty cycle of 1:10) which resulted in an average output power of ~6 mW per beam. Wavelength control was provided using a birefringent filter having a thickness of 0.84 mm. The shortest pulses generated had durations of 130 fs at wavelengths around 930 nm. Intensity autocorrelation and spectral data for such pulses are presented in figure 2.14. The bandwidth of $\Delta\lambda = 7.0$ nm implied a duration-bandwidth product of $\Delta\tau_p\Delta\nu = 0.32$ suggesting that the pulses were free from frequency chirp. The dye concentration was 9.95 x 10^{-4} mol/l. The data plotted in figure 2.15 show how the pulse duration varied with dye concentration for the ring cavity. Tuning curves for the modelocked ring laser are shown in figure 2.16 for three different dye concentrations. It is apparent that the approximate tuning range of this laser covered the 924 - 950 nm spectral region which was similar to that for the linear configuration.

It was possible to obtain unidirectional operation of the ring laser for a certain cavity alignment even in the absence of any additional intra or extra-cavity elements. Interestingly,

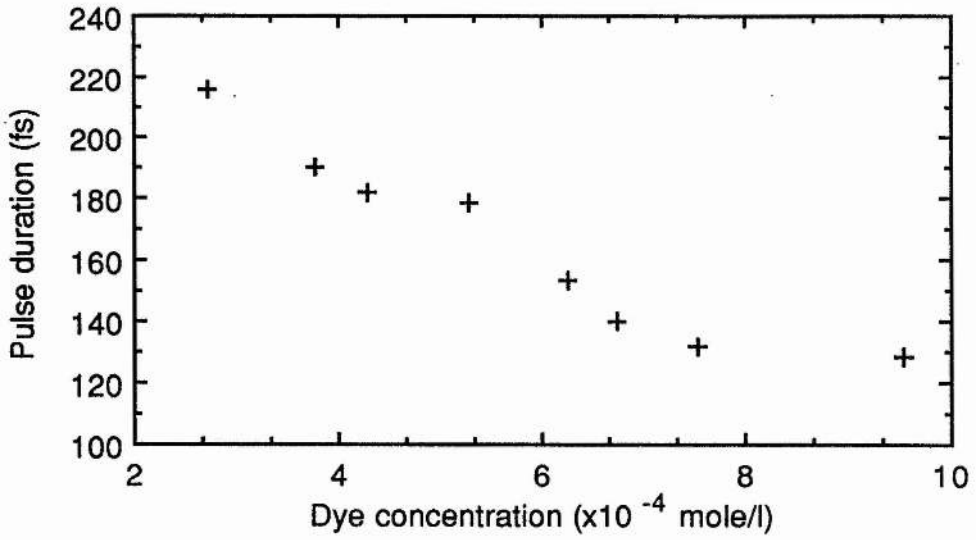

Figure 2.15. Graph showing the variation of the modelocked pulse duration verses saturable absorber dye concentration for the LiF CPM colour-centre laser.

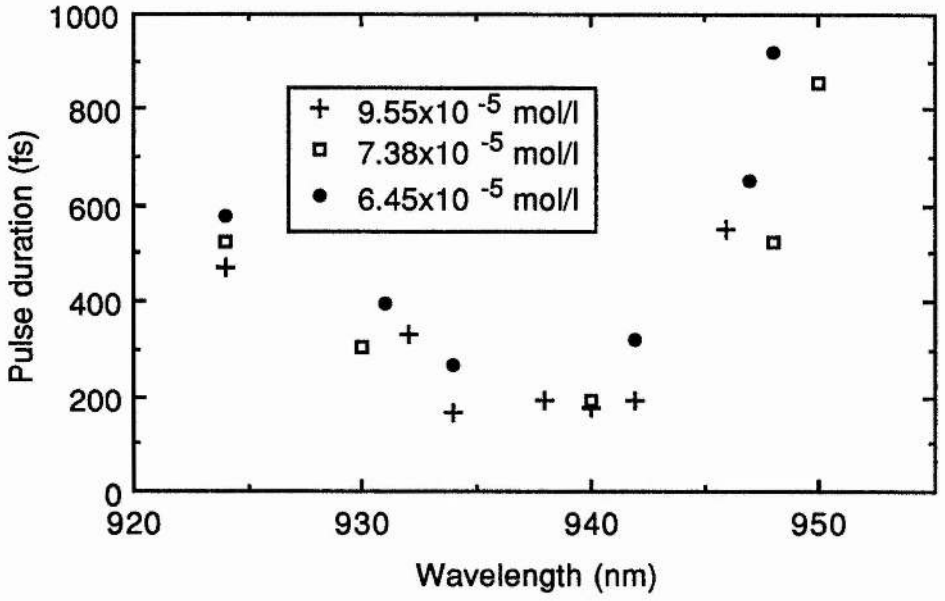

Figure 2.16. Graph showing how the modelocked pulse duration varied with wavelength for three saturable absorber dye concentrations.

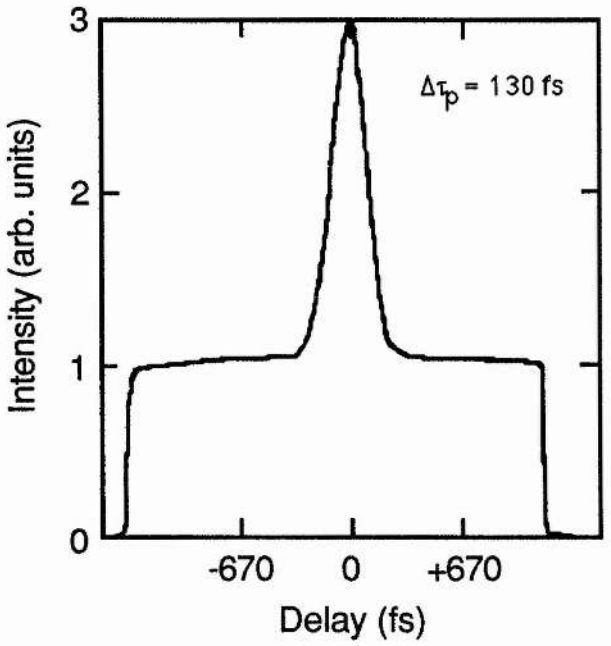

Figure 2.17. Intensity autocorrelation trace of the modelocked pulses from the modelocked unidirectional ring laser.

the pulse durations remained the same as for bi-directional operation, as illustrated by the intensity autocorrelation shown in figure 2.17. This suggested that the CPM mechanism was not contributing to the pulse shortening process. The predicted enhancement in pulse shortening due to the colliding pulses assumes that the pulse widths are long compared with the dye jet thickness[22]. Otherwise the enhanced absorber saturation only occurs over a limited portion of the dye jet. The width of a 130 fs pulse is approximately 40 μm which is already smaller than the 65 μm thick dye jet. It is, therefore, to be expected that the contribution to pulse shortening from the coherent interaction in the absorber would be minimal. However, the CPM configuration did serve to stabilise the laser output[21]. Similar effects to these have been observed in CPM dye lasers.

It has been suggested that the effects of intracavity self-phase modulation (SPM) and group-velocity dispersion (GVD) become increasingly important in lasers generating pulses with durations $\lesssim$100 fs[23] and for the shortest pulses, have a decisive influence on the pulse shortening process[24]. This has been demonstrated experimentally where lasers generating the shortest pulses depend on compensation of second order dispersive effects. It has also been

suggested that a proper balance of SPM and GVD can lead to additional pulse shortening over and above that produced by the passive modulator in the absence of nonlinear and dispersive effects. This additional pulse shaping has been attributed to effects similar to soliton formation in optical fibres and could result in a decrease in pulse duration by a further factor of two[25].

There are several potential sources of frequency chirp and GVD within the colour-centre laser cavity. The most obvious are the material dispersion due to the laser gain medium, cryostat windows and other intracavity elements. Off-resonant transitions in both the absorber and gain media also lead to frequency chirped pulses. The fast optical Kerr effect in the ethelyne glycol jet produces a positive up-chirp where the pulse carrier frequency increases from the front of the pulse to the back. Multiple-stack dielectric mirrors which are commonly used as laser mirrors can also lead to dispersive pulse broadening. It has been shown[26] that within the mirror reflectivity zone there are two regions of differing phase behaviour which are situated almost symmetrically about the central wavelength of the mirror coating. In one region the phase is almost constant and the dispersion is consequently low, where-as the other region exhibits high dispersion. If the wave is primarily reflected from the outer layers of the coating the resulting dispersion will be small. But if the reflection is primarily from the inner layers the wave must also pass twice through the outer layers and the resulting dispersion will be greater. Thus, mirrors which are to be used in modelocked lasers should always be used in the low dispersion side of their reflectivity region. No information was available for the mirrors used in the modelocked LiF:F_2^+ laser and so it was not possible to predict their dispersion characteristics.

For the modelocked operation described here the absorber saturation occurred on the short wavelength side of the resonance, while the gain saturation occurred on the long wavelength side of its resonance. These off resonant transitions can also cause the modelocked pulses to become frequency chirped[27,28]. For passively modelocked dye and colour-centre lasers the pulse energies are often larger than the saturation energy of the saturable absorber. This means that the frequency chirp from this source will occur on the leading edge of the pulses. In the

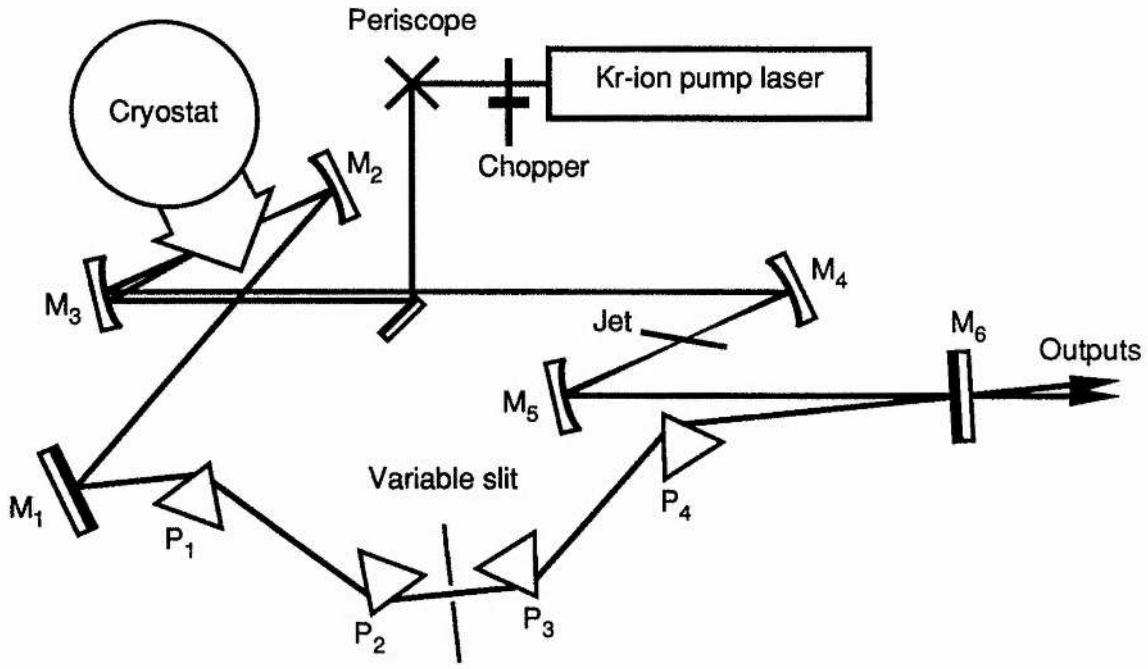

Figure 2.18. Schematic diagram showing the cavity configuration of the dispersion compensated CPM colour-centre laser.

present case, this would result in a down-chirp at the leading edge and an up-chirp over the central part of the pulse. However, these effects are not likely to be significant in this particular case because the laser operated at a wavelength which was relatively near the absorber and gain peak. Since these chirping processes are sensitively dependent on the pulse shape and duration, as well as the energy in the pulse relative to the saturation energy of the gain and absorber and the operating wavelength relative to the absorber and gain peak, the exact nature of the resulting frequency chirp can only be estimated in broad qualitative terms.

The effects of dispersion and frequency chirp can be exploited by introducing additional GVD of the correct sign and magnitude into the laser cavity. For this reason it was decided to introduce a four-prism sequence into the ring cavity to provide the necessary dispersion compensation. The cavity configuration including the prism sequence is shown in figure 2.18. The technique of dispersion compensation using prisms[29] has been discussed in chapter 1. The values for $n(\lambda)$, $dn/d\lambda$ and $d^2n/d\lambda^2$ were calculated using a computer program

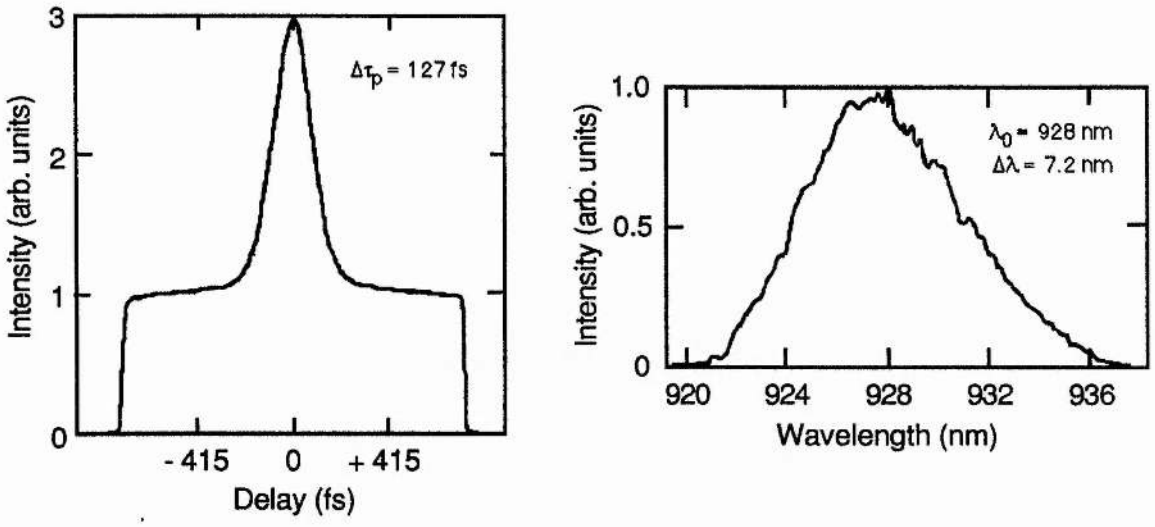

Figure 2.19. Intensity autocorrelation trace and associated pulse spectrum for the dispersion compensated, CPM colour-centre laser.

which fitted tabulated refractive index data to a Sellmeier expansion. The appropriate values for LiF and fused silica (SiO_2) are listed in Table 2.2. Using these values the dispersion due to the various intracavity elements was calculated. It was estimated that the value of ($L\beta_2$) for a single pass of the LiF crystal was ~30 fs^2 while that for both the Suprasil windows was ~116 fs^2. Assuming that the intracavity beam also propagated through ~3 mm of glass in each prism, the material dispersion due to the four prisms was estimated to be 346 fs^2. Using equation 1.25 it was calculated that for a prism separation of $\ell \geq 340$ mm, the dispersion parameter, D, would be positive and the net dispersion would be anomalous.

	LiF	SiO_2
λ (μm)	0.925	0.925
$n(\lambda)$	1.38752	1.45108
$\frac{dn}{d\lambda}$ (μm^{-1})	-9.0763×10^{-3}	-1.3820×10^{-2}
$\frac{d^2n}{d\lambda^2}$ (μm^{-2})	1.0853×10^{-2}	2.0629×10^{-2}
D (ps (nm km)$^{-1}$)	-33.4630	-63.6052

Table 2.2. Refractive index and dispersion data for the LiF laser cavity at 925 nm.

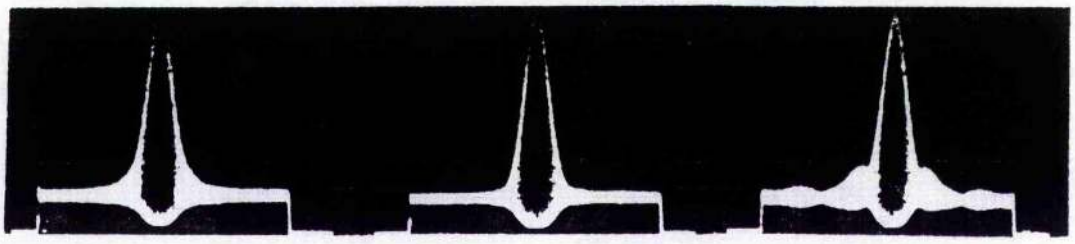

Figure 2.20. Interferometric autocorrelation traces illustrating how the frequency chirp on the modelocked pulses varied with the intracavity glass path.

With the prism sequence inserted into the laser cavity, bandwidth control and wavelength selection was provided using a slit between prisms P_2 and P_3[30]. All the other cavity elements were the same as those used for the linear cavity. With the prism sequence properly adjusted, the minimum pulse duration produced was 127 fs. This was not significantly different from those generated by the non-dispersion compensated laser. For these shortest pulses the average output power was ~7 mW per beam for a pump power of 2.5 W and the laser retained its tuning range of 925 - 950 nm. Intensity autocorrelation and spectral data for the modelocked pulses are presented in figure 2.19. As before, the duration-bandwidth product of $\Delta\tau_p\Delta\nu = 0.32$ implied bandwidth limited pulses.

In addition to the intensity autocorrelation data, real-time interferometric autocorrelation data were also recorded. This technique has been discussed in chapter 1, where the necessity to achieve adequate fringe resolution was pointed out. In this case the real-time interferometric autocorrelation traces were recorded on the autocorrelator by decreasing the scanning frequency of the speaker from the usual 25 Hz to 5 Hz and terminating the input to the oscilloscope. This provided a better impedance match which resulted in sufficient frequency response to enable the interferometric fringes to be recorded. Using this technique it was possible to qualitatively estimate the degree of frequency chirp on the modelocked pulses.

With the prism separation suitably adjusted, it was possible to vary the net intracavity GVD about the point which produced the shortest pulses, ie. those which were bandwidth limited and hence free from frequency chirp. This was achieved by translating one of the prisms in a direction perpendicular to the beam, thus varying the amount of glass within the cavity. In figure 2.20 the variation of the recorded interferometric autocorrelation traces with the intracavity GVD is shown. The position corresponding to chirp free pulses can clearly be identified.

It is apparent from these results that the inclusion of the prism sequence within the laser cavity did not reduce the duration of the pulse generated. This suggests that the intracavity nonlinear and dispersive effects in the non-compensated laser were not large enough to significantly affect the modelocked laser performance for the pulse duration produced. Theoretical predictions and experimental observations for dye lasers suggest that these effects only become significant for pulse durations less than 100 fs[23]. Presumably, a similar situation occurred in this case. The measured pulse durations were most sensitive to the positions of the intracavity focusing mirrors and dye or crystal relative to the beam waists, suggesting that absorber and gain saturation and their relative strengths were still the dominant pulse shaping mechanism in the modelocked laser.

2.7 The Passively Modelocked LiF:F_2^+ Laser with Additional Nonlinear External Cavity

Passive saturable absorber modelocking is a very effective technique which holds the record for the shortest pulses generated from a laser oscillator[28,31†]. However, two

---

† Pulses as short as 60 fs have been generated at 1.5 μm from a soliton laser [F.M. Mitschke and L.F. Mollenauer, Opt. Lett. **12**, 407, (1987)]. Recently pulses as short as 32 fs have been generated at 810 nm from a Ti:sapphire laser. [C-P. Huang, H.C. Kapteyn, J.W. McIntosh and M.M. Murnane, Opt. Lett. **17**, 139, (1992)]. Both of these results are similar to those for the dye laser in terms of the number of optical cycles in the pulse.

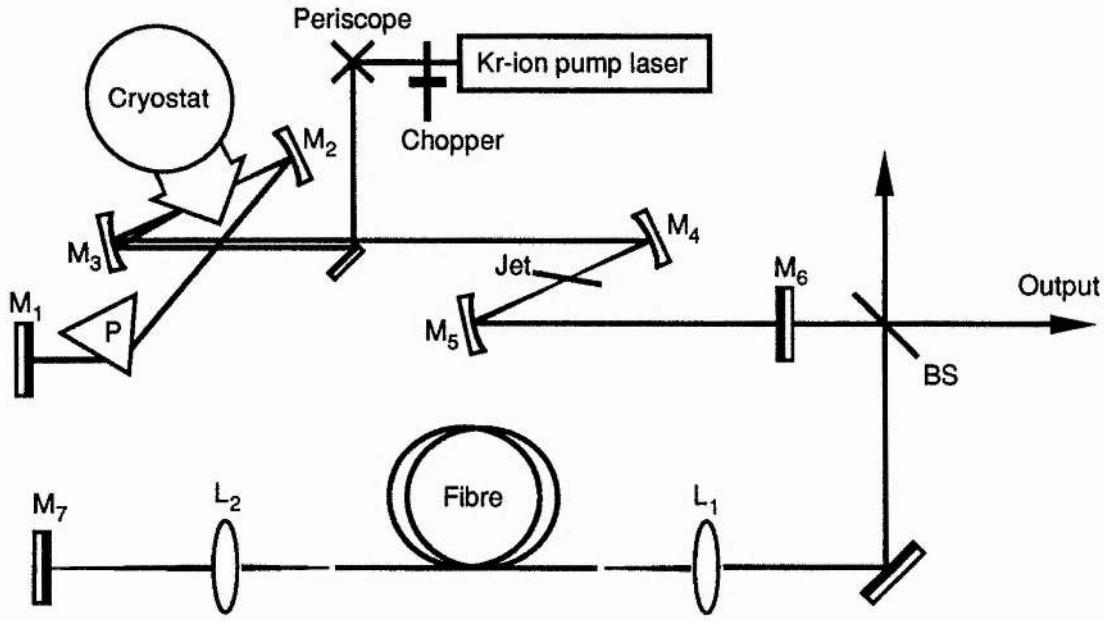

Figure 2.21. Diagram showing the cavity configuration for the passively modelocked colour-centre laser with an additional nonlinear external cavity.

drawbacks with this type of modelocking are: i) the tuning range of the modelocked laser is limited to that covered by the saturable absorber (924 - 946 nm in this case) and ii) the saturable absorber dyes used have a limited lifetime due to optically induced deterioration and are often unpleasant and hazardous to work with. (DaQTeC had a usable lifetime of about 48 hrs.) If an attempt is made to operate the laser outside the parameter range imposed by the passive modelocking technique, the pulse durations dramatically increase and/or the modelocked output becomes unstable or ceases altogether.

The technique of coupled-cavity or additive pulse modelocking[32-35] has been shown to dramatically improve the pulse durations produced from other modelocked colour centre lasers such as the synchronously modelocked KCl:Tl°(1) laser and thus has become a technique for modelocking in its own right. (This will be discussed more fully in chapter 4 with particular reference to the Ti:sapphire laser.) It is sufficient at this stage to say that the technique usually involves optically coupling an interferometrically matched external cavity, containing some suitable nonlinear element, to the main laser cavity. The pulses returned from this nonlinear

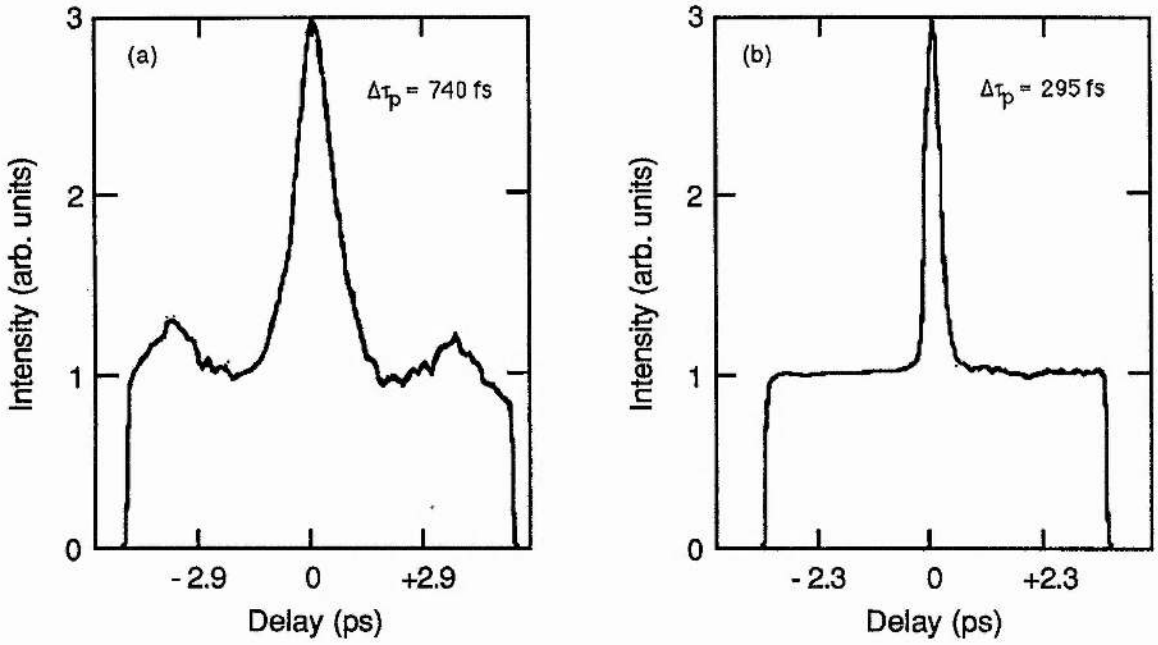

Figure 2.22. Intensity autocorrelation traces of the pulses generated from the passively modelocked laser with old dye at 932 nm, with (a) the coupled cavity blocked and (b) the coupled cavity un-blocked.

termination are frequency chirped and combine with the field in the main cavity resulting in shorter pulses being generated from the laser[36]. It was decided to implement the technique in the case of the passively modelocked LiF laser in the hope that some or all of the restrictions imposed by the saturable absorber might be relaxed, ie. that the modelocked tuning range and/or the usable dye lifetime might be extended.

The cavity configuration for the passively modelocked laser with the coupled-cavity section is illustrated in figure 2.21. The components which formed the main laser cavity remained unchanged, with the exception of the output coupler, M_6, which was changed to one having a transmission of 10% in order to maximise the coupling between resonators. The beam splitter, BS, was 70% reflecting and the remaining 30% of the signal from the main cavity formed the laser output. A length of single mode optical fibre formed the nonlinear element in the external cavity. Initially 4.5 m of Andrew Corporation fibre (Type no. 48280-1-P) was used. This had a elliptical core diameter of 1.25 x 2.5 μm^2 and was

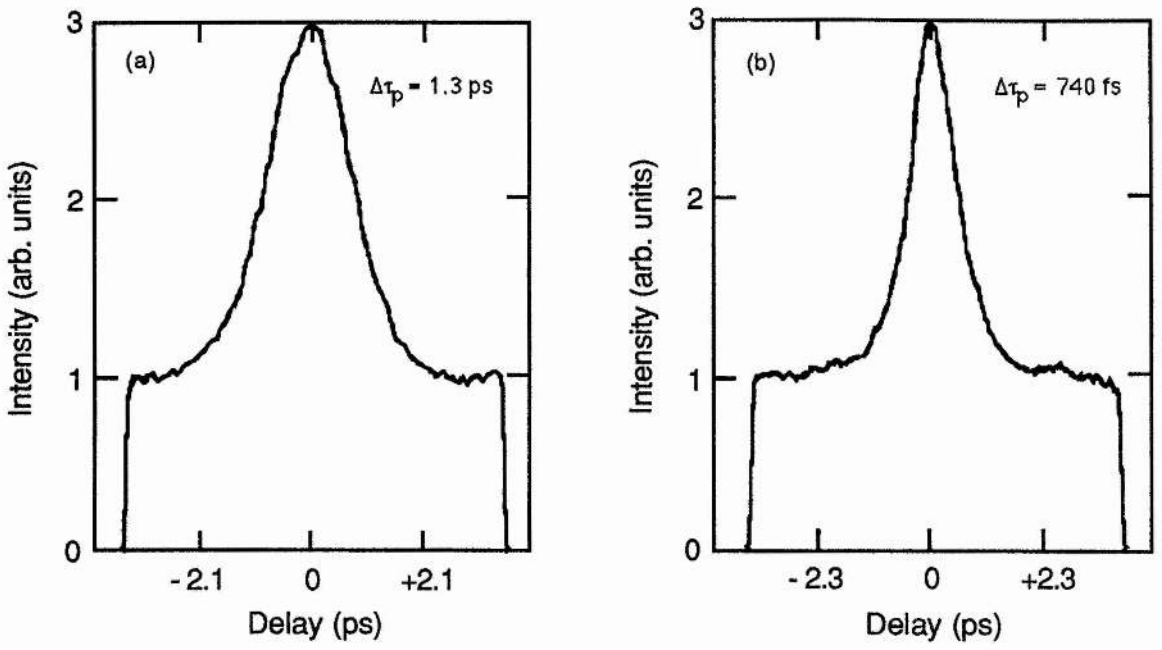

Figure 2.23. Intensity autocorrelation traces of the pulses generated from the passively modelocked laser at 900 nm, with (a) the coupled cavity blocked and (b) the coupled cavity un-blocked.

polarisation preserving and single mode for wavelengths greater than approximately 800 nm. Light was coupled into the length of fibre using x20 microscope objectives, L_1 and L_2, (Vikers AA7726) which were anti-reflection coated for a wavelength region centred on 850 nm. The mirror M7 was used to retro-reflect the light back along the fibre and into the main cavity and was mounted on a translation stage to permit cavity length matching. The coupled-cavity section measured 910 cm in length which was five times the length of the main laser cavity.

The saturable absorber dye solution had a concentration of ~9 x 10^{-5} mol/l and was already several days old at the start of the experiment. The pump power was fixed at 2.2 W, the average power launched into the fibre was approximately 30 mW and the useful average laser output power was ~15 mW. The single pass fibre throughput was about 40 - 50%. Firstly, with the laser tuned to a wavelength of 932 nm and the coupled-cavity section blocked, pulses having durations of 740 fs were generated. When the external cavity was unblocked, and its length suitably adjusted, the pulse duration was reduced to around 300 fs.

Intensity autocorrelation traces showing the recorded pulses with the cavity open and blocked are shown in figure 2.22, where the enhancement in modelocked operation is evident. Secondly, the laser wavelength was tuned to around 900 nm where pulse durations of 1.33 ps were recorded with the coupled-cavity section blocked. With the control-cavity open, the measured pulse durations were reduced to 740 fs. Intensity autocorrelation traces for these pulses are illustrated in figure 2.23.

With the coupled-cavity section properly aligned, the enhancement in the modelocked operation started and dropped out randomly, as the interferometric match between the two cavities varied due to random perturbations from the surrounding environment. It was, therefore, necessary to capture the results presented here using a storage oscilloscope. Coupled-cavity modelocked lasers can be stabilised against these perturbations using an electronic feed-back circuit which will be described in more detail in chapter 4[37]. However, the use of such a stabilisation scheme is made more difficult in the case of the LiF laser due the quasi-cw nature of its operation resulting from the chopped pump beam. This experiment does, however, illustrate that the technique can be used, at least in principle, to improve and extend the modelocked performance of this passively modelocked laser.

2.8 Conclusions

In this chapter the operation of a LiF:F_2^+ colour-centre laser has been described. It has been shown that cw (chopped) operation can be achieved over a wavelength range which extends from 820 nm to 1.0 μm with an average output power of as much as 400 mW when pumped by ~2.5 W from a Kr-ion laser. Data have been presented for a range of pump powers and wavelengths.

Experimental results have been presented for the laser when passively modelocked using the dye, DaQTeC, as a slow saturable absorber. Pulses having durations as short as 170 fs at 930 nm were generated by the basic laser with an average output power of 10 mW and a corresponding peak power of more than 700 W. The modelocked laser was also operated in a CPM cavity configuration, in which pulses having durations as short as 127 fs were

generated, with average and peak output powers of 7 mW and 720 W respectively. In this configuration the pulse durations were just as short as for uni-directional operation of the ring cavity, suggesting that the CPM process did not significantly effect the pulse shaping mechanism. However, the CPM configuration did lead to improved stability of the modelocked output. The technique of dispersion compensation was also implemented in the ring cavity, but this also did not significantly affect the minimum pulse duration. This observation suggested that dispersive and nonlinear effects did not play a significant role in determining the final pulse durations. The results suggested that gain and absorber saturation were still the dominant processes governing the final pulse durations generated. Finally, the technique of coupled-cavity modelocking was used to supplement the passive saturable absorber. This allowed the wavelength range of the modelocked laser to be extended to ~900 nm and also allowed the interval between dye changes to be extended.

At the time this work was carried out the LiF colour centre laser represented a practical alternative to the dye laser in the 0.8 - 1.0 μm spectral region for both narrow linewidth and modelocked operation. However, both of these laser sources have now been superseded by the Ti:sapphire laser, which is able to produce higher powers and shorter pulses over an extended wavelength range. The operation of the Ti:sapphire laser will be considered in the remainder of this thesis.

2.9 References

1. J.H. Schulman and W.D. Compton, in 'Color Centers in Solids', International Series of Monographs on Solid State Physics, Perganom Press, Oxford, (1962), Ch. 1.

2. C.R. Pollock, J. of Lumin. **35**, 65, (1986).

3. S.C. Rand and L.G. De Shazer, Opt. Lett. **10**, 481, (1985).

4. B. Henderson, Opt. Lett. **6**, 437, (1981).

5. F. Seitz, Rev. Mod. Phys. **26**, 9, (1954).

6. R. Herman, M.C. Wallis and R.F. Wallis, Phys. Rev. **107**, 87, (1956).

7. M.A. Aegerter and F. Luty, Phys. Stat. Solid. (b) **43**, 227, (1977).

8. J. Nahum, Phys. Rev. **158**, 814, (1967).

9. L.F. Mollenauer, Rev. Sci. Instrum. **49**, 809, (1978).

10. E. Rzepka, M. Bernard, S. Lefrant, H. Dubost, R. Charneau and J.P. Galaup, Opt. Commun. **62**, 174, (1978).

11. K. Smith, Ph.D Thesis, Univ. of London, (1985), Ch. 4.

12. See, for example 'Color Center Lasers', Burleigh Instruments, Inc., NY.

13. L.F. Mollenauer, in 'Tunable Solid State Lasers', J.C. White and L.F. Mollenauer eds., Springer-Verlag, Berlin, (1987), Ch. 6.

14. H.W. Kogelnik, E.P. Ippen, A. Dienes and C.V. Shank, IEEE J. Quant. Electron. **QE-8**, 373, (1972).

15. A.E. Siegman, in 'Lasers', University Science Books, Mill Valley, California, (1986), Ch. 12.

16. N.J. Langford, Ph.D. Thesis, University of London, (1988), Ch. 5,6.

17. N. Langford, K. Smith and W. Sibbett, Opt. Lett. **12**, 903, (1987).

18. C.I. Johnston, D.E. Spence, R.S. Grant and W. Sibbett, Opt. Commun. **73**, 370, (1989).

19. G.H. New, IEEE J. Quant. Electron. **QE-10**, 115, (1974).

20. H.A. Haus, IEEE J. Quant. Electron. **QE-11**, 736, (1975).

21. R.L. Fork, B.I. Greene and C.V. Shank, Appl. Phys. Lett. **39**, 671, (1981).

22. M.S. Stix and E.P. Ippen, IEEE J. Quant. Electron. **QE-19**, 520, (1983).

23. J.A. Valdmanis and R.L. Fork, IEEE J. Quant. Electron. **QE-22**, 112, (1986).

24. V. Petrov, W. Rudolph, U. Stamm and B. Wilhelmi, Phys. Rev. A **40**, 1474, (1989).

25. O.E. Martinez, R.L. Fork and J.P. Gordon, Opt. Lett. **9**, 156, (1984).

26. P. Laporta and V. Magni, Appl. Opt. **24**, 2014, (1985).

27. A. Finch, Ph.D. Thesis, University of St. Andrews, (1989).

28. A. Finch, G. Chen, W. Sleat and W. Sibbett, J. Mod. Opt. **35**, 345, (1988).

29. R.L. Fork, O.E. Martinez and J.P. Gordon, Opt. Lett. **9**, 150, (1984).

30. R.L. Fork, Opt. Lett. **11**, 629, (1986).

31. J.A. Valdmanis, R.L. Fork and J.P. Gordon, Opt. Lett. **10**, 131, (1985).

32. L.F. Mollenauer and R.H. Stolen, Opt. Lett. **9**, 13, (1984).

33. K.J. Blow and B.P. Nelson, Opt. Lett. **13**, 1026, (1988).

34. P.N. Kean, X. Zhu, D.W. Crust, R.S. Grant, N. Langford and W. Sibbett, Opt. Lett. **14**, 39, (1989).

35. F. Ouellette and M. Piché, Can. J. Phys. **66**, 903, (1988).

36. K.J. Blow and D. Wood, J. Opt. Soc. Am. B **5**, 629, (1988).

37. F.M. Mitschke and L.F. Mollenauer, IEEE J. Quant. Electron. **QE-22**, 2242, (1986).

Chapter 3
An Introduction to the Ti:sapphire Laser

3.1 Introduction

Chapter 2 described the operation of the LiF:F_2^+ colour-centre laser, which provided an alternative coherent optical source to the dye-laser in the 0.8 - 1.0 μm spectral region. Colour-centre lasers do not suffer from any of the less desirable aspects of organic chemistry which beset dye lasers, such as the flammable nature of many of the dyes and solvents, their possible carcinogenic effects and their tendency to leave permanent stains when spilled. Colour centres, however, do suffer from other problems, such as the deterioration of the laser active centres with time and the requirement that they be operated at cryogenic temperatures. In the remainder of this thesis we will describe some of the properties of a laser based on sapphire doped with titanium (Ti:Al_2O_3) which does not suffer from any of the problems mentioned above. In addition, the Ti:Al_2O_3 laser has a tuning range which is considerably broader than any of its dye or colour-centre laser competitors, spanning the 660 - 1100 nm spectral region, and which can also out-perform its rivals in almost all applications.

Since the first demonstration of laser oscillation in Ti:Al_2O_3 in 1982, the performance and breadth of application of the laser has grown rapidly. The material has not only been used in cw single-frequency and modelocked lasers, but has also been successfully applied to laser pumped, pulsed and cw, oscillator and/or amplifier configurations, as well as flashlamp pumped systems using fluorescence convertors. The broad wavelength region covered by the laser means that its range of applications is widespread. Ti:sapphire based systems have found uses in high resolution linear and nonlinear spectroscopy of atoms, molecules and solids. Semiconductor compounds such as GaAs, InP, CdTe, GaAlAs and GaInAs all have direct bandgap energies which lie within the tuning range of the Ti:Al_2O_3 laser. Applications which use the laser as a pump source for other laser materials (eg. Nd, Ho, Tm, Er doped materials) have also been identified. In particular, operation at 980 nm has provided a versatile laboratory pump source for the study of Er-amplifiers. Research is also being carried out into

the use of high power Ti:Al_2O_3 based systems for remote sensing studies in the atmosphere because of the water vapour absorption bands at 727 and 940 nm and the oxygen band at 760 nm all of which lie within the tuning range of the laser. Finally, the high powers available from Ti:Al_2O_3 oscillators have enabled the efficient generation of frequency-doubled, frequency-mixed and parametrically generated radiation spanning, at present, the 190 nm - 4 μm spectral region. Further developments are continuing and such sources should provide replacements for blue/uv dye lasers and find applications in the spectroscopy of, for example, II-VI semiconductor compounds.

In this chapter we will start by briefly describing the growth and spectroscopy of laser-quality Ti:Al_2O_3 material as well as the important design features of such lasers. Results will be presented which characterise the performance of a cw Ti:Al_2O_3 laser which was tunable over the 700 - 1000 nm spectral region and provided more than 3 W of output power at wavelengths around 850 nm. Finally, the operation of an acousto-optically modelocked Ti:Al_2O_3 laser will be described which produced pulses having durations shorter than 60 ps. This will serve as an introduction to the remaining chapters which describe two other modelocking techniques that have been applied to the laser and which have resulted in both picosecond and femtosecond pulse generation.

3.2 Growth and Spectroscopy of Ti:Al_2O_3

Ti:sapphire is a crystalline material produced by introducing Ti_2O_3 into a melt of Al_2O_3. A boule of single crystal laser quality material is grown from this melt using a variety of techniques. Two common methods used are the vertical-gradient freeze (VGF)[1,2] and the Czochralski[3,4] methods, the latter being used to obtain commercially available crystals like that used in the Spectra-Physics Ti:Al_2O_3 laser.

In the Czochralski growth method, an inductively heated iridium crucible in zirconia insulation is used as the growth chamber and the atmosphere over the crucible is pure N_2. Growth is initiated by touching an oriented sapphire seed onto the top of the melt and pulling at a constant rate. The pull rate is typically around 0.5 cm/h and diameter control is achieved

by measuring the weight of the growing crystal. The crucible charge is usually TiO_2 and Al_2O_3 with the latter in the form of pressed pellets or crackle. Above ~1750°C the TiO_2 is reduced to Ti_2O_3 in the following reaction: $2TiO_2 = Ti_2O_3 + 1/2O_2$. Liquid Ti_2O_3 then reacts and mixes with the molten Al_2O_3 upon reaching a temperature of 2050°C. The miscibility of Ti_2O_3 in Al_2O_3 is only about 1% by weight, and this possess one of the main difficulties in achieving laser quality crystals with high Ti concentrations. By pulling at a very slow rate of ~ 0.025 cm/h, Ti concentrations approaching approximately 0.24 wt % have been achieved, however an absorption which overlaps the fluorescence band becomes unacceptably high at these doping levels and concentrations of ~0.1 wt % are more usual.

A useful figure describing the quality of Ti:Al_2O_3 crystals for laser material is the figure of merit defined as follows[7]

$$\text{F.O.M.} = \frac{\alpha_m}{\alpha_r} = \frac{\text{peak } Ti^{3+} \text{ absorption at 490 nm}}{\text{peak residual infrared absorption at 850 nm}} \qquad (3.1)$$

Values for the FOM in excess of 100 have been achieved. The residual near-infrared absorption is believed to be due to the presence of Ti^{4+} - Ti^{3+} ion pairs in the material[8] Annealing the as-grown samples in a reducing atmosphere at temperatures of ~ 1600°C leads to reduction of the Ti^{4+} to Ti^{3+} ions and results in a considerable decrease in the residual infrared absorption, together with a corresponding increase in the FOM.

The Ti^{3+} in Ti:Al_2O_3 is the active laser ion and the system therefore falls in the 3d transition-metal class of lasers which includes other active ions such as Cr^{3+}, Ni^{2+} and Co^{2+}. The titanium atom has the electronic configuration $1s^22s^22p^63s^23p^63d^24s^2$ and so the Ti^{3+} ion has a single 3d valence electron outside a core which has a closed shell argon configuration. The spectroscopic characteristics of Ti:Al_2O_3 are, therefore, largely determined by this single 3d valence electron and as a result it has the simplest energy level structure of all the laser active transition metal ions.

Un-doped Al_2O_3 is transparent in the NIR from approximately 2000 nm to 400 nm in the

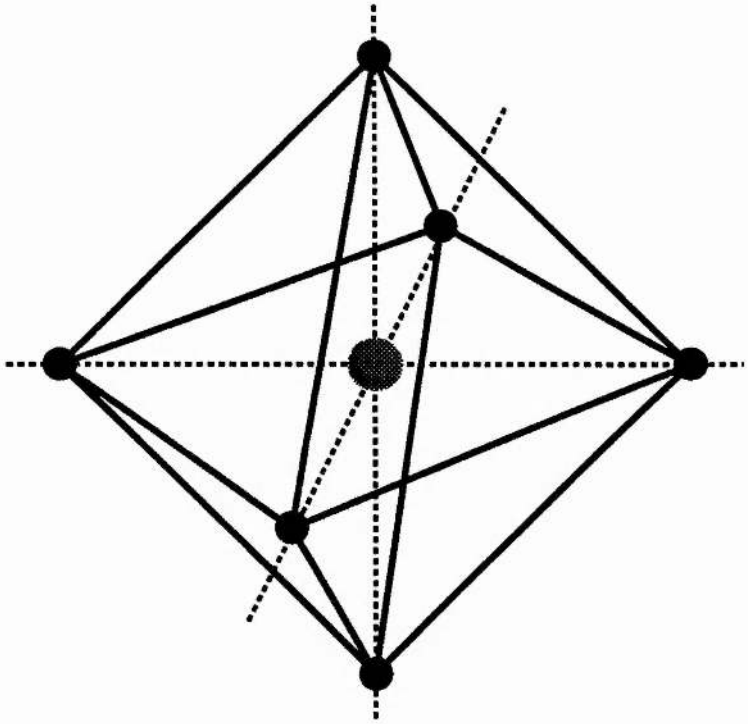

Figure 3.1. The crystal geometry of Ti:Al_2O_3.

visible. In the UV region, between 200 - 400 nm, an absorption arising from the long wavelength tail of the band-edge below 200 nm, increases towards the shorter wavelengths[9]. The Ti^{3+} ions are substituted for a small number of Al^{3+} ions in the sapphire lattice. The Al^{3+} ion lattice symmetry is trigonal but the six O^{2-} ions adjacent to the Al^{3+} site lie at the corners of a slightly distorted octahedron[10]. This geometry is illustrated in figure 3.1. The crystal field seen by the Al^{3+} ions or their substitutes is, therefore, the sum of a dominant cubic component and a much weaker trigonal one so that the resultant field is largely cubic with a small trigonal distortion. In isolation, the 3d electron has a five-fold degeneracy in its lowest energy level (neglecting spin), but once the ion is placed in the crystal host this degeneracy is lifted by the interaction with the host crystal field. The cubic field splits the energy level into a tripley degenerate $^2T_2$ ground state and a doubly degenerate ^2E excited state. The trigonal field also splits the ground state into two further levels and the lower of these is again split by the spin-orbit interaction[11].

The separation between the lowest and higher levels in the $^2T_2$ state is 38 and 107 cm^{-1}

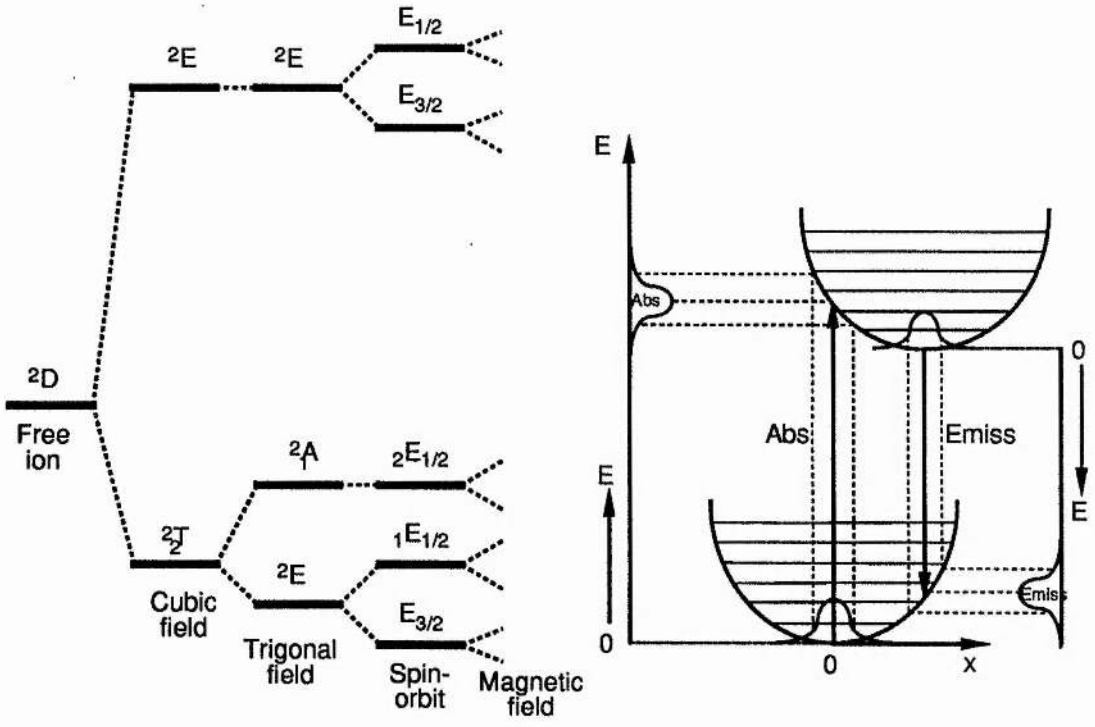

Figure 3.2. Energy levels and configurational-coordinate diagram for Ti:Al_2O_3.

respectively, while the separation between the $^2T_2$ and ^2E states is around 19000 cm^{-1}. Laser action takes place between these latter two states[11]. A schematic energy level diagram together with the configuration-coordinate diagram for the laser transition in Ti:Al_2O_3 is shown in figure 3.2. The main absorption band, which is located in the blue-green spectral region (~400 - 600 nm) and peaks at approximately 490 nm, is illustrated in figure 3.3. This band is due to the phonon-coupled excitation of the Ti^{3+} ions, ie. an electronic transition which is accompanied by the simultaneous emission (or possibly absorption at high temperatures) of one or more lattice phonons. These phonon-terminated electronic transitions are also known as vibronic transitions and lasers based on them are often referred to as vibronic lasers. It is this absorption band that results in the pink colour of Ti:Al_2O_3. The $^2T_2$ and ^2E electronic orbitals interact differently with the surrounding ionic environment and as a result the equilibrium value of the configurational-coordinate is different for each level (see figure 3.2) so that there is a Stokes shift between the absorption and fluorescence spectra which are broad-band due to the vibrational broadening. There are also other absorption peaks

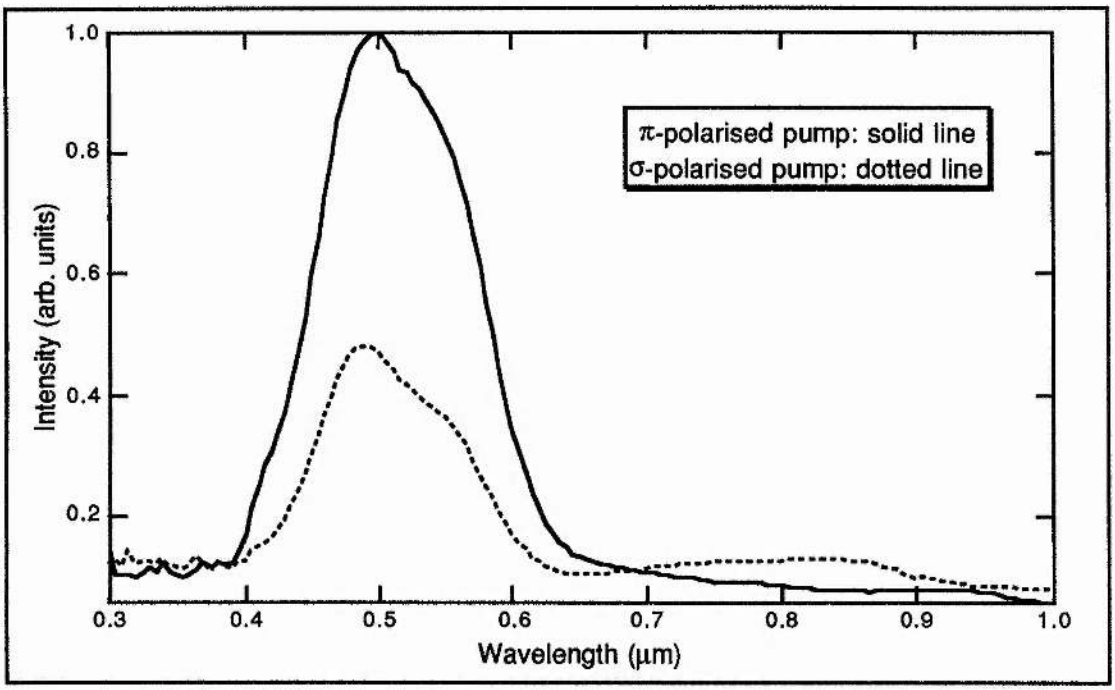

Figure 3.3. Measured absorption spectrum of Ti:Al_2O_3.

in the UV spectral region at approximately 266, 216 and 185 nm, but their origin is not well understood[4].

Optical pumping of the laser transition produces the broad fluorescence band extending from approximately 600 - 1200 nm and peaking at approximately 790 nm, which is shown in figure 3.4. Except at the shortest wavelengths, the luminescence is not reabsorbed by the ground state ions due to the Stokes shift between the absorption and emission bands. Laser action has been achieved over a broad wavelength region extending from ~660 nm to 1100 nm, however, the laser performance is impaired by the relatively weak, broad absorption band that peaks between 800 and 850 nm in the NIR, and extends approximately over the 650 - 1600 nm spectral region[8]. The Ti-ions can occupy the Al^{3+} sites in the form of either Ti^{3+} or Ti^{4+} ions. The residual absorption has been attributed to Ti^{3+} - Ti^{4+} ion pairs and is due to the excitation of the 3d electron in the Ti^{3+} ion which is perturbed by the Ti^{4+} ion's Coulomb field and/or associated Al^{3+} vacancy. (Charge compensation for the Ti^{4+} ions most likely occurs via the formation of an Al^{3+} vacancy for every three Ti^{3+} converted

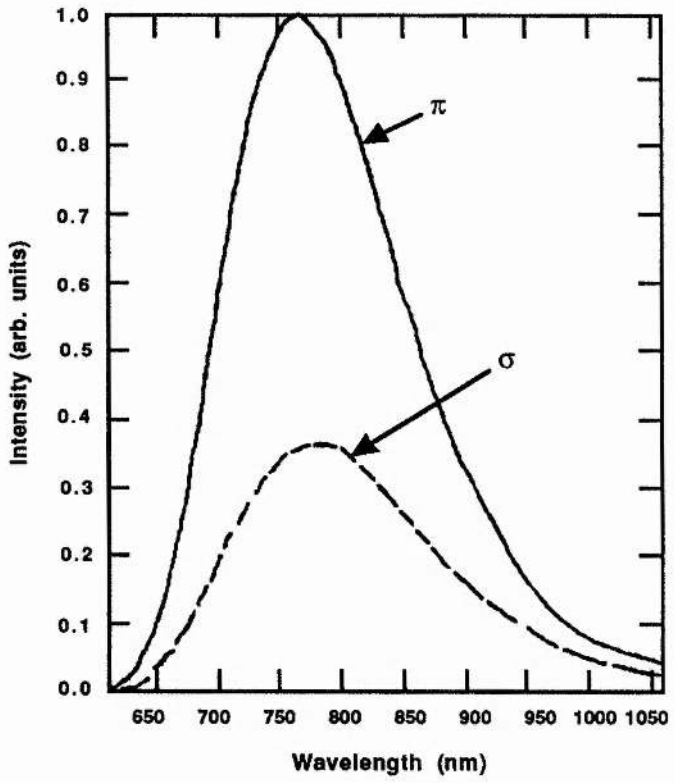

Figure 3.4. Fluorescence spectrum of Ti:Al_2O_3. (Taken from reference 11.)

into Ti^{4+}, ie $3Ti^{3+}(Al) + 3/4O_2(gas) = 3Ti^{4+}(Al) + V^{3-}(Al) + 3/2O$.) This residual absorption has been the most significant problem associated with the development of Ti:Al_2O_3 as a laser material. The strength of the absorption seems to be dependent on the conditions under which the crystals are grown and much improvement has been made in the production of residual absorption-free material.

As is evident from the figures, the absorption and fluorescence are polarisation dependent. This polarisation anisotropy is probably due to the direction of orientation of the bonding orbitals in the material[12]. The main absorption is stronger for π (polarisation parallel to c-axis) than for σ (polarisation perpendicular to c-axis) polarised light, while the reverse is true for the residual absorption. It is clear, therefore, that the optimum laser performance will be achieved for π-polarised pump and laser radiation, requiring light propagation perpendicular to the c-axis in the rod. The dependence of the fluorescence decay time on temperature is

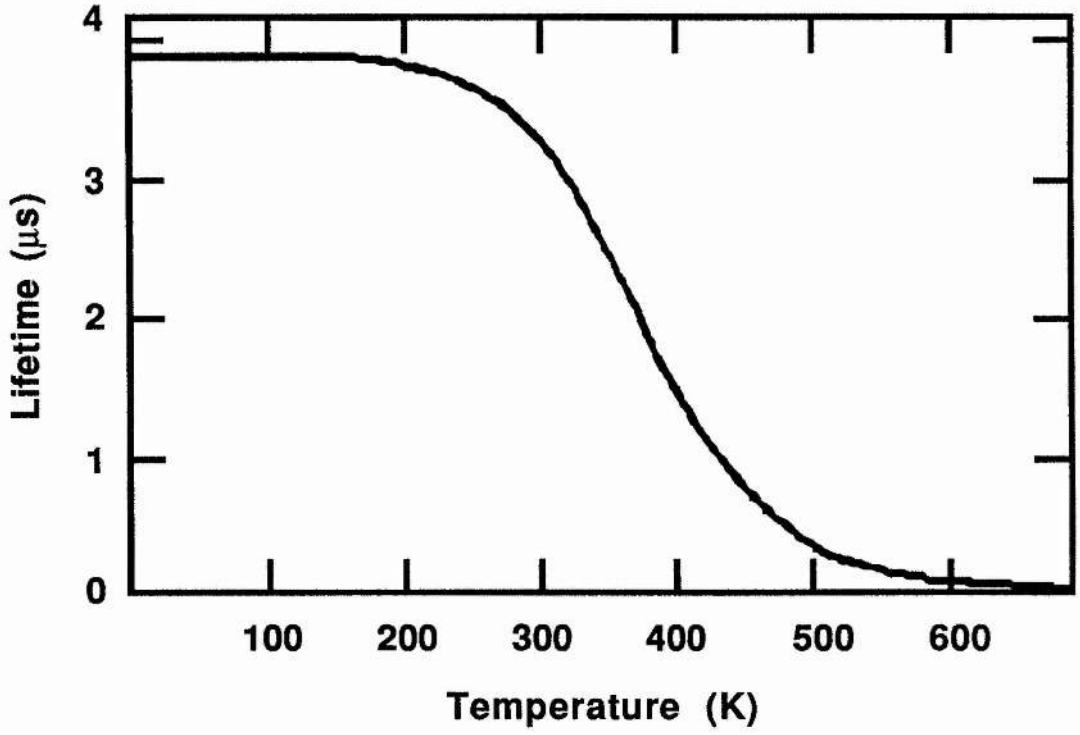

Figure 3.5. Graph showing the temperature dependence of the fluorescence decay time. (Taken from reference 6.)

illustrated in figure 3.5. The rapid reduction in lifetime with increasing temperature is characteristic of fluorescence quenching due to multi-phonon, non-radiative decay[13]. The low temperature lifetime of $\tau_r = 3.85$ μs is purely radiative. Fortunately, this fluorescence quenching is not serious at room temperatures, where $\tau_r \approx 3.1$ μs and this allows Ti:Al_2O_3 lasers to be operated with very simple water cooling arrangements. Finally, it is worth noting that the higher energy states of the Ti^{3+} ion require excitation out of the 3d shell. This requires energy which is large compared to the photon energies involved in the pump or laser transitions, so unlike other 3d transition metal ion laser materials, performance is not compromised by excited state absorption of either the pump or the laser light.

3.3 Design Considerations for Ti:Al_2O_3 Lasers

The short upperstate lifetime of Ti:Al_2O_3 makes direct lamp pumping schemes difficult because of the high pumping rate per unit volume necessary to achieve a population inversion[14]. The high currents required to obtain sufficient pump energy result in the lamp

having a high colour temperature which lies mostly outside the Ti:Al_2O_3 pump band. Such high colour temperatures may also lead to colour centre and Ti^{4+} ion formation resulting in a degradation of the gain medium. As a result, most of the work on cw Ti:Al_2O_3 lasers has used another laser - typically an Ar-ion or frequency-doubled Nd:YAG as a pump source. Fortunately, the physical properties of sapphire permit high pump levels without major optical distortions or destruction of the host material.

In any laser system high efficiency and low threshold are obvious design goals. Threshold is minimised by choosing a cavity mode with a small beam radius in the gain and pumping within that region so that a high inversion will be reached easily, with relatively low pump

Property	Typical value at 300 K
Chemical symbol	Ti:Al_2O_3
Thermal conductivity	0.33 W cm^{-1} K^{-1} (10 W cm^{-1} K^{-1} at 77 K)
Ti^{3+} concentration	1 - 5 x 10^{19} cm^{-3}
n	1.76
n_2	3 x 10^{-16} cm^2 W^{-1}
σ_{abs}	5 - 8 x 10^{-20} cm^2
σ_{gain}	3.7 x 10^{-19} cm^2
α_p	0.7 - 3.0 cm^{-1}
α_r	0.0025 - 0.0065 cm^{-1}
$(\lambda_{abs})_{pk}$	490 nm
$(\lambda_{emiss})_{pk}$	790 nm
Line width ($\Delta\lambda_{gain}$)	3500 cm^{-1}
τ	3.21 μs
η	~70%

Table 3.1. Some important properties of Ti:Al_2O_3 laser crystals.

powers. As this is difficult to achieve over the whole volume of the Ti:Al_2O_3 rod, which is perhaps several millimetres in diameter, the pump beam and laser cavity mode are focused to a narrow waist within the rod and made to overlap[7]. High efficiency requires a long gain medium to achieve maximum absorption of the pump radiation and an optimised output coupling for the peak absorption, ie. Ti^{3+} ion concentration, and cavity losses. Inevitably, there will be some trade-off between increased efficiency and low threshold.

The peak emission cross-section in Ti:Al_2O_3 is only a factor of two smaller than in Nd:YAG at 1.06 μm, however, because of the much lower active ion concentrations used in Ti:Al_2O_3, rod lengths of a few centimetres are necessary to achieve adequate pump absorption, while tightly focused pump and cavity modes are used to minimise the oscillation threshold as noted above. In dye and colour-centre lasers the gain jet or crystal are usually quite thin and the pump and cavity modes need not be exactly overlapped. In Ti:Al_2O_3, however, the longer gain length and lower emission cross-section require close alignment of the pump and cavity modes over the full length of the crystal.

Optimising the Ti:Al_2O_3 oscillator is thus achieved by carefully choosing such constants as α_p and α_e, the absorption and emission coefficients (which are properties of the material and are dependent on the active ion concentration); the crystal length, L; the pump and cavity beam waists and the output coupling. Numerical modelling suggests that choosing $1.5 < \alpha_p L < 2.0$ provides best efficiency for crystals having a wide range of figures of merit[7]. Thus, provided $\alpha_p L$ has been optimised, the FOM is the critical value in determining the cw laser performance. Some important parameters for Ti:Al_2O_3 laser crystals are given in Table 3.1.

The most efficient transfer of pump energy to oscillator output is achieved using a longitudinal pumping geometry which provides maximum overlap of the pump and cavity modes. A four mirror cavity such as that shown in figure 3.6 can be used to satisfy the requirements of tightly focused beams in the crystal together with reasonably sized, collimated

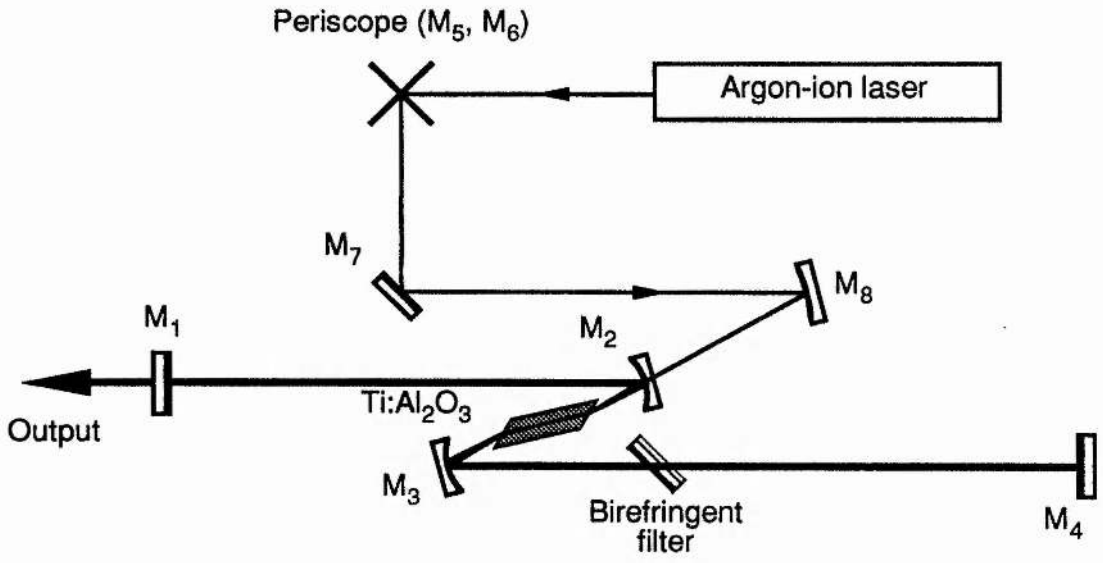

Figure 3.6. Schematic diagram of the 4-mirror cavity used in the $Ti:Al_2O_3$ laser.

beams outside. This cavity can be astigmatically compensated by proper choice of folding angle, so that aberration in the output beam is minimised. Astigmatism within the rod is still present so the pump beam is also focused via a concave mirror used at a suitably chosen angle of incidence. In this way astigmatism is introduced into the pump beam providing efficient coupling between the pump and cavity modes and resulting in higher conversion efficiencies. Perfect mode matching is still not possible over the entire rod length since pump and cavity beams are at different wavelengths. The best power transfer and performance is achieved with the best average match between these two modes. Longitudinally pumped laser cavities such as these have been analysed by several groups and typical results have been published in reference 7 for a $Ti:Al_2O_3$ laser.

3.4 The Spectra-Physics Model 3900 $Ti:Al_2O_3$ Laser

The work based upon $Ti:Al_2O_3$ described in this thesis was carried out using a modified Spectra-Physics Model 3900 system. The basic configuration of this laser will now be described, while the modifications will be discussed in the relevant sections of the following chapters. The laser configuration is illustrated schematically in figure 3.6 and uses a four mirror, longitudinally pumped cavity configuration.

The pump laser was either a Spectra-Physics Model 2030-20 or 2040E-15 argon ion laser. These lasers were operated in the visible using all the transitions in the 457.9 - 514.5 nm spectral region. Under these conditions the maximum output power was typically between 15 and 25 W depending on plasma tube specification and age. It is interesting to note that the overall electrical to optical efficiency of such a laser was only about 0.03% (60 kW/15 W) and that nearly all of the energy loss was in the form of heat from the plasma discharge, magnet and power supply. Water cooling was therefore essential for laser operation and this was obtained from a boost pump providing a flow of more than 20 l/min at approximately 70 psi. The ion laser cavity consisted of a flat high-reflecting end mirror and an 8 m radius of curvature output coupler. On the Model 2040E this output mirror was mounted on a piezo-electrically variable mount which was controlled by a suitable servo loop from a quadrant photodetector. In this way the transverse position of the output beam could be stabilised. This BeamLok™ system enabled immediate use without an initial warm up period and maintained stable operation throughout the day without the need to adjust the alignment of the laser. The introduction of economic and reliable high-power laser diodes should lead to the development of diode-pumped, frequency-doubled Nd:YAG lasers with sufficient power output to pump Ti:Al_2O_3 lasers. This would greatly improve the efficiency, reliability and output noise performance of the Ti:Al_2O_3 laser[15].

Wavelength tunability was provided by means of a birefringent filter[16] consisting of three crystalline quartz plates oriented at the Brewster angle inside the cavity[17]. These plates were polished parallel to the optic axis and their birefringence caused the linearly polarised input to become elliptical at the output due to the phase delay introduced between the polarisation components parallel to the fast and slow axes. The filters were designed so that for one frequency within each free-spectral-range, the phase shift between the two components at the output would be 2π (or some multiple thereof) so that light at this frequency would remain unchanged. Due to the presence of the Brewster angles within the cavity all elliptically polarised light experienced higher reflection losses and failed to reach oscillation threshold. By changing the angle of the optic axis with respect to the polarisation plane of the cavity (ie.

by rotating the filter) the oscillating wavelength of laser could be varied. The plates supplied with the Spectra-Physics laser had thicknesses of 5.36 mm, 1.34 mm and 0.34 mm, thus the thickness ratio was 16:4:1. Best results (ie. greatest wavelength selectivity) should be obtained if the optic axis of the filter is near 45° to the plane of polarisation[18]. The plate thickness determined the oscillation bandwidth, with a thinner plate having a broader FWHM filter response. The free spectral range of the three-plate filter used in the Ti:Al_2O_3 laser was just over 150 nm and this, together with the reflectivity range of the cavity optics permitted oscillation at only one wavelength within the laser tuning range for any particular setting of the filter.

The tuning of the laser was further complicated by the fact that the Ti:Al_2O_3 crystal was itself birefringent. Proper tuning was achieved only when the the c-axis of the rod was aligned to be coplanar with the polarisation of the electric field within the cavity. Since the filter and rod together consisted of a total of eight Brewster surfaces, losses were minimised and tuning optimised only if all eight surfaces were properly aligned and the rod was properly oriented. To achieve this, a special rod mount was used in the Spectra-Physics system to compensate for the unavoidable errors introduced during manufacture, cutting and polishing.

The Ti:Al_2O_3 laser cavity, illustrated in figure 3.6, consisted of a plane, 3.5% transmitting output coupler, M_1, two concave folding mirrors, M_2 and M_3, having a radius of curvature of R = 10 cm and an incident angle of ~15°, and a plane high reflector, M_4. These cavity mirrors were dichroic - highly reflecting in the near-infrared and highly transmitting for wavelengths near 500 nm. They were also wedged to eliminate etalon effects in the laser resonator. The arm containing the output coupler had a length of 27 cm while the other arm was 19 cm in length which resulted in a total cavity length of 60 cm. The cavity was astigmatically compensated in the output, while astigmatism was introduced into the pump beam by the off-axis mirror to provide maximum conversion efficiency. The required folding angle for the cavity mirrors was confirmed by simple calculation to be approximately 15.2°. The pump beam was routed via mirrors M_5 and M_6, which formed a periscope arrangement to

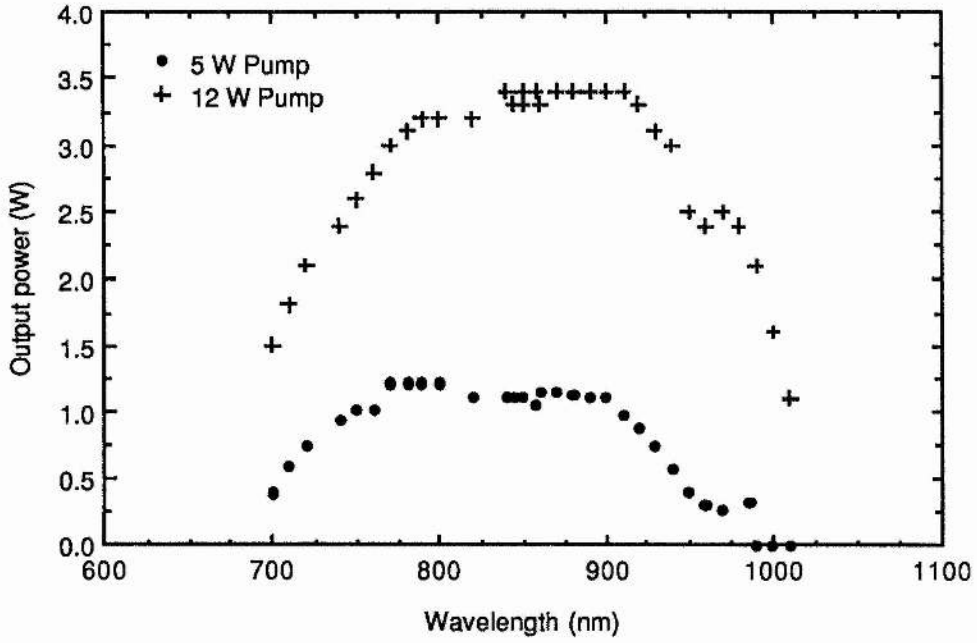

Figure 3.7. Graph showing the variation of output power with wavelength for the cw Ti:Al_2O_3 laser.

rotate the vertically polarised pump light to a horizontal polarisation. Mirror M_7, was a flat highly reflecting steering mirror and M_8 (figure 3.6) was a concave mirror with $R \approx 23$ cm and $\theta_i \approx 10°$, which focused the pump radiation into the Ti:Al_2O_3 crystal. This crystal was 20 mm in length and Brewster-angled for light at wavelengths near 800 nm.

When operated as a cw system with 5 W pump power, the laser could be tuned from 700 - 858 nm with the low wavelength optics set installed and from 845 - 986 nm when using the high optics set. With the pump power increased to 12 W the tuning range with the low wavelength optics did not change, but the longer wavelength range was increased to 1010 nm. With the improved crystal growth technology together with extended optics sets the latest Spectra-Physics Ti:Al_2O_3 lasers can be tuned over a range extending from 660 - 1100 nm. An experimental tuning curve for the laser used in the work presented here is given as figure 3.7. Typically, the laser linewidth was approximately 0.1 nm. The laser threshold was in the region of 1 W for operation in the 800 - 900 nm spectral region.

3.5 The Acousto-optically Modelocked Ti:Al_2O_3 Laser

The scattering of light by sound provides a convenient means of controlling the frequency, intensity and direction of an optical beam of light. Acousto-optic devices using this principle are commonly employed as the active modelocking element in lasers. A travelling or standing acoustic wave in an acousto-optic medium sets up associated travelling or standing layers of spatial refractive index inhomogeneities from which optical waves can be scattered. These variations in index result from the coupling between the refractive index and the strain of the material due the the photoelastic effect, as described by the photoelastic constant[19]. The sound wave causes a sinusoidal perturbation of the density of the material and a resulting sinusoidal modulation of the refractive index. In the linear approximation the change in n is proportional to the strain[20].

The process can be viewed either as a collision involving photons and phonons or as a diffraction process where the optical wave is diffracted by a periodic index grating. In either case both energy and momentum must be conserved so that

$$\omega_d = \pm\omega_s + \omega_i \tag{3.2}$$

$$\mathbf{k}_d = \mathbf{k}_s + \mathbf{k}_i \tag{3.3}$$

where the latter equation implies that the diffracted waves must constructively interfere. If the modulator operates in the Raman-Nath diffraction regime[21] several diffracted orders are produced symmetrically located about the zeroth-order beam. This was the scheme used for the work described here. Alternatively, the modulator can be operated in the Bragg diffraction regime, where the angle between the two waves is the Bragg angle and only a single diffracted beam is generated. An optical beam interacting with a travelling acousto-optic wave will emerge from the medium with a depleted, but time-independent intensity, while the diffracted wave is shifted in frequency and direction. If, on the other hand, the incident wave interacts with a standing acousto-optic wave, the output intensity is modulated in time. It is this effect that is used in acousto-optic modelockers.

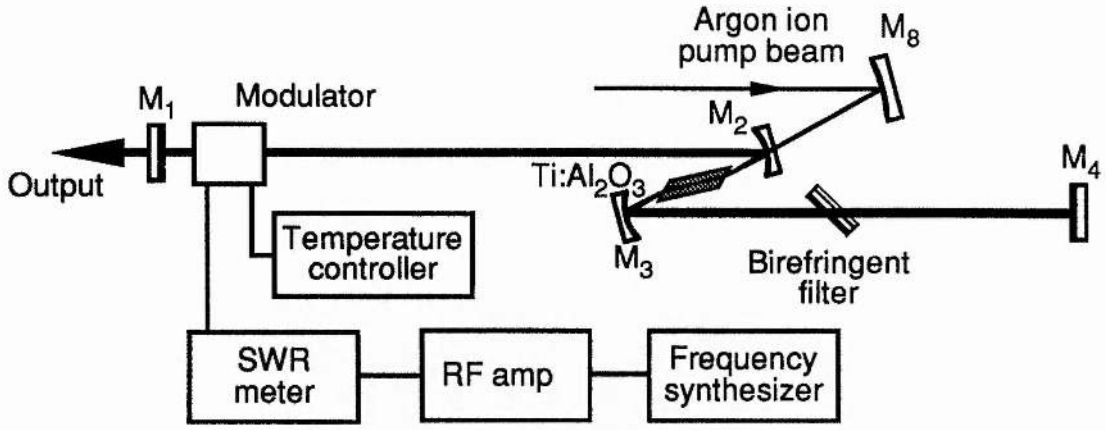

Figure 3.8. Schematic diagram for the acousto-optically modelocked $Ti:Al_2O_3$ laser.

In such devices, a piezo-electric transducer is used to launch acoustic waves into the material (typically a quartz block). If the thickness of the block is an integer multiple of $\lambda_s/2$, then a resonant standing acoustic wave is established. This in turn produces a variation in refractive index which is also periodic in time and space and acts as a bulk diffraction grating, forming a loss element by diffracting light out of the laser resonator. Since the grating formed by a standing-wave modulator will disappear and re-establish itself at a frequency which is twice the driving frequency, the optical modulation will also be at twice this frequency. Accurate temperature control is essential because the speed of sound in the medium is critically dependent on the temperature. Thus, the insertion of a standing-wave acousto-optic modulator in the laser cavity results in a time-varying loss which can lead to short pulse formation as outlined in chapter 1. For a polarised optical input wave, it can be shown that the index change is directly proportional to the square root of the acoustic power[20].

The acousto-optically modelocked laser is illustrated schematically in figure 3.8. The system used an acousto-optic standing wave modulator manufactured by Newport Electro-Optics Systems, which was designed to be operated at frequencies near 41 MHz. It consisted of a quartz block measuring 20 mm in length by 100 mm^2 and had a broad-band anti-reflection coating, covering the wavelength range 750 - 900 nm, on both the optical input and output surfaces. A piezo-electric transducer was deposited on the top of the quartz block

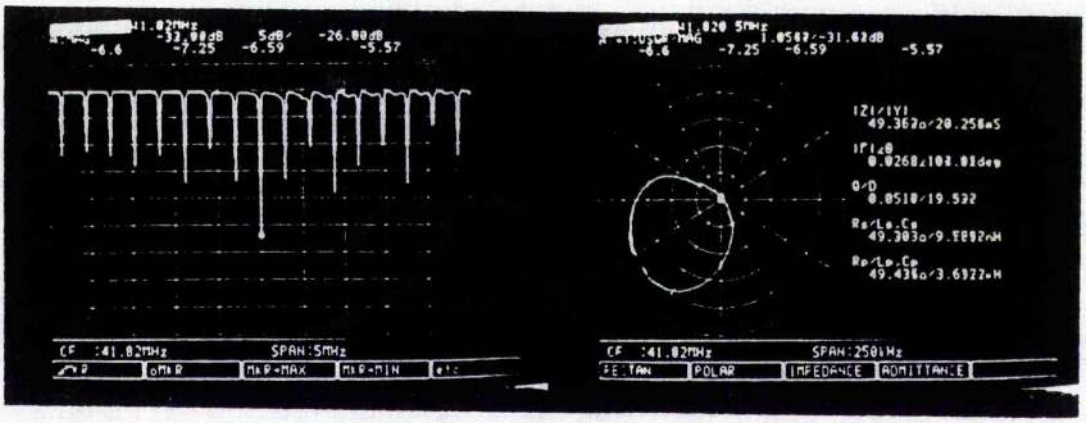

Figure 3.9. Network analyser traces illustrating the rf characteristics of the acousto-optic modulator: Trace (a) shows a number of resonances near 42 MHz and trace (b) shows the characteristics of the strongest resonance near 42 MHz.

and had a thickness of approximately 70 μm. The modulator was placed in an electrically heated oven which maintained a constant temperature using a thermistor controlled feedback circuit. This was set to keep the device several degrees above normal room temperature. The modulator used in these experiments had resonance frequencies which were separated by 300 kHz. Figure 3.9 shows network analyser traces which illustrate the electrical performance of the modulator. The trace in part (b) of the figure is for the strongest resonance near 42 MHz. The modulator had a measured intensity modulation efficiency on resonance, of ~25% at 633 nm for 500 mW of rf power.

The circuit used to provide the rf drive signal to the modelocker is also illustrated in figure 3.8. This circuit consisted of a frequency synthesizer (Racal, model no. 9081; or Marconi Instruments, model 2019), a rf amplifier, and an SWR meter. For the experiments described here, the modulator was driven at a frequency of 41.85218 MHz at rf power levels in the range 0.5 - 0.75 W. This operating frequency was close to one of the resonance frequencies of the modulator. This represented the case when the transducer frequency enabled acoustic standing waves to be established in the quartz crystal block and thus allowed maximum power transfer from the rf drive signal into the acousto-optic grating. When operated away from a resonance, the rf power could not be efficiently coupled into acoustic

waves and was reflected back and forth along the cable resulting in an apparent increase in cable loss.

The critical temperature dependence of the speed of sound in quartz meant that accurate temperature control was essential for stable operation. The rf power coupled into the modulator also caused an increase in the temperature of the crystal and this resulted in a corresponding rise in the resonance frequency. Provided the modulator was operated at a frequency below the resonance, a negative feedback effect ensured that reasonably stable operation occurred. In this case an increase in temperature caused a corresponding increase in the resonance frequency which resulted in less rf heating because the device was pushed away from resonance. However, if the rf drive frequency was to high, a positive feed back effect occurred so that a change in temperature could cause the system to slip out of resonance. This process is known as thermal runaway. The oven control helped prevent temperature changes in the environment from disturbing the resonance frequency. Under normal operating conditions, the modulation efficiency was estimated to be ~15%.

The rf drive frequency of 41.8 MHz resulted in a modulation frequency of 83.6 MHz when applied to the acousto-optic modulator. Since, in the simplest case, this will also be the round trip frequency of the modelocked pulses, the laser cavity length was extended to ~1.79 m. This was achieved by removing the output coupler and high reflector from their mounts within the box and holding them separately in translatable mounts situated externally and directly on the optical table. In this extended cavity configuration, the gain medium was placed close to the centre of the cavity. The laser was operated with a pump power of approximately 10 W at a wavelength close to 848 nm. The output power in this case was typically 600 mW. The cavity length was finely adjusted by means of the translation stage in order to generate the shortest pulses.

The resulting modelocked pulse sequence was monitored using a silicon avalanche photodiode (APD) (Telefunken BPW 28) having an electrical bandwidth of approximately

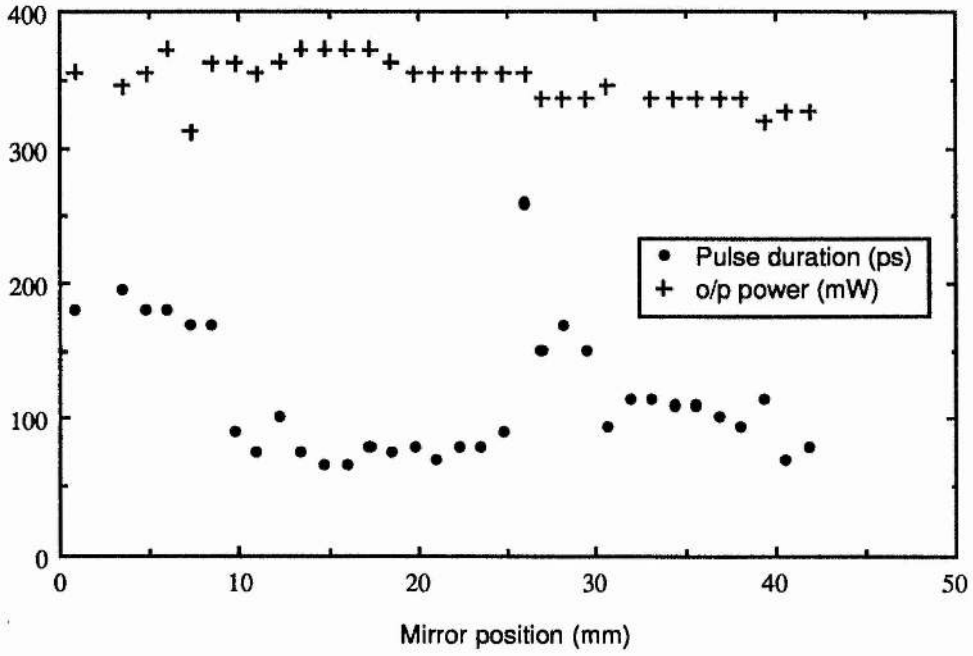

Figure 3.10. Graph illustrating the variation of the modelocked pulse duration with the distance between the output coupler and the modulator.

2 GHz and an oscilloscope having a bandwidth of approximately 400 MHz (Tektronix 7834 or 7904). Somewhat better temporal resolution was obtained when the modelocked pulses were monitored using AlGaAs PIN or APD photodiodes whose bandwidths were in the 20 GHz range together with a sampling oscilloscope (Tektronix 7603 with S6 sampling head). This photodiode and sampler combination had a resolution of approximately 60 ps. The modelocked pulses had typical durations shorter then 100 ps with pulses as short as 60 ps being recorded. These pulses were too long to be recorded on the second-harmonic generation autocorrelator which could not accurately measure pulse durations longer than ~30 ps.

Figure 3.10 shows how the pulse duration varied with the distance between the modelocker and the output coupler, while figure 3.11 shows a typical sampling scope trace of one of the shortest pulses recorded. The variation in pulse duration with the separation

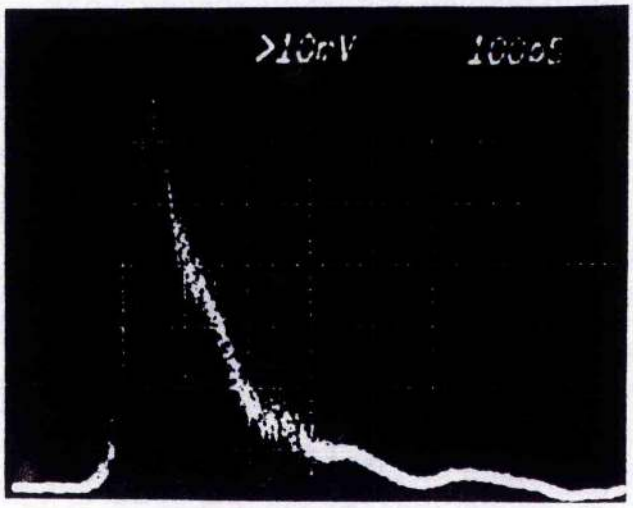

Figure 3.11. Oscillogram showing a 60 ps pulse from the acousto-optically modelocked laser recorded with a photodiode and sampling oscilloscope. (This represents the resolution limit of the detection system.)

between the mirror and modulator may be due to interference effects between the diffracted light on consecutive passes through the modulator[22]. Depending on the distance, the interference can be either constructive or destructive, resulting respectively in either increased or decreased modulation depth. Since $\tau_p \propto \Delta_m^{-1/4}$, a change in modulation depth will also result in a change in pulse duration. Approximate calculations[22] suggest that in this case, constructive interference will result if the separation is an integral multiple of 2 cm. This agrees approximately with the results presented as figure 3.10.

The acousto-optically modelocked laser was tuneable over the 845 - 900 nm wavelength range and generated pulses having durations less then 100 ps over this entire region. The lower limit was due to the reflectivity of the mirrors and the modelocked operation could be extended by using the lower wavelength mirror set.The upper wavelength limit was due to the AR coating on the modulator.

It is interesting to compare the measured pulse durations with those predicted by the Kuizenga-Siegman analysis mentioned in chapter 1[23]. The round-trip saturated voltage gain g_o is given approximately by

$$g_o \approx \frac{1}{2} \ln\left(\frac{1}{R}\right) \tag{3.4}$$

where R is the effective power reflectivity of a mirror and includes all losses. In the case of the Ti:Al_2O_3 laser described here, it was assumed that $R \approx 0.9$, while $f_m = 83.70436$ MHz and Δf was estimated to be ~3 THz. From equation (1.3), this gives a value for τ_p of

$$\tau_p = 0.5 \times \frac{0.5}{\Delta_m^{1/4}} \times 60 \text{ ps} \tag{3.5}$$

The voltage transmission of the modelocker is given by

$$t_{am} = \exp\left[-\Delta_m (1 - \cos \omega_m t)\right] \tag{3.6}$$

so that the minimum intensity transmission is given by $\exp(-4\Delta_m)$. For an intensity modulation of 0.15, $\Delta_m = 0.03$ and so τ_p is approximately 40 ps which is not far from the measured, resolution limited duration of 60 ps.

3.6 Conclusions

In this chapter an introduction to the Ti:Al_2O_3 laser has been given. A brief review of the most important growth techniques and spectroscopy of Ti:Al_2O_3 laser crystals has been presented and some of the properties which are important for laser oscillation have been summarised. Some of the design goals which should be considered when building a cw laser and the ways in which they can be achieved in practice, have briefly been discussed. The performance of a cw Ti:Al_2O_3 laser has been characterised with laser oscillation being achieved over a wavelength region spanning more than 300 nm from 700 to 1010 nm, with more than 3 W output power at wavelengths near 850 nm.

Finally, the operation of an actively modelocked Ti:Al_2O_3 laser has been described. This laser generated pulses having durations less than 100 ps over a wavelength range from 845 - 900 nm, with durations of less than 60 ps at 848 nm. This tuning range was limited by the optical coatings.

3.7 References

1. R.E. Fahey, A.J. Strauss, A. Sanchez and R.L. Aggarwal, in 'Tunable Solid State Lasers II', Springer Series in Optical Sciences vol. 52, A.B. Budgor, L. Esterowitz and L.G. De Shazer, eds., Springer-Verlag, New York, (1987), p. 82.

2. A.J. Strauss, R.E. Fahey, A. Sanchez and R.L. Aggarwal, Proc. SPIE vol. 681, 62, (1987).

3. G.A. Keig, J. Cryst. Growth **2**, 356, (1968).

4. P. Lacovara, L. Esterowitz and M. Kokta, IEEE J. Quant. Electron. **QE-21**, 1614, (1985).

5. P. Moulton, Optics News, (Nov/Dec 1982), p.9.

6. A. Sanchez, A.J. Strauss, R.L. Aggarwal and R.E. Fahey, IEEE J. Quant. Electron. **QE-24**, 995, (1988).

7. A.J. Alfrey, IEEE J. Quant. Electron. **QE-25**, 760, (1989).

8. R.L. Aggarwal, A. Sanchez, M.M. Stuppi, R.E. Fahey, A.J. Strauss, W.R. Rapoport and C.P. Khattak, IEEE J. Quant. Electron. **QE-24**, 1003, (1988).

9. A. Sanchez, A.J. Strauss, R.L. Aggarwal and R.E. Fahey, IEEE J. Quant. Electron. **QE-24**, 995, (1988).

10. R.R. Joyce and P.L. Richards, Phys. Rev. **179**, 375, (1969).

11. P.F. Moulton, J. Opt. Soc. Am. B **3**, 125, (1986).

12. E.W.J. Mitchell, J.D. Ridgen and P.D. Townsend, Phil. Mag. **5**, 1013, (1960).

13. P. Albers, E. Stark, and G. Huber, J. Opt. Soc. Am. B **3**, 134, (1986).

14. P. Lacovara, L. Esterowitz and R. Allen, Opt. Lett. **10**, 273, (1985).

15. J. Harrison, A. Finch, D.M. Rines, G.A. Rines and P.F. Moulton, Opt. Lett. **16**, 581, (1991).

16. J.W. Evans, J. Opt. Soc. Am. **39**, 229, (1949).

17. D.R. Preuss and J.L. Gole, Appl. Opt. **19**, 702, (1980).

18. G. Li and Y. Li, Appl. Opt. **29**, 3462, (1990).

19. D.A. Pinnow, IEEE J. Quant. Electron. **QE-6**, 223, (1970).

20. H.A. Haus, in 'Waves and Fields in Optoelectronics', Prentice-Hall Series in Solid State Physical Electronics, N. Holonyak, Jr., ed., Prentice-Hall inc., Englewood Cliffs, (1984), Ch. 9.

21. C.V. Ramman and N.S. Nath, Proc. Ind. Ac. Sci. **2**, 406, (1935).

22. D. von der Linde, Appl. Phys. Lett. B **39**, 201, (1986).

23. D.J. Kuizenga and A.E. Siegman, IEEE J. Quant. Electron. **QE-6**, 694, (1970).

Chapter 4
The Coupled-Cavity Modelocked Ti:sapphire Laser

4.1 Introduction

Chapter 3 ended with a presentation of results for an actively modelocked Ti:Al_2O_3 laser which generated pulses having durations in the sub-100 ps regime. In this chapter results will be presented for a coupled-cavity modelocked Ti:Al_2O_3 laser, in which the modelocking process was self-starting and which could produce pulses having durations of <3 ps over a wavelength range extending from 750 - 960 nm. Near 860 nm pulses as short as 1.3 ps were generated. These pulses had average powers >100 mW and peak powers which exceeded 1 kW. Results are also presented which show how the performance of the laser varied with some of the important operating parameters such as wavelength and fibre length. The laser produced chirped pulses which could be directly compressed outside the cavity to 290 fs. The results show that dispersion played a key role in determining the duration of the pulses generated.

By using the technique of dispersion compensation in the coupled-cavity section of the laser, the pulse durations were reduced from ~4 ps to 1.3 ps with some frequency chirp remaining. By dispersion compensating the main laser resonator, the pulse durations were reduced to 120 fs. The average power was ~200 mW which corresponded to a peak power of more than 20 kW. The shortest pulses were generated by using dispersion compensation in both cavities. With this scheme the pulse durations were as short as 90 fs. The results show how the pulse durations depended on the magnitude and sign of the dispersion and suggest that the shortest pulses were obtained with a small negative dispersion. Finally, the stability of the modelocked output will be discussed. First, a brief review of coupled-cavity modelocking is given and some of the important theoretical points which explain the operation of the modelocked Ti:Al_2O_3 laser are discussed.

4.2 Coupled-Cavity Modelocking

The technique of coupled-cavity modelocking (or additive-pulse or interferential modelocking) has been successfully employed for ultrashort pulse generation from a wide variety of laser systems. Initially, it was used to generate femtosecond pulses from colour-centre lasers such as KCl:Tl°(1) or NaCl:OH^-, but more recently has been applied to solid-state lasers such as Ti:Al_2O_3 as well as Nd:YAG/YLF/glass. In some of these systems active modulation is necessary to initiate short pulse generation, while in others the process self-starts from noise or longitudinal mode beating in the laser.† It is a particularly useful technique for lasers for which no suitable saturable absorber is available and does not impose the same wavelength restrictions which often apply to saturable-absorber-based modelocking.

In its most common form the coupled-cavity modelocked laser consists of a main laser resonator which is coupled to a second optical cavity through a common partially transmitting mirror, as shown schematically in figure 4.1. The auxiliary cavity contains some nonlinear medium, such as a length of optical fibre[1,2], a semiconductor diode amplifier[3], a frequency doubling crystal[4] or a multiple quantum well semiconductor sample[5]. The nonlinear medium causes the pulses in the control cavity to experience an intensity-dependent nonlinear phase shift which can lead to pulse shortening in the main laser by coherent addition of the pulses from the two cavities at the common interface. For this reason, the modelocking mechanism has also been termed additive-pulse or interferential modelocking[6,7].

The predecessor to the generic coupled-cavity systems was the soliton laser[8] which used a length of soliton supporting optical fibre in the control cavity. This system was based on a synchronously pumped KCl:Tl°(1) colour-centre laser and was thought to depend on the domination of the strong soliton pulse shaping occurring in the control cavity, over the weaker gain shaping provided by the pump pulses[9]. It was realised at this time that once the weak

---

† In fact, self-starting operation has been observed in all these lasers, but it is considerably more difficult to achieve in some systems than in others. This point is discussed in more detail later in the text.

pulse shaping effects of synchronous pumping had initiated pulsing, the influence of the fibre-cavity could take over completely and the modelocking process would become essentially passive in nature. Experimental results suggested that the laser often operated in a regime where the pulses in the control cavity were nearly N=2 solitons. The technique led to the generation of pulses as short as 60 fs[10], but was obviously limited to lasers operating in the 1.5 μm spectral region where the group-velocity dispersion (GVD) of optical fibres was negative.

Blow and Wood were the first to consider that soliton formation in the external cavity might not be the crucial ingredient for short-pulse operation[11]. They studied numerically the more general case where the coupled cavity contained either a saturable absorber or a saturable amplifier. Although the latter lead to pulse broadening in the external cavity, their model suggested that net pulse shortening in the laser could result in either case, if the returned wave had the correct phase mismatch with the main cavity field so that it subtracted preferentially from the low-intensity parts of the laser signal for saturable amplification and added preferentially to the high intensity parts of the pulse for the case of saturable absorption. They suggested that the modelocking mechanism induced coupling between the longitudinal modes of the master laser cavity and thus permitted more efficient communication of phase information to the edges of the laser bandwidth. Significantly, the results showed that any nonlinear response to the optical field in the external cavity could lead to short pulse generation provided the two cavities had the correct phase mismatch. Independently, a CO_2 laser was passively modelocked by placing a germanium crystal (the nonlinear medium) in one arm of a Michelson interferometer which was added to the laser cavity[12]. This interferometer behaved as a nonlinear mirror which exhibited an enhanced reflectivity with higher incident optical intensities, due to the interference of the main pulse with the phase modulated version of itself returned from the nonlinear branch.

At the same time, a general time-domain model termed additive-pulse modelocking was developed in an attempt explain the experimental results from lasers coupled to both soliton

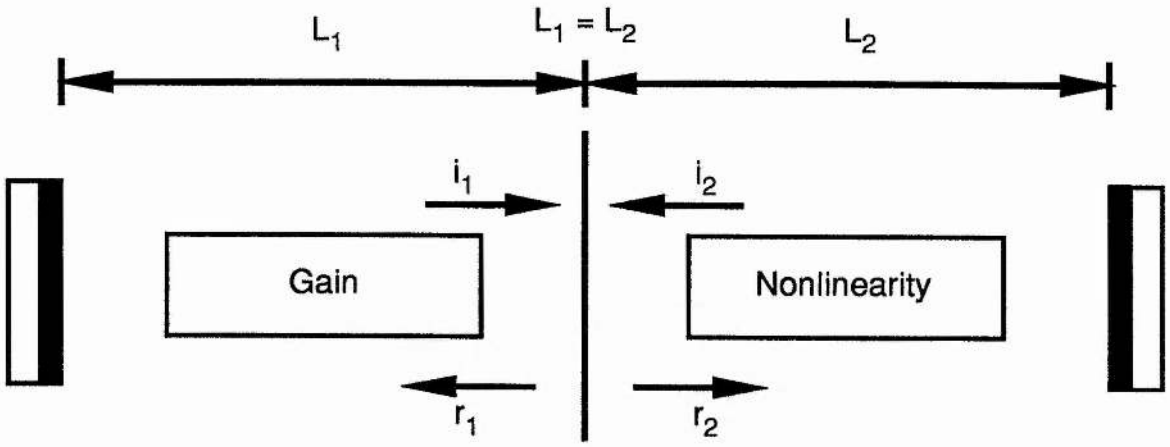

Figure 4.1. Schematic diagram showing the basic construction of a coupled-cavity laser.

and non-soliton supporting cavities[6,13]. The model suggested that self-phase modulation (SPM) in the external resonator could lead to pulse shortening in the main resonator by coherent addition of the two cavity fields at the common interface. Pulse interference required that both cavities be maintained at the same length with interferometric accuracy. The reflectivity from the common interface, as seen by the main cavity, depends on the instantaneous phases of the fields on both sides of the mirror. Since the nonlinear phase shift in the external cavity will vary across the pulse, the reflectivity of the mirror will also be a rapidly varying function of time. With the proper choice of static phase mismatch between the two cavities, this dynamic reflectivity can be enhanced in the centre of the pulse and reduced in the wings, thus producing pulse shortening. The coupled cavity therefore acts as a termination of the main laser that returns a pulse having a shorter duration than the one incident upon it. This suggests that increasing the frequency chirping in the control cavity should produce shorter pulses because the destructive interference in the wings of the main cavity pulse, which leads to pulse shortening, can occur closer to the peak. Significantly, the mechanism can shorten the laser pulses without any temporal pulse shaping in the nonlinear resonator.

In figure 4.1 the incident and reflected wave amplitudes are i_1, r_1 on the laser side and i_2,

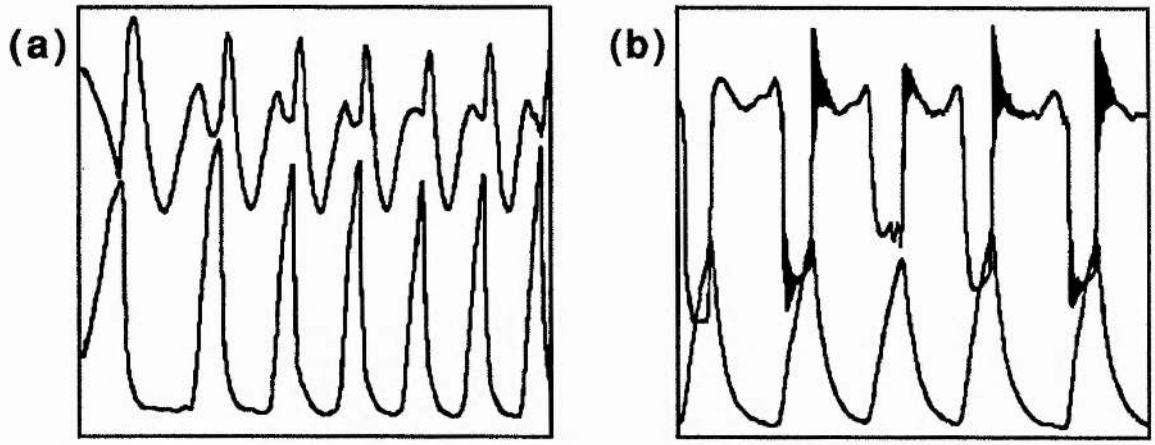

Figure 4.2. Variation of (a) the average laser intensity and (b) the average feedback intensity from the coupled cavity and the second harmonic intensity (bottom traces), with the phase bias of the external cavity.

r_2 on the auxiliary cavity side so that the amplitude reflection coefficient is $\Gamma = r_1/i_1$. Neglecting dispersion, if the nonlinear phase shift, Φ (defined so that Φ is zero at the peak of the pulse and negative in the wings) is small, then it can be shown that the maximum change in $|\Gamma|$ with Φ occurs for a phase bias of $\phi = -\pi/2$ and is given approximately by

$$|\Gamma| \approx r + \mathcal{L}(1 - r^2)\Phi \tag{4.1}$$

where $\mathcal{L}$ is an attenuation factor for the nonlinear cavity which is assumed to be much less than unity. Thus Γ is a maximum at the peak of the pulse and decreases in the wings. Since this approximation is only valid in the limit of low dispersion and small nonlinear phase shift, more generally, the optimum value for ϕ may not be $-\pi/2$. Unlike saturable absorber modelocked dye or colour-centre lasers where the pulse shortening velocity is constant for pulses having constant energy, in the case of coupled-cavity modelocking the pulse shortening velocity can increase as the pulses get shorter.

Although the modelocking mechanism does not depend on dispersion for its operation, it is affected by it. It is the GVD which balances the pulse shortening velocity and eventually determines the steady-state pulse durations. Interestingly, negative GVD in the control cavity is more detrimental than positive GVD because the former tends to directly cancel the effects

of the SPM. Also, the temporally compressed pulses returning from the control cavity cannot interfere effectively with the wings of the main cavity pulses. This situation is reversed for positive GVD when the pulses in the coupled cavity will be broadened and the rate of change of phase across the centre of these pulses (the part which will interfere with the main pulse) will be reduced so that the pulse shortening is again compromised. The effects of GVD become particularly important for solid-state lasers such as Ti:Al_2O_3, which operate below 1.0 μm, where the magnitude of the GVD is particularly large.

The traces shown as figure 4.2 illustrate how the average laser output power and second harmonic power varied with the phase of the external cavity for a coupled-cavity modelocked Ti:Al_2O_3 laser[14]. These traces were recorded by monitoring the appropriate signals while sweeping the external cavity length by applying a voltage ramp to a piezo-electric translator on which one of the coupled-cavity mirrors was mounted. The exact shapes of the curves are quite complicated, but illustrate some general trends. Short pulse formation occurred only on certain portions of the cycle when the phase of the external cavity was negative. The variation in the effective reflectivity of the common output mirror caused a corresponding variation in the laser output power which is also clearly visible. It is also evident how this behaviour can be used to derive an error signal to stabilise the laser output. Stabilisation is necessary because the optimum phase for maximum cw gain is different from that for maximum nonlinear reflectivity change (a negative phase bias is required) so that it is necessary to actively hold the cavities at a position of lower reflectivity[15]. Finally, it should be noted that the assumptions of low dispersion and phase shift are not always satisfied, particularly in coupled-cavity modelocked solid-state lasers such as Ti:Al_2O_3. However, the theory nevertheless provides a good insight into the modelocking process.

Experimental observations have shown that any forced modelocking influence becomes unimportant once short pulse formation has been established, ie. the laser essentially becomes passively modelocked. However, if reliable coupled-cavity modelocking is to be achieved, at least in colour-centre lasers, the forced modelocking influence has been necessary to initiate the process. On the other hand, coupled-cavity modelocking in the Ti:Al_2O_3 laser is self-

starting and does not require the influence of additional forced modulation[16]. The dynamic reflectivity of the common output mirror may be equivalently represented as a dynamic change in the round-trip gain which is similar to the effect produced by a fast saturable absorber modelocker[17,18]. Assuming that the gain recovery time is slow compared to the duration of any fluctuation of the cw intensity and that the nonlinear response is fast, it has been shown[17] that modelocked pulses can build up provided

$$\frac{\kappa}{g} > \beta\sigma\tau_p \tag{4.2}$$

where g is the saturated gain prior to a fluctuation having a duration τ_p, σ is the gain cross section, β is a parameter dependent on the pulse shape ($\beta = 0.85$ for $sech^2$ pulses and 0.75 for gaussian pulses) and κ is a constant which depends upon the nonlinearity, the loss and the coupling between the two cavities. This condition ensures that a temporary peak in the laser radiation will experience a net gain. The gain cross section for Ti:Al_2O_3 is ~10^{-19} cm^2, while it is ~10^{-17} cm^2 for KCl:Tl°(1), thus the Ti:Al_2O_3 laser should self-start more easily, as is observed in practice. Experimental observations show that the coupled-cavity modelocked Ti:Al_2O_3 laser starts from mode-beating or random noise[19], while the colour centre lasers need to be synchronously pumped. Self-starting has been observed in coupled-cavity modelocked colour-centre lasers by either eliminating stray reflections or enhancing the initial mode-beating[20,21]. In all cases the effect is to shorten the duration of any intensity fluctuations within the laser in agreement with the trend predicted by equation (4.2). Reliably self-starting coupled-cavity modelocked colour-centre lasers still seem to require some external forced modulation.

Conventional fast saturable absorbers have a very limited application as modelocking elements because of the conflicting requirements of having a fast response, large absorption change and low insertion loss. The coupled-cavity scheme works so well because of the relatively large number of easily adjustable parameters, which make it possible to satisfy these requirements simultaneously. The technique is especially applicable to laser materials such as Ti:Al_2O_3, Nd:YAG/YLF, etc which have long upper-state lifetimes since dynamic gain

saturation is not required, but care must also be taken to avoid Q-switching in some of these systems.

Self-starting operation in Ti:Al_2O_3, Nd:YAG/YLF, etc require high intensities for initiating the modelocking process, which imply strong nonlinear phase shifts at the pulse peaks. In addition, these lasers operate at wavelengths where the material dispersion of both the optical fibre and gain media are large. Strong interactions between the nonlinear phase shifts and the GVD can thus be expected. In such systems the interaction between SPM and GVD (which maybe artificially produced by prisms) may provide considerable pulse shaping in addition to that provided by the (real or artificial) saturable absorber which also provides stability by preventing the growth of noise fluctuations before and after the pulses[22,23].

In such lasers, theoretical considerations and experimental results suggest that for overall positive GVD, the pulses are relatively long and highly frequency chirped. In this regime gain dispersion or other bandwidth limitation provides an additional pulse shaping mechanism by shaving off the high and low frequency wings[23,24], ie. only the central portion of the pulse where the instantaneous frequency shift is small will fall inside the effective gain bandwidth. The pulse duration is kept in balance by the broadening due to the GVD while the spectral narrowing provided by the frequency filter is balanced by the spectral broadening produced by SPM. In this regime, the pulse shortening provided by the action of the coupled cavity strongly affects the pulse durations, which, in contrast, are not a strong function of the amount of SPM. Thus, the effective fast saturable absorption is necessary for pulse shortening and stable modelocked operation. Increasing the amount of positive GVD should lead to the generation of longer, more highly chirped pulses, as experimentally confirmed.

The positive GVD in the main resonator due to the gain medium, birefringent filter etc. will lead to pulse broadening and frequency chirping in the usual way. This frequency chirp on the pulses in the main resonator is also modified on each round trip due to the addition of the chirped pulse from the auxiliary cavity. As a result, the pulses entering the auxiliary cavity will also have an initial chirp which interacts with the positive GVD of the fibre to broaden the

pulse durations and decrease the amount of nonlinear frequency chirp. Since these pulses are fed back into the main cavity temporally broadened and with reduced nonlinear phase shift, the pulse shortening effect of the coupled cavity will also be weakened. This is one difference between the effect of conventional fast saturable absorbers and the self-amplitude modulation provided by the coupled cavity - the latter not only produces an effective gain change, but can also produce a nonlinear frequency chirp due to the addition of the two differently chirped and shaped pulses. In this regime the pulses can be compressed outside the laser to obtain durations which are approximately limited by the inverse of the oscillating bandwidth. However, it should be noted that the pulse bandwidths are smaller for positive GVD than for negative GVD, so that the shortest pulses will be generated with intracavity compression techniques.

In the presence of negative GVD, short pulses can be produced which are relatively chirp free. The influence of SPM and GVD produce pulse shaping in a way analogous to soliton shaping[25], which has been discussed in chapter 1. In this case the GVD and SPM cooperate to produce pulse compression inside the laser which leads to additional pulse shortening. Here the amount of SPM has a stronger influence on the pulse duration compared to the pulse shortening effect of the coupled cavity. The latter is still required to provide stability by ensuring that there is a net loss before and after the pulse. This is necessary for two reasons: to prevent the growth of cw radiation in the cavity arising from noise; and to prevent breakup in the wings of the main pulse due to incomplete compensation of the nonlinear frequency chirped portions of the pulse by the negative GVD.

Decreasing the net negative GVD, for a fixed amount of SPM and self-amplitude modulation, leads to the generation of shorter pulses until the laser finally becomes unstable. The size of this unstable region depends on the strength of the SPM and effective fast saturable absorption. Obviously, the larger the SPM, the more negative the dispersion that is required to maintain stable operation. The instability results because light which has a finite bandwidth will require more gain at the centre frequency, because the frequencies which are

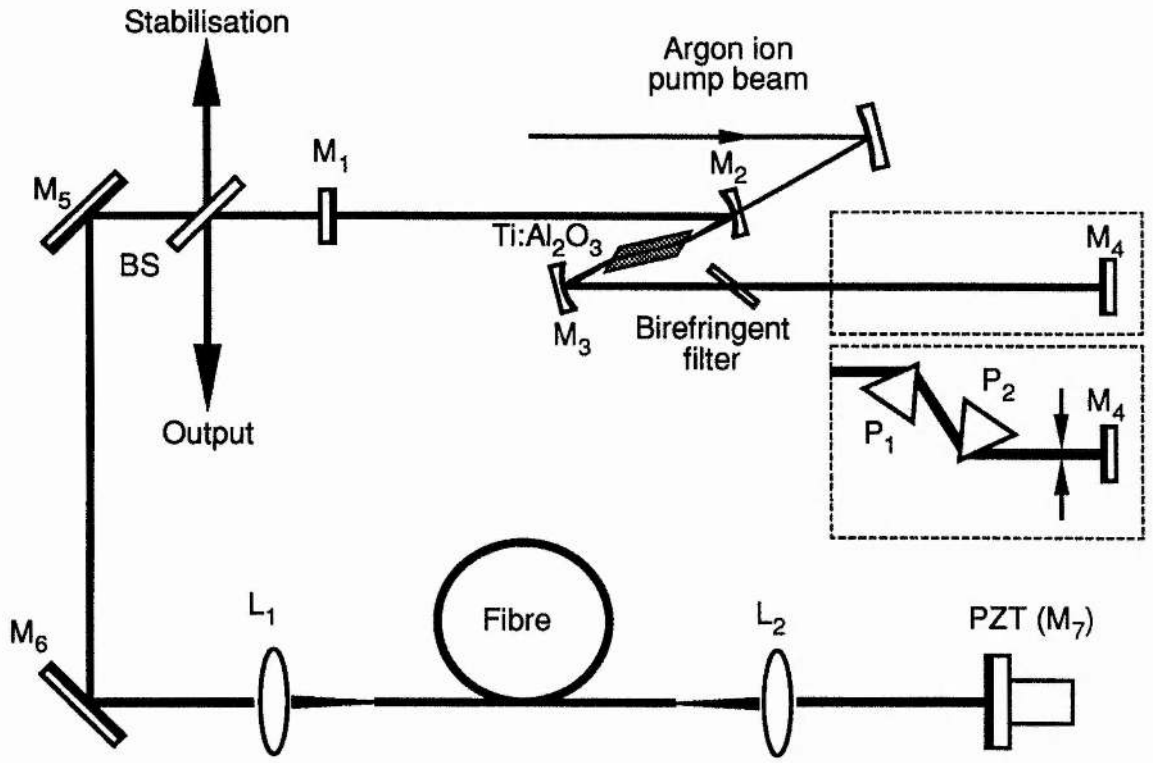

Figure 4.3. Schematic diagram of the cavity configuration for the coupled-cavity modelocked Ti:Al_2O_3 laser.

off line centre will see less gain and as a result the gain at line centre must rise above the loss during the occurrence of a pulse. Some loss modulation is therefore necessary to ensure that this gain window is closed before and after the pulse has passed if stable operation is to be maintained. The addition of properly balanced SPM and dispersion can result in the generation of shorter pulses than for zero SPM[22,23,25]. The shortest pulses can therefore be obtained for GVD which is less than or equal to zero, with a relatively small amount of loss modulation. The nonlinearity necessary to achieve these moderate amounts of loss modulation (~1%) is easily achievable in optical fibres of the type used in coupled-cavity modelocked lasers.

The key parameters determining the pulse durations in lasers such as the Ti:Al_2O_3 are, therefore, the intracavity SPM and GVD together with saturable absorption (real or artificial). With proper control of these parameters it is possible to generate pulses having durations in

the sub-100 fs regime. On the other hand improperly balanced SPM and GVD can result in pulses broadening and/or instabilities.

4.3 The Experimental System

The experimental arrangement for the coupled-cavity modelocked Ti:Al_2O_3 laser is illustrated schematically in Figure 4.3. The Spectra-Physics Model 3900 system, described in chapter 3, formed the bases for the modelocked laser. The main resonator, consisting of mirrors M_1 to M_4, was extended to between 1.5 m and 1.8 m by removing the two plain mirrors (M_1, M_4) from the laser enclosure and placing them in separate mounts attached directly to the optical table in appropriate locations. The cavity was extended in such a way that the 20 mm long Brewster-angled Ti:Al_2O_3 gain medium was located near the centre of the resonator. The standard Spectra-Physics Model 3900 cavity optics (see chapter 3) were used. It is worth noting that both of the plane mirrors (M_1, M_4) were anti-reflection (AR) coated on their second surface and were also wedged to minimise spurious Fabry-Perot effects. This was necessary in the modelocked laser where large oscillating bandwidths were required. It was especially important for the coupled-cavity laser because it is known that spurious reflections can increase the self-starting threshold for passive modelocking by inhibiting the laser mode coupling[26]. The pump laser was either a Spectra-Physics Model 2030 or Model 2040E argon-ion laser which operated on all-lines in the visible at powers up to 15 W in a TEM_{00} mode. This laser has already been described in chapter 3. The Ti:Al_2O_3 laser was tuned by means of either a three-plate Lyot filter or a single-plate birefringent filter (BRF).

The nonlinear external-cavity section was formed between the laser output coupler, M_1, and the mirror M_7, which was mounted on a piezoelectric translator (PZT). This mirror was made by evaporating a thin layer of gold onto a microscope coverslide where the intention was to keep its weight to a minimum to avoid a significant decrease in the resonance frequency of the PZT/mirror combination. A length of optical fibre which provided the nonlinearity was

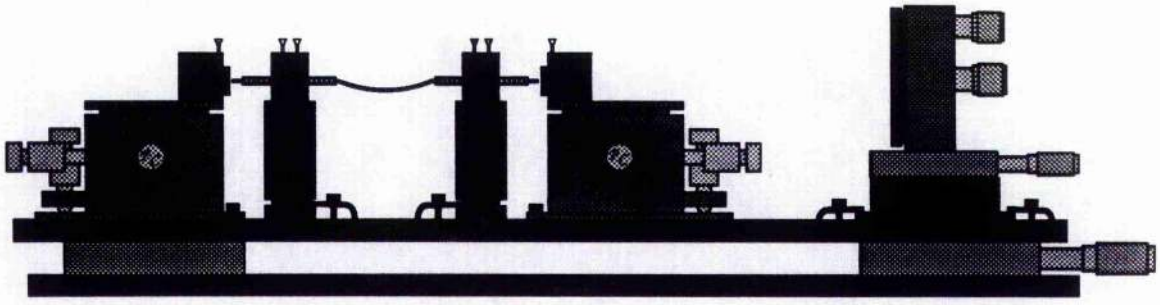

Figure 4.4. Diagram of the breadboard arrangement used to hold the optical fibre and cavity end mirror in the coupled-cavity modelocked laser.

placed within this coupled-cavity section and both ends of the fibre were cleaved and mounted securely in fibre-retaining chucks. The laser radiation was coupled into and out of the fibre using diode collimating lenses (Melles Griot) which had a numerical aperture of 0.500, and a working distance of 1.13 mm. In order to reduce back reflections, these objectives were AR-coated on all surfaces except the one which faced the fibre-end. The space between the fibre-end and the objective was filled with Polyalphdolefin compound gel (n = 1.465), used as index matching fluid to suppress similar reflections from the other objective surface and from the fibre. This oil had sufficient viscosity so that no elaborate means of containing it was necessary - it would stick between the lens and fibre chuck, aided only by a piece of plastic placed below the objective. The fibre chucks were held in fixed mounts, while the objective lenses were held in Microblocks (Photon Control Series) which provided xyz translation. It was found that angular adjustment was not essential to achieve good coupling efficiencies (typically > 60% throughput was obtained) provided reasonable care was taken when initially locating the components. It is worth mentioning that lighter halocarbon series compounds were also tried as index matching fluids, but it was found that these could not withstand the high optical intensities incident on the fibre ends.

The PZT mirror, M_7, was mounted on a translation stage and positioned approximately 10 - 15 cm from the end of the optical fibre. The objective lens which collected the light from the fibre, was positioned so that this light was focused onto the mirror which was aligned to retroreflect it back into the fibre. The optical fibre and coupling optics were

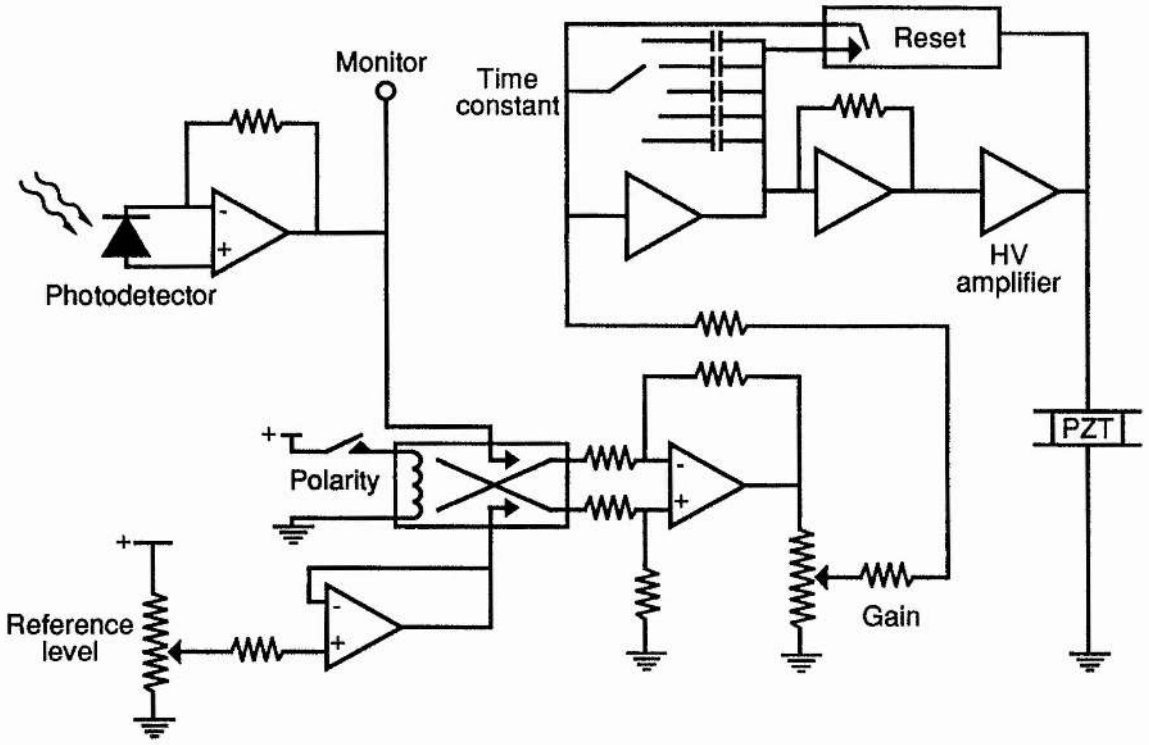

Figure 4.5. Schematic diagram of the electronic feedback circuit used to stabilise the coupled-cavity modelocked laser.

mounted on a movable bread-board so that the length of the external cavity could be varied easily without affecting the fibre coupling arrangement. This scheme is illustrated in figure 4.4. The laser output was taken via the beam splitter, BS, which typically had an intensity transmission of between 60 - 70% depending on the exact laser wavelength. The beam-splitter was partially reflection coated on one surface and AR-coated on the other. A variable neutral-density filter wheel was sometimes included in the external cavity enabling the losses and hence the degree of nonlinearity in this cavity to be varied.

Stable operation of the coupled-cavity laser required that an interferometric match be maintained between the main and external cavities so that an electronic stabilisation loop was used to control the length of the control cavity by varying the position of the mirror M_7[9]. The input error signal for the servo loop was usually derived from the average power fed back into the laser from the external cavity, but the average output power from the laser was also occasionally used. These were useful error signals because their average levels varied

periodically with the phase bias of the external cavity as illustrated in figure 4.2. The optical bandwidth of the monitored error signal was sometimes restricted by using a diffraction grating together with an aperture in front of the photodiode. A simplified circuit diagram for the servo loop is given in figure 4.5. The scheme used standard feedback loop techniques. The input signal was compared with an electronic reference voltage, which represented an optical power level from the laser cavity, and the difference was amplified and fed to a high voltage amplifier which drove the PZT. In these experiments, the PZT (Photon Control MGS 15) could provide a total movement of ~15 μm for a voltage change of 150 V. The gain control and variable time constant enabled the total phase shift through the loop to be kept below π at frequencies where the loop gain approached unity, thus permitting stable operation for a range of experimental conditions.

4.4 The Coupled-Cavity Modelocked Laser

It had been demonstrated that the coupled-cavity modelocking process in the Ti:Al_2O_3 laser could easily self-start with no active modulation, unlike its colour-centre laser counterparts. Initially, the aim was to reproduce the results obtained by other workers and fully characterise the system. With this in mind, the laser was constructed as described above with the three-plate BRF inserted as the tuning element. A 2 m length of optical fibre (York Technology Type No SM 800), having a cut-off wavelength of ~800 nm, was inserted into the external cavity which was set to be approximately twice the length of the main resonator. This relatively long length was chosen so as to give the modelocking process the maximum possible chance of self-initiation.

With the fibre coupling efficiency maximised, single-pass throughputs of between 50% and 60% could usually be achieved. The Ti:Al_2O_3 laser was pumped with an all-lines argon-ion laser power of 6 - 10 W, which resulted in average output powers of between 300 mW and 500 mW from the main resonator. Of this output, 70% was sent to the coupled-cavity section so that the fibre launch power was between 200 and 400 mW and the power measured before the retroreflecting mirror, M_7, ranged from 100 mW to 200 mW. The laser

wavelength was set at approximately 850 nm. The alignment of both cavities was optimised and the length of the external resonator was varied about the matching point. However, no increase in the level of the second harmonic generated in the autocorrelator was observed, indicating that no short pulse generation was occurring. In fact, it was not certain that the two cavities were properly matched as no obvious variation in the power from either cavity could be detected.

It was decided to actively modelock the Ti:Al_2O_3 laser so as to relax the starting conditions for coupled-cavity modelocking by reducing the value of τ_p in equation (4.2), in the hope that the cavity lengths could be more easily matched and enhanced modelocking observed. The main resonator length was set to 1.82 m and an acousto-optic (A/O) prism modulator was inserted as close to the highly reflecting plane mirror as possible. The laser was actively modelocked as described in chapter 3. The coupled cavity was again optimised and its length adjusted until the matching point was found, as evidenced by the variation in average power from the laser. (The A/O modelocked laser made it relatively easy to match the cavity lengths.) As the external cavity length was varied about the matching point the second harmonic signal could be seen to periodically increase by several orders of magnitude, indicating that short pulse generation was taking place. If the cavity lengths were left fixed and closely matched the second harmonic would increase at random intervals, as expected for any coupled-cavity laser that is not actively stabilised. Once the cavities were matched and the feasibility of the modelocking technique demonstrated, the A/O modulator was switched off and, as anticipated, the modelocking did self-start.

Once self-starting operation had been demonstrated, the A/O modulator was removed from the cavity and the laser would reliably self-start provided the coupling efficiency and intra-fibre power were high enough for the particular configuration adopted. First, the laser was actively stabilised using the technique described above, by monitoring the average power returned from the control cavity. This was achieved relatively easily by setting the external cavity length so that the modelocked operation could be seen to occur randomly and then

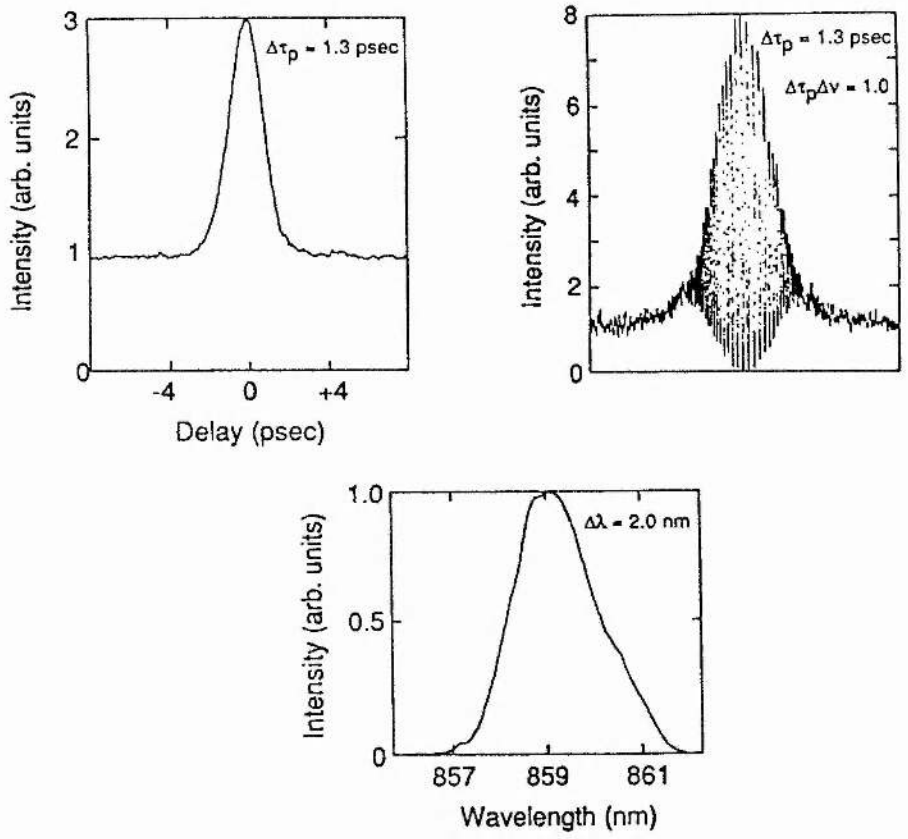

Figure 4.6. Autocorrelation and spectral data for the pulses generated from the coupled-cavity modelocked Ti:Al_2O_3 laser.

closing the stabilisation loop and suitably adjusting the reference level. Once stabilisation had been achieved, the servo loop gain and time constant could be adjusted to give the best operation. With the loop controls optimised, stable modelocked operation could be maintained for periods of several hours. The laser would still drop out as a result of strong environmental perturbations which the feedback circuitry could not track. In this case the loop could usually restabilise the laser so that modelocked operation would continue after the perturbation had ceased, without the need for re-alignment. On the other hand, the inevitable drifts in cavity length, fibre coupling efficiency, etc. which occurred with time meant that eventually the regime of stable operation would fall outside the capture range of the PZT, or the intra-fibre power would fall below the critical level required for proper modelocking and some optimisation would be required before modelocked operation could again begin. Results were taken which enabled the operation of the modelocked laser to be characterised under various operating conditions - these results will be described in the following paragraphs.

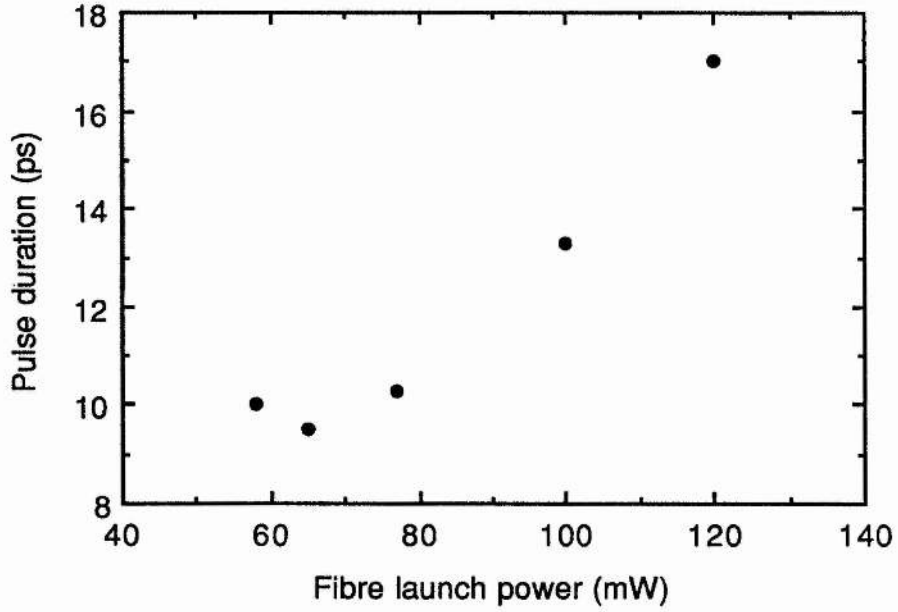

Figure 4.7. Graph illustrating the variation in pulse duration with the average power launched into the 105 cm length of fibre in the external cavity.

The length of optical fibre in the external cavity was replaced with approximately 30 cm of Andrew Corporation fibre (Andrew Corp. Type 48280-1-P). This fibre had an elliptical core having major and minor diameters of 2.5 x 1.25 μm^2 and a Δn of 0.033. It was polarisation preserving and had a cut-off wavelength of ~800 nm. Single-pass coupling efficiencies in excess of 60% could be achieved with the use of index-matching fluid. The use of index matching fluid was not essential provided the coupling efficiency could be maintained above ~60%. If it dropped below this level the laser would not modelock even if the intra-fibre power was proportionately increased, suggesting that the back-reflection into the laser was too strong. This observation agrees with the theoretical considerations presented in reference 26. In practice, the laser was usually operated with matching fluid because of the less stringent requirements placed upon the fibre coupling. In this configuration, the pump power was approximately 6 W, which resulted in an average modelocked output power of 110 mW. The laser was tunable between 830 nm and 960 nm using the three-plate BRF.

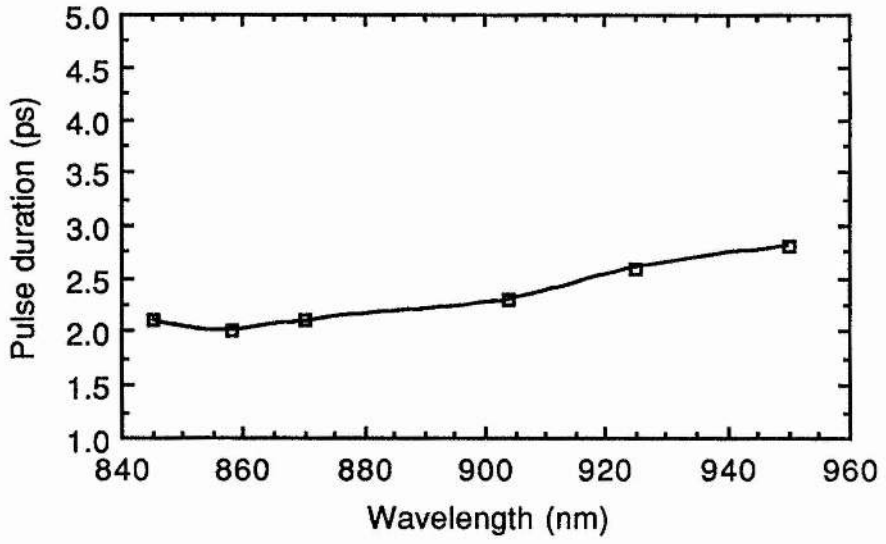

Figure 4.8. Graph illustrating the variation in pulse duration with wavelength for the coupled-cavity modelocked laser.

Pulses having durations less than 3 ps were produced across this entire tuning range. The lower end of this range was determined by the reflectivity of the optics used in the laser. Similar results have been achieved in the 750 - 850 nm spectral region using the low wavelength optics set and suitable optical fibre. The upper end of the tuning range was determined by the increasing losses in the control fibre as the wavelength was increased and by the reduction in the gain available from the Ti:Al_2O_3 as the wavelength approached 1 μm. In both cases the power available was neither sufficient to start nor to sustain the short-pulsed operation.

The shortest pulses were generated with the three-plate BRF at wavelengths near 860 nm and had durations of approximately 1.3 ps.† The peak pulse powers were in excess of 1 kW. Intensity and interferometric collinear autocorrelation traces of these pulses are presented in

† Hyperbolic-secant squared intensity profiles are assumed throughout this chapter.

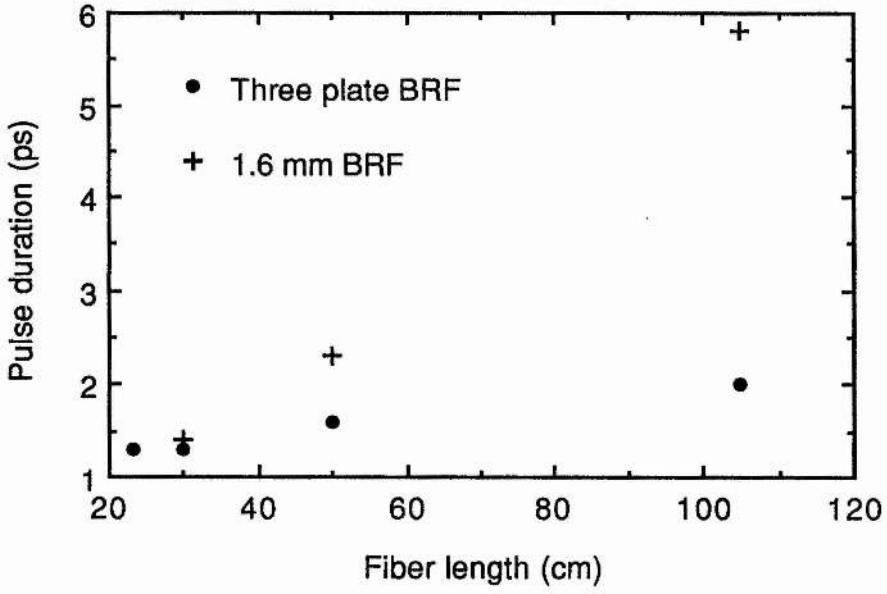

Figure 4.9. Graph illustrating the variation of the pulse duration with the length of fibre in the external cavity for two BRF thicknesses.

figure 4.6, together with the associated pulse spectrum. The calculated duration-bandwidth product for these pulses of $\Delta\tau_p\Delta\nu \approx 1.0$ is rather larger than the value of 0.32 expected for bandwidth-limited pulses. This suggested that the pulses had some degree of frequency chirp. This was further confirmed by the interferometric autocorrelation trace in figure 4.6, where the loss of coherence in the wings of the pulse profile is characteristic of chirped pulses. This behaviour agrees with that predicted by the theory for lasers with overall positive GVD as outlined in section 4.2, which suggests that the pulses should be highly chirped so that spectral filtering provides additional pulse shaping.

The plot included as figure 4.7 illustrates how the pulse duration from the modelocked laser varied with the power launched into the optical fibre in the control cavity. These results were taken when the laser was tuned to approximately 860 nm using a BRF having a thickness of 1.6 mm. The pump power was ~6 W and the average output power was ~100 mW. The launch power was varied using a variable neutral-density filter wheel placed

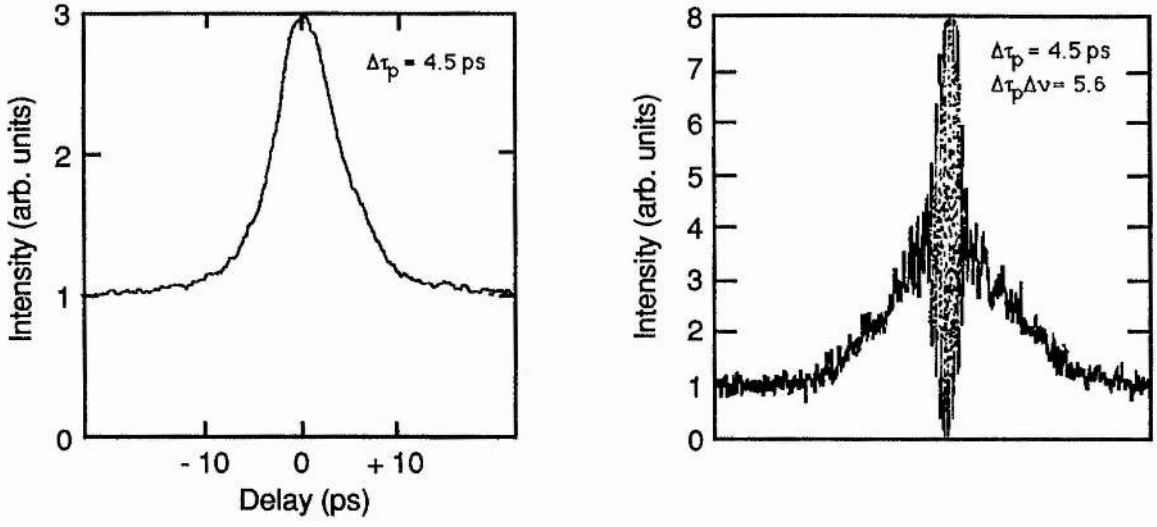

Figure 4.10. Autocorrelation traces showing the modelocked output from the laser before pulse compression.

before the optical fibre which was approximately 105 cm in length. It is clear that there existed an optimum power level for the generation of the shortest pulses. Obviously, increasing the nonlinearity should decrease the pulse duration, but if this nonlinearity becomes too large the pulse shortening will be reduced and the laser can become unstable. In figure 4.8, the data show how the pulse duration varied as the laser was tuned. These data were taken under similar pumping conditions to those for figure 4.7. In this case the laser was tuned using the three-plate BRF and the fibre launch power was ~200 mW. The dependence of the pulse duration on the length of fibre used in the external cavity was also studied, and the results are presented as figure 4.9. The pumping power was again ~6 W resulting in an average output power of ~100 mW. The fibre launch power was kept constant at ~200 mW. Results are included for both the three-plate and 1.6 mm BRF. As explained in section 4.1, low dispersion in the control cavity is preferred for short pulse generation and this explains why shorter lengths of fibre lead to the generation of shorter pulses. Shortening the fibre also increased the self-starting threshold. This behaviour is consistent with the trend predicted by equation (4.2) since decreasing the fibre length effectively decreases the nonlinearity parameter, κ.

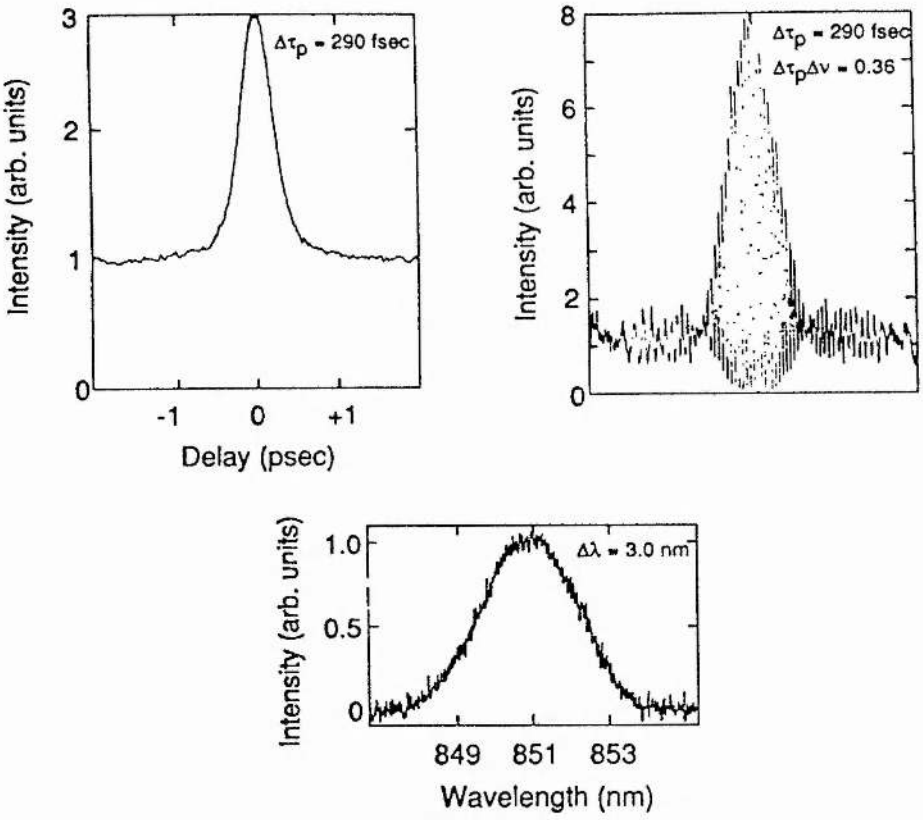

Figure 4.11. Autocorrelation and spectral data for the modelocked pulses after compression in a diffraction grating pair.

4.5 Extra-cavity Pulse Compression

It was evident from the duration-bandwidth products and interferometric autocorrelation traces that the pulses produced from the modelocked Ti:Al_2O_3 laser exhibited a substantial degree of frequency chirp. As illustrated in figure 4.9 the shortest pulses were generated with the thickest BRF. Thinner filters merely resulted in broader pulse durations with increased amounts of frequency chirp. The envelope shape of the interferometric autocorrelation trace suggested that this frequency chirp was linear. It follows, therefore, that these chirped pulses could be efficiently compressed outside the laser to obtain shorter pulse durations as well as higher peak power levels.

The theory of pulse compression has been outlined in chapter 1. A grating-pair pulse compressor was constructed using components which were readily available at the time. This consisted of two holographic diffraction gratings, blazed for 1.06 μm and having

1200 lines/mm. These were placed in the laser output and their separation was varied to produce the shortest pulse durations. The pulse durations were monitored using the intensity autocorrelator, while the degree of frequency chirp remaining on the compressed pulses was monitored using the interferometric autocorrelation technique.

The laser was operated with the 1.6 mm birefringent tuning element and had 29 cm of Andrew Corp. fibre in the control cavity. This provided ~150 mW of useful output power for a pump power of 14 W at a wavelength of ~850 nm. Frequency-chirped pulses having durations of 4.5 ps were generated in this configuration. These uncompressed pulses had duration-bandwidth products of $\Delta\tau_p\Delta\nu \approx 5.6$ and are illustrated in figure 4.10. It was found that a grating separation of 30 mm provided the best pulse compression. This separation resulted in an equivalent dispersion which was calculated to be -0.095 ps^2. Intensity and interferometric autocorrelation traces and an associated spectrum for the compressed pulses are presented as figure 4.11. The compressed pulse durations were 290 fs which implied a duration-bandwidth product of $\Delta\tau_p\Delta\nu \approx 0.36$, which was close to that expected for transform-limited $sech^2$ pulses. The compressed durations represented a compression factor of approximately x15 from the original pulses. The duration-bandwidth product and interferometric autocorrelation trace suggested that while the compressed pulses were close to the transform limit, some residual frequency chirp remained. This was almost certainly due to the presence of a small amount of nonlinear chirp which could not be compensated by the grating pair.

It should be pointed out that the throughput efficiency of the diffraction grating pair at 850 nm was less than 30%. Thus for an average laser output of 150 mW, approximately 40 mW was transmitted after the compressor. This still resulted in a net increase in the peak pulse power from ~400 W before compression to ~1.9 kW afterwards. With properly optimised gratings, transmissions in excess of 80% should be achievable which would result in peak powers in excess of 5 kW.

4.6 Intracavity Dispersion Compensation of the Coupled-Cavity Modelocked Laser

While the technique of extracavity pulse compression provides one means of obtaining shorter laser pulses which are (nearly) chirp-free, it nevertheless suffers serious drawbacks. Most importantly, even optimised grating compressors are relatively lossy. Because diffraction gratings are optimised for a limited wavelength range it is not possible to construct a compressor which is relatively free from losses over a spectral region which is compatible with the tuning range available from Ti:Al_2O_3 lasers. Thus, grating compressors lose useful power which could be made available for experiments. One solution, which will be illustrated in chapter 5, is the use of a prism sequence as an alternative to the diffraction gratings. However, prisms provide much less dispersion than gratings and so the required separation becomes unacceptably large when moderate amounts of frequency chirp arise. Careful choice of prism material and arrangements which provide high dispersion can partially solve this problem, but these configurations almost always have correspondingly large higher-order dispersion as well, which can lead to additional nonlinear pulse chirping.

Because the coupled-cavity modelocked Ti:Al_2O_3 laser produced frequency chirped pulses directly, this chirp must originate within one or both of the laser resonators. It was logical, therefore, to compensate for this chirp within the laser rather that outside it. This overcomes the problems associated with extracavity compression and provides a more compact ultrashort

	SiO_2	ZnSe
λ (μm)	0.866	0.866
$n(\lambda)$	1.45	2.51
$\frac{dn}{d\lambda}$ (μm^{-1})	-0.0153	-0.193
$\frac{d^2n}{d\lambda^2}$ (μm^{-2})	0.0290	0.766
D (ps (nm km)$^{-1}$)	-83.6	-2212

Table 4.1. Refractive index and dispersion data for the external cavity.

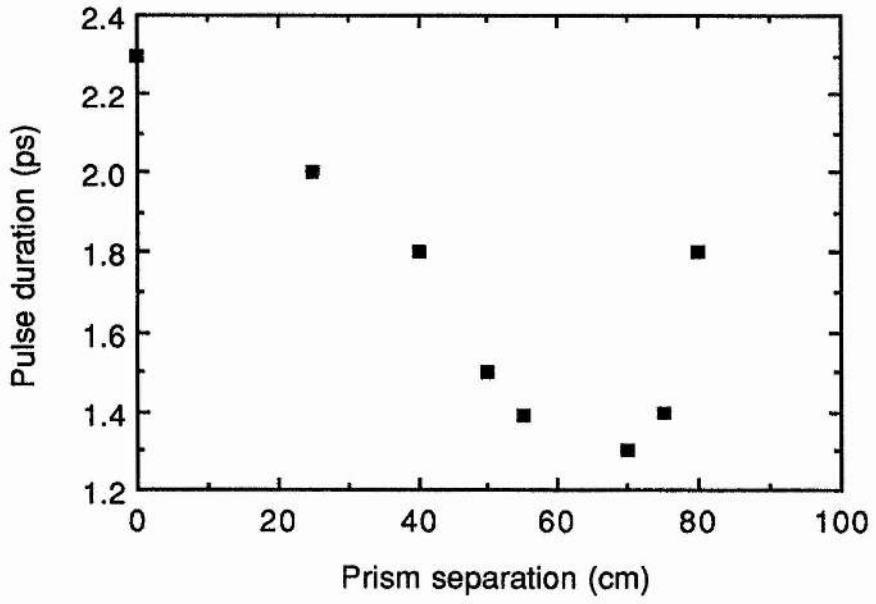

Figure 4.12. Graph illustrating the dependence of the pulse duration on the ZnSe prism separation in the external cavity.

pulse source. It might also be expected to lead to the production of shorter pulses through a soliton-like pulse shaping mechanism. An obvious source of dispersion within the laser was the optical fibre in the external cavity. The dependence of the pulse duration on the fibre length can be seen with reference to figure 4.9 where it can be seen that shorter pulses were generated with shorter lengths of fibre. Using very short fibre lengths was not an ideal solution because, although the dispersion would be reduced, the nonlinearity would also be reduced resulting in an increase in the self-starting threshold and possibly a decrease in the pulse shortening provided by the coupled cavity A preferred approach was, therefore, to introduce dispersion compensation into the external cavity with the aim of minimising the pulse broadening effects of dispersion without affecting the degree of available nonlinearity.

The amount of dispersion in the external cavity can be estimated by considering the material dispersion of the fibre. (To a first approximation, the waveguide dispersion can be ignored.) The refractive index and its derivatives can be calculated from the Sellmeier

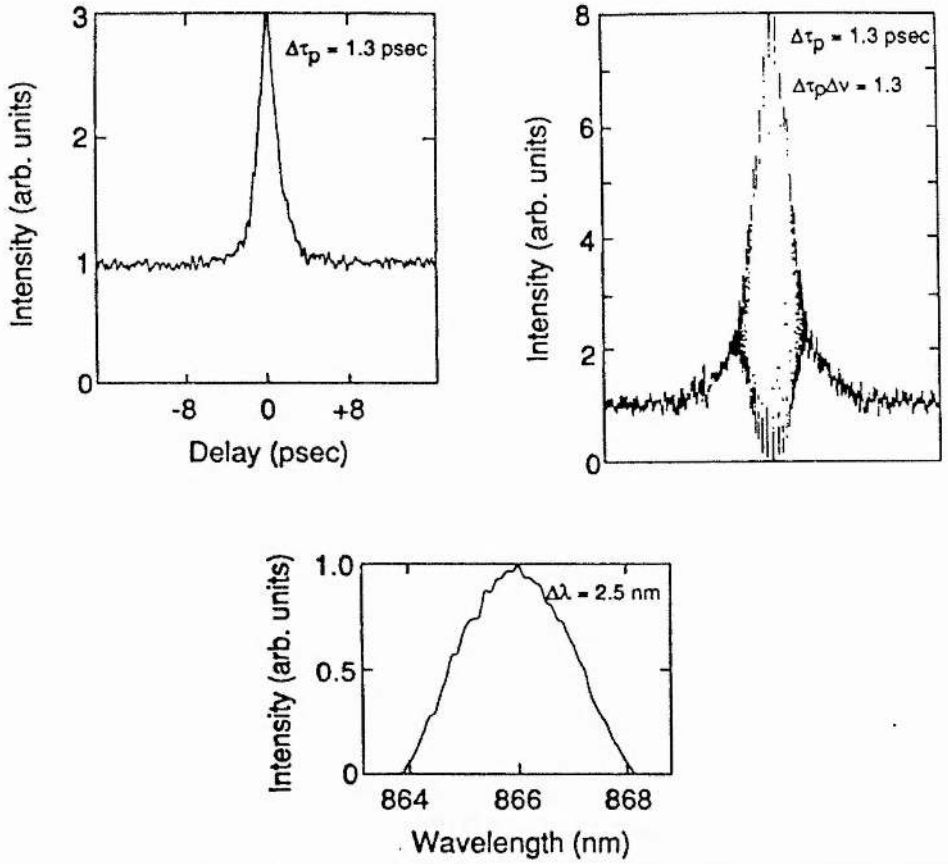

Figure 4.13. Autocorrelation and spectral data showing the modelocked pulses generated by the coupled-cavity laser with dispersion compensation in the external cavity.

expansion for SiO_2. The calculated figures are included in Table 4.1. For a 50 cm length of fibre at 866 nm the single-pass material dispersion was calculated to be 0.0167 ps^2. In order to compensate for this relatively large amount of dispersion without having to use excessively large external cavity lengths, zinc selenide (ZnSe) was chosen for the prism material. The refractive index data for ZnSe is also included in Table 4.1. Four ZnSe prisms, which were cut for minimum deviation at the Brewster angle (at ~850 nm), were included in the control cavity. By varying the separation between the prisms the magnitude and sign of the dispersion could be varied in the usual manner.

The laser was operated with a 1.6 mm tuning element in the main cavity and the separation of the prisms in the external cavity was varied to find the arrangement that gave the

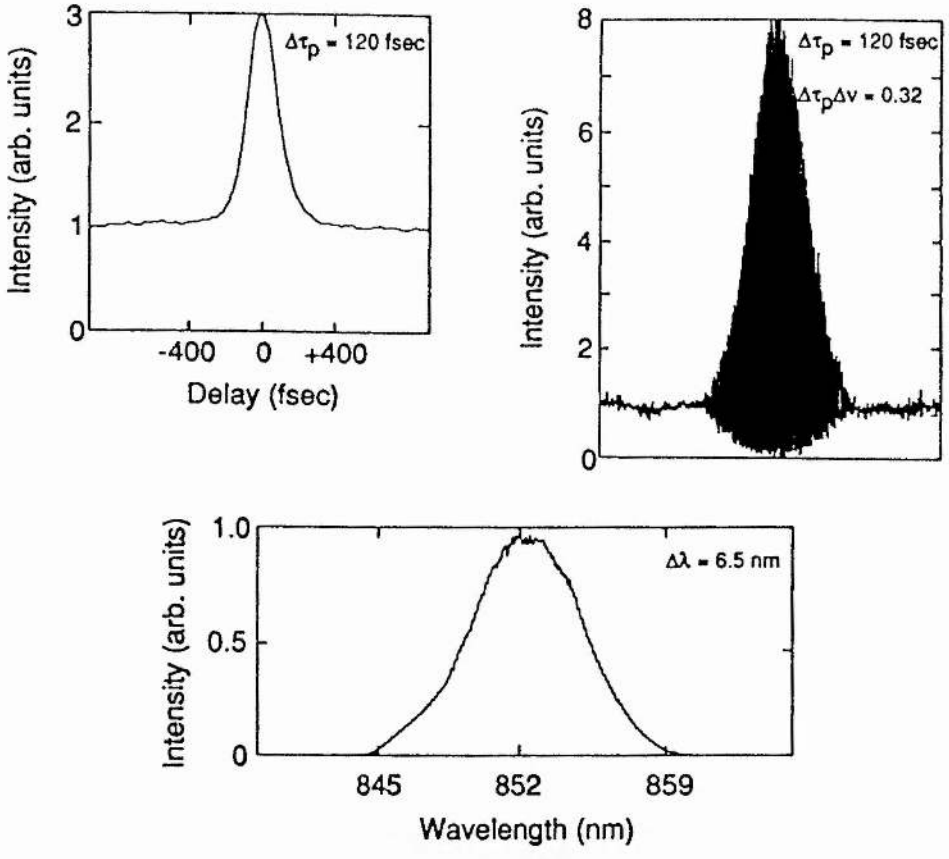

Figure 4.14. Autocorrelation and spectral data showing the modelocked pulses generated by the coupled-cavity laser with dispersion compensation in the main cavity.

shortest pulses. In this case the pump power was fixed at 5 W, which resulted in an average output power of 70 mW and a fibre launch power of 130 mW. The data obtained, as presented graphically in figure 4.12, show how the pulse durations from the laser varied with the separation between the prisms. It follows that the optimum separation was approximately 70 cm. The resulting pulses had durations of 1.3 ps, which taken with the recorded bandwidth implied a duration-bandwidth product of $\Delta\tau_p\Delta\nu \approx 1.3$. These pulses had peak powers of ≈0.7 kW. With the prism separation of 70 cm the net dispersion in the external resonator was estimated to be -0.408 ps^2.

The autocorrelation and spectral data for the pulses produced from this configuration are presented as figure 4.13. The duration-bandwidth product and interferometric autocorrelation trace suggest that there was still a substantial degree of frequency chirp associated with these

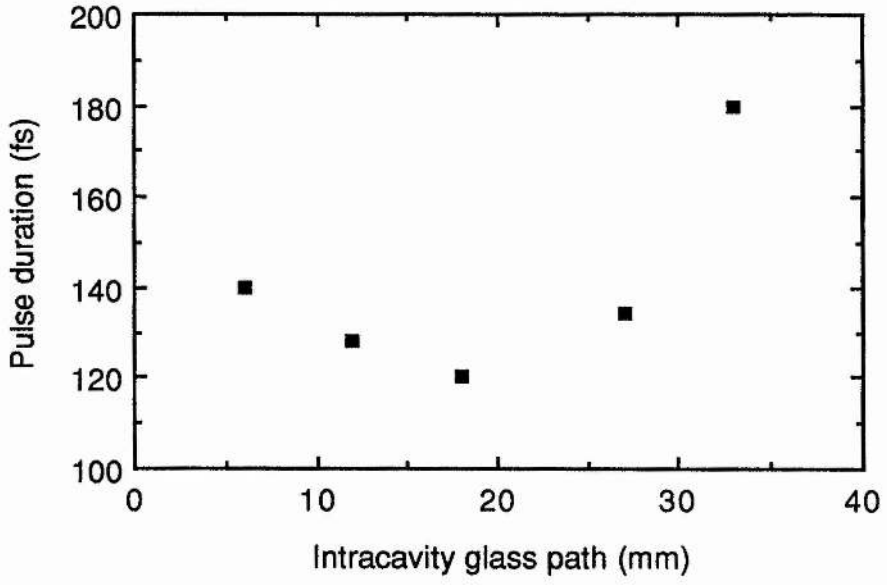

Figure 4.15. Graph illustrating the variation in the modelocked pulse duration with the glass path length for near optimum dispersion compensation by SF14 prisms in the main resonator.

pulses. The calculated prism separation for zero GVD in the control cavity was ~11 cm, however this separation did not result in a significant degree of pulse compression. Even with the substantial amount of negative GVD provided by the much larger prism separation, the compression factor was only about 3, compared with 15 for the extracavity case. It could, therefore, be concluded that the remaining chirp must be a result of processes occurring in the main resonator. In particular, the Ti:Al_2O_3 gain medium must contribute a significant amount of GVD and SPM within the main cavity.

To compensate for these effects two SF14 prisms were placed in the main cavity between the BRF and the plane mirror, M_4. In this configuration the birefringent tuning element was replaced by an aperture located between the prism, P_2 and mirror, M_4, which could be translated in a direction perpendicular to the beam. The prism separation was again varied until the length which gave the shortest pulses was found. This corresponded to a prism separation

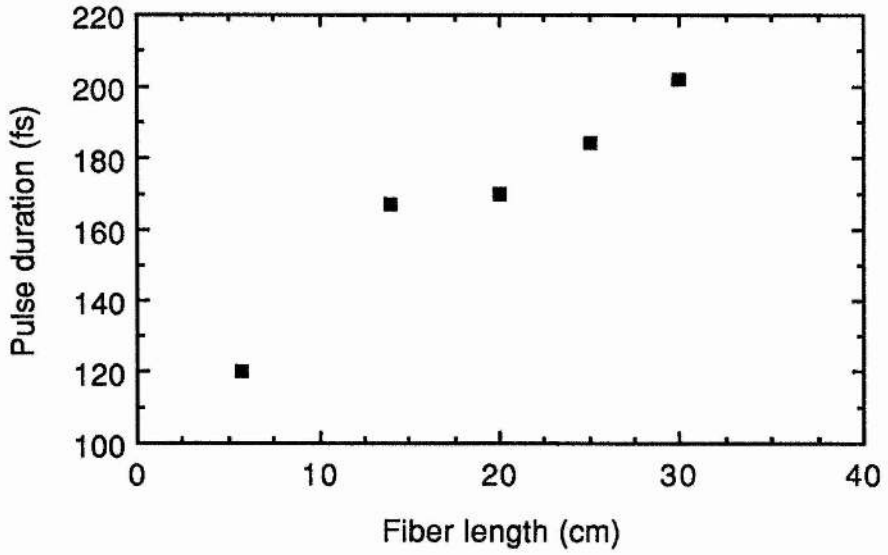

Figure 4.16. Graph showing the variation in pulse duration with the length of optical fibre used in the control cavity of the modelocked laser with dispersion compensation in the main resonator.

of ~35 cm. For this experiment, the length of fibre used in the control cavity was 5.7 cm. The laser was operated with 7.5 W of pump power which resulted in a modelocked output of 200 mW. The optical power incident on the length of optical fibre was 230 mW. In this configuration, the laser generated pulses as short as 120 fs at a wavelength of 852 nm. This represented a compression factor of ~40, which was more than twice that obtained with

	SF14	$Ti:Al_2O_3$
λ (μm)	0.852	0.852
$n(\lambda)$	1.74	1.76
$\frac{dn}{d\lambda}$ (μm^{-1})	-0.0459	-0.0239
$\frac{d^2n}{d\lambda^2}$ (μm^{-2})	0.148	0.0473
D (ps (nm km)$^{-1}$)	-421	-134

Table 4.2. Refractive index and dispersion data for the main cavity.

extracavity compression. The resulting peak pulse powers were >20 kW. The autocorrelation and spectral data for these shortest pulses are presented in figure 4.14. The calculated duration-bandwidth product was $\Delta\tau_p\Delta\nu = 0.32$ which is consistent with transform-limited $sech^2$ pulses. The absence of frequency chirp on the modelocked output is further confirmed by the interferometric autocorrelation trace where interference fringes are observed throughout the pulse profile.

With the position of the prism sequence in the main cavity fixed, the total GVD could be adjusted by varying the amount of prism material through which the cavity beam passed. This enabled fine adjustments to be made while the laser was operating. However, the amount of glass in the beam could only be changed a little at a time because it also changed the length of the main laser cavity. This length change had to be followed by the coupled cavity whose PZT could only move ±6 μm before resetting. Nevertheless, it was possible to easily optimise the pulse durations by controlling the GVD in this way. The variation of the pulse duration with the amount of glass in the beam is illustrated in figure 4.15. It is evident from this plot that there existed an optimum amount of GVD for which the shortest pulses were generated. The primary sources of dispersion within the main cavity were the Ti:Al_2O_3 laser rod and the prism sequence itself. The appropriate refractive index data and its derivatives for these components were again calculated using Sellmeier expansions and this data is included as

	Ti:Al_2O_3	SF14	ZnSe	SiO_2
λ (μm)	0.858	0.858	0.858	0.858
$n(\lambda)$	1.76	1.74	2.51	1.45
$\frac{dn}{d\lambda}$ (μm^{-1})	-0.0236	-0.0450	-0.199	-0.0155
$\frac{d^2n}{d\lambda^2}$ (μm^{-2})	0.0457	0.144	0.801	0.0303
D (ps (nm km)$^{-1}$)	-131	-141	-2292	-86.8

Table 4.3. Refractive index and dispersion data for both cavities.

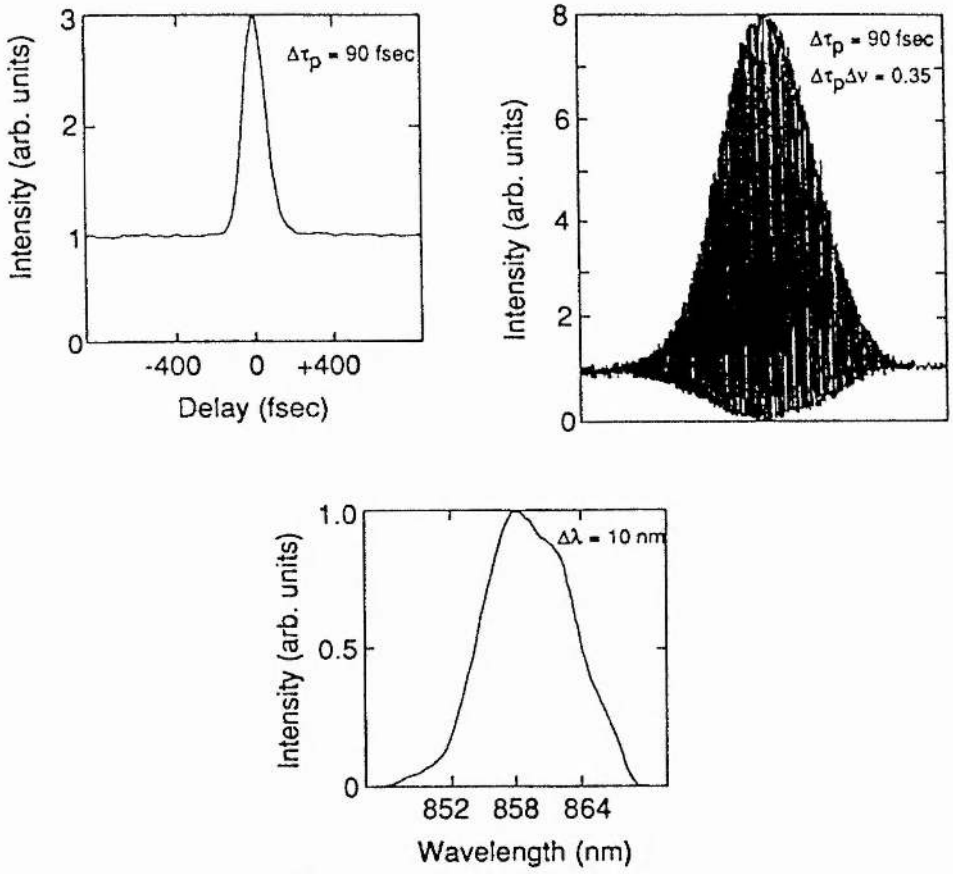

Figure 4.17. Autocorrelation and spectral data for the modelocked pulses from the coupled-cavity laser with dispersion compensation in both cavities.

Table 4.2. For the prism separation of 35 cm, the net GVD within the main cavity was calculated to be -418 fs^2.

With the dispersion compensation in the main cavity optimised, it was observed that the pulse duration still showed a dependence on the length of fibre used in the control cavity. This dependence is illustrated by the graph included as figure 4.16. One implication of this behaviour was that the dispersion in the external cavity still played some role in broadening the pulses produced in the laser. In order to generate the shortest pulses from the Ti:Al_2O_3 laser it was, therefore, necessary to provide dispersion compensation in both the main and external cavities. The autocorrelation and spectral data obtained with this arrangement are presented in figure 4.17. The laser was able to generate pulses as short as 90 fs at a wavelength of 858 nm. These pulses had duration-bandwidth products of 0.35. This,

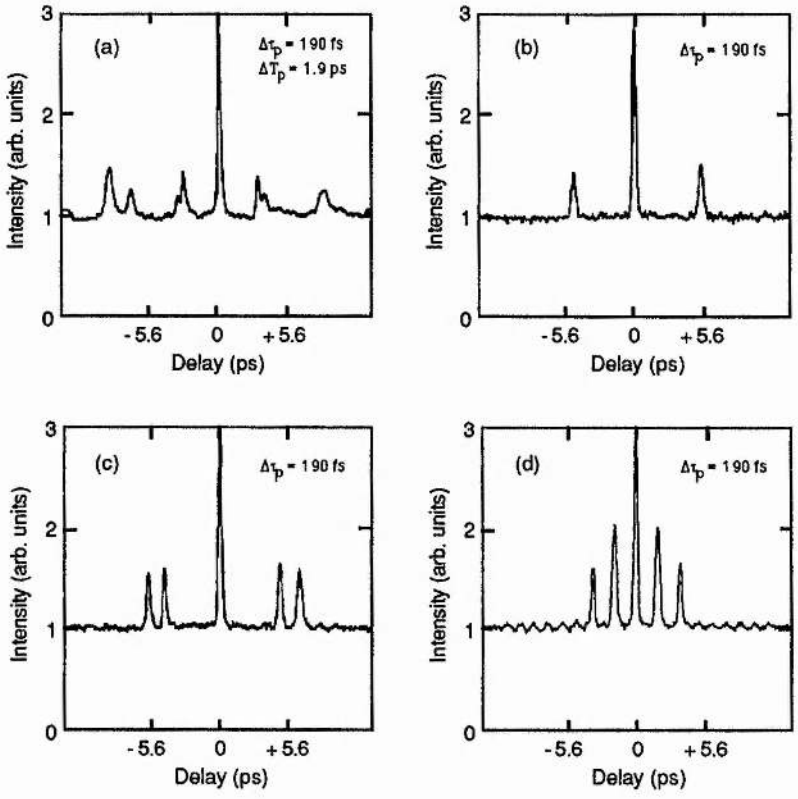

Figure 4.18. Intensity autocorrelation traces showing various stable multipulsing states of the modelocked laser.

together with the interferometric autocorrelation trace in figure 4.17 implies that the pulses were well compensated for frequency chirp. These results were taken for a pump power of 8 W, for which the average output power was 80 mW and the resulting peak pulse powers were ~11 kW. Approximately 110 mW was launched into the 25 cm length of optical fibre used in the control cavity.

The net dispersion for both the main and external cavity was calculated for the laser configuration producing the shortest pulses. The appropriate refractive index data calculated from the Sellmeier expansions is given in Table 4.3. For the prism separation of 14.5 cm in the external cavity the resulting net dispersion was calculated to be -0.046 ps^2. Similarly, for the prism separation in the main cavity of 35 cm, the net dispersion was calculated to be -376 fs^2. These findings again agree with the theoretical modelling which suggest that the

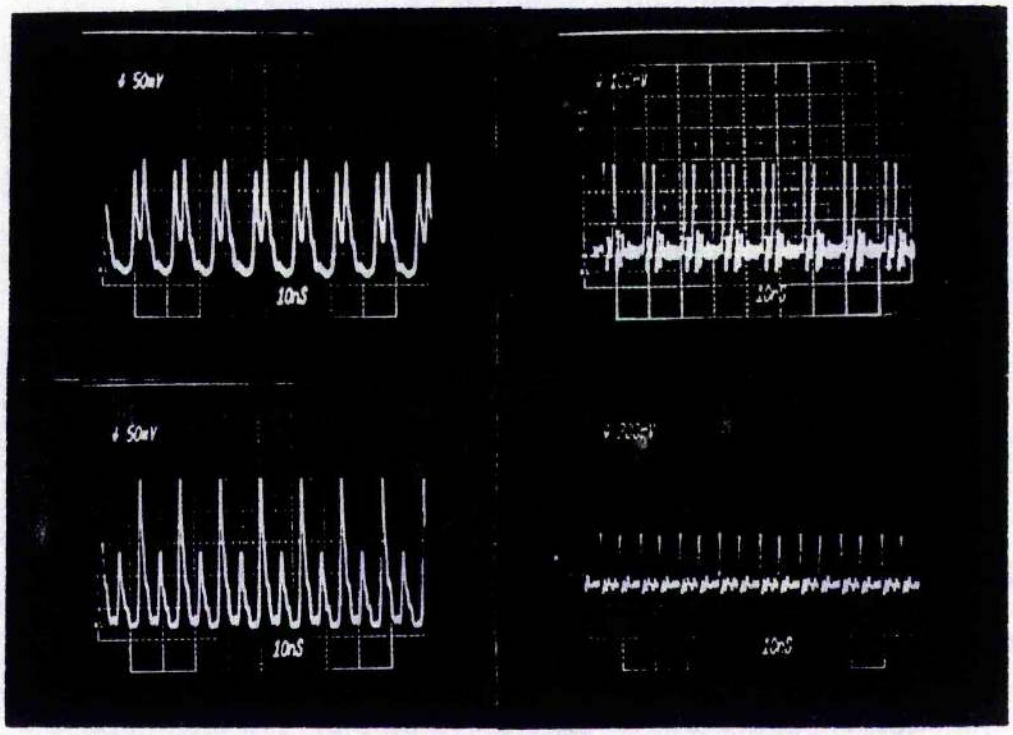

Figure 4.19. Oscillograms showing stable multipulsing states of the modelocked laser where the sub-pulses were relatively far from the main pulse.

shortest pulses are generated with small negative GVD. In all cases the self-starting threshold was observed to decrease with increasing dispersion compensation. This experimental observation implied that low GVD was beneficial even during pulse evolution and led to an effective increase in κ in equation (4.2).

4.7 Instabilities in the Coupled-Cavity Modelocked Ti:Al_2O_3 Laser

Although it was possible to find stable operating regimes within which good modelocking could be achieved, many other stable states were observed in which some aspect of the modelocked operation was compromised. The laser often showed a tendency towards multiple-pulse operation when as many as six pulses were present within one cavity period. The sub-pulses either occurred close to the main pulse and equally spaced from it, or at regular intervals during the cavity period. The intensity autocorrelation traces in figure 4.18

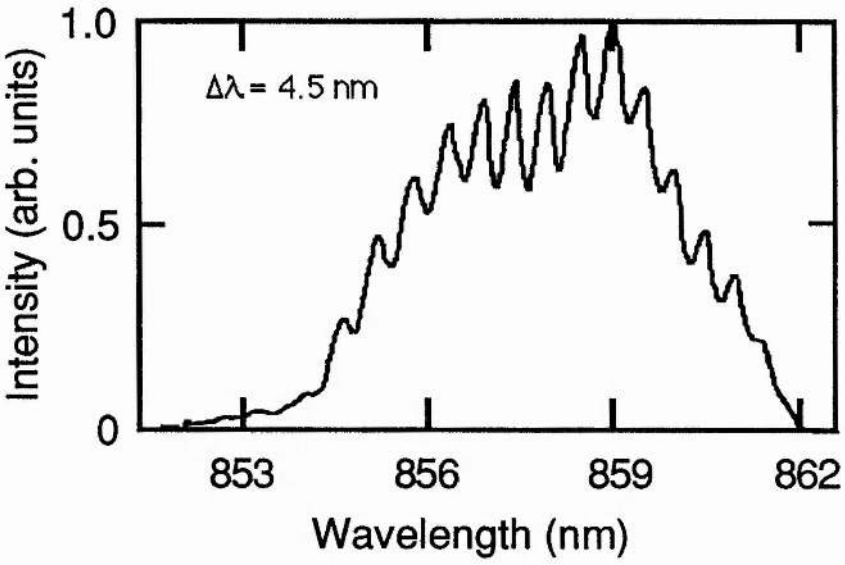

Figure 4.20. Modelocked spectrum corresponding to the multipulsing state shown in figure 4.18(a). The modulation period corresponds to the pulse separation in the time domain.

show some of the commonly observed states where the satellite pulses were close to the main pulse. The oscillograms in figure 4.19 show the pulse train for states where the sub-pulses were further from the main pulse. In all cases these multiple-pulsing features were accompanied by a modulation on the spectrum, similar to that shown in figure 4.20.

The modelocked spectrum did not change in any other way when the laser was multipulsing, in particular, the pulse bandwidth did not increase. The frequency of the modulation on the spectrum corresponded to the separation of the sub-pulses in the time domain. This implied that the sub-pulses occupied the same frequency space as the main cavity pulses and that interference occurred between them (see figure 4.18(a) and 4.20). The timing of the sub-pulses was generally not fixed relative to the main pulses and they could often be seen to drift along between the main cavity pulses, taking anything from approximately one tenth of a second to several seconds to do so. Such a state is illustrated in figure 4.21.

Another common operating regime was characterised by the presence of relatively narrow

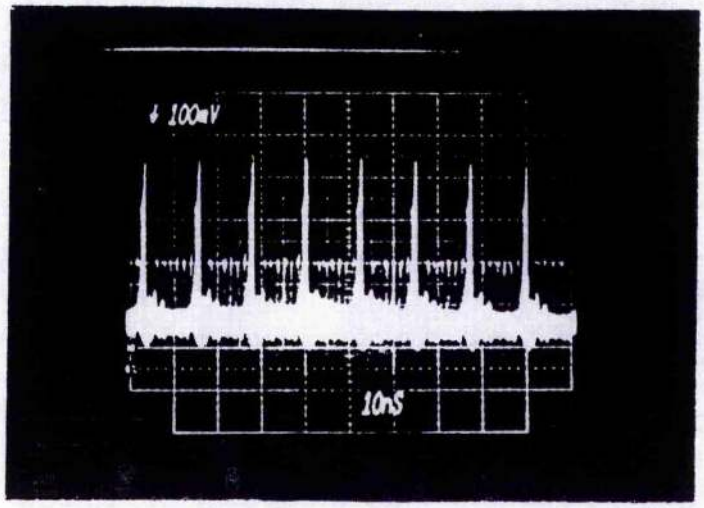

Figure 4.21. Oscillogram showing a 'stable' multipulsing state where the sub-pulse drifted along with respect to the main cavity pulse.

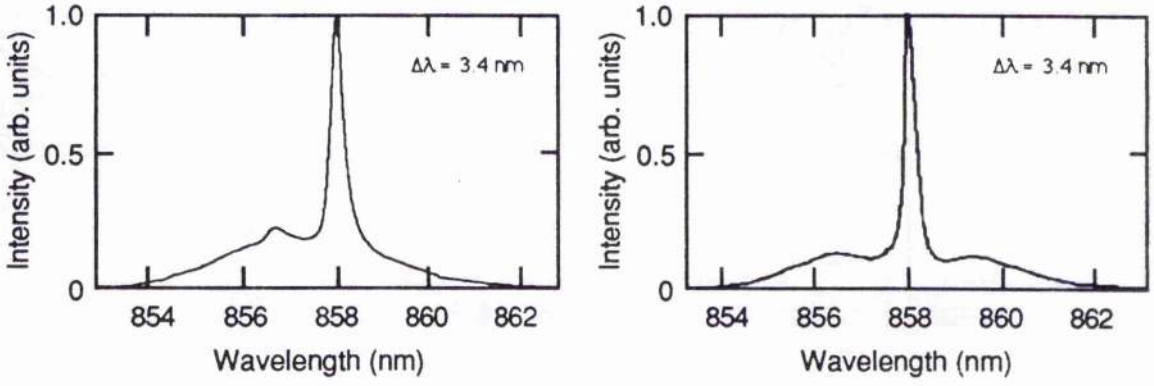

Figure 4.22. Spectra illustrating two of the most commonly observed states characterised by the presence of narrow spikes superimposed on the modelocked spectrum.

spikes superimposed on the spectrum of the modelocked laser as illustrated in figure 4.22. These spikes could appear anywhere across the spectrum, and were sometimes present at wavelengths well removed from the modelocked spectrum when sufficient gain was available in these regions. Although these spike features were readily observed in the frequency domain it was significant that the monitored modelocked pulse train and autocorrelation traces offered no evidence of their existence. We believe that these features corresponded to the spectrum of the unmodelocked laser breaking through the much broader modelocked spectrum. When these spectral spikes were present it was most likely that the laser output consisted of either modelocked pulses with a broad, low energy pedestal, or a modelocked pulse train which

coexisted with a very low intensity cw beam. Several distinct states have been monitored which were characterised by significantly different levels of second harmonic intensity even though the pulse duration and the total average power from the laser remained constant. This was due to different ratios of modelocked to unmodelocked radiation in the laser.

All of these effects were associated with a high level of peak pulse power in the fibre, which in turn corresponded to a greater nonlinear phase shift than was desirable for modelocking. Excess phase shifts lead initially to the generation of broader pulses. With even higher peak powers, the peak phase shift could exceed 2π so that there existed more than one point of optimum interference. Eventually, the pulses became totally unstable. Within the parameter range required for self-starting operation, the peak nonlinear phase shift in the fibre was estimated to often exceed 2π. This could be one explanation of the multiple pulsing. Another possible cause could be the presence of nonlinear frequency chirp resulting in pulse splitting because the linear GVD compensation could not compress the wings of the pulses. The laser seemed able to accommodate excess peak power levels by either multiple-pulsing, or by confining some of the energy into unmodelocked radiation such that in each case, there was a corresponding decrease in the peak pulse power.

The obvious way by which these undesirable effects could be avoided was to reduce the power launched into the fibre, but this made the self-starting conditions for modelocking more difficult to satisfy. Often the stable operating window for good modelocking seemed to lie at power levels which were below the threshold for self-starting such that the modelocked laser would tend to exhibit some of the undesirable effects mentioned above. It was difficult to precisely identify the stable operating window for a particular operating regime. In practice one had to achieve modelocked operation and then carefully adjust the pump power, the coupling efficiency and the relative phase mismatch between the cavities, the wavelength and the average power in the fibre until satisfactory stable modelocking was observed.

A coupled-cavity scheme has also been used with an acousto-optically modelocked

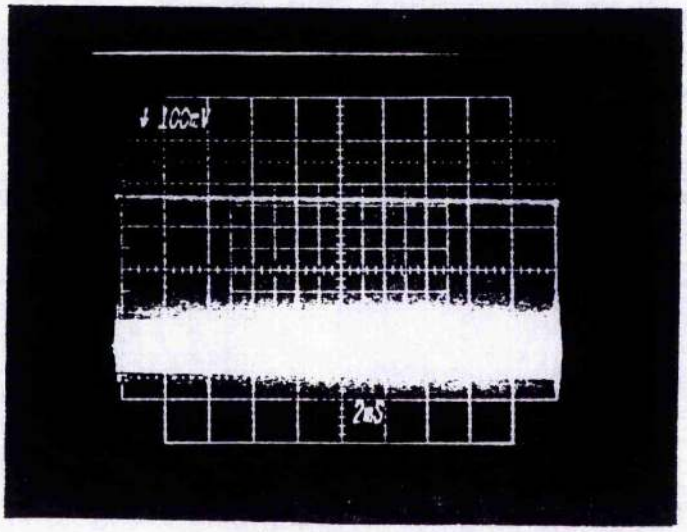

Figure 4.23. Oscillogram showing a stable modelocked pulse sequence.

Ti:Al_2O_3 laser. With the laser already producing relatively short pulses (~100 ps), the pulse shortening effects of the nonlinear external cavity could be utilised more easily than in the self-starting regime. The behaviour of the laser in terms of pulse duration was similar to the self-starting case, although it was possible to operate with much lower intra-fibre powers so that the undesirable effects mentioned above could be more easily controlled. For this reason the acousto-optic modelocked, coupled-cavity laser still represents a serious option for reliable ultrashort pulse generation as compared to the purely passive self-starting laser.

The behaviour of the modelocked laser did not show any particular dependence on the length of the laser resonator provided the two coupled-cavities were interferometrically matched. Modelocking has been observed with cavity lengths ranging from approximately 70 cm to over 2 m. These limits were merely set by the practical constraints imposed by the physical size of the laser and the space available on the optical table. The laser was most often operated with cavity lengths close to 1.7 m as this provided the best compromise between size, stability and high peak pulse powers. It was observed, however, that the stability and degree of modelocking was much better if both the main resonator and the coupled cavity had the same period rather than one being a multiple of the other. This was not surprising as the latitude of stability has been shown to decrease for the latter condition[27].

The stability of the laser for all of the above assessments was good. With the stabilisation electronics switched off and depending on the conditions in the lab, modelocked operation

could be achieved for periods of a few milliseconds to several minutes. When the stabilisation was switched on the laser would remain modelocked for periods of up to several hours, only dropping out as a result of excessive perturbations or gradual relaxation of the alignment. The peak-to-peak amplitude fluctuations on the output of the laser were typically less than 10%. The major contributions to this noise were at frequencies of 50 Hz and 300 Hz and could be traced directly to noise on the output of the pump laser.† The oscillogram in figure 4.23 shows the modelocked pulse train under normal operating conditions. In an attempt to further improve the amplitude stability of the output, an acousto-optic modulator was placed in the pump beam and used as a noise suppressor. However, thermal lensing in the modulator material meant that the usable pump power had to be kept below 6 W if pump beam degradation was to be avoided. In practice this was not a satisfactory solution because of the severe limitations it placed upon the output power available from the laser.

4.8 Conclusions

This chapter has discussed the operation of a coupled-cavity modelocked Ti:Al_2O_3 laser in which the modelocking was self-starting. The modelocked output was tunable from 750 - 900 nm with pulse durations of less than 3 ps being generated throughout. Pulses as short as 1.3 ps were produced at wavelengths near 860 nm. These pulses had average powers of more than 100 mW and peak powers greater than 1 kW. The modelocked pulses exhibited a substantial amount of frequency chirp and could be directly compressed outside the laser cavity to 290 fs. The shortest pulses had durations of 90 fs and were generated with intracavity dispersion compensation in both the main and nonlinear cavities. The operation of the laser, in terms of pulse duration, was shown to depend significantly on the amount of dispersion within the cavities, with the shortest pulses being generated for small overall anomalous dispersion. The operation of the system was also sensitive to other parameters such as the fibre length, the intra-fibre power and the amount of bandwidth restriction.

---

† The amplitude noise on the output of the Model 2040E Ar-ion laser was much better than that on the Model 2030.

Qualitative conditions for stable operation were also identified. The importance of limiting the peak nonlinear phase shift to controllable levels was pointed out and some of the undesirable operating states were also illustrated. The necessity of maintaining the interferometric match between the two cavities was demonstrated. It is this requirement which most of all, limits the simplicity of the modelocking technique. Solutions have been demonstrated which use either resonant nonlinearities[5] in the control cavity, multimode laser outputs[28] or single cavity schemes[29]. In the next chapter another solution to this problem is demonstrated. The self-modelocked Ti:Al_2O_3 laser does not require the use of an external cavity at all, thus removing the need for length matching and is also capable of generating shorter pulses.

4.9 References

1. K.J. Blow and B. Nelson, Opt. Lett. **13**, 1026, (1988).
2. P.N. Kean, X. Zhu, D.W. Crust, R.S. Grant, N. Langford and W. Sibbett, Opt. Lett. **14**, 39, (1989).
3. R.S. Grant, P.N. Kean, D. Burns and W. Sibbett, Opt. Lett. **16**, 284, (1991).
4. J.R.M. Barr and D.W. Hughes, Appl. Phys. B **49**, 323, (1989).
5. U. Keller, W.H. Knox and H. Roskos, Opt. Lett. **15**, 1377, (1990).
6. J. Mark, L.Y. Liu, K.L. Hall, H.A. Haus and E.P. Ippen, Opt. Lett. **14**, 48, (1989).
7. M. Morin and M. Piché, Opt. Lett. **14**, 1119, (1989).
8. L.F. Mollenauer and R.H. Stolen, Opt. Lett. **9**, 13, (1984).
9. F.M. Mitschke and L.F. Mollenauer, IEEE J. Quant. Electron. **QE-22**, 2242, (1986).
10. F.M. Mitschke and L.F. Mollenauer, Opt. Lett. **12**, 407, (1987).
11. K.J. Blow, and D. Wood, J. Opt. Soc. Am. B **5**, 629, (1988).
12. F. Ouellette and M. Piché, Can. J. Phys. **66**, 903, (1988).
13. E.P. Ippen, H.A. Haus and L.Y. Liu, J. Opt. Soc. Am. B **6**, 1736, (1989).
14. D.E. Spence and W. Sibbett, J. Opt. Soc. Am. B **8**, 2053, (1991).
15. H.A. Haus, U. Keller and W.H. Knox, J. Opt. Soc. Am. B **8**, 1252, (1991).
16. J. Goodberlet, J. Wang, J.G. Fujimoto and P.A. Schulz, Opt. Lett. **14**, 1125, (1989).
17. E.P. Ippen, L.Y. Liu and H.A. Haus, Opt. Lett. **15**, 183, (1990).
18. H.A. Haus, J. Appl. Phys. **46**, 3049, (1975).
19. J. Goodberlet, J. Wang, J.G. Fujimoto and P.A. Schulz, Opt. Lett. **15**, 1300, (1990).
20. R.S. Grant and W. Sibbett, Opt. Commun. **86**, 177, (1991).
21. G. Sucha, Opt. Lett. **16**, 922, (1991).
12. H.A. Haus and Y.S. Silberberg, IEEE J. Quant. Electron. **QE-22**, 325, (1986).
23. H.A. Haus, J.G. Fujimoto and E.P. Ippen, J. Opt. Soc. Am. B **8**, 2068, (1991).
24. D. von der Linde, Appl. Phys. B **37**, 1, (1985).
25. O.E. Martinez, R.L. Fork and J.P. Gordon, J. Opt. Soc. Am. B **2**, 753, (1985).
26. H.A. Haus and E.P. Ippen, Opt. Lett. **16**, 1331, (1991).
27. M.N. Kong, J.K. Chee and J.M. Liu, Opt. Lett. **16**, 73, (1991).
28. E.C. Cheung, J.M. Liu and J.K. Chee, Opt. Lett. **16**, 1671, (1991).
29. T.F. Carruthers and I.N. Duling, Opt. Lett. **15**, 804, (1990).

Chapter 5
The Self-Modelocked Ti:sapphire Laser

5.1 Introduction

The previous chapter described the operation of a coupled-cavity modelocked Ti:Al_2O_3 laser, which was able to generate pulses having durations in the sub-100 fs range. In this chapter the implementation of another modelocking technique is discussed which can lead to pulses shorter than 100 fs being generated when applied to the Ti:Al_2O_3 laser. The term 'self-modelocked' was chosen because this type of laser generated pulses in the absence of any modelocking elements within the cavity, by exploiting the Kerr nonlinearity within the gain medium. The experimental results for this self-modelocked laser were similar in many respects to those obtained for the coupled-cavity modelocked laser.

Experimental data will be presented describing the operation of the basic laser, which was able to generate pulses as short as 2 ps and was continuously tunable from 750 - 950 nm. For a pump power of 8 W, the average modelocked output power was ~450 mW which corresponded to a peak pulse power of 2.6 kW. These pulses exhibited significant amounts of frequency chirp and could be temporally compressed outside the laser cavity using diffraction gratings or ZnSe prisms to obtain pulses having durations as short as 380 fs. An intracavity prism sequence, consisting of two SF14 prisms, was included to provide dispersion compensation and this resulted in the generation of pulses as short as 60 fs. For these shortest pulses, the average power was ~600 mW (for ~8 W pump power) and the corresponding peak power was ~110 kW. Using an extra-cavity fibre-prism pulse compressor, pulses as short as 45 fs were produced. Although the self-modelocking process was not self-starting it was self-sustaining. In order to overcome the self-starting problem, an acousto-optic modulator was included in the cavity. This was driven regeneratively from the intracavity laser intensity and provided sufficient modulation to assist the femtosecond pulse initiation.

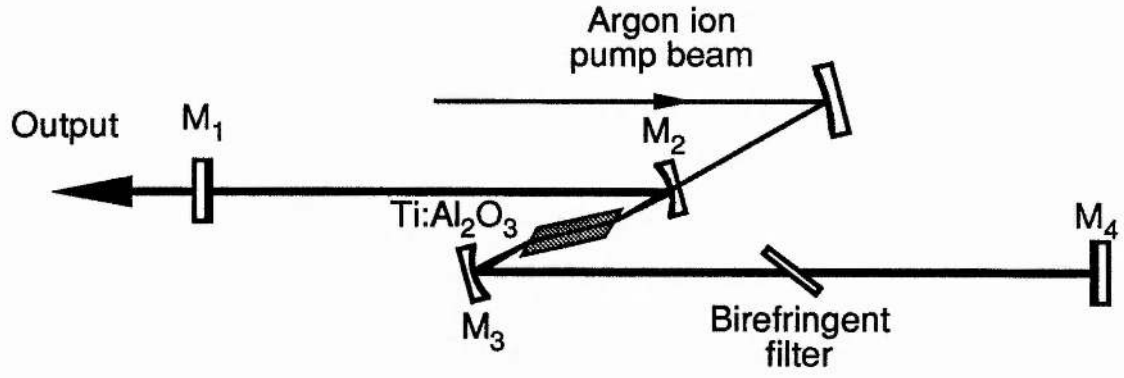

Figure 5.1. Schematic diagram of the cavity configuration of the self-modelocked $Ti:Al_2O_3$ laser.

The chapter will conclude with a review of the current theories concerning the operation of the self-modelocked laser. Several other techniques have enabled the generation of sub-100 fs pulses from $Ti:Al_2O_3$ lasers where passive (saturable absorber dye), active, synchronous modulation, and various coupled-cavity schemes using resonant nonlinearities and even empty external cavities have been used. It is suggested that all of these techniques, including the coupled-cavity scheme described in the last chapter, involve similar basic mechanisms for the generation of femtosecond pulses. These techniques should then be generally applicable to other solid-state laser types.

5.2 The Self-Modelocked Laser Configuration and Operation

As in the the $Ti:Al_2O_3$ laser configurations described in previous chapters, the self-modelocked laser was based on a modified Spectra-Physics Model 3900 laser. The cavity configuration, illustrated in figure 5.1, consisted of an extended resonator measuring between 1.5 and 2.0 m in length with a Z-folded focusing section comprising of two concave mirrors (M_2, M_3) which each had a 10 cm radius of curvature and contained the 20 mm long Brewster angled gain medium. The two long arms of the cavity were arranged approximately symmetrically about this folded section. The output coupling mirror M_1, had an intensity transmission of approximately 3.5% and, as with the other resonator mirrors, was designed to operate over the 850 - 1000 nm spectral region. The laser was tuned by means of a suitably

chosen birefringent filter (BRF). The pump laser was either a Spectra-Physics Model 2030 or 2040E argon-ion system which provided 15 W of all-lines visible power in a TEM_{00} mode. This pump radiation was focused into the Ti:Al_2O_3 crystal via a concave mirror which had a radius of curvature of 23 cm.

In this configuration the laser was able to produce pulses having durations as short as 2 ps without the addition of any discrete modelocking element[1]. In order to achieve modelocking, the following procedure was adopted. The laser output was monitored using a real-time second-harmonic generation autocorrelator together with a photodiode and oscilloscope having a bandwidth of ~400 MHz. The average intensity was also monitored using a photodiode and oscilloscope with a slower response. Initially the laser was tuned to a wavelength which experienced reasonably high gain (typically <900 nm) and aligned for maximum output power. Fine adjustments were made to the alignment to produce strong mode beating as observed on the oscilloscope. This could be facilitated by tapping one of the mounts which held the cavity optics or by sweeping the cavity length and thus enhancing the mode beating effect. These intensity fluctuations could be maximised by carefully optimising the distances between the curved mirrors and the ends of the Ti:Al_2O_3 rod. Minor changes in the alignment of the resonator were made in this way until a tap on one of the cavity mirrors initiated the self-modelocked process. Further adjustments could be made at this stage to improve the stability of the modelocked output. Once a pulse sequence had built up, the laser remained modelocked until some external perturbation caused the process to stop. In general, the self-modelocked operation was not self-starting and required some external influence to restart short-pulse generation once it had ceased.

Initially the laser operated with the output consisting of the TEM_{00} mode together with a higher order transverse mode such as the TEM_{05}. It was later observed that multi-transverse mode operation was not essential for modelocked operation, particularly when the laser produced pulses having durations in the femtosecond regime. In this case the output was greater than 99% TEM_{00}.

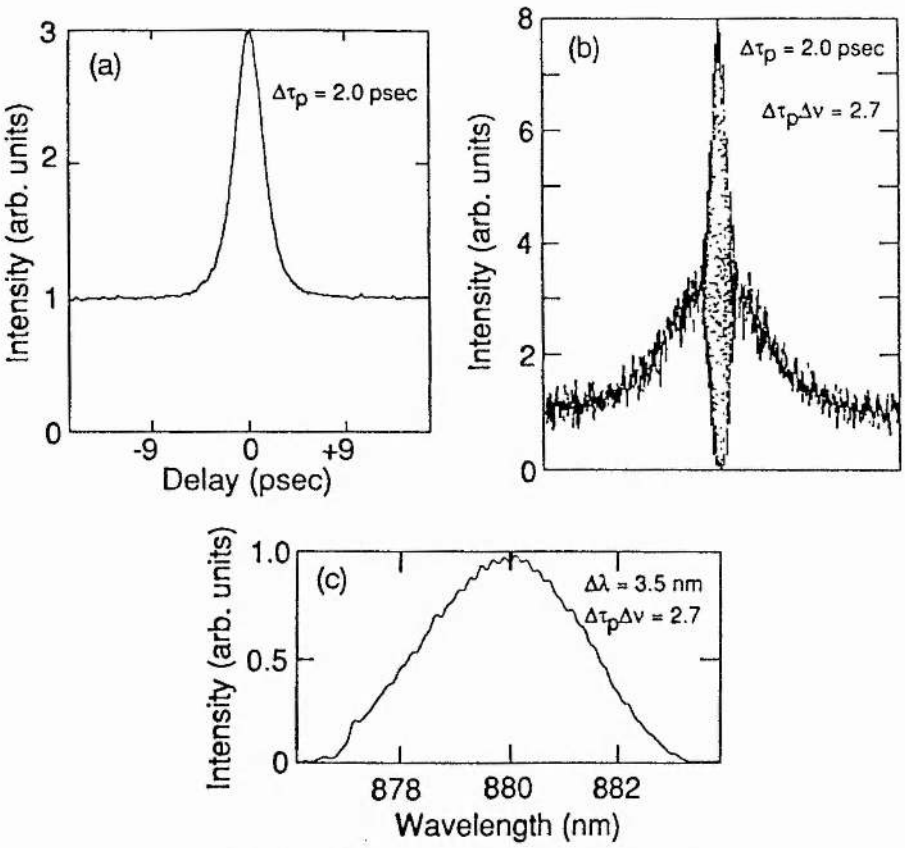

Figure 5.2. Autocorrelation and spectral data for the self-modelocked Ti:Al_2O_3 laser.

In this basic configuration the laser had a threshold that corresponded to an all-lines argon-ion pump power of approximately 1 W. Self-modelocked operation could be achieved for pump powers ranging from approximately 4 - 12 W. With pump powers outside this latter range, the laser output reverted to cw un-modelocked operation. The laser typically produced pulses as short as 2 ps in a configuration with a 1.6 mm thick BRF as the intracavity tuning element. For a pump power of 8 W the average modelocked output power was approximately 450 mW which represented a peak pulse power of 2.6 kW for a repetition frequency of 86 MHz. Second harmonic generation (SHG) intensity and interferometric autocorrelation traces for the modelocked output are illustrated in figure 5.2, together with the associated spectrum. Modelocking could be achieved continuously over a spectral region extending from approximately 830 nm to 950 nm with a single optics set. The lower bound of this region was determined by the reflectivity of the optics. Modelocked operation was also observed

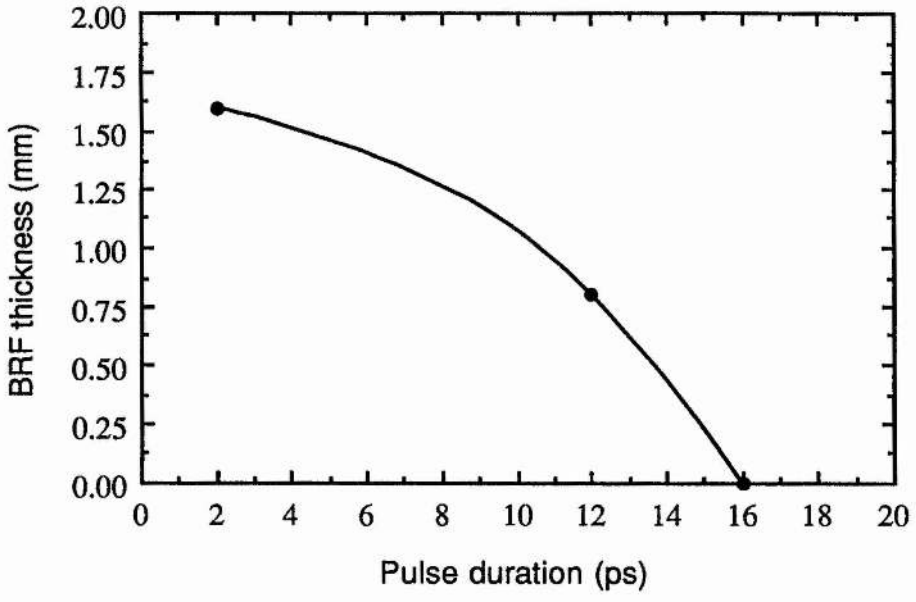

Figure 5.3. Graph showing the variation in modelocked pulse duration with the BRF thickness.

over the 750 - 850 nm wavelength range with alternative optics which were reflection coated for the 700 - 850 nm region. The upper and lower bounds of this modelocked tuning range at 750 nm and 950 nm were due to insufficient gain being available beyond these wavelengths. It is expected that wavelengths outside this range could be achieved with suitable optics. Significantly, it was observed that this modelocked operation depended on exceeding a certain threshold level of intracavity intensity.

It is important to note that the self-modelocked laser was continuously tunable within the spectral regions mentioned above, in contrast to other ultrashort pulse sources. For instance, in the coupled-cavity modelocked laser described in chapter 4, the different amounts of dispersion in the two cavities limited the range of continuous tunability because of the requirement that the cavity lengths be interferometrically matched. The thickness of the BRF used did not significantly affect the tuning range of the self-modelocked laser, but strongly influenced the pulse durations obtained as illustrated graphically in figure 5.3. Generally, the characteristics of the self-modelocked laser (in terms of the choice of tuning element, the

wavelength of operation, etc.) had similarities with those of the coupled-cavity modelocked system described in the previous chapter.

For all of the above measurements the stability of the modelocked output was adequate. Stability depended primarily on the amount of noise in the environment - perturbations which were strong enough could cause the modelocked operation to cease with the laser reverting to the cw regime. Such perturbations could also initiate the modelocked output. The noise and stability of the laser are illustrated by the traces in figure 5.4, where the oscillograms in figure 5.4 (a) show that the noise superimposed on the pulse train is due primarily to mains ripple on the pump laser and occurs at frequencies of 50 Hz and 300 Hz. Figure 5.4 (b) shows the average SHG signal from the modelocked laser and illustrates that the laser could remain modelocked for periods in excess of 30 minutes with only minor fluctuations in SHG output. However, it should be emphasised that the noise on the pump laser represented a major source of instability in the system and could cause the modelocked operation to cease, or to start spontaneously. This is illustrated by the oscillogram presented as figure 5.5 in which the top trace shows the real-time SHG intensity autocorrelation function of the laser output and the bottom trace represents the (inverted) variation in the average pump power. It is evident that this variation could seriously influence the stability and noise associated with the modelocked Ti:Al_2O_3 output.

In order to try to improve both the stability and noise characteristics of the output from the laser, an acousto-optic modulator (Intra-Action Corp. Model AFM 402) was inserted into the pump beam before the Ti:Al_2O_3 oscillator. The modulator was biased so as to deflect ~20% of the power out of the zeroth order, the latter being used as the pump beam. The pump intensity which remained in the zeroth order was monitored using a photodiode and this signal was fed into an electronic servo loop, similar to the one described in chapter 4 for stabilising the coupled-cavity modelocked laser. The low voltage output from the integrator, instead of driving a high voltage amplifier, was fed directly into the external modulation input of the rf oscillator/amplifier used to drive the acousto-optic modulator. This enabled the diffraction

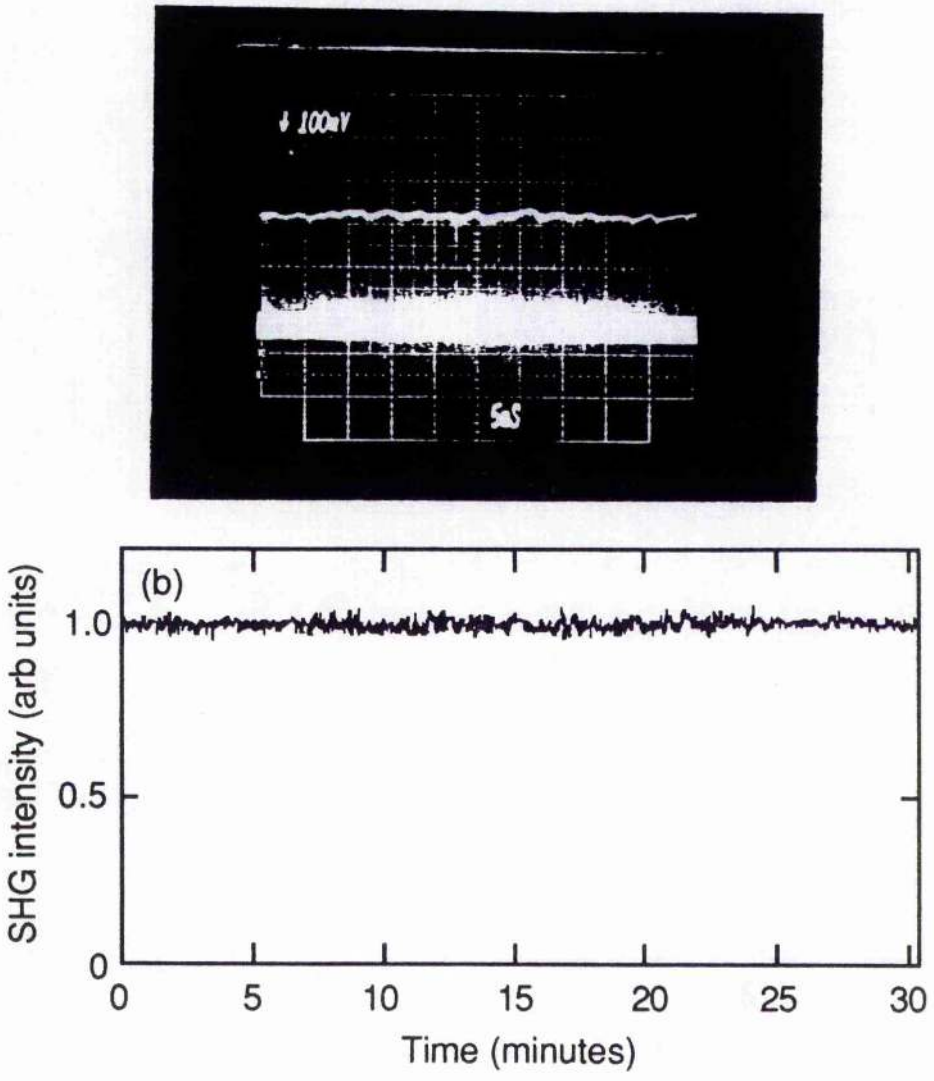

Figure 5.4. Traces illustrating the noise and stability of the self-modelocked laser: (a) oscillogram showing amplitude noise on the modelocked pulse train with predominant contributions at 50 and 300 Hz; and (b) trace showing the long term stability of the SHG output.

efficiency of the modulator to be varied. When the servo loop was closed, the system acted as a 'noise-eater' by varying the amount of optical power diffracted out of the first order in an attempt to maintain the monitored intensity at a preset reference level. With this system in operation, the noise features and stability of the self-modelocked Ti:Al_2O_3 laser were improved considerably. The best performance was achieved by monitoring as the error signal, the average intensity from the output of the modelocked Ti:Al_2O_3 laser, rather than the average

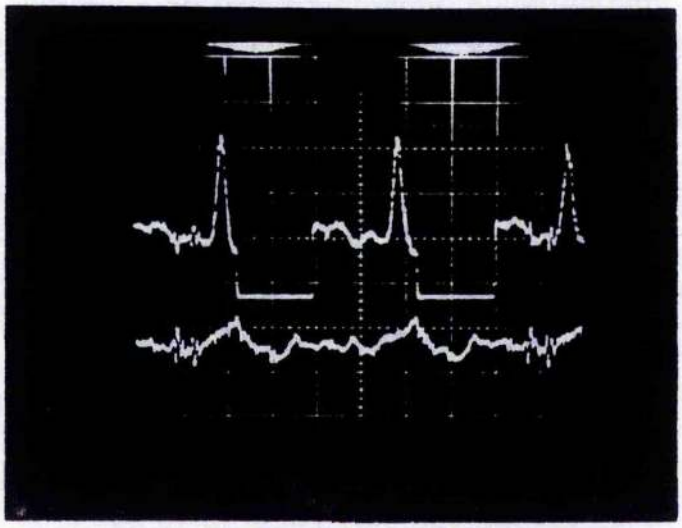

Figure 5.5. Oscillogram showing how the amplitude noise of the pump laser could affect the stability of the modelocked Ti:Al_2O_3 laser: the top trace shows the intensity autocorrelation function and the bottom trace represents the inverted variation in the average pump power.

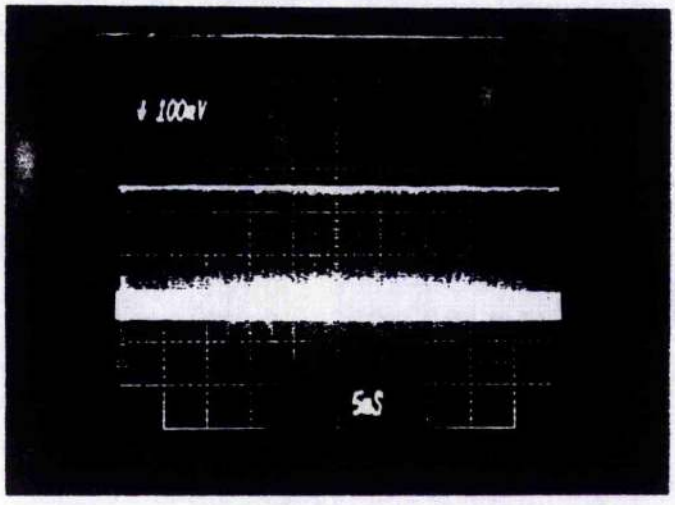

Figure 5.6. Oscillogram showing the amplitude-stabilised modelocked pulse train.

pump intensity. The oscillogram in figure 5.6 illustrates a typical stabilised pulse sequence. Unfortunately, the quality of the pump beam was seriously affected by thermal lensing in the modulator material so that at best, the Ti:Al_2O_3 laser output efficiency was seriously compromised. Generally, self-modelocked operation could not be achieved at all for pump powers exceeding ~5 W which seriously limited the usefulness of the device. Other workers have made similar observations concerning the use of noise eaters with high power ion lasers[2]. If a satisfactory modulator material could be found, the use of noise eaters would dramatically improve the Ti:Al_2O_3 laser stability in many cw applications. Unfortunately, it

was decided that the disadvantages associated with the noise-eater outweighed its advantages and so it was not included as a standard part of the laser system.

It is evident from the interferometric autocorrelation trace shown in figure 5.2 and the associated duration-bandwidth product of $\Delta\tau_p\Delta\nu = 2.7$, that the pulses produced from the laser had a large amount of frequency chirp associated with them. As observed for the coupled-cavity modelocked system, the pulse duration and the frequency chirp increased as the bandwidth of the spectral filter in the cavity was increased. In the self-modelocked laser, this chirp must originate from within the Ti:Al_2O_3 resonator and result primarily from the group-velocity dispersion (GVD) and self-phase modulation (SPM) within the gain medium. It should, therefore, be possible to compress the pulses outside the laser resonator using techniques similar to those described in chapter 4.

The amount of GVD in the main resonator could be estimated from the dispersion data obtained from the Sellmeier expansions for Ti:Al_2O_3 and quartz as discussed in chapter 1. The relevant data for this case are included in Table 5.1. It has been estimated from the data in Table 5.1 that the total intracavity dispersion was approximately 3000 fs^2. In the first instance, the diffraction grating pulse compressor, which has been described in chapters 1 and 4, was used outside the laser cavity. The laser was operated with the 1.6 mm BRF and

	Ti:Al_2O_3	SiO_2	SF14	ZnSe
λ (μm)	870	870	870	870
$n(\lambda)$	1.76	1.45	1.74	2.51
$\frac{dn}{d\lambda}$ (μm^{-1})	-0.0231	-0.0153	-0.0433	-0.190
$\frac{d^2n}{d\lambda^2}$ (μm^{-2})	0.0427	0.0290	0.135	0.750
D (ps (nm km)$^{-1}$)	-124	-84	-391	-2174

Table 5.1. Refractive index and dispersion data for the Ti:Al_2O_3 laser cavity.

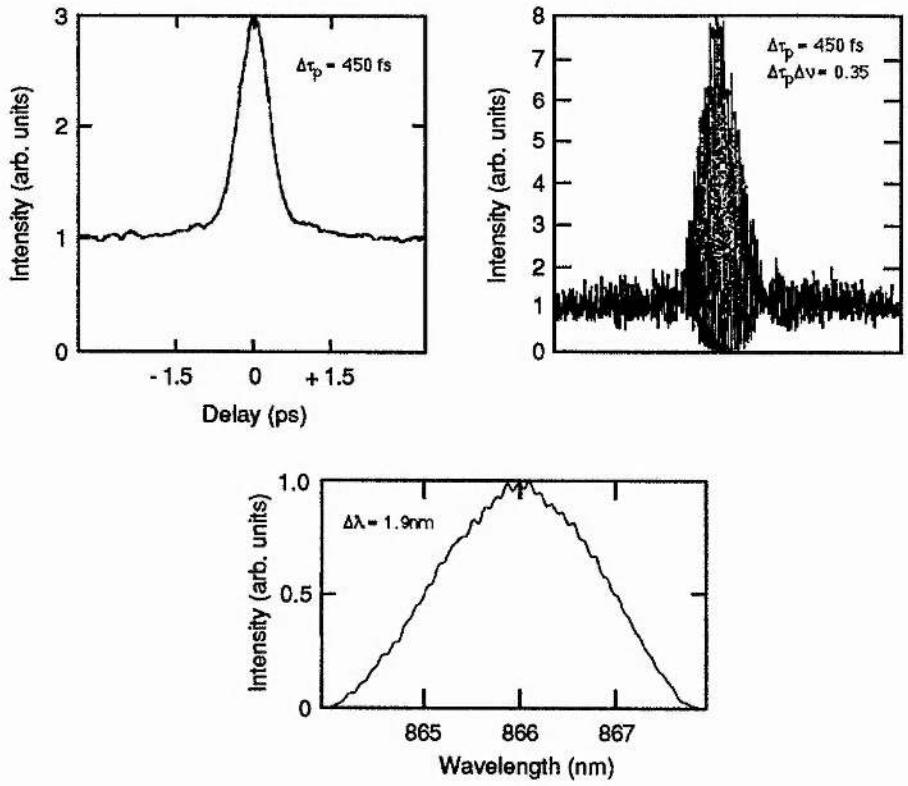

Figure 5.7. Autocorrelation traces and associated pulse spectrum for the modelocked pulses after compression with a diffraction grating pair.

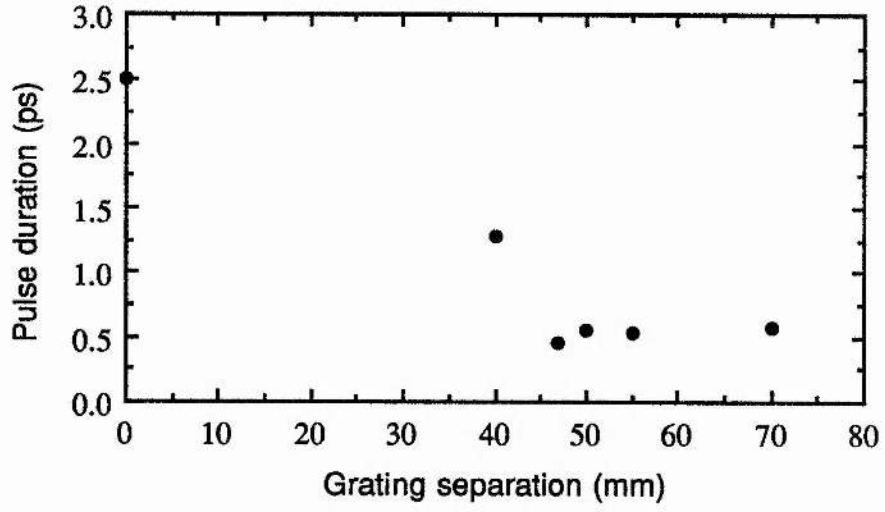

Figure 5.8. Graph illustrating the variation in the compressed pulse duration with the separation between the diffraction gratings.

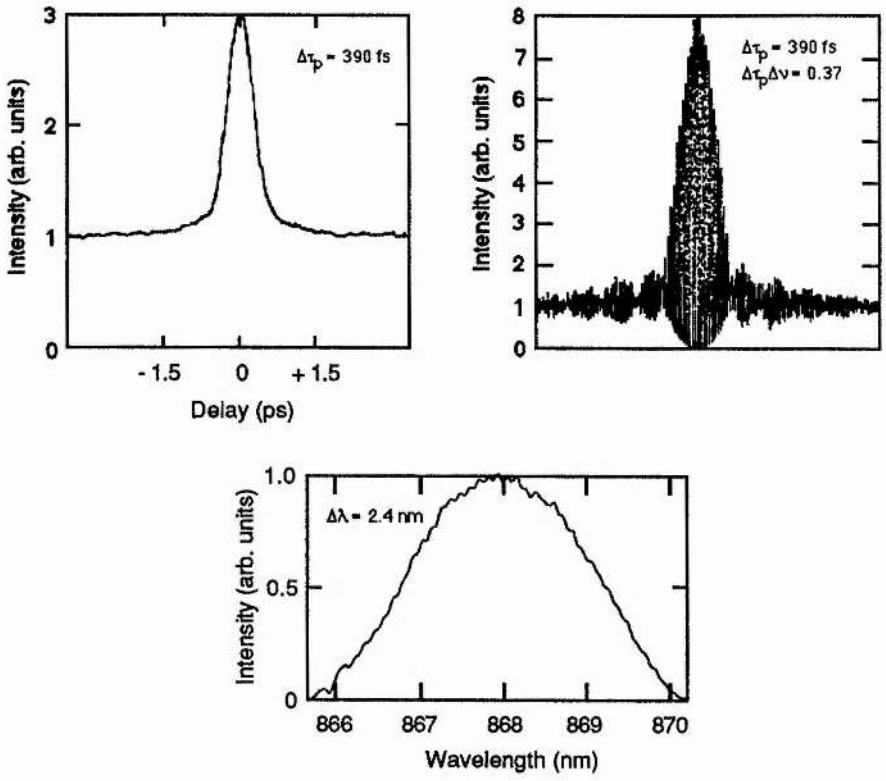

Figure 5.9. Autocorrelation and spectral data for the modelocked pulses after compression with ZnSe prism sequence.

when the optimum grating separation had been found, the pulses measured after the grating pair had durations of 450 fs. This represented a compression factor of ~6. Intensity and interferometric autocorrelation traces of these compressed pulses are presented as figure 5.7. It is evident that some residual frequency chirp still remained after compression. The graph in figure 5.8 illustrates how the compressed pulse duration varied with the separation between the gratings. The output power from the laser was approximately 280 mW for a pump power of 7 W. The diffraction grating pair had a throughput of approximately 33% so that ~100 mW of average power was measured at the compressor's output which represented a peak pulse power in excess of 3 kW. The effective negative dispersion provided by the grating pair can be estimated using the method described in chapter 1. In this case the compressor had an effective dispersion of -0.16 ps^2.

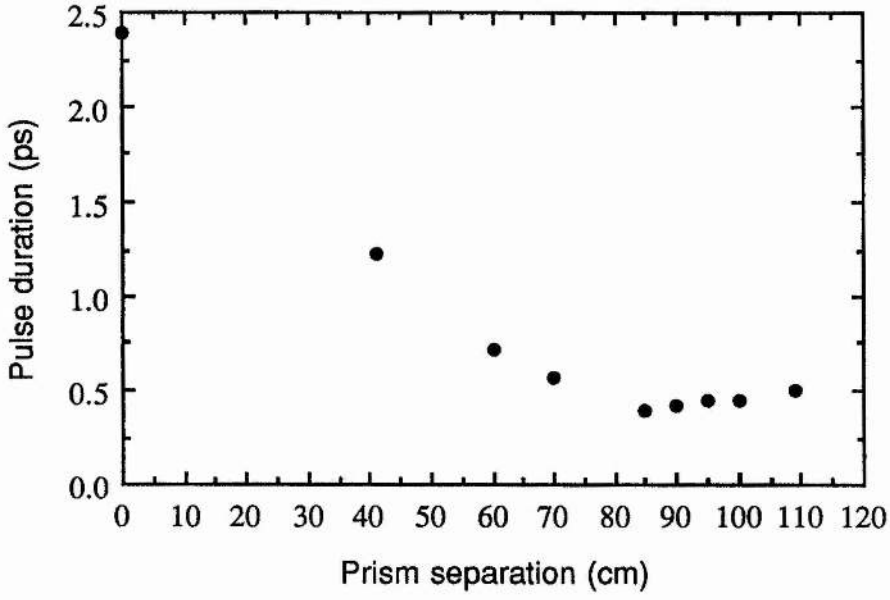

Figure 5.10. Graph illustrating the dependence of the pulse duration on the separation between the prisms in the extracavity pulse compressor.

As an alternative to the grating compressor, four zinc selenide prisms were placed outside the laser cavity in the normal configuration used to provide intracavity dispersion compensation. In this case the optimum prism separation which provided the shortest pulses was found to be ~85 cm. The compressed pulses are presented in figure 5.9 where the shortest pulse duration were 390 fs. The dispersion provided by the prism sequence was estimated to be approximately -0.25 ps^2. The relevant dispersion data for this case are also included in Table 5.1. The dependence of the compressed pulse duration on the prism separation is illustrated in figure 5.10.

5.3 The Intracavity Dispersion-Compensated Self-Modelocked Ti:Al_2O_3 Laser

It was pointed out in chapter 4 that the technique of intracavity dispersion compensation provided a more efficient means of controlling the frequency chirp of modelocked laser

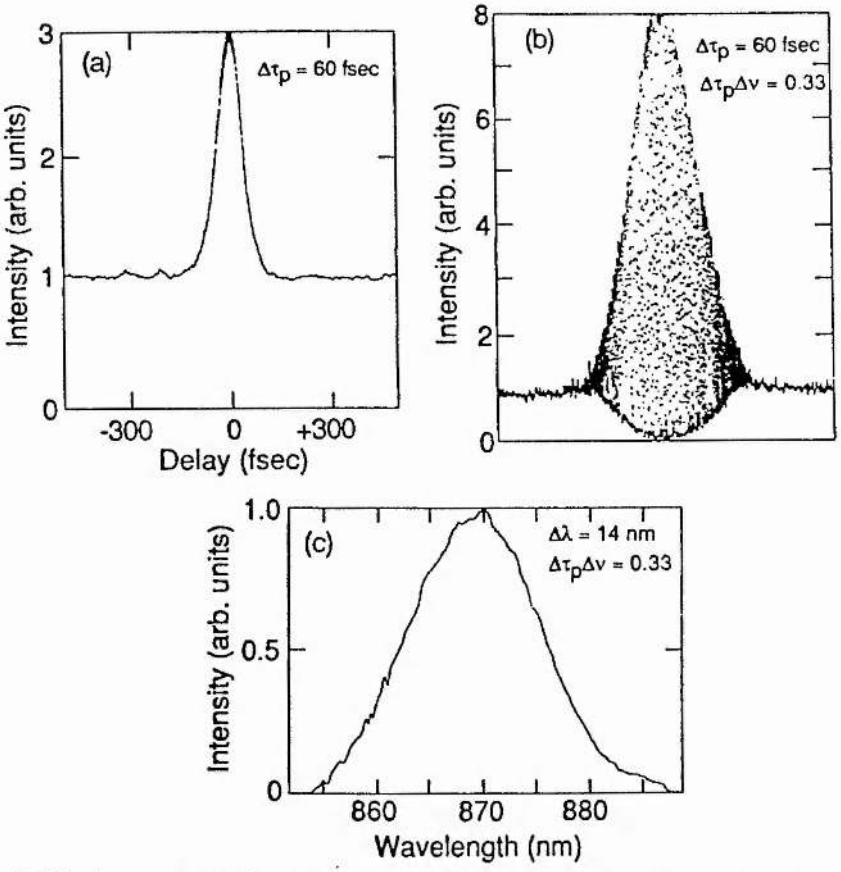

Figure 5.11. Autocorrelation and spectral data for the modelocked pulses from the dispersion-compensated, self-modelocked Ti:Al_2O_3 laser.

pulses. This technique had the advantage of providing higher output powers since all of the output was available for use. In addition, it led to the generation of shorter pulses due to a soliton-like pulse shaping process[3]. An obvious modification was, therefore, to extend the technique to the self-modelocked Ti:Al_2O_3 laser. Two SF14 prisms, which were Brewster-angled for minimum deviation at ~850 nm, were inserted into the main laser cavity in the arm containing the highly reflecting plane mirror. Provided the prisms were properly aligned, their insertion did not significantly affect the threshold or the cw operation of the laser. With the prism sequence in place it was convenient to use a variable aperture slit between the second prism and the highly reflecting plane mirror to achieve wavelength and bandwidth control.

The prism separation which resulted in the generation of the shortest pulses was found to be approximately 35 cm, with the shortest pulses having durations of 60 fs. These pulses were generated at a wavelength of 870 nm . The laser was tunable over a similar wavelength

region to that for the non-compensated, self-modelocked laser. The pulse duration was not seriously affected by the exact centre wavelength, although minor adjustments to the amount of prism material in the cavity were necessary to achieve the shortest durations over the entire tuning range. Intensity and interferometric autocorrelation traces together with the associated pulse spectrum for the shortest pulses are presented in figure 5.11. Reference to the interferometric autocorrelation trace and duration-bandwidth product of $\Delta\tau_p\Delta\nu = 0.33$ show that the pulses are almost free from frequency chirp. The small remaining frequency chirp was most likely a result of higher order processes such as third-order dispersion resulting from the cavity elements and the prism sequence and from un-compensated dispersion outside the laser resonator. Intracavity dispersion compensation cannot fully compensate for these unavoidable dispersive effects outside the cavity. It is worth mentioning at this point that in order to obtain symmetric autocorrelation traces, a glass microscope slide had to be placed in one arm of the autocorrelator to compensate for the beam splitter. This illustrates that such sources of dispersion can have significant effects on the shortest pulses. As with the coupled-cavity modelocked Ti:Al_2O_3 laser, the inclusion of intracavity dispersion compensation relaxed the starting condition for modelocked operation so that short-pulsed operation could be achieved more easily.

The intracavity dispersion could also be estimated for the dispersion-compensated laser. The refractive index data for Ti:Al_2O_3 and SF14 were fitted to appropriate Sellmeier expansions from which the dispersion data were obtained. The relevant data is presented in Table 5.1. Using this data the net dispersion in the laser resonator was estimated to be -300 fs^2. Thus the laser was operating with a small amount of anomalous dispersion. The graph included as figure 5.12 shows how the pulse duration depended on the variation of dispersion near the optimum value. Typically, for a pump power of 8 W, the laser produced ~450 mW of average output power. For pulse durations of 60 fs this represented peak pulse powers of 90 kW.

The self-modelocked laser displayed similar instabilities to those observed in the coupled-

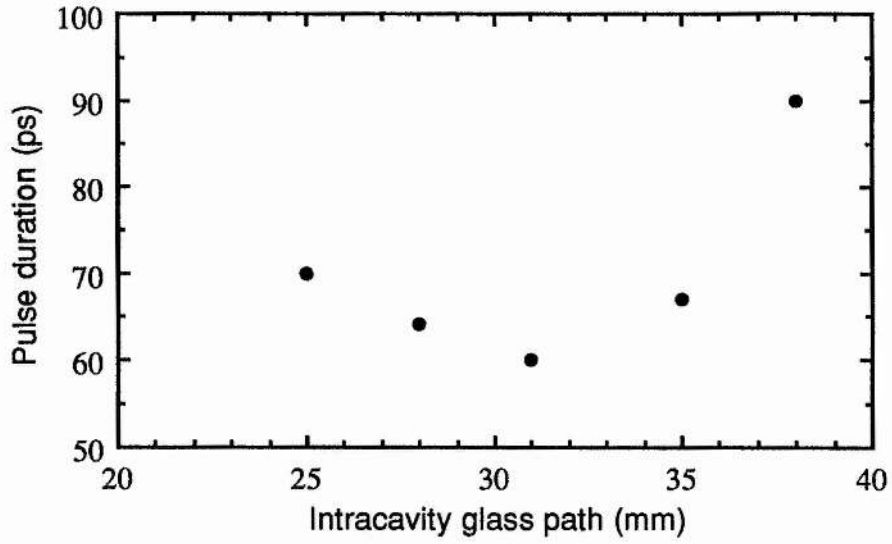

Figure 5.12. Graph showing the dependence of the modelocked pulse duration on the intracavity glass path length.

cavity laser. Multiple-pulsing was observed when the sub-pulses were spaced close to the main pulse. As with the coupled-cavity laser, several sub-pulses could be present. Sub-pulses were also observed further away from the main pulse. In general, the secondary pulses could be located anywhere relative to the main pulse and were accompanied by a modulation on the spectrum as discussed in chapter 4. Their intensities were also variable and could be equal to that of the main pulse. Equally spaced pulses of similar intensity were observed so that the laser repetition frequency was ~172 MHz. Narrow spectral spikes were also observed, similar to the coupled-cavity laser. Again these indicated that part of the laser output was in the form of cw radiation or a relatively broad, low intensity pedestal. Stable operation of the laser required careful adjustment of the intracavity GVD, the bandwidth restriction and the average laser power (ie. the pump power). These instabilities were so similar to those discussed in chapter 4 that further illustration is not necessary here.

If even shorter pulse durations are required, it would be necessary to compensate for the third order dispersion which also significantly influences the shortest modelocked pulses. It is not easy to achieve intracavity compensation for higher-order dispersion and while it is

possible to compensate for its effects outside the resonator the benefits in terms of a reduction in pulse duration and an increase in peak power would be relatively small. One solution would be to carefully choose the material used in the prism sequence so that the third order dispersion is minimised. This technique has recently been demonstrated experimentally and pulse durations as short as 30 fs have been reported[4]. An alternative solution would be to use pulse compression techniques which first chirp the pulses in a length of optical fibre. This technique has been discussed in chapter 1. It was decided to try to further reduce the pulse durations in this way because a pulse compressor could be easily constructed using equipment readily available in the laboratory.

Using the simple results quoted in chapter 1 it was possible to estimate the length of optical fibre and grating separation required to provide the optimum compression. For the calculation it was assumed that the laser pulse duration was ~100 fs with an average power of 300 mW which corresponded to a peak pulse power of ~36 kW, assuming a cavity period of ~12 ns. Andrew Corporation optical fibre similar to that used for the coupled-cavity modelocked Ti:Al_2O_3 laser was used for the first section of the compressor. The optimum length was calculated to be ~5 cm, and the resulting compressed pulse durations were estimated at ~40 fs. The pulse compressor was set up using four zinc selenide prisms in preference to a diffraction grating pair. The main advantage of the prisms was that they had a much higher transmission, typically 85%, than the gratings. Using a 5.7 cm length of fibre (the shortest length which could conveniently be held in the fibre chuck) and a prism separation of ~9 cm the pulses measured after the fibre had durations as short as 45 fs. With approximately 300 mW incident on the length of fibre, 100 mW was measured after the prism sequence. This implied that the compressed pulses had a peak power of the order of 25 kW. Autocorrelation traces of these compressed pulses are included as figure 5.13.

The results agree reasonably well with the calculated value for the compressed pulse duration. The discrepancies arise because the theory assumes initially unchirped pulses and neglects higher order dispersion. As already mentioned, the pulses from the laser are not

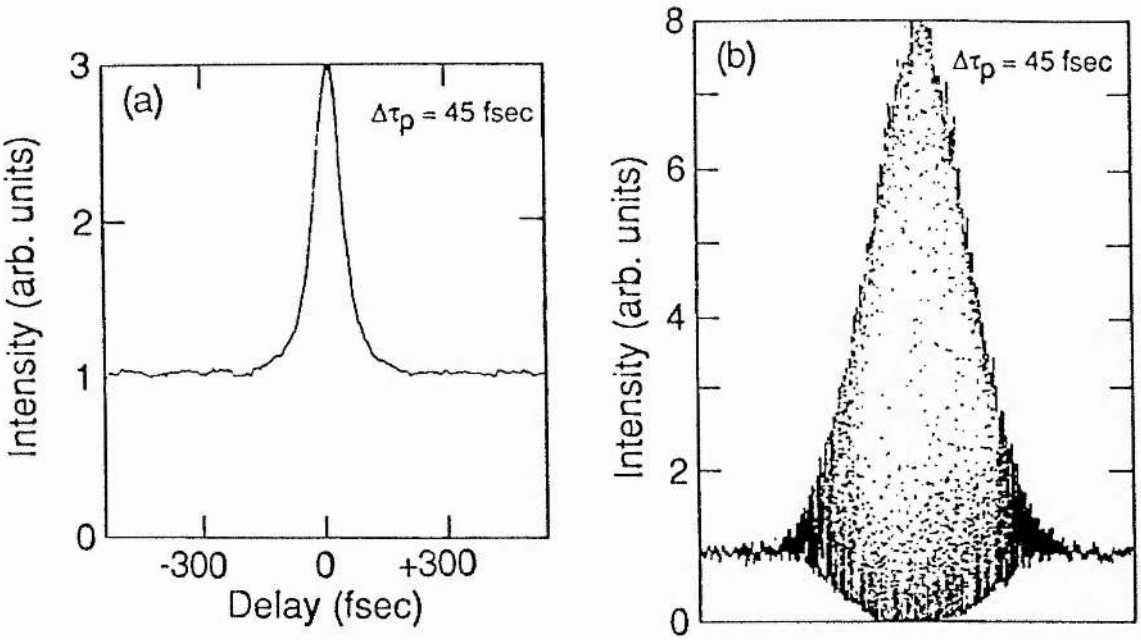

Figure 5.13. Intensity and interferometric autocorrelation traces of the pulse compressed, self-modelocked laser output.

completely free from such chirp. The ZnSe prism sequence most likely exhibited relatively large third order dispersion. Of course, the input pulse parameters are also only estimates and in practice the actual input pulse durations and power differed somewhat from those used in the calculation.

5.4 The Regeneratively Initiated Self-Modelocked Ti:Al_2O_3 Laser

The stability of the basic self-modelocked Ti:Al_2O_3 laser has already been discussed in section 2 of this chapter. Although this laser represented a considerable improvement over other femtosecond Ti:Al_2O_3 lasers in terms of simplicity and pulse characteristics, it had a major drawback because the modelocking process was not self-starting. This meant that stable operation could not be guaranted for an extended period. Thus, in spite of its many advantages, the system's applicability to many areas of research was limited. Both the experimental results and the theory for modelocking with a fast saturable absorber imply that there is a threshold for self-starting in such lasers, which depends on several initial parameters, including the initial duration of any intensity fluctuations in the cavity[5,6]. The

process of tapping one of the cavity mirrors or sweeping the cavity length merely served to enhance these fluctuations so that the threshold for modelocking was achieved.

If this self-starting threshold could be reached under normal operating conditions, it was expected that the modelocked operation would self-start and the general stability of the laser with regard to random dropouts should improve. Unfortunately, unlike the coupled-cavity modelocked laser, there were relatively few adjustable initial parameters for the self-modelocked laser. For example, in the former, the nonlinearity could be increased simply by lengthening the control fibre or increasing the coupling between the cavities. It was, however, possible to adjust the initial pulse duration in the self-modelocked laser. Several schemes have emerged which use this technique, such as the use of weak saturable absorbers[7,8], various coupled-cavity schemes[9,10], active cavity length modulation and synchronous pumping[11]. In this section we describe a technique which used an acousto-optic modulator to help initiate the pulse shortening process[12]. This had the advantage of retaining the all-solid-state nature of the laser while keeping the system relatively simple to set up and operate and did not introduce additional noise into the laser output. The modulation could be applied continuously so that the laser always produced pulses of a few hundred picoseconds. These were sufficiently short that the self-starting threshold could be exceeded more easily and with the proper cavity alignment, self-modelocking could be obtained. In addition, the modulation not only initiated the modelocking process, but also provided a stabilising influence against perturbations which would otherwise interrupt the short-pulse mode of operation.

The laser configuration was based on that used for the dispersion-compensated system described in the previous section. The acousto-optic modulator (obtained from Newport Electro-Optics Systems), which was maintained at a constant temperature, was placed in the cavity as close to the output coupler as was possible. This was the same device used for active modelocking in the system described in chapter 3. It was designed to be driven with up to 1 W of rf power at a frequency close to 42 MHz. Initially the rf signal was derived from a frequency synthesizer (Marconi Model 2019) and amplified using a broad band rf amplifier (Motorola CA2832) which provided ~30 dB of gain at 43 MHz. The modulator was driven

at one of its resonance frequencies with an rf power of ~500 mW. Under these conditions the laser produced pulses having durations as short as 60 ps, as discussed in chapter 3. However, with the proper cavity alignment and length, the the duration of the modelocked pulses would instantaneously shorten to <100 fs with no loss in average output power. In practice, the laser cavity was aligned to self-modelock in the way already described with the rf drive to the modulator switched off. The laser was then adjusted to obtain optimum actively modelocked operation. At this stage a minor adjustment to the alignment resulted in spontaneous femtosecond pulse operation.

It was obvious that these ultrashort pulses had durations which were much shorter than those expected from active modelocking alone. It was also significant that the laser repetition frequency became dependent only on the length of the laser resonator, suggesting that the modelocking process was passive in nature. This was confirmed by monitoring the modelocked pulse train using a fast photodiode and rf spectrum analyser or frequency counter. When the laser produced pulses in the hundred picosecond regime the exact pulse repetition frequency was determined by the modelocker drive frequency. Because the self-modelocked pulse repetition rate was no longer determined by the active modulation frequency, stable operation of the laser required that the laser cavity frequency be exactly matched to the rf drive frequency. If these frequencies were not matched, the two signals would beat together resulting in a modulation on top of the modelocked pulse train at the beat frequency. Furthermore, if these two frequencies were separated by more than a few hundred Hertz, the femtosecond pulse generation would cease altogether. Conversely, initiation of self-modelocking also required the two frequencies to be matched with a similar accuracy. This fact obviously presented a problem to the stable operation of the laser since cavity length drifts of a few hundred Hertz (~4 μm) were not uncommon, and a modulated pulse sequence would be unsatisfactory for most applications.

In order to avoid the necessity of maintaining a fixed cavity length, it was decided to derive the rf drive signal for the modulator from an intensity component of the modelocked

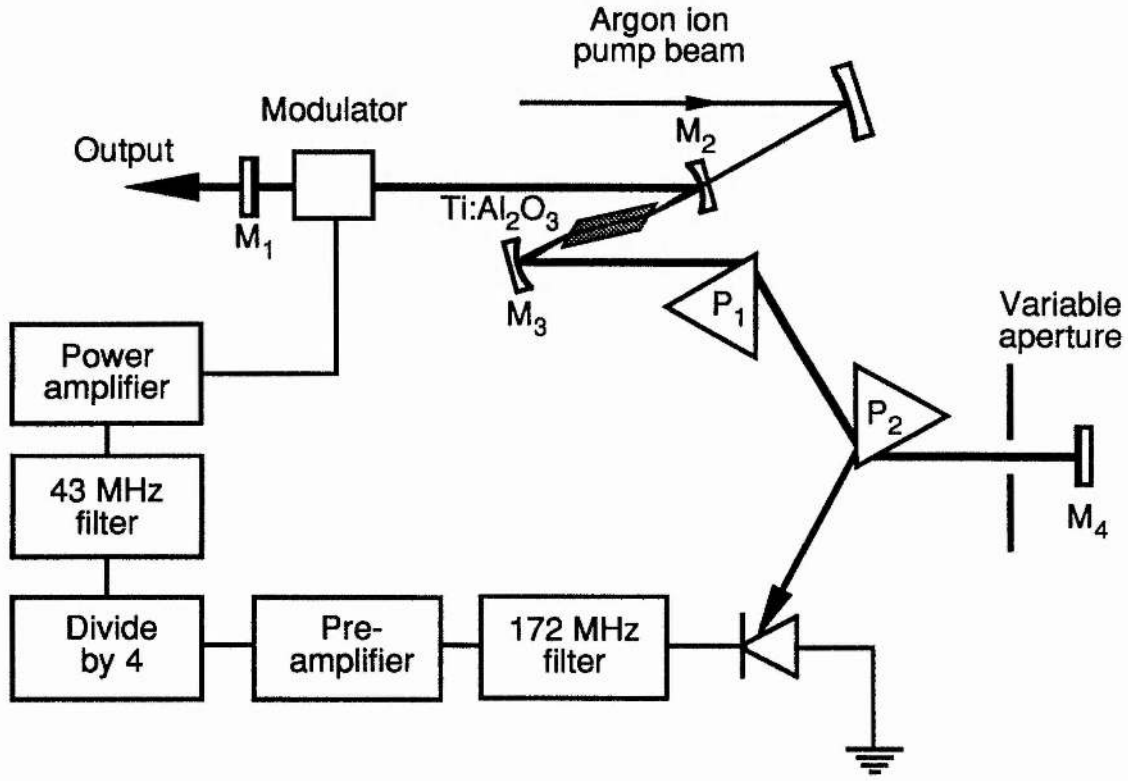

Figure 5.14. Schematic diagram of the cavity configuration and regenerative electronics for the self-modelocked Ti:Al_2O_3 laser.

pulse train, so that the two would always be in synchronism irrespective of the cavity length. This scheme was first reported by Huggett[13] as a technique for active mode-coupling and was termed 'regenerative modelocking'. In this approach a small component of the optical intensity within the laser resonator was sampled, amplified to a suitable level and applied to the intracavity modelocking element. In this way the modulator drive frequency was always matched to the cavity frequency. With appropriate electronic circuitry, even if the laser was initially not modelocked, there was still a sufficient modulation of the intracavity intensity at the cavity frequency to initiate pulse formation through weak acousto-optic modulation.

The electronic circuitry used for driving the modulator in these experiments is illustrated schematically in figure 5.14. A small fraction of the intracavity intensity was directed onto a fast photodiode (RS Components Ltd BPX 65) having a bandwidth of ~500 MHz. The optical signal could conveniently be derived from the reflection from one of the intracavity prisms. The second harmonic frequency, at 172 MHz, of the diode output was selected using

a passive bandpass filter having a bandwidth of approximately 10 MHz, and amplified using a hybrid rf amplifier (Philips OM 335). This amplified signal was applied to the input of a integrated 'divide by 4' circuit to provide the necessary drive signal at ~43 MHz. This signal was first filtered at 43 MHz, amplified to a level of approximately 400 mW and passed through a variable delay line before being applied to the modulator.This design was chosen simply because of the availability of a suitable 'divide by 4' circuit.

When the Ti:Al_2O_3 laser was initially switched on the regenerative electronics would drive the modulator resulting in actively modelocked pulses. The shortest pulses were generated when the phase of the regenerative drive signal was optimised to ensure that the active modulation was in phase with the modulation on the intracavity field. By following the same procedure already described for the actively driven system, the laser could by aligned to generate pulses having durations in the femtosecond regime. The stability of the output was significantly improved because the active modulation frequency was automatically held in synchronism with the pulse repetition frequency. The active modulator not only helped to initiate the self-modelocking process but also made the laser more tolerant to disturbances caused by external noise sources. The amount of active modulation provided was very small. It was possible to drive the modulator at a frequency midway between its resonances at rf power levels of a few hundred milliwatts and still achieve ultrashort pulse generation from the laser. Under these conditions, the modulation provided by the modulator could be as little as 0.5% of the total incident intensity. This ability to drive the system at frequencies away from its resonances avoided complication caused by the π phase shifts which occur in the vicinity of the resonance.

The laser performance was not significantly affected by the presence of the acousto-optic modulator in the cavity. Intensity and interferometric autocorrelation traces together with an associated spectrum for the pulses generated by this regeneratively initiated laser are reproduced in figure 5.15. It is evident that the pulse durations remained unchanged at 60 fs and the interferometric autocorrelation trace and duration-bandwidth product of

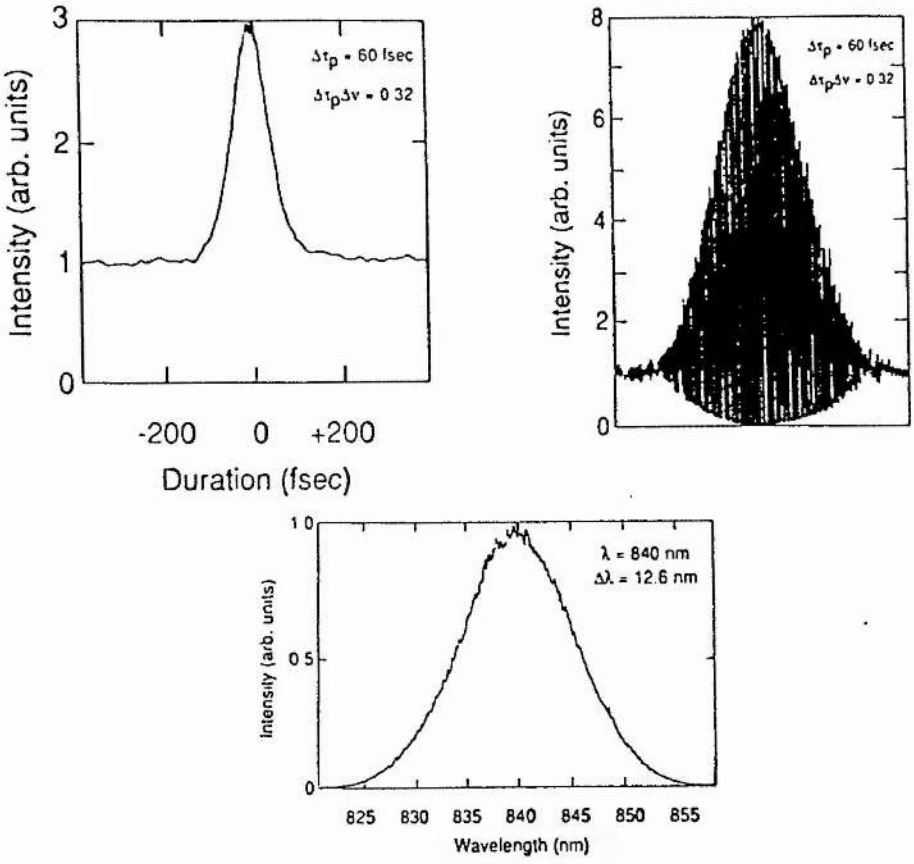

Figure 5.15. Autocorrelation traces and associated pulse spectrum for the modelocked output from the regeneratively initiated, self-modelocked Ti:Al_2O_3 laser.

$\Delta\tau_p\Delta\nu = 0.32$ confirmed that the pulses were still essentially free from frequency chirp. Of course a minor adjustment had to be made to the prism sequence in order to compensate for the increased dispersion introduced by the modulator material. This can easily be estimated using the methods already described above. The modulator element introduced an estimated additional dispersion of 1300 fs^2 into the resonator and the net dispersion after compensation was -430 fs^2. The laser was tunable over the 750 - 900 nm spectral region. The decrease in the tuning range at longer wavelengths was due to the characteristics of the anti-reflection coating on the modulator. For 7 W of pump power the laser generated an average output power of 600 mW which corresponded to a peak pulse power in excess of 110 kW.

5.5 Mechanisms for Self-Modelocking

The term self-modelocking was applied to the Ti:Al_2O_3 laser described in this chapter because it was able to generate modelocked pulses without the addition of any conventional

modelocking elements. Self-modelocking was first observed in He-Ne lasers in 1965 and soon after in solid-state lasers and was thought to be due to a nonlinear interaction between the laser medium and the radiation in the cavity, which under 'proper conditions', could force the resonator modes to maintain a fixed phase relationship with one another[14]. Typically, such self-modelocked lasers produced pulses having durations ~1 ns. In most cases reliable operation required that the cavity round trip time be greater than or equal to the atomic decay time and that the laser was not operated too far above threshold.† Later, however, doubts regarding the interpretation of the early pulse measurement techniques cast a question-mark on these results. Some workers believed that only partial modelocking occurred in solid-state lasers[15]. In contrast, the ability of the self-modelocked Ti:Al_2O_3 laser to produce high quality modelocked pulses has been demonstrated by several independent groups. This section aims to review the current views regarding the mechanisms responsible for ultrashort pulse generation in such a Ti:Al_2O_3 laser.‡

Modelocked Ti:Al_2O_3 lasers producing femtosecond pulses possess some characteristic features which distinguish them from their dye laser counterparts. The relatively long gain media and high intracavity powers result in considerable SPM in these systems. The physical length of the gain material also imply a relatively high amount of normal dispersion, since the lasers operate at wavelengths in the sub-1 μm spectral region. It can be expected that the interaction of this SPM and GVD will have a considerable influence on the modelocked pulses[3,16]. This has already been demonstrated for the case of the coupled-cavity modelocked laser discussed in chapter 4. Thus, the processes which can be expected to influence the modelocked pulse during its passage through the laser cavity are: gain, GVD, SPM, amplitude modulation, and linear loss and phase shift. These effects are not restricted to the Ti:Al_2O_3 laser, but can be expected to be generally applicable to femtosecond, passively modelocked, solid-state lasers. Experimental data confirm that the pulse durations produced in

---

† These conditions do not hold in the self-modelocked Ti:Al_2O_3 laser.

‡ At the time of writing the exact mechanism responsible for the self-modelocking process was not fully understood.

such lasers do indeed depend strongly on the interaction of intracavity SPM and GVD, and that dispersion compensation is necessary for the generation of pulses having durations in the femtosecond regime. Furthermore, calculations suggest that the optimised dispersion-compensated Ti:Al_2O_3 laser operates with net small negative intracavity GVD (see, for example, reference 7). This suggests that an additional soliton-like pulse shaping mechanism is taking place within the laser resonator where the SPM is balanced by the negative dispersion. Of course, modelocking can also be demonstrated when the net GVD is positive, when the resulting pulse durations are considerably longer. In this regime additional pulse shaping is provided by frequency filtering the chirped pulses.

Self-phase modulation has been exploited in a number of laser types to generate shorter pulses[17]. However, it should be stressed that SPM by itself, is not sufficient to produce modelocking because it cannot discriminate between the pulses and the noise. An additional element having an intensity dependent transmission is necessary for stable passive modelocking, both to initiate pulse buildup and to maintain stability by ensuring that there is a net loss before and after the pulse in the steady-state. In conventional passively modelocked dye and colour-centre lasers, for example, this additional element is a saturable absorber.

As the modelocked pulse duration shortens, the effect of the Kerr nonlinearity increases. Typically, in Ti:Al_2O_3 lasers, the cavity mode is focused to a beam waist of the order of a few tens of microns in the gain medium. The resulting high intensities mean that for the shortest pulses, spatial nonlinear effects such as self-focusing also become significant[18-20]. These spatial effects can be used in conjunction with an aperture to transform the phase nonlinearity into an amplitude modulation. This happens because the nonlinear medium acts as an intensity dependent lens producing a smaller beam waist for higher intensities. If an aperture is placed at a suitable location within the laser cavity, where the beam size decreases with increasing intensity, it will have a higher transmission for a high intensity beam than for a low intensity beam. Thus, the cavity losses are intensity dependent and the system sees a higher gain with increasing intensity. The aperture does not necessarily need to be a hard-edged physical aperture because the spatial profile of the pump beam results in a corresponding spatial gain

profile which increases towards the centre where the pump intensity is highest. Consequently, reducing the size of the intracavity waist in a suitably designed resonator will increase the net gain seen by the laser and the dynamic self-focusing effect can simulate the action of a fast saturable absorber.

The influence of this nonlinear lens can be illustrated by approximating the self-focusing effect in the laser rod by a self-induced quadratic index gradient. The cavity mode is assumed to be gaussian and is approximated by a parabola so that the spatial intensity profile is given by

$$I(r) = I_0 \exp\left(\frac{-2r^2}{w_0^2}\right) \approx I_0\left(1 - \frac{2r^2}{aw_0^2}\right) \tag{5.1}$$

where a is a correction factor for the higher order terms which are ignored in the parabolic beam approximation and which can take a value between approximately 3 and 7, depending on the severity of the nonlinear phase distortion[21]. The Kerr nonlinearity leads to the usual intensity dependent refractive index given by $n = n_0 + n_2 I$. The origin of the spatially varying quadratic index profile is evident because the refractive index is highest at the centre of the mode where the intensity is highest (assuming a positive n_2). This refractive index profile causes an effective converging lens in the Kerr material, the strength of which depends on the instantaneous intensity of the optical signal and leads to the well known self-focusing and self trapping of gaussian beams in nonlinear media which have been outlined in chapter 1. By using the normal ABCD matrix methods[22] for gaussian beam propagation the focal length of the effective nonlinear lens can be expressed as

$$f_{NL} \approx \frac{\pi\, a\, w_0^4}{8\, n_2\, P_0\, z} \tag{5.2}$$

where w_0 is the 1/e amplitude beam radius, P_0 is the instantaneous peak power (given by $P_0 = \pi w_0^2 I_0/2$) and z is the interaction length[20]. For the self-modelocked Ti:Al_2O_3 laser described here, the radial dimensions of the beam waist in the crystal were calculated as (20 x 30) μm^2. We can get a first approximation of the nonlinear interaction by setting $z = L_{eff} \equiv \pi n_0 w_0^2/\lambda$, where L_{eff} is the effective interaction length[23] and by assuming a~5. If

we take the average intracavity power in the laser to be ~8 W, then the pulse energy is ~99 nJ assuming a repetition rate of 86 MHz. For 100 fs pulses this implies that $f_{NL} \approx 6$ mm, where we have taken n_2 to be 3×10^{-20} m^2W^{-1}. For 1 ps pulses $f_{NL} \approx 6$ cm and $f_{NL} \approx 6$ m for 100 ps pulses. We can use the ABCD law to estimate what effect this nonlinear lens will have on the beam waist in the crystal. The results indicate that the waist can decrease by as much as 15% for 100 fs pulses and by ~1% for 1 ps pulses. These simple calculations show that the self-focusing effects can be significant for modelocked pulse durations in the picosecond and femtosecond regime, especially with the introduction of a hard aperture in the laser cavity. Numerical simulations have shown that amplitude modulation of only ~1% can be sufficient to sustain modelocked operation[24].This self-focusing effect can, therefore, provide the self-amplitude modulation required for stable passive modelocking.

The critical power for beam collapse can be estimated from the following equation

$$P_{cr} = \frac{a\,\lambda^2}{8\,\pi\,n_0\,n_2} \tag{5.3}$$

For $Ti:Al_2O_3$, P_{cr} ~2.5 MW, which is only about a factor of two greater than the typical intracavity peak powers present when the modelocked pulse durations are $\lesssim$100 fs. This simple analysis has ignored the effects of gain saturation and gain guiding in the laser medium which will tend to decrease the effect of the self-focusing. In a more exact analysis, the effect of the total rod length should be taken into account by splitting the rod into segments which are much shorter than the Rayleigh length and using an iterative procedure from one segment to the next. The effect of the nonlinear lens on the overall stability of the resonator and efficiency of the laser should also be included. In any case, since the amount of self-focusing depends on the beam size, which in turn depends on the self-focusing, an exact solution to the problem is difficult and at present no detailed theoretical analysis has been performed. However, this effect has been observed experimentally in both the laser gain medium and in discrete intracavity bulk nonlinear materials and has been shown to be significant in the operation of such modelocked lasers[19,25].

In the previous chapter the action of the coupled-cavity was compared to that of a fast saturable absorber and a threshold condition for self-starting was given. It was pointed out that the coupled-cavity modelocked Ti:Al_2O_3 laser should self-start more easily than the corresponding colour-centre lasers because of its lower gain cross-section. The latter usually require additional modulation which provide shorter initial intensity fluctuations so that the self-starting threshold can be reached. Since the dynamic self-focusing effects in the self-modelocked Ti:Al_2O_3 laser also simulate fast saturable absorption, a self-starting threshold should also be expected in this case. However, because the self-focusing effects are relatively weak for pulse durations in the 0.1 - 1 ns range, the self-starting threshold is not normally reached by the cw laser system and such lasers do not normally self-start. Some additional modulation must be provided. Tapping one of the cavity mirrors has the effect of inducing a sufficiently short intensity fluctuation in the cavity so that modelocked operation can build up. A more satisfactory solution is to include some weak modulation in the laser so that the self-starting threshold can be exceeded automatically. Various schemes have been demonstrated such as the regeneratively driven AO modulation described here, synchronous pumping[11], weak dye[7] and solid state[8] saturable absorbers and various schemes using resonant[9] and non-resonant nonlinear and linear[10] coupled-cavities. All of these achieve the same purpose of providing initial fluctuations which have sufficient intensity to exploit the Kerr effect in the nonlinear material so that the self-modelocking process can build up when the laser cavity is suitably aligned.

Thus far the probable sources of amplitude modulation in the self-modelocked Ti:Al_2O_3 laser have been mentioned. Of equal importance are the effects of GVD and SPM. The combined influence of these processes in the coupled-cavity Ti:Al_2O_3 laser has been discussed in chapter 4 and their effects can be expected to be similar in both of the modelocking schemes. This is confirmed by the experimental observations which show that the behaviour of both types of modelocked laser have much in common with respect to the control of intracavity GVD and SPM. In the region of net positive GVD the pulses are relatively long and strongly chirped. In this regime additional pulse shaping is provided by the action of the

frequency filter (bandwidth limitation) as it shaves off the high and low frequency wings of the pulse, as well as by the (artificial) fast saturable absorber. Similarly, in the region of net negative GVD, additional pulse shaping is provided by a soliton-like mechanism and the self-amplitude modulation has a much weaker effect. For the shortest pulses, the interplay between SPM and GVD can dominate the pulse shortening process. The effects of GVD and SPM on pulse propagation have already been discussed in chapter 1.

There are some important differences between the well known fibre based soliton supporting systems and the dispersion-compensated laser resonator which have not been mentioned before. Solid-state lasers tend to have regions of discrete gain and loss within the resonator. This situation is in some ways similar to long distance soliton propagation in optical fibres using lumped amplification[26,27]. It has been shown that the solitons are remarkably resilient to large variations in energy and dispersion provided the characteristic length scale of these variations (ie. the amplifier spacing and fibre draw lengths) are considerably smaller than the soliton period - the length scale over which nonlinear and dispersive effects become significant[26-28]. Typical soliton periods are ten to twenty times longer than the amplifier spacing in such experiments. We can estimate the equivalent parameter for the self-modelocked Ti:Al_2O_3 laser cavity from equation (1.33) by letting $\bar{\beta}_2$ represent the dispersion averaged over one cavity round trip. For 100 fs pules, the effective soliton period is ~40 m, assuming $\bar{\beta}_2 = -120\ fs^2m^{-1}$. If we assume that the round trip cavity length represents the characteristic length for amplifying and dispersive effects in the laser, it is evident that the modelocked laser is operating in a similar regime to that of long distance soliton propagation in fibres and that a stable soliton-like pulse shaping mechanism might reasonably be expected.

In lasers, other effects must be considered such as the positive GVD of the Kerr medium, the third order dispersion of the intracavity prism sequence and gain medium and gain dispersion. The latter can usually be neglected in Ti:Al_2O_3, however, the discreteness of the Kerr nonlinearity and the negative GVD mean that in general, the pulses will exhibit some nonlinear frequency chirp in the wings. As a result, the GVD compensation can only

compress the central linearly chirped portions of the pulses. This effect leads to pulse breakup at the wings of the main pulse and eventually to instability. For this reason some amplitude modulation will always be required to maintain stability in such lasers even in the absence of perturbations. This might be one possible explanation of the multipulsing behaviour observed in the self-modelocked Ti:Al_2O_3 laser. The discrete nature of the pulse shaping elements may also result in slightly different pulse durations at different locations within the resonator.

As with the coupled-cavity modelocked laser, increasing the SPM and negative GVD does not lead to arbitrarily short pulses because the laser goes unstable once the effective gain available for the pulses falls below the level for cw operation. Increased amplitude modulation is also required if stability is to be maintained. Recent theoretical studies have shown that the pulse shapes can deviate significantly from the ideal bandwidth limited pulses as the ratio of the SPM to amplitude modulation increases, before the instability region is finally reached[29].

The similarities between the pulse shaping mechanisms in the coupled-cavity and self-modelocked Ti:Al_2O_3 lasers are clear - both utilise the interaction between SPM and GVD to provide additional pulse shortening and both require self-amplitude modulation if the modelocked pulses are to evolve and remain stable against perturbations. In the former scheme this is provided by the coupled-cavity modelocking process while in the latter it is provided by dynamic self-focusing. Both of these techniques are different methods of achieving the same goal - that of converting a phase nonlinearity into an amplitude modulation. The influence of both of these has been shown to be fundamentally equivalent to that of fast saturable absorption. It is not surprising, therefore, that the self-modelocked and coupled-cavity modelocked lasers should display certain similarities in their operation. The results indicate that the lasers operate best with a small overall negative GVD and that excessive peak power levels can lead to instabilities. This is also confirmed by theoretical analysis. The self-starting conditions are the same as those which are generally applicable to fast saturable absorber modelocking. The inclusion of an additional source of modulation in the cavity can lead not only to lower self-starting thresholds, but also to improved stability.

The self-modelocking process has the advantage that it does not require active stabilisation and therefore provides a much simpler source for femtosecond pulse generation.

5.6 Conclusions

This chapter has described the operation of a self-modelocked Ti:Al_2O_3 laser which generated pulses having durations as short as 2 ps and which was continuously tuneable over the 750 - 950 nm spectral region. This laser had an average power output of ~450 mW, for 8 W pump, which corresponded to peak pulse powers of 2.6 kW. The results showed that these pulses were highly frequency chirped and could be directly compressed outside the laser cavity to 380 fs. By using intracavity dispersion compensation pulses as short as 60 fs were generated. These pulses were subsequently compressed outside the cavity to 45 fs. A regeneratively driven acousto-optic modulator was incorporated into the laser cavity to lower the self-starting threshold of the laser by inducing shorter initial intensity fluctuations. This laser also generated pulses as short as 60 fs with average powers of 600 mW, which corresponded to peak pulse powers of 110 kW.

Finally the concepts underlying this type of modelocking in solid-state lasers such as Ti:Al_2O_3 were reviewed. These suggest that there are two distinct regimes of operation depending on the sign of the intracavity dispersion. For overall positive GVD the pulses generated were relatively long and exhibited substantial frequency chirp, while for net negative GVD, the pulses were much shorter and relatively free from frequency chirp. The experimental results described in this chapter agree with the theoretical simulations by other workers. These studies suggest that additional pulse shortening is most likely provided by spectral filtering for the case of net positive GVD and by a soliton like mechanism for net negative GVD. In both regimes, stability is maintained by self-amplitude modulation provided by the action of an effective fast saturable absorber. In the self-modelocked laser this can be provided by dynamic self-focusing in the gain medium. This effect is not strong enough to lead to reliable self-starting and so some additional amplitude modulation should be provided. This description should be generally applicable to femtosecond solid-state lasers, so that many

of the practical designs which have emerged can be viewed as variations of the same basic type of modelocking process.

5.7 References

1. D.E. Spence, P.N. Kean and W. Sibbett, Opt. Lett. **16**, 42, (1991).

2. J.D. Kafka, private communication.

3. O.E. Martinez, R.L. Fork and J.P. Gordon, J. Opt. Soc. Am. B **2**, 753, (1985).

4. C-P. Huang, H.C. Kapteyn, J.W. McIntosh and M.M. Murnane, Opt. Lett. **17**, 139, (1992).

5. K. Krausz, T. Brabec and Ch. Spielmann, Opt. Lett. **16**, 235, (1991).

6. H.A. Haus and E.P. Ippen, Opt. Lett. **16**, 1331, (1991).

7. N. Sarukura and Y. Ishida, Opt. Lett. **17**, 61, (1992).

8. N. Sarukura, Y. Ishida, T. Yanagawa and H. Nakamo, Appl. Phys. Lett. **57**, 229, (1990).

9. U. Keller, G.W. 'tHooft, W.H. Knox and J.E. Cunningham, Opt. Lett. **16**, 1022, (1991).

10. P.M.W. French, D.U. Noske, N.H. Rizvi, J.A.R. Williams and J.R. Taylor, Opt. Commun. **85**, 185, (1991).

11. Ch. Spielmann, F. Krausz, T. Brabec, E. Wintner and A.J. Schmidt, Opt. Lett. **16**, 1180, (1991).

12. D.E. Spence, J.M. Evans, W.E. Sleat and W. Sibbett, Opt. Lett. **16**, 1762, (1991).

13. G.R. Huggett, Appl. Phys. Lett. **13**, 186, (1968).

14. M.A. Crowell, IEEE. J. Quant. Electron. **QE-1**, 12, (1965).

15. M.A. Duguay, J.W. Hansen and S.L. Shapiro, IEEE. J. Quant. Electron. **QE-6**, 725, (1970).

16. H.A. Haus and Y. Silberberg, IEEE. J. Quant. Electron. **QE-22**, 325, (1986).

17. J. Comley, A. Yariv and E. Garmire, Appl. Phys. Lett. **15**, 148, (1969).

18. S. Chen and J. Wang, Opt. Lett. **16**,1689, (1991).

19. F. Salin, J. Squier and M. Piché, Opt. Lett. **16**, 1674, (1991).

20. M. Piché, Opt. Commun. **86**, 156, (1991).

21. M. Sheik-Bahae, A.A. Said, D.J. Hagan, M.J. Soileau and W.W. Van Stryland, Opt. Eng. **30**,1228, (1991).

22. A.E. Siegman, in 'Lasers', University Science Books, Mill Valley, California, (1986).

23. G.P. Agrawal, in 'Nolinear Fiber Optics', Academic Press Inc. (London) Ltd., London, (1989), Ch. 2, 5.

24. H.A. Haus, J.G. Fujimoto and E.P. Ippen, J. Opt. Soc. Am. B **8**, 2068, (1991).

25. G. Gabetta, D. Huang, J. Jacobson, M. Ramaswamy, E.P. Ippen and J.G. Fujimoto, Opt. Let. **16**, 1756, (1991).

26. L.F. Mollenauer, M.J. Neubelt, S.G. Evangelides, J.P. Gordon, J.R. Simpson and L.G. Cohen, Opt. Lett. **15**, 1205, (1990).

27. L.F. Mollenauer, S.G. Evangelides, H.A. Haus, IEEE. J. Lightwave Technol. **9**, 170, (1991).

28. J.P. Gordon and L.F. Mollenauer, IEEE. J. Lightwave Technol. **9**, 170, (1991).

29. T. Brabec, Ch. Spielmann and F. Krausz, Opt. Lett. **16**, 1961, (1991).

Chapter 6
Measurement and Suppression of Phase Noise on the Self-Modelocked Ti:sapphire Laser

6.1 Introduction

The modelocked pulse sequences generated by real lasers generally exhibit some degree of random fluctuations in the pulse duration, pulse energy (amplitude noise) and pulse timing (phase noise), so that individual pulses in the sequence are not perfect replicas of one another. Many applications require the synchronisation of optical and electrical pulses or optical pulses from two different sources. The minimum temporal resolution of any measurements made in such circumstances is directly related to the relative timing jitter between the two oscillators, whether they be electrical or optical. As a result the characterisation and reduction of phase noise or pulse timing jitter is of great practical significance.

This chapter begins with a brief review of the principles involved in the measurement of phase noise in modelocked lasers. A technique which is based upon rf spectrum analysis of the laser repetition frequency will be outlined and it will be shown how useful information about the pulse timing jitter can be deduced. The use of a synchronously operating electron-optical streak camera in the evaluation of pulse timing jitter is also demonstrated. A system used to measure the phase noise of the self-modelocked Ti:Al_2O_3 laser will be described and the experimental results obtained will be presented. These show that this laser had a pulse timing jitter of ~10 ps over frequencies up to 5 kHz. In the 5 - 50 kHz region the measured jitter was limited by the noise floor of the detection system and was less than 500 fs.

A general technique which can be used to reduce the pulse timing jitter of passively modelocked lasers is also described and results are included which illustrate its application to the self-modelocked Ti:Al_2O_3 laser. By phase locking the laser cavity frequency to that of a crystal reference oscillator the phase noise of the laser output was reduced to 350 fs (100 - 500 Hz), 250 fs (500 Hz - 5 kHz) and 240 fs (5 - 50 kHz). The probable sources of the phase noise are discussed and the section concludes with a discussion of the

limitations to the locking technique used. In section 6.5 the technique is extended to two self-modelocked lasers in an attempt to reduce the relative timing jitter between them. An absolute relative timing jitter between the lasers of a few picoseconds has been measured. At frequencies above a few tens of Hz this jitter was reduced to a few hundred femtoseconds. The two lasers retained their independence in all respects so that different pulse durations, wavelengths and output powers could be selected as required.

6.2 Theory and Measurement of Noise

A simple but powerful technique which enables one to quantify the noise content in modelocked lasers involves illuminating a fast photodiode with the laser output and analysing the resulting electrical power spectrum of the laser intensity using a microwave spectrum analyser. Such spectral analyses have been widely used to determine the phase stability of radio and microwave oscillators. A theoretical treatment of the characterisation of noise in modelocked lasers was first presented by von der Linde[1]. The power spectral density of the laser intensity is given by the Fourier transform of the intensity autocorrelation function. The experimentally measured power spectrum is truncated due to the finite bandwidth of the measurement system (the detector diode, interconnecting cables and spectrum analyser).

For small phase deviations the power spectrum can be expanded in frequency as an infinite summation to second order over three terms. These terms represent the spectrum which would be produced by a perfectly modelocked laser, the spectrum due to the amplitude fluctuations and the spectrum due to the phase fluctuations. The power spectrum, therefore, consists of a series of δ-functions spaced at the laser repetition frequency, accompanied by a series of associated amplitude noise sidebands and phase noise sidebands. (This is illustrated in figure 6.1.) The small signal approximation is valid when the noise sideband content is sufficiently small so that no secondary sidebands are produced - typically the maximum phase deviation per decade should be less than 0.2 rad.. The important point to note from the analysis is that the amplitude noise sidebands remain constant with increasing harmonic

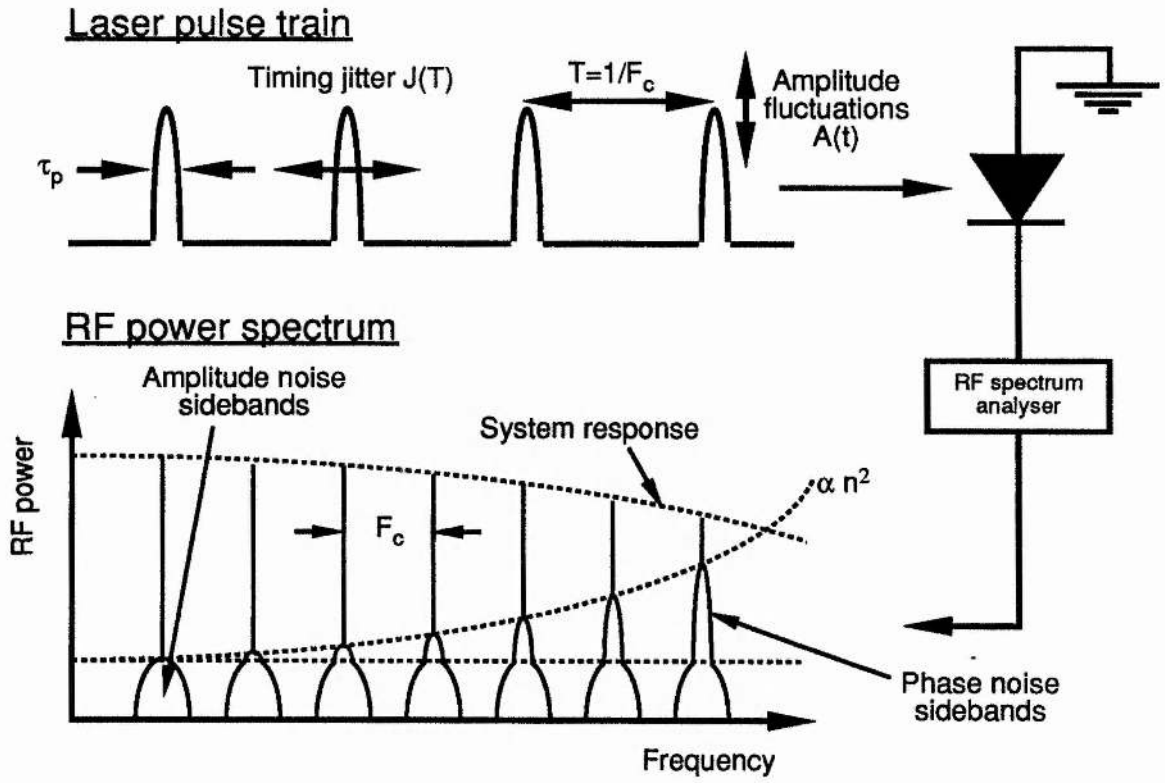

Figure 6.1. Schematic diagram showing the detection of a noisy laser pulse train with a spectrum analyser. The amplitude fluctuations appear as constant energy sidebands on the rf power spectrum, while the phase noise appears as sidebands whose power is proportional to the square of the harmonic number, n.

number while the power of the phase noise sidebands increase quadratically with the harmonic number. Thus the amplitude noise contribution will be dominant at low harmonic numbers while the phase noise contribution will dominate at higher harmonics. By comparing the relative power of the laser harmonic and its sidebands for low and high harmonics it is possible to determine the spectral density of both the amplitude noise and the phase noise.

Spectrum analysers measure the power density P(f), integrated over the resolution bandwidth. It is useful to express the noise content of the recorded signal in terms of the single-sideband noise spectral density of the fundamental, $L_1(f)$, which may by presented as a log-log plot versus frequency[2]. This parameter was originally used to measure the phase stability of microwave oscillators and is defined as the ratio of the power in one phase modulated sideband, in a one Hertz integration bandwidth, to the power in the carrier, P_c. L(f)

has units of dBc per Hz. $L_n(f)$, the noise spectral density for the n-th harmonic, is calculated using equation (6.1)

$$L_n(\Delta f) = 10 \log_{10}\left[\frac{P(nf_0+\Delta f)}{1.2\ B\ P_c}\right] \tag{6.1}$$

where f_0 is the laser repetition frequency, and Δf is the frequency offset from the carrier. The factor of 1.2 is included to normalise the filter response of the spectrum analyser to a rectangular function and accounts for the equivalent noise bandwidth of the device. If the power spectra of the fundamental and a high harmonic are recorded on the spectrum analyser, the corresponding functions $L_1(f)$ and $L_n(f)$ can be calculated from (6.1). Once these functions have been determined, the phase noise spectrum, $L_J(f)$ and amplitude noise spectrum, $L_A(f)$ can be obtained from equations (6.2) - (6.4), where

$$L_J(f) = 10 \log_{10}\left[\frac{10^{L_n(f)/10} - 10^{L_1(f)/10}}{(n^2 - 1)}\right] \tag{6.2}$$

$$L_A(f) = 10 \log_{10}\left[\frac{n^2\ 10^{L_1(f)/10} - 10^{L_n(f)/10}}{(n^2 - 1)}\right] \tag{6.3}$$

$$= 10 \log_{10}\left[10^{L_1(f)/10} - 10^{L_J(f)/10}\right] \tag{6.4}$$

It is also possible to calculate the root-mean-squared (rms) values of the pulse timing jitter, σ_J, and amplitude noise, σ_A, within a frequency range $f_l \le f \le f_h$, which are defined as follows.

$$\sigma_J[f_l,f_h] = \sqrt{\langle J^2(t)\rangle} = \frac{1}{2\pi f_0}\sqrt{\frac{P_{sb}}{P_c}} \quad \text{where } P_{sb} = \int_{f_l}^{f_h} \frac{2\ P_J(f)}{B}\, df \tag{6.5}$$

$$\text{so that } \sigma_J[f_l,f_h] = \frac{1}{2\pi f_0}\sqrt{2\int_{f_l}^{f_h} 10^{L_J(f)/10}\, df} \tag{6.6}$$

where J(t) is the timing fluctuations of the pulse train. Note that the rms phase noise is given by $\phi_{rms} = 2\pi f_0 \sigma_J$. Similarly, if A(t) is the normalised pulse intensity fluctuations, then

$$\sigma_A[f_l,f_h] = \sqrt{\langle A^2(t)\rangle} = \sqrt{\frac{P_{sb}}{P_c}} \quad \text{where } P_{sb} = \int_{f_l}^{f_h} \frac{2\,P_A(f)}{B}\,df \tag{6.7}$$

$$\text{so that } \sigma_A[f_l,f_h] = \sqrt{2\int_{f_l}^{f_h} 10^{L_A(f)/10}\,df} \tag{6.8}$$

In practice, f_l is set by the measurement acquisition time which in turn depends on the sensitivity of the detection system, while f_h is usually determined by the bandwidth of the detection system.

In general, actively modelocked systems such as the acousto-optically (AO) modelocked Ar-ion laser or the synchronously modelocked dye laser exhibit phase noise which results primarily from the active modulation[1]. For example, the low frequency phase noise of a synchronously modelocked dye laser is an exact replica of the noise on the pump laser. This laser also exhibits amplitude and pulse duration fluctuations which have been attributed to the random noise nature of the pulse substructure. The timing jitter of the AO modelocked Ar-ion laser used to pump the dye laser has been attributed to plasma current fluctuations resulting from power supply noise. The phase noise of the electronic rf drive for the modelocker will also result in timing jitter on the laser output.

In contrast, the repetition frequency of passively modelocked lasers is determined by their cavity length, so that the phase noise of these systems can be expected to arise from cavity length fluctuations. Additional amplitude and phase noise can result from amplitude fluctuations on the pump laser, particularly those which result from power supply noise. Slow changes in cavity length over several hours due to thermal effects result in drifts of hundreds of Hertz in the laser repetition frequency. Vibration of the optical components used in the laser cavity resulting from mechanical and acoustic noise in the local environment also produce both amplitude and phase noise on the laser output. Laser cavities containing dye jets suffer from further noise produced by vibrations, nonuniformities and flow perturbations in the jet stream. Since most of the noise is mechanical or acoustical in origin it occurs at frequencies lower than a few kHz.

If periodic variations, δL, occur in the laser cavity length, L, the corresponding frequency variation, δf_L, in the laser repetition frequency, f_L, is given by

$$\delta f_L \approx \frac{\delta L}{L} f_L \tag{6.9}$$

provided $\delta L \ll L$. If these variations occur at a modulation frequency f_m, then the corresponding phase modulation is given by

$$\delta\phi = \frac{\delta f_L}{f_m} = \frac{\delta L}{L}\frac{f_L}{f_m} \tag{6.10}$$

This implies that the rms timing variation of the pulse train at the frequency f_m is

$$\sigma_J(f_m) = \frac{\delta t_{max}}{2\sqrt{2}} = \frac{\delta L}{4\sqrt{2}\,\pi\,L\,f_m} \tag{6.11}$$

It is interesting to use equation (6.11) to estimate the timing jitter which would result from a cavity length change of 10 nm at a frequency of 100 Hz. For a cavity length of 1.74 m, the resulting rms timing jitter is 1.6 ps. In reality, the cavity length changes are distributed over the entire frequency spectrum, but it is evident from this example that a substantial amount of timing jitter can arise from extremely small, low frequency changes in cavity length.

It is also possible to obtain a measure of the relative timing jitter on a laser output by monitoring the modelocked pulses on a synchronously operating electron-optical streak camera. It is well known that the presence of phase noise between the pulse train and the deflection voltage sinusoid applied to the streak camera will lead to a loss of temporal resolution because many streak images are integrated on the phosphor screen. This integration time is ~30 ms[3]. The phase noise can originate either in the deflection electronics or on the laser pulse sequence. It is possible to vary the effective integration time and thus the lower frequency bound of the measurement by shuttering the input to the camera.

6.3 Phase Noise Measurements on the Self-Modelocked Ti:Al_2O_3 Laser

The self-modelocked laser on which the measurements were made was similar to that described in chapter 5. Measurements were made on both the basic laser and the regeneratively initiated system. The cavity length was set to ~1.74 m and the dispersion compensating prism sequence was adjusted to generate chirp-free femtosecond pulses. The laser was operated with a pump power of 6 - 8 W and typically generated sub-100 fs pulses with an average power output of a few hundred milliwatts. As before, tuning was accomplished using a variable aperture. The noise spectrum of the laser was determined as described above using spectrum analysis. A portion of the laser output was directed onto a silicon avalanche photodiode (APD) (Telefunken BPW 28) which had a 3 dB bandwidth of ~2 GHz. This APD was biased at 130 V using a mains power supply which had a high degree of electrical smoothing. (An InGaAs PIN diode was also used, but the APD was preferred because of its larger output signal which reduced the overall noise floor of the measurement system. The PIN diode was biased at between 3 - 10 V, provided by a battery supply.)

The incident laser intensity was adjusted so that the photodiode provided the maximum possible output signal before becoming detectably nonlinear, as evidenced by the appearance of spurious sidebands on the rf spectrum analyser trace. Under these conditions, the diode signal was typically greater than -16 dBm. This signal was coupled to a Hewlett-Packard 71000 series spectrum analyser which had a frequency range of 50 kHz - 22 GHz and 10 Hz resolution bandwidth. The manufacturer's quoted figures for the spectral purity of the local oscillator were: -108 dBc/Hz at 10 kHz offset over 0 - 2.9 GHz and -108 dBc/Hz at 30 kHz offset over 2.7 - 22 GHz. The minimum displayed noise level was -129 dBm over 10 MHz - 2.9 GHz. The spectrum analyser was used to record several power spectra for the laser, each one having a progressively smaller span and resolution bandwidth, down to a span of 1 kHz and a resolution bandwidth of 10 Hz. These measurements were made for the fundamental frequency and for selected higher harmonics. The data were then down-

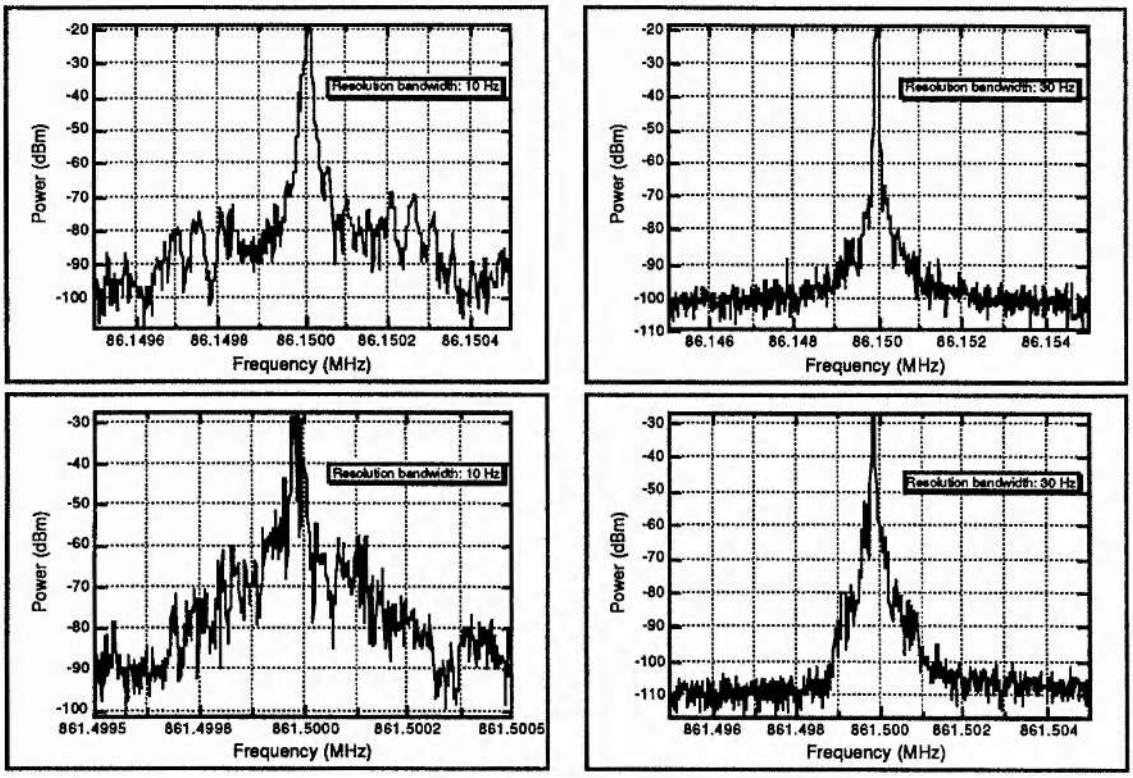

Figure 6.2. Power spectra of the 1st and 10th harmonics of the self-modelocked laser.

loaded into a computer for processing. The computer provided plots of the calculated noise spectrum and associated timing jitter figures.

Data were recorded for the self-modelocked laser using the PIN diode initially. Traces were taken of the fundamental and of the 10th harmonic. The power spectra obtained from the spectrum analyser are given in figure 6.2 for spans of 10 kHz and 1 kHz. It is evident from these traces that the sideband power for frequency offsets of less than a few kHz increased by approximately 20 dB over ten harmonics which is consistent with the presence of phase noise on the laser pulse train. There was no advantage in recording harmonics higher than the 10th because of the relatively large timing jitter in the pulses. From these data, the single sideband phase noise spectrum was obtained as described in section 6.2 and is reproduced in figure 6.3. It is again evident that most of the noise was concentrated at frequencies below a few kHz. At higher frequencies, the noise had dropped to a level which represented the noise

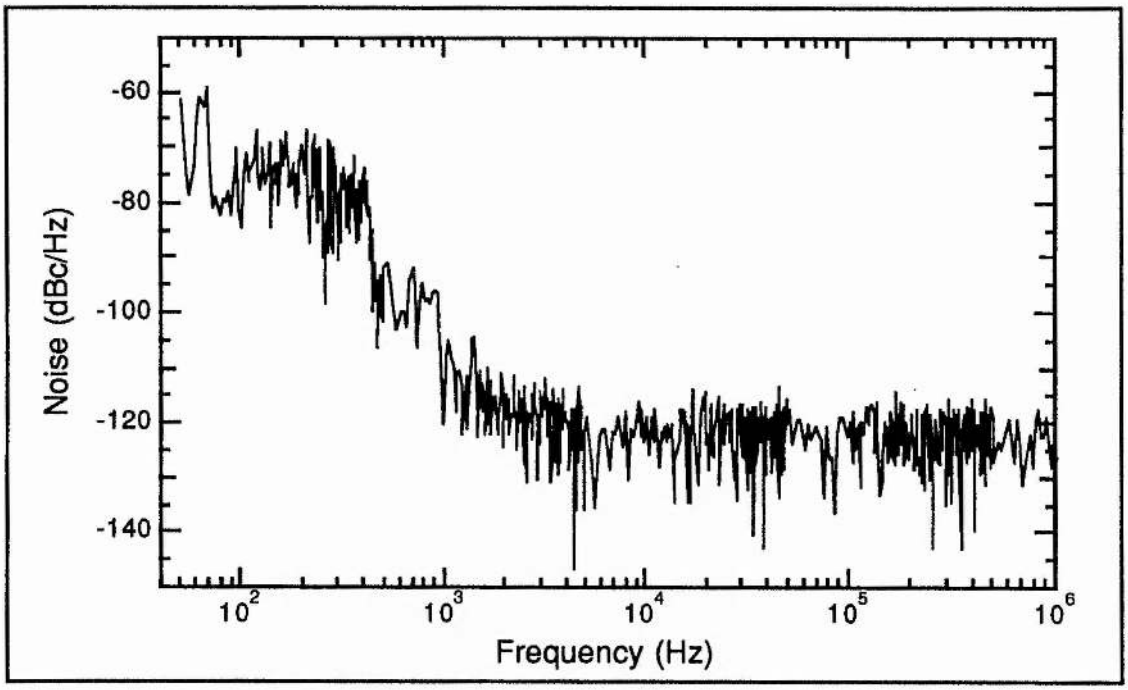

Figure 6.3. Single sideband phase noise spectrum of the self-modelocked laser calculated using the 1st and 10th harmonics.

floor of the measurement system. This behaviour is characteristic of passively modelocked systems where most of the noise results from mechanical and acoustic noise in the environment. The exact sources of the noise on this Ti:Al_2O_3 laser will be discussed more fully in section 6.4. The noise was particularly dominant at frequencies of 50 Hz, 150 Hz and 300 Hz and appeared to correspond to amplitude noise on the Ar-ion pump laser due to inadequate power supply electrical smoothing.† The pulse timing jitter figures calculated for the laser from this data were: 8.6 ps (100 - 500 Hz), 1.1 ps (500 Hz - 5 kHz) and 495 fs (5 - 50 kHz). These figures are summarised in Table 6.1. The lowest frequency limit of 50 Hz was chosen by considering the resolution bandwidth of the spectrum analyser.

† Unfortunately it was not possible to use a noise-eater to remove this noise for the reasons described in chapter 5.

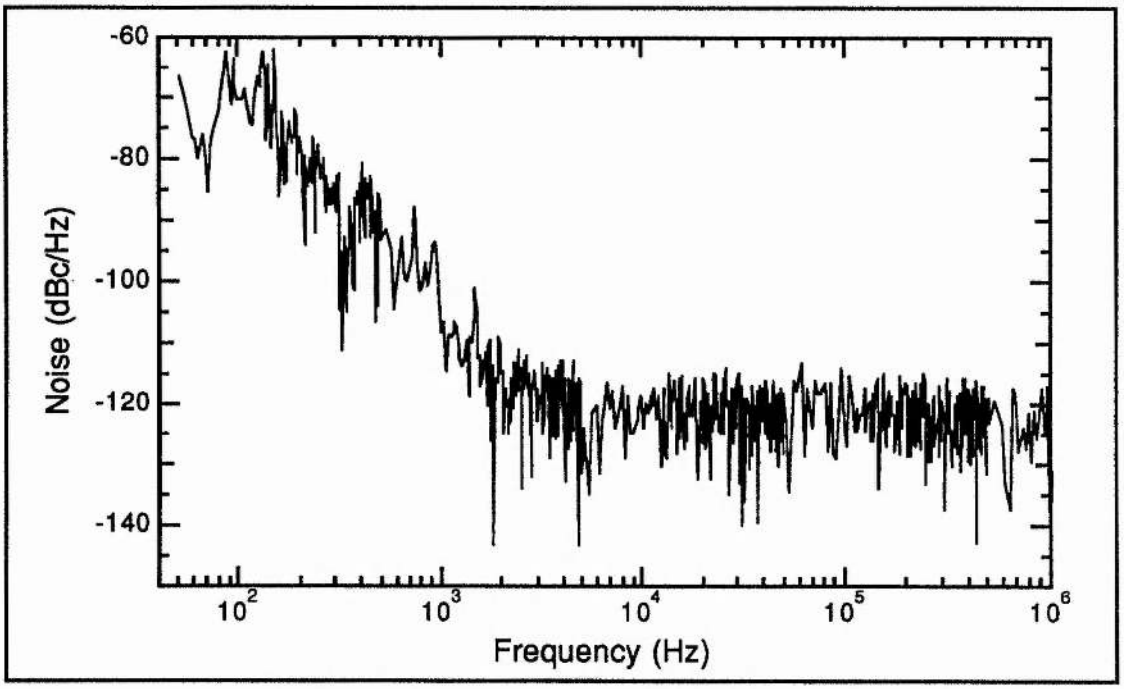

Figure 6.4. Single sideband phase noise spectrum of the regeneratively initiated, self-modelocked Ti:Al_2O_3 laser calculated using the 1st and 10th harmonics.

Similar measurements were repeated for the regeneratively initiated, self-modelocked laser. In this case the silicon APD was used as the detection diode. The results obtained were qualitatively similar to those for the basic laser. The calculated noise power spectrum is presented as figure 6.4, from which the pulse timing jitter was calculated to be: 8.9 ps (100 - 500 Hz), 850 fs (500 Hz - 5 kHz) and 470 fs (5 - 50 kHz). These

	Timing jitter (ps) (100 - 500 Hz)	Timing jitter (ps) (500 Hz - 5 kHz)	Timing jitter (ps) (5 - 50 kHz)
Self-modelocked laser	8.6	1.1	0.50
Regenerative, self-modelocked laser	8.9	0.85	0.47

Table 6.1. Pulse timing jitter figures for the self-modelocked Ti:Al_2O_3 laser.

figures are also summarised in Table 6.1. The similarity between the two sets of results suggests that the operation of the regeneratively driven modelocker did not affect the noise properties of the laser. This was further confirmed because it was possible to disconnect the modelocker drive without any observable change in the power spectrum. This also confirms that the modulator had no noticeable effect on the passive nature of the modelocking process.

6.4 Phase Noise Reduction in the Ti:Al_2O_3 Laser

Cotter[4] first suggested a method by which the phase noise (measured relative to some independent oscillator) of an actively modelocked laser could be reduced by using a phase-locked loop feedback circuit. In this system a photodiode monitored the laser pulse train and the phase of its fundamental frequency was compared with that of an ultra-stable electronic reference oscillator (which also provided the signal for the AO modelocker) to generate a phase error signal. This signal was subsequently amplified and filtered and used to vary the phase of the modelocker driver via a voltage-controlled phase shifter. Given an ideal servo loop the system continuously adjusted the phase of the laser pulse train to equal that of the oscillator so that the relative phase noise between the two was suppressed. The performance of the system was limited by spurious outputs from the phase detector and by the finite loop gain and bandwidth. The absolute suppression of noise was also limited by the phase noise of the reference oscillator. This scheme was also implemented by Rodwell et. al.[2] to reduce the phase noise of an AO-modelocked and pulse compressed Nd:YAG laser which generated pulses having durations of 1.25 ps. The relative timing jitter of this laser was reduced from 20 ps to 0.3 ps over a 0.25 Hz - 25 kHz range.

A similar technique is applicable to passively modelocked systems if the phase error signal is used to vary the cavity length of the laser since it is this variable which determines the repetition frequency of the pulses[5,6]. By considering equation (6.11) and the discussion following, it is apparent that the cavity length must be controlled to a accuracy of the order of a nanometer at frequencies up to a few kilohertz. Piezo-electric translators (PZT's) are well

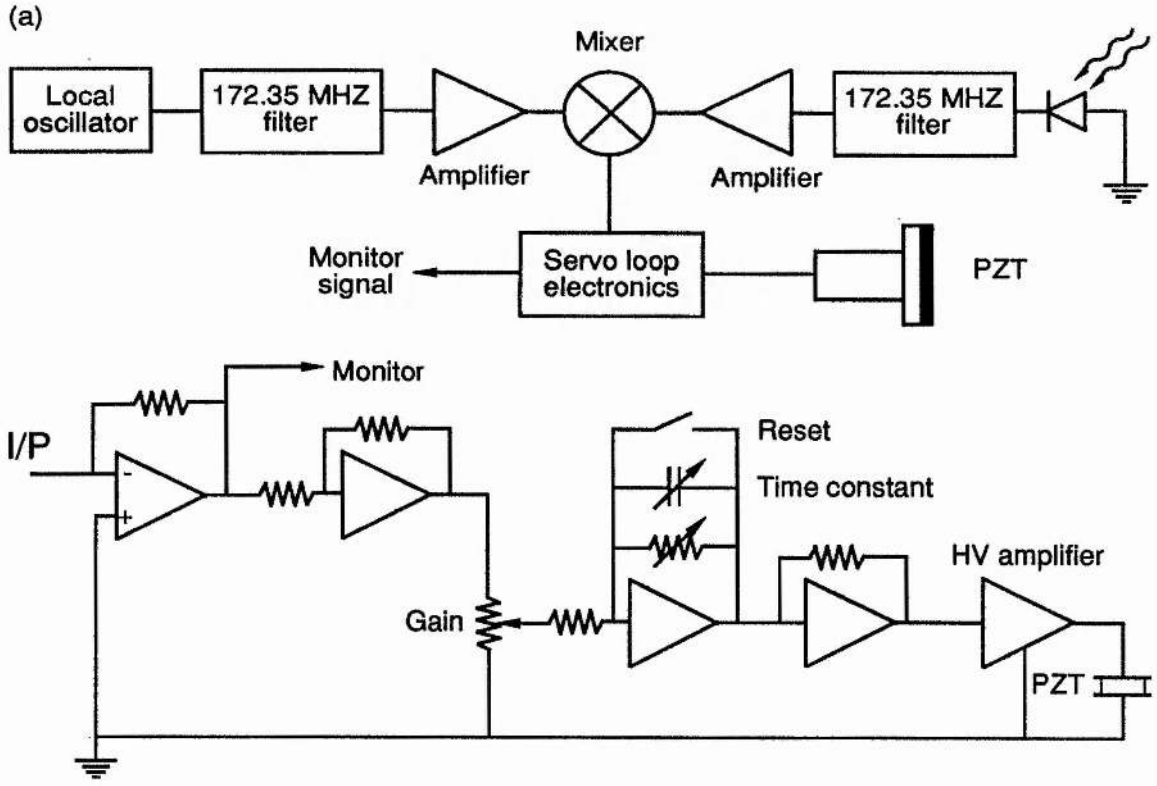

Figure 6.5. Schematic diagrams of the electronics used to phase lock the laser cavity frequency.

suited for this task. Previous work on relative phase noise reduction between a passively modelocked laser and electronic oscillator used the laser oscillator as the frequency reference[7] (with the exception of references 5,6). This is not an ideal technique because the absolute laser noise remains poor and the electronic oscillator is forced to follow this poor reference.

The arrangement used to phase lock the self-modelocked Ti:Al_2O_3 laser is illustrated schematically in figure 6.5. The laser repetition frequency was monitored using a fast photodiode (silicon PIN diode - RS Components Ltd BPX 65) which had a specified cut-off frequency of ~500 MHz. In practice this was the same diode as was used to drive the regenerative modelocker. The diode signal was filtered using a ~5 MHz bandpass passive filter tuned to 172.35 MHz - the second harmonic of the laser repetition frequency. The filter had an insertion loss of < 2 dB. This filtered signal was pre-amplified using a wide-band hybrid rf amplifier (Philips OM 335) which typically provided 27 dB gain with a specified

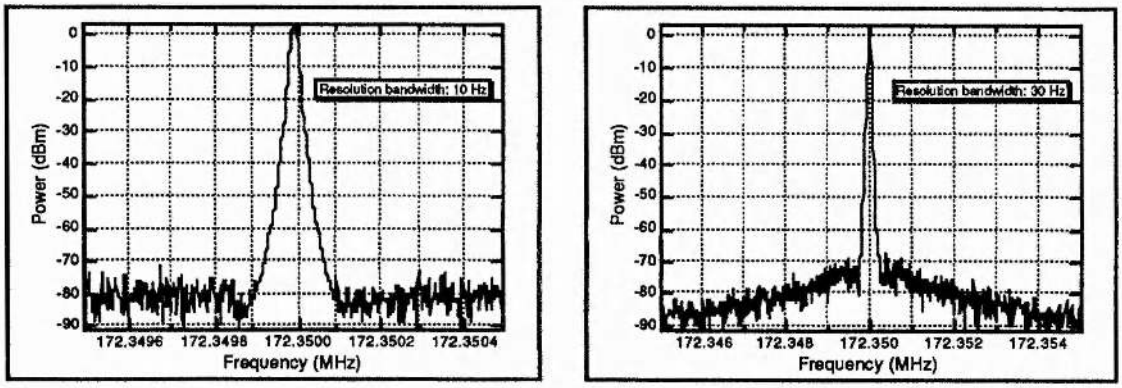

Figure 6.6. Spectrum analyser traces of the output from the electronic crystal oscillator used as the frequency reference.

noise figure of ~5.5 dB. The second rf amplifier was again a wide-band device (Motorola CA 2832) which provided approximately 30 dB of gain with a quoted noise figure of 6 dB at 40 MHz. This amplified signal had its phase compared with that of an ultra-stable electronic crystal reference oscillator. The phase-comparator was a high level (level 13) double-balanced mixer of the diode ring type (Minicircuits SRA-1MH) which had an rf-to-if conversion of approximately -6 dB and a quoted dc offset of <200 μV at the specified drive power of +13 dBm LO and +9 dBm RF. The mixer was typically operated with input powers approximately 3 dB above these values. The reference oscillator had a measured spectral purity of ~-85 dBc at 500 Hz and ~-90 dBc at 5 kHz. Spectrum analyser traces of the output from this device are presented in figure 6.6. The output from the phase-comparator was passed through the circuit shown schematically in figure 6.5 (b) which provided further amplification, together with a variable gain and time constant before being applied to a high voltage amplification stage used to provide an output for the PZT.

The laser cavity configuration used for the experiment is shown schematically in figure 6.7. A plane mirror, which had been ground down to a weight of approximately 100 mg, was attached to the PZT using cyanoacrylate adhesive. This mirror was made as light as practically possible to avoid a serious reduction in the inherent resonance frequency of the piezo. The PZT used was a low voltage type, supplied by Physik Instruments (Model

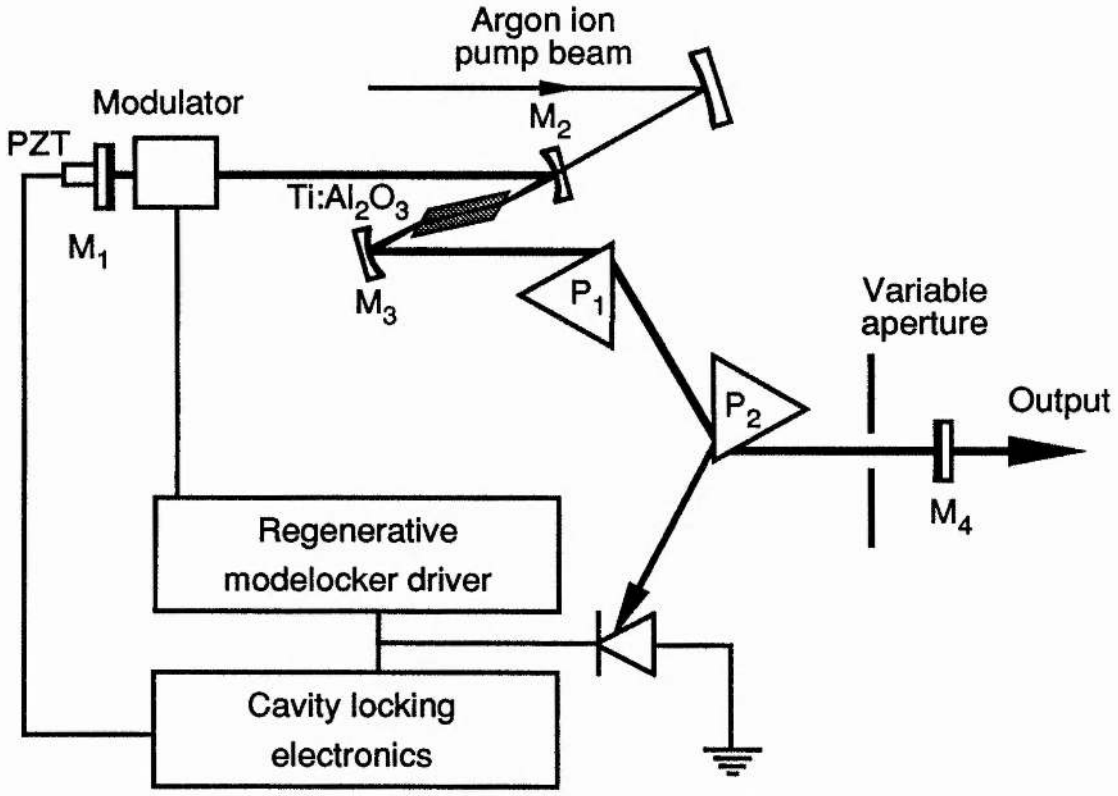

Figure 6.7. Schematic diagram showing the phase-locked laser cavity configuration.

No. P-820.10) and provided ~15 μm movement for a voltage change of 120 V. It had an unloaded resonance frequency greater than 20 kHz. The laser output was taken from the opposite end of the cavity via the 3% transmitting output coupler and the signal for the servo loop was taken from a reflection off one of the dispersion-compensating prisms.

The operation of the laser in this configuration did not significantly affect the noise characteristics of the unlocked system - this was confirmed by repeating the noise measurements described in the previous section. With the laser self-modelocked, the cavity length was adjusted using the translation stage on which the output coupler was mounted in order to match the cavity frequency with that of the reference oscillator. This was achieved by observing the monitor signal from the servo loop. When the cavity length was within the capture range of the electronics, the loop was closed with the gain set to a minimum. Once a loose lock had been achieved, the gain could be increased to the maximum possible value

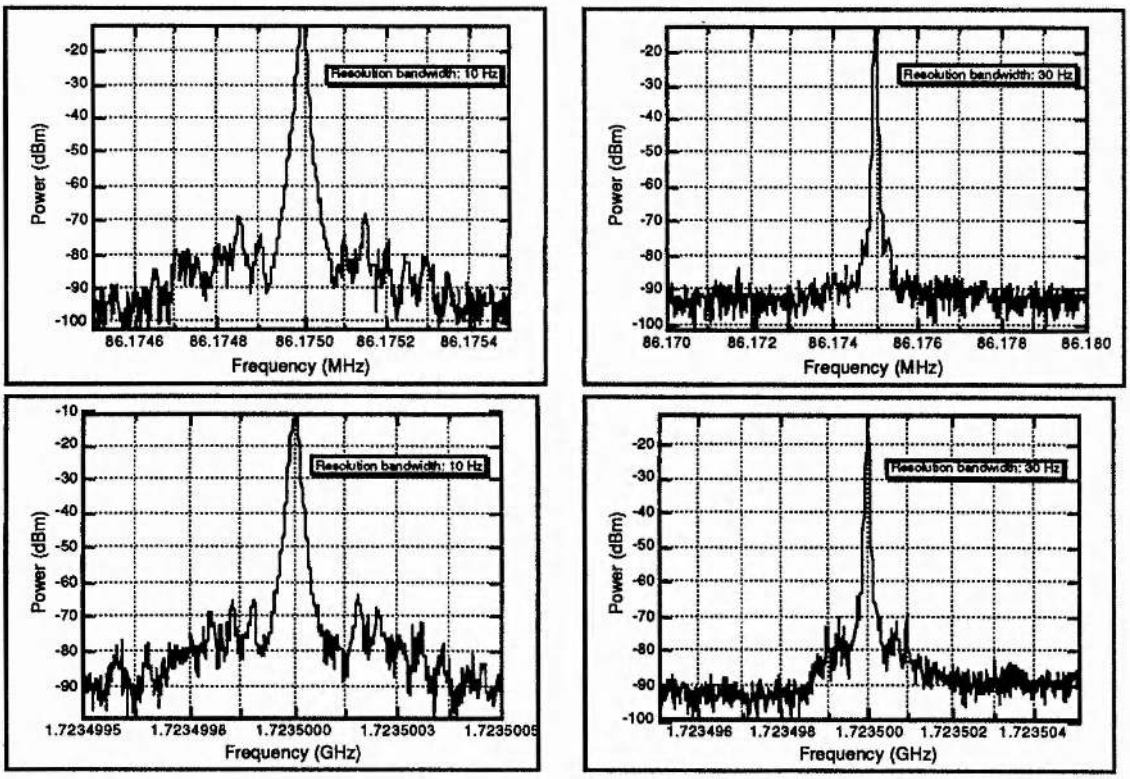

Figure 6.8. Power spectra of the phase-locked laser showing the 1st and 20th harmonics.

which permitted stable operation. The noise measurements were repeated for the phase-locked laser by recording the power spectra for the fundamental and twentieth harmonics. The spectrum analyser data obtained from these harmonics are shown in figure 6.8 for spans of 1 kHz and 10 kHz, while the computed single sideband phase noise spectrum is presented as

	Timing jitter (fs) (100 - 500 Hz)	Timing jitter (fs) (500 Hz - 5 kHz)	Timing jitter (fs) (5 - 50 kHz)
Phase locked to electronic oscillator	350	250	240
Phase locked to optical oscillator (see section 6.5)	369	214	241

Table 6.2. Pulse timing jitter for the phase-locked self-modelocked Ti:Al_2O_3 laser.

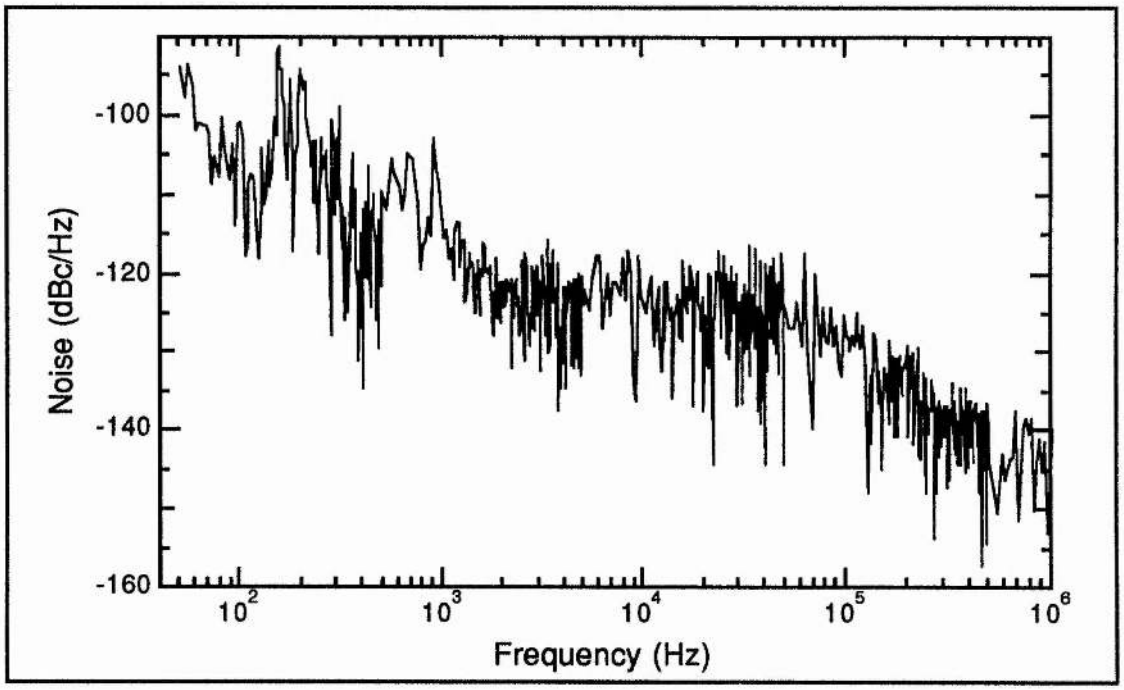

Figure 6.9. Single sideband phase noise spectrum of the phase-locked laser calculated using the 1st and 20th harmonics.

figure 6.9. It can be seen that the noise spectrum retains its characteristic shape but that the noise level has been reduced by almost two orders of magnitude for the lowest frequencies and by a factor of 2 - 3 for frequencies above a few kilohertz. (The reduction is consistent with a loop bandwidth of approximately 1 kHz.) This improvement is confirmed by the calculated pulse timing jitter figures of 350 fs (100 - 500 Hz), 250 fs (500 Hz - 5 kHz) and 240 fs (5 - 50 kHz), which are summarised in Table 6.2. Again, the noise recorded at the higher frequencies was more representative of the noise floor of the measurement system so that the relative laser phase noise at these frequencies could not be accurately determined. It is interesting to note that these figures together with equation (6.11) imply that the cavity length is controlled to a accuracy of $\sim 10^{-9}$ m.

The power spectra and noise spectrum obtained again indicate the presence of relatively dominant amplitude and phase noise components at frequencies of approximately 150 Hz, 200 Hz, 600 Hz and 900 Hz. It is believed that this noise was due to various mechanical

resonances driven by background acoustic noise in the laboratory. This has been confirmed by using a loudspeaker to deliberately induce vibrations within a frequency range of approximately 10 Hz to 10 kHz. The speaker was operated at low power and was placed both in contact with and separate from the optical table top. It was thus possible to identify the exact frequencies which most strongly affected the phase noise characteristics of the modelocked laser. These effects were investigated using an accelerometer in conjunction with an audio frequency spectrum analyser (Brüel & Kjaer Type 2033). This low frequency device was also used to monitor the error signal from the mixer when the laser was loosely phase locked to the reference oscillator.

In this way it was discovered that the original Ti:Al_2O_3 enclosure was responsible for the component near 150 Hz, which was by far the most dominant of all the resonances. Vibration of the laser cover was also responsible for the component near 900 Hz. Interestingly, the component at 200 Hz was caused by a resonance of the optical table top (this was consistent with the frequency response data for the table supplied by the manufacturer - Newport Corporation). The component at a frequency near 600 Hz was caused by ambient acoustic noise arising from the water pump which was incorporated into the cooling system of the argon-ion laser. Finally the component at 100 Hz was attributable to power supply noise. It is possible that a reduction in the level of ambient noise in addition to an improved laser enclosure would diminish the amplitude of the mechanical vibrations at these frequencies, but it is not certain that this would lead to a significant reduction in the phase noise characteristic of the laser because this noise was already heavily suppressed by the servo loop.

When the laser was phase locked the remaining error signal measured approximately 5 - 10 mV peak to peak with most of the noise arising at frequencies below one kilohertz. Thus, although much of the laser noise was suppressed, a small amount remained. The origin of most of the remaining noise has been discussed above. There are several possible reasons why the servo loop was unable to completely remove all of this noise. It is possible for the servo loop to introduce phase noise into the laser by a process referred to as amplitude modulation to phase modulation (AM-PM) conversion[2]. This can occur in the phase

comparator because its output is a function of both phase and amplitude. If this device has a non-zero dc offset (as all real mixers do), changes in the amplitude of the input signals result in corresponding variations of the phase detector's output which ultimately leads to closed-loop timing jitter. The obvious practical solution to this problem is to ensure large input signal levels so that the effects of the dc offset are minimised. However, if any of the components in the loop begin to saturate so that their response becomes nonlinear, AM-PM conversion will again occur. The servo loop cannot distinguish between real laser timing fluctuations and spurious phase modulation occurring through AM-PM conversion from either of these sources. Obviously inherent noise in the amplifiers and other components of the phase detection system can also result in spurious outputs. A compromise has to be made when choosing high signal levels which minimise the spurious noise terms but which do not cause significant AM-PM conversion through saturation effects.

The obvious requirement that the servo loop be well damped limits the achievable loop gain and bandwidth so that all of the laser noise cannot be completely removed. The requirement that the gain be small in the region of the piezo resonance (<20 kHz) limits the loop bandwidth to a few kilohertz. A final source of absolute phase noise† results from the timing jitter of the reference oscillator because the servo loop attempts to maintain zero phase difference with respect to this signal. In practice it is not difficult to obtain relatively low noise reference oscillators so that the noise contribution from this source is usually small. To summarise, the major contributions to the pulse timing jitter of the phase-locked laser arise from mechanical vibrations in the laser components and phase errors in the electronic servo loop.

---

† The ultimate cause of phase noise on a laser output is quantum mechanical in nature and is due to spontaneous emission in the gain medium. However, the noise from this source is not likely to be significant compared to that introduced by the environmental sources discussed in the text.

6.5 Time Synchronisation Between Two Self-Modelocked Ti:Al_2O_3 Lasers

Applications such as electro-optic (EO) sampling[8] require the synchronisation between an optical oscillator and an electronic oscillator and the technique described in the previous section can be used to achieve this. More elaborate EO sampling experiments, or dual-wavelength pump probe measurements may require the synchronisation of two independent laser oscillators, perhaps with a third electronic oscillator. Previously, dual-wavelength pump-probe measurements have necessarily involved the complicated technique of continuum generation[9] using high peak power laser sources which usually include pulsed amplifiers having repetition frequencies limited to a few kilohertz. Such schemes are also limited by their relative inefficiency which severely restrict the useful power output available for the experiment. Clearly, the discussions already presented in this chapter, illustrate that the use of two independently modelocked lasers is not a practical technique for these measurements because of the presence of pulse timing jitter on both laser outputs. Passive modelocking schemes generally result in the shortest pulses having the highest peak powers and the random nature of the pulse evolution further complicates the problem of synchronisation.

It has been demonstrated that it is possible to phase lock one passively modelocked laser to an electronic reference oscillator. In this section the techniques just described are modified, to enable two passively modelocked lasers to be phase locked to a third reference oscillator, or to one another. Both lasers retain their independence in all respects so that different wavelengths and/or pulse durations can be selected as required. To obtain a cross-correlation between the outputs of two passively modelocked lasers their cavity periods must be precisely matched and the pulses must be initially synchronised. If one of the laser cavity lengths subsequently change, the two pulse trains will temporally walk off due to the change in repetition frequency. If the cross-correlation is to be re-established, the cavity lengths must not only be matched again, but they must be matched in such a way as to bring the pulses back into phase and then maintain their temporal coincidence. Thus, it is not sufficient to lock the cavity frequencies together, the cavities must be locked together in phase.

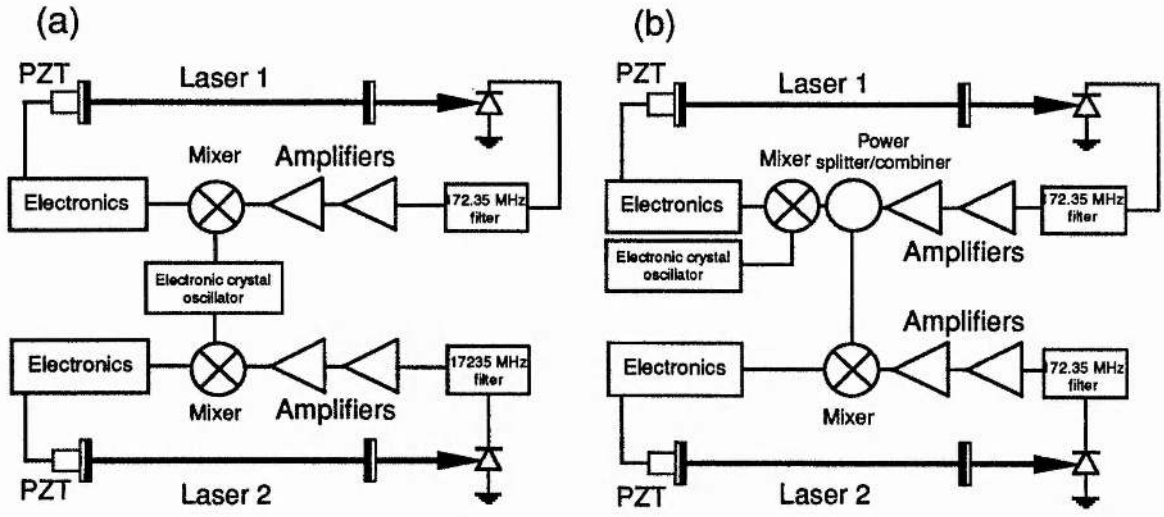

Figure 6.10. Schematic diagram showing the schemes used to phase lock two passively modelocked laser together: (a) both lasers locked to the same reference oscillator; (b) first laser locked to reference oscillator and second laser locked to first.

The use of a streak camera to measure the timing jitter of a modelocked laser has already been briefly mentioned. Such a device is a useful tool for obtaining an upper limit on the timing jitter of one or two modelocked lasers with respect to the signal used to drive the camera deflection. By shuttering the optical input to the camera it is also possible to deduce the frequency limit below which the predominant phase noise occurs, because shuttering effectively decreases the overall integration time. If the drive signal for the deflection system is obtained from the same electronic reference oscillator used to phase lock the laser cavity, then the recorded streak durations will give a measure of the relative timing jitter between the laser output and the reference oscillator, within the limitations set by the temporal resolution of the streak camera. Alternatively, the camera can be driven by a signal derived from one of the laser outputs and used to measure the pulse duration of the other laser. In this case the recorded streak durations give an indication of the relative phase noise between the two laser oscillators.

The two lasers systems used for the synchronisation experiment were similar to those described in the previous section of this chapter and both were made as similar as possible.

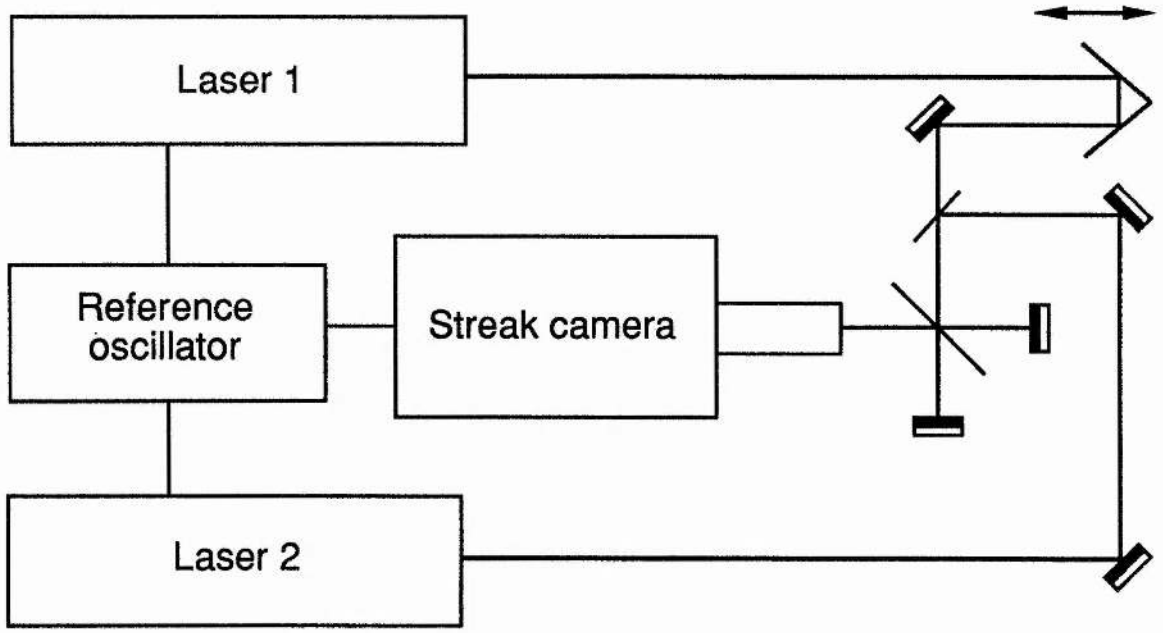

Figure 6.11. Schematic diagram showing the experimental arrangement used to measure relative timing jitter on the streak camera.

Phase noise measurements were repeated on both systems with the servo loops both on and off. The results for each individual laser were not significantly different to those described above and indicate that the performance of both lasers was indeed similar. Two approaches to the problem of time synchronising the laser outputs have been compared. One involved locking both lasers independently to the same electronic reference oscillator, while the other involved locking one of the lasers to the reference oscillator and locking the second laser to the first. These two experimental schemes are illustrated schematically in figure 6.10.

In order to obtain an upper bound on the relative timing jitter between the two lasers, both modelocked outputs were simultaneously monitored on a synchronously operating streak camera. The camera tube used for these measurements was a Photochron II C, which had an extended red (S25) photocathode[10]. Under the experimental conditions described here, this tube had a measured limiting resolution of 1.8 ps. The streak images were recorded using an optical spectrum analyser (B&M Type OSA 500). The deflection voltage applied to the camera was derived from the electronic reference oscillator at 172.35 MHz as illustrated

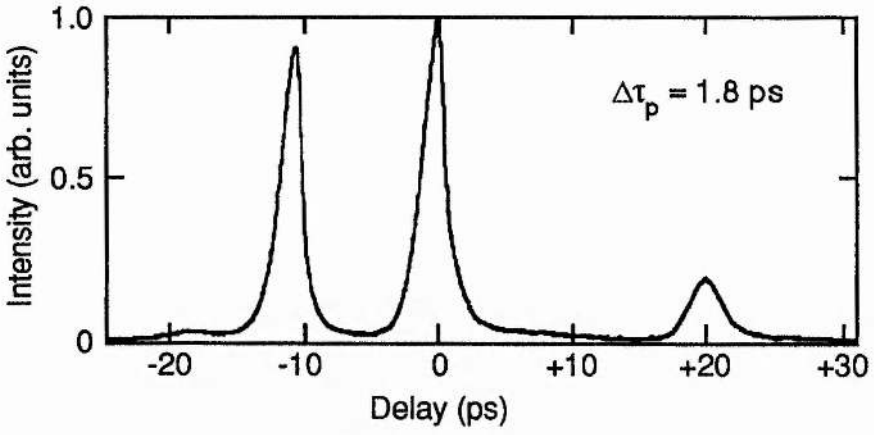

Figure 6.12. Streak images for pulse sequences from each laser. The delay between the 2nd and 3rd pulses is 20 ps, and the recorded streak durations are 1.8 ps.

schematically in figure 6.11. With this scheme, any phase noise relative to the reference oscillator would be evident as a broadening of the recorded streak images. Note that as the laser pulse durations were <100 fs, the measured streak durations in the absence of phase noise, should be equal to the resolution limit of the camera. With both lasers phase locked to the reference oscillator and the optical path lengths between the laser outputs and the camera suitably adjusted, streak images of the pulses from each laser could be observed. The condition that the signals applied to the LO and RF inputs of the phase comparators be held in phase-quadrature ensured that the two pulse sequences were maintained continuously in temporal synchronism when the servo loops were in operation.

A typical streak profile for the pulses is presented as figure 6.12. A calibration for the trace is provided by the second and third pulses from the left which were obtained from the same laser but with a delay equivalent to 20 ps. This implies that the streak durations were 1.8 ps for both lasers. Because the durations of these recorded streak images were limited by the temporal resolution of the camera they could only represent an upper bound for the timing jitter.

An alternative synchronisation scheme (presented schematically in figure 6.10 (b))

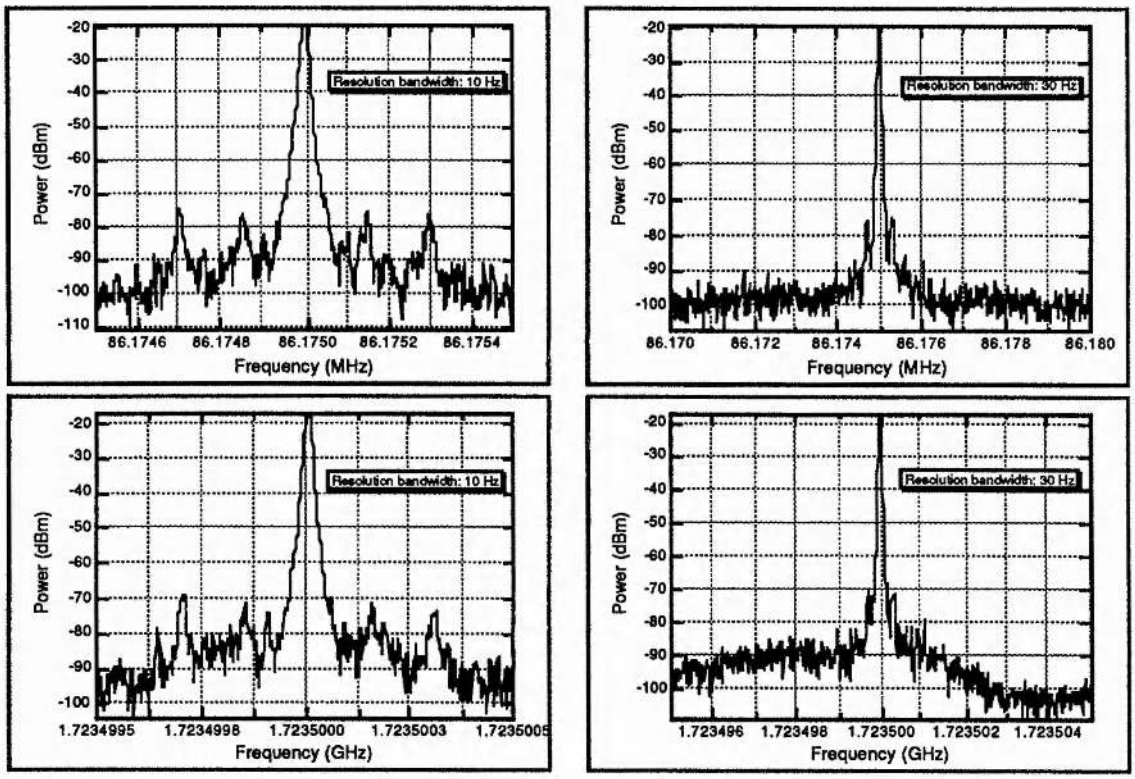

Figure 6.13. Power spectra for the 1st and 20th harmonics of the laser when phase locked to the first laser.

involved phase locking one of the lasers to the other, ie. using one laser as an optical reference oscillator. In practice this optical reference oscillator was first phase locked to the electronic oscillator. This had the advantage of reducing the absolute phase noise of both lasers and also resulted in more reliable phase-locked operation of the second laser. Power spectrum data were recorded for this scheme as before. As expected, the timing jitter of the laser which was locked directly to the electronic reference did not differ significantly from that already recorded (see Table 6.2). The data obtained for the second laser, which was locked to the optical reference, is presented as figure 6.13. The single sideband phase noise spectrum calculated from this data is shown in figure 6.14. Qualitatively, the timing jitter of both lasers were similar. The calculated timing jitter figures for the second laser were 369 fs (100 - 500 Hz), 214 fs (500 Hz - 5 kHz) and 241 fs (5 - 50 kHz) and are summarised in Table 6.2. The jitter in the frequency range 100 - 500 Hz was marginally worse than before, but it must be

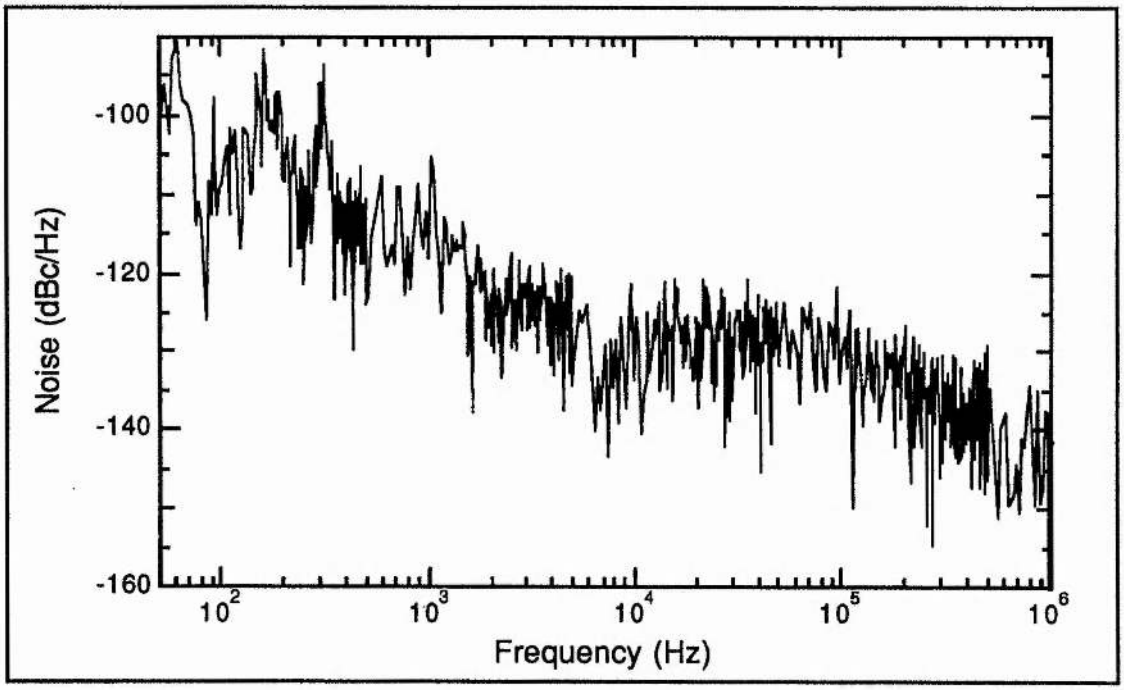

Figure 6.14. Single sideband phase noise spectrum, calculated using the 1st and 20th harmonics, for the self-modelocked laser when phase locked to the first laser.

remembered that the optical reference oscillator had a higher noise spectrum than the electronic oscillator. As has already been mentioned, noise on the reference oscillator will affect the absolute phase noise of the system. Thus, in this case, the measured noise of laser 2 relative to the spectrum analyser's local oscillator was worse, but this does not necessarily imply that the relative noise between the two lasers was also poorer. In practice the first scheme was preferred because it resulted in improved long term stability for both lasers.

In order to measure the absolute timing jitter between both lasers an attempt was made to measure the second-order cross-correlation function of the two modelocked outputs. The crosscorrelator was based on a modified second-harmonic generation (SHG) autocorrelator in which the degree of overlap of a pulse from one laser with a pulse from the other was varied in the nonlinear crystal, while the resulting SHG output was monitored. This did not provide an entirely satisfactory measurement because the integration time of the detection system was insufficiently long. Although the observed cross-correlations had estimated durations of a few

hundred femtoseconds, the recorded profiles did not remain stationary on the oscilloscope, but randomly varied their positions at low frequencies (of the order of 20 Hz) with a total deviation of 1 - 2 ps. Consequently, an accurate calibration of the crosscorrelator was not possible, but the observations are consistent with the other data. It is most likely that this low frequency phase noise was due to phase errors in the electronic amplifiers and mixers used in the servo loops.

The servo system used the second harmonic of the lasers' repetition frequency at 172.35 MHz for phase locking. In general it might be advantageous to use the higher harmonics for phase comparison because of the increase in the ratio of phase-to-amplitude noise in proportion to the square of the harmonic number. However, this has a interesting side effect for the problem of obtaining a cross-correlation between the two laser pulse trains. The reference frequency, in this case, was twice the lasers' repetition frequency and thus there were two possible positions at which a lock could be achieved. The pulses could be overlapped at some reference point but could equally well be separated by 6 ns - half of the cavity period. Obviously, as the reference frequency is increased, the number of possible points in a cavity period where a lock can be achieved also increases. For a practical system which would provide reliable cross correlations some means of ensuring that phase locking always occurred at the right phase would be a helpful addition to the system. In these experiments, if the lasers locked up with the pulses separated by 6 ns, the cross-correlation could usually be restored by momentarily interrupting the operation of the servo loop and then allowing it to recapture lock with the correct phase.

One solution to this problem would involve having a second phase sensitive detector which compared the phases of the fundamental laser repetition frequency and reference oscillator output. These fundamental signals could be derived from their higher harmonics by frequency division. The resulting fundamental phase error signal would be fed into a comparator and integrator. If the input signal to the comparator was below a predefined level the output would be zero and only the high harmonic phase error signal would affect the position of the PZT. However, if the laser cavity locked at the wrong position, the output

from the fundamental detector would be large enough to trigger the second loop which would force the PZT to the correct position, after which the first loop would again take over and provide accurate cavity stabilisation as before.

Equation (6.11) implies that if the timing jitter is to be reduced to the order of a pulse width, at frequencies less that 100 Hz, then the cavity length must be controlled to an accuracy of better than 0.5 nm (greater than 1 part in 10^9). Bearing this in mind it is interesting to note that a change in air temperature of 1°C at 20°C results in an equivalent length change of ~1.0 μm/m, which results in an equivalent timing drift of more than 50 ps/ms. This underlines the importance of ensuring good temperature stability in the lab and, in particular, the avoidance of air currents within the experimental set-up. Another point worth mentioning concerns the positioning of the reference diodes for the servo loop. Because the pulses originating from different lasers travel over different paths, synchronism maintained at the reference diodes does not necessarily imply that the pulses will be overlapped everywhere. In practical systems it would, therefore, be advisable to position the reference diodes as close as possible to the sample under examination. Of course, both of these effects will only have a minor influence when compared with the other primary sources of noise.

The data described in this section can be reviewed by summarising all of the results obtained for the synchronised lasers. Firstly, the SHG cross-correlation data suggested that the two lasers had a relative timing jitter of a few hundred femtoseconds, or 2 - 4 times the pulse duration on a time-scale of ≤50 ms, but that the overall jitter could be in the region of 1 - 2 ps. Streak camera measurements confirmed that the total jitter was in this range. Time synchronisation of two femtosecond lasers does not, therefore, seem feasible unless improvements in the noise characteristics of both the electronic and laser systems are made. On the other hand, this technique is capable of synchronising two lasers producing pulses in the picosecond regime.

6.6 Conclusions

In this chapter the main concern has been with the pulse timing jitter of the self-modelocked Ti:Al_2O_3 laser. Following a general discussion of the technique used for measuring the phase noise on modelocked lasers, its application to this laser was described. Results have been presented showing that the timing jitter over a frequency range between 50 Hz and 5 kHz was ~10 ps. The probable sources of this jitter have been identified as being acoustic and mechanical background noise in the laboratory.

A technique which can be generally used to reduce phase noise on passively modelocked lasers was then discussed. This involved locking the phase of the modelocked pulse sequence to that of an ultrastable electronic reference oscillator. Some of the most important limitations to this technique were pointed out and the results obtained for the the reduced timing jitter on the Ti:Al_2O_3 laser were presented. These results show that the jitter was reduced to 350 fs (100 - 500 Hz), 250 fs (500 Hz - 5 kHz) and 240 fs (5 - 50 kHz).

In the final section of the chapter the technique was extended to two self-modelocked lasers and the relative phase noise between the two systems was recorded. The absolute jitter between the lasers was 1 - 2 ps. This jitter decreased to a few hundred femtoseconds at frequencies above a few tens of Hertz. Because both of these lasers retained their independence in all respects, this technique could have applications to dual wavelength pump-probe experiments and other schemes requiring synchronised picosecond pulses at two different wavelengths. The technique is particularly useful because it can be used to synchronise the laser repetition frequency to any reference oscillator - optical or electrical.

6.7 References

1. D. von der Linde, Appl. Phys. Lett. B **39**, 201, (1986).

2. M.J. Rodwell, D.M. Bloom and K.J. Weingarten, IEEE. J. Quant. Electron. **QE-25**, 817, (1989).

3. A. Finch, W.E. Sleat and W. Sibbett, Rev. Sci. Instrum. **60**, 839, (1989).

4. D. Cotter, 'Techniques for highly stable active modelocking', in Ultrafast Phenomena IV, D.A. Auston and K.B. Eisenthal, eds., New York, Springer-Verlag, (1984), p.78.

5. S.B. Darack, D.R. Dykaar and G.T. Harvey, Opt. Lett. **16**, 1677, (1991).

6. D.R. Walker, D.W. Crust, W.E. Sleat and W. Sibbett, IEEE. J. Quant. Electron. **QE-28**, 289, (1992).

7. G.T. Harvey, M.S. Heutmaker, P.R. Smith, M.C. Nuss, U. Keller and J.A. Valdmanis, IEEE. J. Quant. Electron. **QE-27**, 295, (1991).

8. K.J. Weingarten, M.J.W. Rodwell and D.M. Bloom, IEEE. J. Quant. Electron. **QE-24**, 198, (1988).

9. F.Salin, J.Squier and G. Mourou, Opt. Lett. **16**, 1964, (1964).

10. W. Sibbett, W.E. Sleat and W. Krause, Proceedings of the European Space Agency Workshop on Laser Applications and Technology, (Les Diablerets, Switz.), **ESA SP-10**, 171, (1984).

Chapter 7
General Conclusions

The work described in this thesis has been concerned with the generation of ultrashort pulses in the 700 nm - 1000 nm region using tunable, solid state laser materials. Such lasers are highly desirable because of the breadth of applications for both cw and modelocked sources at these wavelengths. Although this spectral region is well covered by available organic dyes, solid state gain media offer many advantages such as cleanliness, extended operating lifetimes, greater power output and potentially better stability. In this thesis, the operation of a passively modelocked LiF:F_2^+ colour-centre laser was initially studied, although most of the work concentrated on the Ti:Al_2O_3 laser. This latter system was first actively modelocked using an acousto-optic modulator. Of more interest were the passive techniques of coupled-cavity modelocking and self-modelocking which were used extensively. In this concluding chapter the results which have been presented are briefly summarised and some of the areas where future work might be concentrated are identified.

Before the advent of materials such as Ti:Al_2O_3, the LiF:F_2^+ colour-centre laser represented the most promising solid-state alternative to the dye laser at wavelengths in the sub-1 μm region. However, the colour-centre gain medium presented its own difficulties. Of most importance was the requirement that it be maintained at liquid nitrogen temperature to prevent the thermal destruction of the laser active centres. After a brief review of the physics of colour centres, the necessary storage and handling precautions for the F_2^+ colour centre were outlined in chapter 2. The construction and operation of a laser based on these colour centres was described. This laser was continuously tunable over the 820 - 1000 nm spectral region with up to 400 mW of average power (chopped with a duty cycle of 1:10). Provided adequate cryogenic cooling was maintained, the laser crystals had useful lifetimes of approximately 200 hrs.

The technique of passive modelocking, using the organic dye, DaQTeC, was applied to the laser in a linear cavity configuration and pulses having durations of approximately 170 fs

were generated. The modelocked laser was tunable over the 925 - 950 nm region and produced average powers of approximately 10 mW, which corresponded to peak powers of ~700 W. The passively modelocked laser was also configured in a ring geometry which enabled pulses as short as 127 fs to be generated with an average power of ~7 mW per output beam. In this configuration, the ring laser was also observed to operate in a unidirectional mode, with the pulse durations remaining unchanged. An intracavity prism sequence was included in the modelocked laser cavity to provide dispersion compensation. Again, the measured pulse durations did not change significantly. These observations suggest firstly, that the expected enhancement in pulse shortening due to colliding pulses in the absorber was not significant. This might be explained by the fact that the pulse width was already shorter than the dye jet thickness, which has been shown to decrease the effectiveness of the additional pulse shortening mechanism[1]. Secondly, the GVD compensation did not effect the modelocked pulse durations. This implied that the effects of dispersion and nonlinearity in the modelocked laser were not significant. This could be expected for the operating conditions of the laser, where the intracavity powers were relatively small, the pulse durations were greater than 100 fs and the operating wavelengths were close to the peak of both the gain and absorber transitions[2]. The dominant pulse shaping mechanisms were, therefore, likely to be due to dynamic gain and absorber saturation. The observed critical dependence of the position of the gain and absorber with respect to the intracavity beam waists supported this fact.

A severe limitation of this passively modelocked laser, was its relatively restricted tunability and the short lifetime of the saturable absorber dye. In an attempt to extend both of these, a nonlinear external cavity was added to the laser. With this addition, the laser was able to generate modelocked pulses at wavelengths as low as 900 nm and operate for longer periods between dye changes. However, due to the necessity for actively stabilised cavities, which was not feasible at the time, these results could only demonstrate the viability of the technique.

With the introduction of new materials such as Ti:Al_2O_3, both dye and colour-centre lasers covering the 700 - 1000 nm spectral region became largely obsolete for most applications. Chapter 3 began with a brief review of the growth and spectroscopy of laser quality Ti:Al_2O_3 material. The operation of a commercially available cw Ti:Al_2O_3 laser was characterised. This system was tunable from 700 - 1000 nm and could provide up to 3 W of average output power at wavelengths around 850 nm. The basic configuration was modified to enable the laser to be actively modelocked and pulses as short as 60 ps were measured.

Generally, passive modelocking produces shorter pulses than active techniques. However, the relatively small gain cross-section and long upperstate lifetime of Ti:Al_2O_3, means that it is not ideally suited to traditional saturable absorber based methods where dynamic gain saturation is required for stable modelocked operation. The technique of coupled-cavity modelocking provides an alternative form of passive modelocking which does not require dynamic gain saturation to achieve pulse shortening. This scheme was applied to a modified Ti:Al_2O_3 laser and resulted in the generation of pulses as short as 1.3 ps. Coupled-cavity modelocked operation was observed to reliably self-start without any active modulation. This laser generated pulses which were approximately linearly frequency chirped and which could be effectively compressed outside the laser cavity using diffraction gratings or prisms. Compressed pulses having durations of 290 fs were recorded.

It was realised that the relatively high amounts of normal dispersion in both the external cavity and the main cavity must influence the performance of the laser. Initially a four prism sequence was added to the coupled-cavity section in an attempt to compensate for the fibre dispersion. This led to a reduction in pulse duration from 4 ps to 1.3 ps, however the modelocked output still showed evidence of frequency chirp. With a prism sequence in the main resonator only, the pulse durations were reduced to 120 fs and by inserting a prism sequence in both cavities the shortest pulses were obtained with durations of 90 fs. The results showed that the magnitude and sign of the intracavity GVD played and important role in determining the pulse durations generated from the laser.

It was also observed that the coupled-cavity modelocked laser often operated in stable states were the output consisted of more than one pulse per round trip, or in which the modelocked output was accompanied by a weak cw background. Results were presented which illustrated some of these modes of operation and their occurrence was linked to high levels of intracavity peak power. Since these high power levels were primarily required to achieve self-starting, it is probable that more satisfactory laser operation could be achieved with the introduction of some active modulation. This would lower the power level at which the coupled-cavity modelocking process started and consequently would allow the laser to be operated with lower intracavity peak powers. For example, the inclusion of a regeneratively driven acousto-optic modulator in the main laser cavity should allow reliable self-starting operation at reduced powers, without adversely affecting the passive nature of the coupled-cavity modelocking process.

Stable operation of coupled-cavity lasers required that the lengths of the two cavities be matched, except for a constant phase bias, which was achieved by using an active feedback loop to control the length of the external resonator. This complicated the laser configuration and added a potential source of instability because an interferometric match was required. One system which overcame this difficulty was the self-modelocked Ti:Al_2O_3 laser which was discussed in chapter 5. In the basic configuration, the laser generated pulses having durations of 2 ps and was continuously tunable over the 750 - 950 nm region, with up to 500 mW of average power being produced. These picosecond pulses were frequency chirped and could be directly compressed outside the laser cavity to durations as short as 380 fs. Using intracavity dispersion compensation, the laser produced pulses as short as 60 fs with an average power of ~600 mW which corresponded to a peak power of more than 100 kW. Using conventional pulse compression techniques, the pulse durations could be further reduced from ~100 fs to 45 fs. The self-modelocking process was self-sustaining but not self-starting. By including a regeneratively driven acousto-optic modulator within the laser cavity, the self-starting threshold was lowered sufficiently, so that femtosecond pulse

generation could be reliably obtained. The results again showed that the pulse durations depended on the magnitude and sign of the intracavity GVD.

In order to generate shorter pulses from the Ti:Al_2O_3 laser, it would be necessary to compensate for the effect of third, as well as second order dispersion. The situation can be improved by choosing suitable material, which has small third order dispersion for the intracavity optical elements, particularly the prisms. The length of the intracavity material through which the pulses travel should also be minimised. These approaches have already led to some success[3]. Direct compensation of third order dispersion within the laser cavity is difficult because the most straight forward method requires the use of diffraction gratings which are too lossy for intracavity use[4]. The use of a Gires-Tournois interferometer (GTI)[5] is a second possibility, but these are relatively inefficient and difficult to design, particularly if broad tunability is required. A third technique which has been demonstrated outside the resonator with some success uses a slightly bent mirror located at the filter plane of a femtosecond pulse shaper[6]. An alternative approach to the generation of shorter pulses is the use of extracavity pulse compression techniques.

The construction of the crosscorrelator described in chapter 1 would provide a useful tool for accurate measurements of the shape and phase of the modelocked pulses generated from the Ti:Al_2O_3 laser and from similar modelocked, solid state oscillators. The self-modelocking process has already been demonstrated in Nd:YLF[7] and Cr:LiSAF and should be applicable to other gain media such as Cr:LiCAF, Cr:YAG, etc. Some of these materials are currently under investigation at St. Andrews.

The tunability and high powers available from the Ti:Al_2O_3 laser make it ideally suited as a pump source for various nonlinear phenomena. Processes such as parametric oscillation, second harmonic generation and sum frequency generation can be used to further extend the wavelength range available from the basic laser. Second harmonic generation at wavelengths near 860 nm has been used in this laboratory to provide short pulses in the blue spectral region for the study of II - VI semiconductor compounds and further work is planned in this

area. Work is also in progress with the aim of constructing a Ti:Al_2O_3 pumped OPO based on KTP and LBO which will extend the wavelength range out to the 2.8 μm region. Such a femtosecond OPO may be one alternative means of simultaneously generating synchronised pulses at two different wavelengths.

In chapter 6, the relative phase noise, or pulse timing jitter, of the self-modelocked Ti:Al_2O_3 laser was measured using a technique based upon rf spectrum analysis of the laser repetition frequency. The results suggested that the laser had a timing jitter of ~10 ps at frequencies below 5 kHz and of <500 fs at frequencies in the 5 - 50 kHz region. A method to reduce the phase noise of passively modelocked lasers was described and was applied to the Ti:Al_2O_3 laser. This involved phase locking the laser repetition frequency to that of an electronic reference oscillator. Using this technique, the pulse timing jitter was reduced to 350 fs over the 100 - 500 Hz range and to <250 fs over the 0.5 - 5 kHz and 5 - 50 kHz ranges. The remaining noise on the laser was attributable to environmental acoustic and mechanical vibrations in the laser components.

The technique just described was also applied to two similar modelocked Ti:Al_2O_3 oscillators and the relative phase noise between them was measured. The total timing jitter was found to be <5 ps. At frequencies above about 20 Hz this jitter was reduced to 200 - 300 fs. The technique is, therefore, not suitable for synchronising two femtosecond lasers, but could be used for picosecond pulses. It has the advantage of allowing the laser repetition frequency to be synchronised to any reference source - optical or electrical.

Low phase noise optical sources have direct applications in electro-optic sampling experiments. Another area of interest at St. Andrews is the evaluation of synchronously operated streak cameras having femtosecond resolution. Low phase noise between the optical pulses and the camera deflection signal is an obvious requirement in such circumstances. The scheme described in chapter 6, to measure the timing jitter of the modelocked laser has also been used to reduce the timing jitter between the laser output and the camera deflection signal so that the best performance can be achieved. Further work is being carried out in this area.

One drawback with laser materials such as Ti:Al_2O_3 is the necessity for optical pumping with inefficient ion lasers. The development of efficient diode pump sources for such materials would, therefore, be of considerable interest. Other materials, such as Cr:YAG can be pumped directly by diode pumped Nd:YAG systems. The Ti:Al_2O_3 laser would require a frequency doubled, diode pumped system. This has already been demonstrated[8] and with the continual improvement in high power diode laser technology, should become a practical and economic reality. The Cr:LiSAF laser is of interest because of its ability to be directly pumped by laser diodes in the 670 - 750 nm region. Such all solid state modelocked (and cw) systems would benefit not only from improved efficiency, but should also have improved noise and stability characteristics.

References

1. M.S. Stix and E.P. Ippen, IEEE J. Quant. Electron. **QE-19**, 520, (1983).

2. J.A. Valdmanis and R.L. Fork, IEEE J. Quant. Electron. **QE-22**, 520, (1983).

3. C-P. Huang, H.C. Kapteyn, J.W. McIntosh and M.M. Murnane, Opt. Lett. **17**, 139, (1992).

4. C.H. Brito Cruz, P.C. Becker, R.L. Fork and C.V. Shank, Opt. Lett. **13**, 123, (1988).

5. K.D. Li, W.H. Knox and N.M. Pearson, Opt. Lett. **14**, 450, (1989).

6. J.P. Heritage, E.W. Chase, R.N. Thurston and M. Stern, Conference on Lasers and Electro-Optics, CLEO Tech. Digest Series **10**, paper CTuB3, (1991).

7. G.P.A. Malcolm and A.I. Ferguson, Opt. Lett. **16**, 1967, (1991).

8. J. Harison, A. Finch, D.M. Rines, G.A. Rines and P.F. Moulton, Opt. Lett. **16**, 581, (1991).

Acknowledgements

I would like to thank my supervisor, Professor Wilson Sibbett, for his continued support and guidance throughout this project. I am particularly grateful to Dr Bill Sleat for all his advice and for his invaluable assistance with electronics. I am also grateful to Mr Bob Mitchell for his advice and for help with the vacuum and cryogenic systems. Thanks are also due to the technical staff, in particular, Mr Jimmy Lindsey, for constructing many of the mechanical components. I would like to thank Mr David Crust for writing much of the computer software used. Thanks must also go to Dr Colin Johnston and all the members of the "WS" research group for practical help and for useful discussion. Finally, I am grateful to Dr John Dudley for proof reading the manuscript and for accepting responsibility for any remaining errors; (but not for breaking the ND-wheel mentioned in chapter 4).

I am indebted to the Department of Education for Northern Ireland for financial support.

Publications

FEMTOSECOND PULSE GENERATION IN THE 900–950 nm REGION FROM A PASSIVELY MODELOCKED LiF:F_2^+ COLOUR CENTRE LASER

C.I. JOHNSTON, D.E. SPENCE, R.S. GRANT and W. SIBBETT

J.F. Allen Physics Research Laboratories, Department of Physics and Astronomy, University of St Andrews, North Haugh, St. Andrews, Fife, KY16 9SS Scotland, UK

Received 14 June 1989

The passive mode-locking characteristics of a LiF:F_2^+ colour centre laser operating around 930 nm using the saturable absorber DaQTeC are described. For a standing-wave cavity configuration pulses of 170 fs duration were generated and implementation of colliding-pulse-modelocking in a travelling-wave ring cavity led to pulse duration reduction to 130 fs. Experimental data relating to laser configurations involving either the intracavity compensation of group velocity dispersion or the technique of coupled-cavity modelocking are also presented and discussed.

1. Introduction

The application of passive mode-locking to cw dye lasers has led to the development of a range of ultrashort optical pulse sources for the visible and near-infrared spectral regions [1–3]. Sub-30fs pulse durations have been reported for colliding-pulse-modelocked (CPM) ring dye lasers in which self-phase-modulation and group velocity dispersion effects arising in the laser cavity have been controlled [4,5]. More recently, by passively modelocking a LiF:F_2^+ colour centre laser using the saturable absorber dye IR140 pulse durations of 180 fs have been obtained at operating wavelengths around 850 nm [6]. In this letter we describe the passive mode-locking of a similar LiF:F_2^+ laser operating in the 930 nm wavelength region and we report the generation of stable pulses as short as 128 fs duration when the saturable absorber dye DaQTeC was employed. The potential applicability of the coupled-cavity modelocking scheme [7] to enhance the pulse evolution kinetics at the spectral extremes of the saturable absorber dye absorption or where the effectiveness of the saturable absorber dye decreases (through aging for example) will also be discussed.

2. Experimental

Our inhouse designed LiF:F_2^+ colour centre laser [8] was used initially in conjunction with the six mirror standing-wave cavity illustrated in fig. 1. This arrangement had the convenience that it could be readily modified to form a travelling-wave ring cavity by suitable reorientating mirrors M1 and M6 as shown in fig. 1. Mirrors M1 to M5 had 100% reflectivity within the tuning range of the LiF:F_2^+ gain medium, (i.e. 800–1000 nm) and the output coupler M6 was 3% transmitting over this range. The focusing mirrors M2 and M3 were of 10 cm radius of curvature which provided a beam waist in the gain medium of approximately 20 μm. Mirror M3 also acted as a focusing mirror for the 647 nm, 676 nm pump beam ($\sim$3 W) from a krypton-ion laser. Efficient coupling for the pump beam into the gain medium was ensured by the selection of a double stack dielectric sequence with the IR reflector deposited on top so that phase distortion in the pulses could be minimised [9]. The focusing mirrors M4, M5 around the saturable absorber dye jet were of 5 cm radius of curvature thus ensuring that the "S parameter" was appropriate for stable passive modelocking of this laser [10,11]. The saturable absorber used here was the photosensitive dye 1-diethyl-2,13-acetoxy-1,2-quinotetracarbocyanine perchlorate (DaQTeC) [12]

0 030-4018/89/$03.50 © Elsevier Science Publishers B.V. (North-Holland Physics Publishing Division)

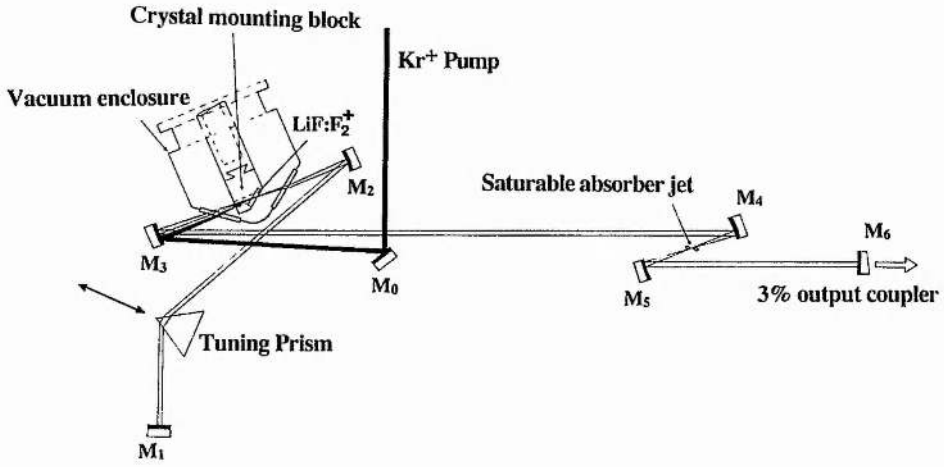

Fig. 1. The passively mode-locked LiF: F_2^+ standing-wave laser cavity. The alternative ring cavity configuration is formed by the reorientation of mirrors M_1 and M_6.

which has been used (in iodide form) by other workers [13] to produce ~230 fs pulses by hybrid modelocking of dye lasers near 975 nm. The DaQTeC was dissolved in a small amount of ethanol before being added to a free flowing 65 μm thick jet of ethylene glycol placed at the beam waist of mirrors M4 and M5. Pulse durations were deduced from data for a standard collinear intensity second harmonic generation autocorrelation technique where $sech^2$ intensity profiles were assumed.

The laser was initially passively mode-locked in the standing-wave configuration of fig. 1 where the cavity round-trip period was 12 ns. Stable pulse trains were obtained over the spectral region 924 nm to 946 nm in this regime for a saturable absorber dye concentration of 0.6×10^{-5} ML^{-1}. The shortest pulses had durations of 170 fs at wavelengths around 930 nm with a corresponding spectral bandwidth of 6.25

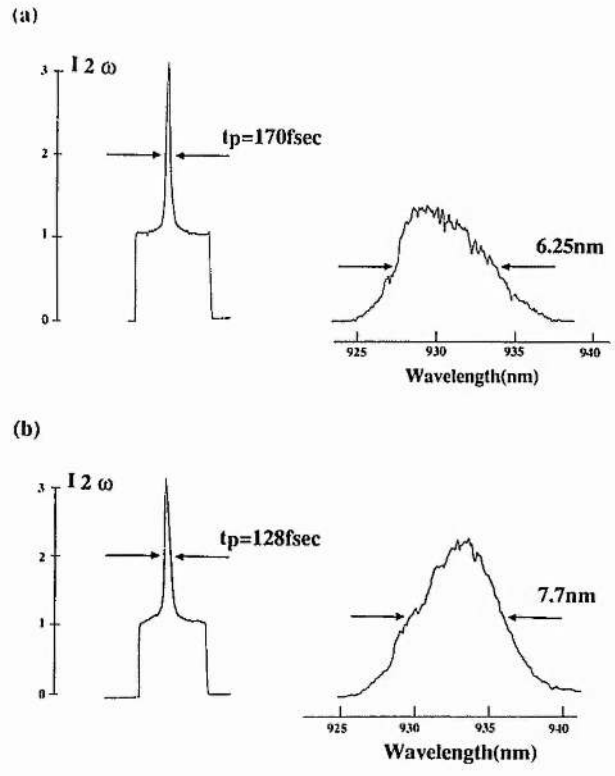

Fig. 2. Autocorrelation trace and associated spectra for the shortest pulses produced in (a) the standing-wave cavity and (b) the CPM ring cavity.

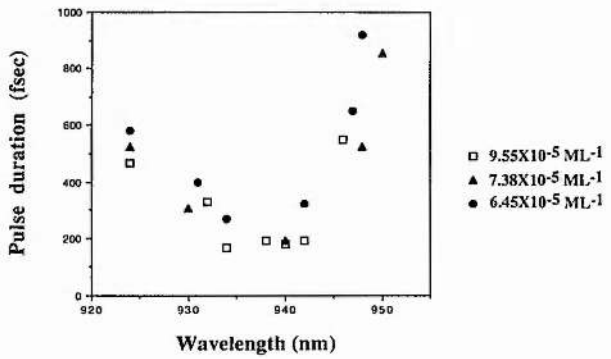

Fig. 3. The dependence of the pulse duration as a function of wavelength for several saturable absorber dye concentrations.

nm which implies a duration–bandwidth product of 0.37. These were obtained at a pump power of 2.3 W (chopping duty cycle of 10) where the time-averaged output power of the colour centre laser was 10 mW. An intensity autocorrelation trace of these shortest pulses is reproduced in fig. 2(a) together with the spectral profile and in fig. 3 the variation of the pulse duration as a function of wavelength is presented for a range of saturable absorber dye concentrations.

By suitably adjusting the orientations of mirrors M1 and M6 to constitute a colliding-pulse ring cavity configuration stable pulses having the somewhat shorter durations of ~130 fs were obtained around

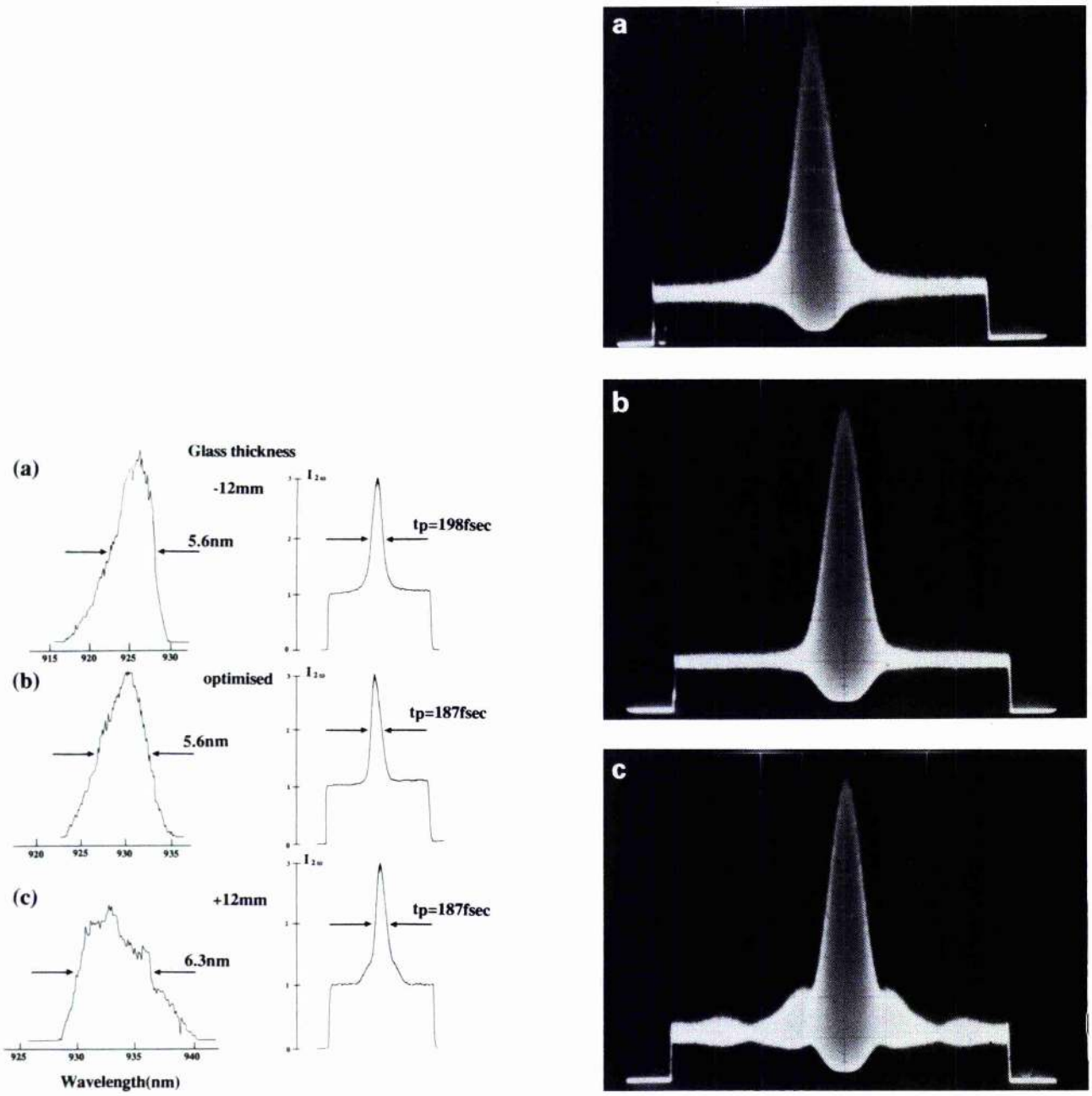

Fig. 4. Intensity and interferometric autocorrelation traces and associated pulse spectra for pulse trains with different intracavity glass path lengths showing evidence of low frequency chirp within the laser cavity.

932 nm for dye concentrations $\sim 1\times10^{-4}$ ML^{-1}. The corresponding bandwidth of these pulses was 7.7 nm which implies a duration–bandwidth product of 0.34. This is consistent with the presence of a relatively small amount of frequency chirp which arises due to self-phase-modulation in the saturable absorber dye jet [14,15]. An intensity autocorrelation trace of these pulses and the associated spectrum are included as fig. 2(b). The cavity period in this case was 13 ns and for pump laser powers of 2.3 W the time averaged power available in each output beam was 6 mW. (The chopping factor of 10 was retained.)

Although the duration–bandwidth product was close to the Fourier transform limit of 0.315 for sech^2 pulse profiles it was decided to insert an intracavity prism sequence by which the intracavity group velocity dispersion (GVD) could be controlled [6,16]. The inclusion of this prism sequence served merely to retain the stability of the pulse train with essentially no effect on the observed pulse durations and we conclude that this is consistent with the presence of a low degree of frequency-chirp for the operating conditions of the laser described here. Confirmation of this was evidenced by the intensity and interferometric autocorrelation data and corresponding pulse spectra as shown in fig. 4 for various amounts of intracavity GVD [17]. This can be contrasted to the previously reported passive modelocking characteristics of this laser in the 850 nm spectral region using the saturable absorber dye IR 140 where significant amounts of frequency chirp were observed [6].

As with most saturable absorber dyes which operate in the near infra-red region of the spectrum the useful lifetime of the saturable absorber DaQTeC was of the order of several days. Beyond this operating period the durations of the mode-locked pulses were observed to increase dramatically and the operating wavelength band of the laser tended towards the peak of the LiF:F_2^+ gain, around 900 nm. Under these operating conditions, when the laser was tuned to operating wavelengths near 930 nm where the shortest pulses were usually obtained, relatively broad pulses (1–2 ps) were generated with frequent evidence of the subpulse structure, as shown in fig. 5(c). At this point it was decided to implement the technique of coupled-cavity mode-locking to the passively mode-locked LiF:F_2^+ colour centre laser as this had the potential to contribute to the pulse shaping and shortening kinetics so that the demand placed upon the saturable absorber could be relaxed. This "hybrid" mode-locking scheme therefore becomes significant for instances where saturable absorber dyes become less efficient through aging or when used in spectral regions at the extremities of their absorption profile.

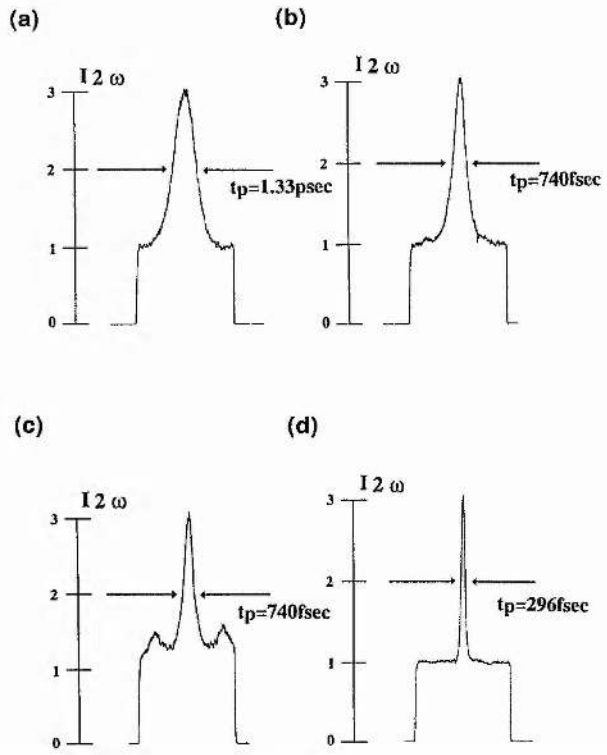

Fig. 5. Intensity autocorrelations for the hybrid mode-locked laser (i.e. passive modelocking together with coupled-cavity mode-locking), (a) pulses from master cavity at 904 nm (coupled-cavity blocked), (b) pulses from CCM laser at 904 nm, (c) pulses from master cavity at 932 nm (coupled-cavity blocked), (d) pulses from CCM laser at 932 nm.

To assess this type of "hybrid" mode-locking, a standing-wave cavity was employed where the positions of mirrors M1 and M6 where suitably adjusted (the 3% output coupler was replaced by a 10% output coupler) and the intracavity prism sequence was removed. The optical fibre used in the control cavity was an elliptical-core (1.25 μm×2.5 μm) polarization-preserving fibre (Andrew Corporation) with a core cladding $\Delta n \sim 0.034$. The fibre length was 4.52 m and the coupled cavity period was twice that of the colour centre laser cavity. Intensity autocorrelation traces for pulses produced from the colour

centre laser operating alone, with a much degraded saturable absorber dye, are reproduced in fig. 5 for the conditions of (a) a much extended operating wavelength of 904 nm and (c) the normal operating wavelength of 932 nm. The corresponding autocorrelation traces for coupled-cavity mode-locked pulse trains are reproduced in (b) and (d) respectively. (For both operating wavelengths the krypton-ion pump power was 2.2 W and the power launched into the fibre was 30 mW). It can be readily seen that the mode-locking is substantially enhanced for the coupled-cavity scheme and this indicates that this approach may be a practical "hybrid" technique for passively mode-locked laser systems.

Acknowledgements

Research studentship support for D.E. Spence from the Department of Education of Northern Ireland (DENI), and for R.S. Grant from the Science and Engineering Research Council (SERC), is acknowledged. Personal support for C.I. Johnston from the Procurement Executive of the Ministry of Defence (MOD) is also gratefully acknowledged. The overall research funding was provided by the MOD and SERC. The authors would also like to thank Mr. R.H. Mitchell for specialist technical assistance concerning the vacuum and cryogenic equipment used in this work.

References

[1] P.M.W. French and J.R. Taylor, Optics Comm. 61 (1987) 224.
[2] P.M.W. French and J.R. Taylor, Appl. Phys. Lett. 50 (1987) 1708.
[3] K. Smith, N. Langford, W. Sibbett and J.R. Taylor, Optics Lett. 10 (1985) 559.
[4] O.E. Martinez, R.L. Fork and J.P. Gordon, J. Opt. Soc. Am. B2 (1985) 753.
[5] A. Finch, G. Chen, W. Sleat and W. Sibbett, J. Mod. Opt. 35 (1988) 345.
[6] N. Langford, R.S. Grant, C.I. Johnston, K. Smith and W. Sibbett, Optics Lett 14 (1989) 45.
[7] P.N. Kean, X. Zhu, D.W. Crust, R.S. Grant, N. Langford and W. Sibbett, Optics Lett. 14 (1989) 39.
[8] N. Langford, K. Smith and W. Sibbett, Optics Lett. 12 (1987) 903.
[9] P. Laporta and V. Magni, Appl. Optics 24 (1985) 2014.
[10] G.H.C. New, IEEE J. Quantum electron. QE-10 (1974) 115.
[11] G.H.C. New, Optics Comm. 6 (1972) 188.
[12] Saturable Absorber Dye purchased from Gallard-Schlesinger Chemical MFG Corp, 594 Minola Ave, Carle Place, NY 11414.
[13] M.D. Dawson, T.F. Boggess and A.L. Smirll, Optics Lett. 12 (1987) 590.
[14] J.J. Fontaine, W. Dietal and J.C. Diels, IEEE J. Quantum Electron. QE-19 (1983) 1467.
[15] R.S. Miranda, G.R. Jacobovitz, C.H. Britocruz and M.A.F. Scarparo, Optics Lett. 11 (1986) 224.
[16] R.L. Fork, O.E. Martinez and J.P. Gordon, Optics Lett. 9 (1984) 150.
[17] J.C. Diels, J.J. Fontaine, I.C. McMichael and F. Simoni, Appl. Optics 24 (1985) 1270.

60-fsec pulse generation from a self-mode-locked Ti:sapphire laser

D. E. Spence, P. N. Kean, and W. Sibbett

J. F. Allen Physics Research Laboratories, Department of Physics and Astronomy, University of St. Andrews, North Haugh, St. Andrews, Fife, KY16 9SS, Scotland

Received July 20, 1990; accepted November 2, 1990

Pulses having durations as short as 60 fsec have been directly generated by a self-mode-locked, dispersion-compensated Ti:sapphire laser. By using an extracavity fiber–prism pulse compressor, pulse durations as short as 45 fsec have been obtained.

Titanium:sapphire ($Ti:Al_2O_3$) has been shown to be an attractive gain medium for laser operation in the near-infrared spectral region. Its broad gain bandwidth means that in addition to a large tuning range it is especially well suited to ultrashort-pulse generation and amplification. $Ti:Al_2O_3$ lasers have been mode locked by using a variety of techniques, including synchronous pumping,[1,2] acousto-optic mode locking,[3–5] passive mode locking,[6] injection seeding,[7] and coupled-cavity (also referred to as additive-pulse or interferential) mode locking,[8,9] in which the mode-locking process may be self-starting.[10]

To date the shortest pulses reported from $Ti:Al_2O_3$ lasers have had durations of 300 fsec and have been generated using injection-seeding techniques.[7] By using a nonlinear external cavity, pulses as short as 800 fsec have been directly generated from an actively mode-locked coupled-cavity laser.[8] By using a diffraction grating pair outside the laser cavity for dispersion compensation, the output from a self-starting coupled-cavity $Ti:Al_2O_3$ laser has been compressed to 200 fsec.[10] With intracavity dispersion compensation, pulses as short as 150 fsec can be directly produced.[9]

In this Letter we present results for a self-mode-locked $Ti:Al_2O_3$ laser from which pulses having durations of 2 psec can be generated. By using an intracavity two-prism sequence for dispersion compensation,[11] the pulse durations can be directly reduced to less than 100 fsec at average laser powers in excess of 400 mW. A further reduction in pulse duration to less than 50 fsec can be achieved by using an extracavity fiber–prism pulse compressor, which incorporates four high-dispersion ZnSe prisms in a configuration that provides adjustable anomalous group-velocity dispersion (GVD).

The self-mode-locked $Ti:Al_2O_3$ laser, illustrated schematically in Fig. 1, is a modified Spectra-Physics Model 3900 system. The main laser cavity, consisting of mirrors M_0 to M_3, was extended to between 1.5 and 2.0 m, with the 20-mm-long Brewster-angled $Ti:Al_2O_3$ gain medium placed in the center of the cavity. The plane output coupler M_0 had a transmission of approximately 3.5% over the 850–1000-nm spectral region, and the spherical mirrors M_1 and M_2 ($r = 10$ cm) were highly reflecting over this wavelength range and highly transmitting for the 488–514-nm pump wavelengths. The pump laser was a Spectra-Physics Model 2030 argon-ion laser that operated on all lines in the visible at as much as 20 W of power in a TEM_{00} mode. The pump beam passed through a periscope arrangement to rotate the plane of polarization by 90° and was focused into the $Ti:Al_2O_3$ gain medium by spherical mirror M_4, which had a radius of curvature of 22.8 cm. The prisms P_1 and P_2 were made from high-dispersion SF14 glass and were Brewster angled for minimum deviation at approximately 850 nm. They constituted the intracavity double-prism sequence for dispersion compensation, as shown in the inset of Fig. 1. For tuning purposes the standard Spectra-Physics three-plate birefringent filter was replaced by either a single-plate birefringent filter or by a variable-aperture slit placed between P_2 and M_3.

The mode-locked pulses from the laser were recorded by using a real-time autocorrelator that provided both intensity and interferometric autocorrelation data. A fast photodiode and oscilloscope combination was used to monitor the pulse sequence, and the spectral characteristics of the pulses were recorded with a 25-cm scanning monochromator that had a resolution of approximately 0.8 nm.

With the cavity arrangement shown in Fig. 1, the pump power threshold for cw laser oscillation was approximately 1 W, and at a pump power level of 6 W the output power of the $Ti:Al_2O_3$ laser was typically ~500 mW. In this configuration the laser could be made to

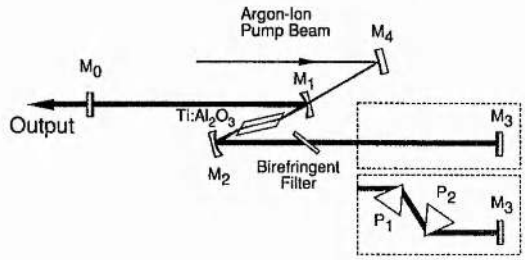

Fig. 1. Schematic of the cavity configuration for self-mode-locked $Ti:Al_2O_3$ laser. The inset shows the intracavity prism sequence for dispersion compensation.

0146-9592/91/010042-03$5.00/0 © 1991 Optical Society of America

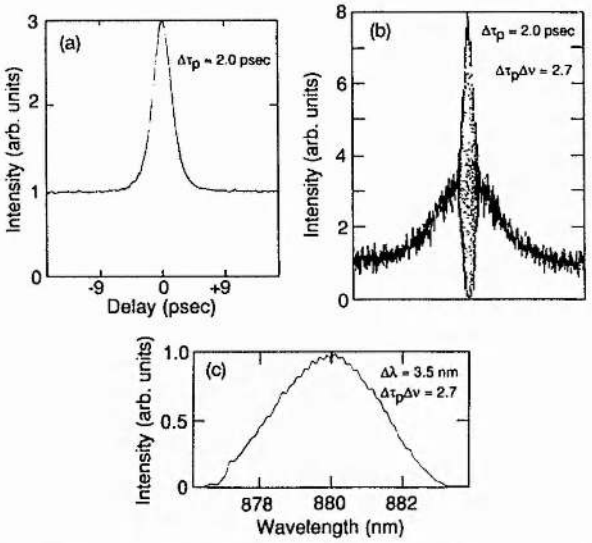

Fig. 2. (a) Intensity and (b) interferometric autocorrelation traces and (c) the associated spectrum for the mode-locked Ti:Al_2O_3 laser.

self-mode lock by simply realigning the cavity slightly using one or both of the end mirrors. This realignment resulted in a reduction of ~40% in average output power, so that for 6 W of pump power the average output was ~300 mW and the threshold for laser oscillation increased to approximately 2 W. The output beam profile also changed from the entirely TEM_{00} mode pattern obtained with optimum alignment to a beam that had ~70% of the average power concentrated in the fundamental mode. The remaining 30% of the laser output power was in a low-order transverse mode such as TEM_{05}.

With an appropriate cavity alignment self-mode-locked operation could be induced by applying some external perturbation, for instance, tapping one of the resonator mirrors. Occasionally the mode-locking process was observed to start spontaneously, although any sudden physical shock could also start or stop mode-locked operation. For a pump power of 8 W the average mode-locked output power was approximately 450 mW. The range of pump powers over which the laser would self-mode lock was found to be between ~4 and 12 W. Outside this range the laser would revert to cw un-mode-locked operation. To date all attempts to eliminate the higher-order transverse modes, by using an intracavity aperture, for example, have also resulted in the collapse of the mode-locked output. With no dispersion compensation the shortest pulses were obtained with the thickest available birefringent filter (1.6 mm) in the cavity, and these had durations of 2.0 psec as typified by the intensity autocorrelation trace in Fig. 2(a) ($sech^2$ intensity profiles are assumed). The laser was also operated with a 0.8-mm birefringent filter, and in this case the pulse duration increased to ~12 psec. Similarly, with no intracavity tuning element the pulse duration again increased to ~16 psec.

When the laser was mode locked its tuning range extended approximately from 845 to 950 nm. The lower value is a result of reaching the low-wavelength limit of the optics, and any attempts to tune below this wavelength either caused the laser oscillations to cease or, more frequently, the wavelength to jump back to that allowed by the neighboring order of the birefringent filter. Beyond the upper end of the mode-locked tuning range the laser continued to oscillate but in an un-mode-locked fashion until eventually laser threshold was not established. Within this wavelength range the laser could be tuned smoothly and continuously while the mode-locked output was maintained, with the shortest pulses being generated near the 870-nm region. This is in contrast to other types of mode-locked Ti:Al_2O_3 lasers, where the range over which the laser may be continuously tuned is restricted by, for example, the effective change in length owing to the dispersion of an optical fiber in an interferometrically matched external cavity. When the shorter-wavelength optics, covering the 700–850-nm spectral region, were used, mode-locked operation could also be obtained between 750 and 850 nm.

Reference to the pulse spectrum shown in Fig. 2(c) indicates that the mode-locked pulses generated from the laser have a very large associated duration–bandwidth product ($\Delta\tau_p\Delta\nu$ = 2.7). This implies that the pulses are strongly frequency chirped, and this is further confirmed by the interferometric autocorrelation trace shown in Fig. 2(b), where the loss of coherence in the wings is characteristic of frequency-chirped pulses.[12] This frequency chirp must originate from within the main laser cavity and is due primarily to the presence of self-phase modulation (SPM) and GVD within the Ti:Al_2O_3 gain medium.

With the two-prism sequence described above and shown in the inset of Fig. 1, the pulse-broadening effects can be overcome. The threshold for laser oscillation and the average output power did not change significantly with the insertion of the prism sequence. The shortest pulses were then generated when the birefringent filter was removed from the laser cavity. The optimum prism separation, for which these short-

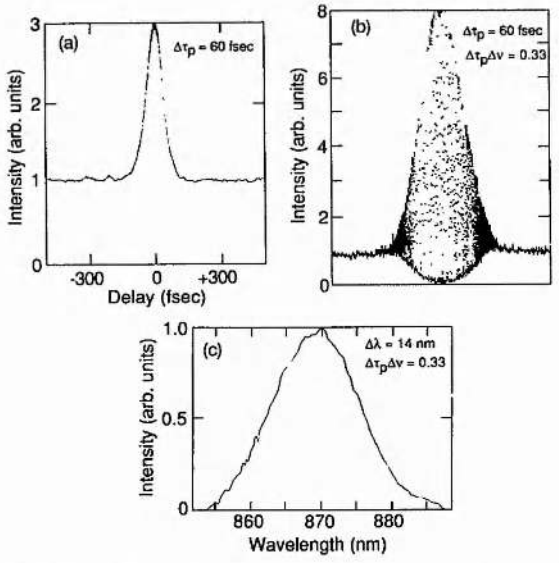

Fig. 3. (a) Intensity and (b) interferometric autocorrelation traces and (c) the associated spectrum for the mode-locked Ti:Al_2O_3 laser.

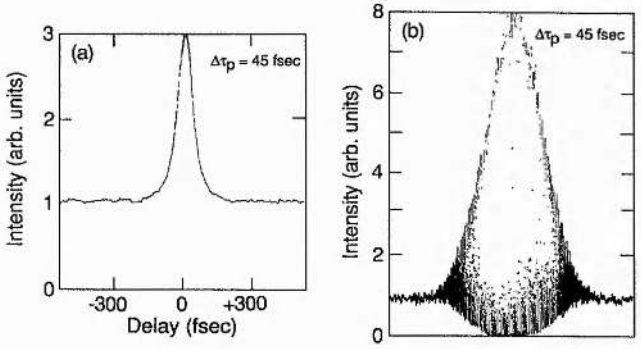

Fig. 4. (a) Intensity and (b) interferometric autocorrelation traces for the mode-locked Ti:Al_2O_3 laser pulses after extracavity pulse compression.

est pulses were produced, was found to be 35 cm. Under these conditions pulses having durations as short as 60 fsec were generated. For a pump power of 8 W the average output power was 450 mW, and thus for a typical cavity period of 12 nsec this represents a peak pulse power of 90 kW.

Typical autocorrelation and spectral data associated with the shortest pulses are presented in Fig. 3. It is clearly evident from the duration–bandwidth product of 0.33, which is close to the Fourier-transform limit of 0.32, that the pulses are essentially free from excess frequency chirp. This is confirmed by the interferometric autocorrelation trace where the fringe visibility extends into the wings of the pulse. For the dispersion-compensated cavity the laser output was still multimode, but the percentage of the average power in the fundamental mode was generally much higher at ~99%.

Self-mode-locked operation could be obtained for cavity lengths that ranged from approximately 1.5 to 2.0 m, which corresponds to a cavity frequency range of 100–75 MHz. Outside this range only a cw unmode-locked output could be obtained, and the resonator did not exhibit multitransverse-mode operation. Within the 75–100-MHz latitude the cavity frequency could be continuously and smoothly varied while mode-locked operation was retained, and there was no evidence that the mode-locked output had any particular dependence on the length of the resonator.

A potential qualitative understanding of the self-mode-locking mechanism can be provided if the two modes within the resonator interact in a manner similar to that of the modes in the main and external cavities of a mode-locked, dispersion-compensated coupled-cavity Ti:Al_2O_3 laser.[9] Thus the operation of the laser can be regarded as a simplified version of coupled-cavity mode locking in which the Ti:Al_2O_3 crystal provides both the gain and the nonlinearity. Further checks on the validity of this proposed interpretation are the subject of ongoing research.

A further reduction in pulse duration could be obtained by using an extracavity fiber–prism pulse compressor. This consisted of a length of optical fiber, chosen so that the GVD linearized the SPM-induced frequency chirp on pulses that had a given peak power. The linearly chirped pulses could then be compressed by using adjustable anomalous dispersion provided by a grating pair or, as in this case, a four-prism sequence. The prisms were preferred to the grating pair because higher transmissions of ~85% could be achieved. For an average output power of 300 mW and pulse durations of 90 fsec and assuming a 50% coupling efficiency into the fiber, the correct length of fiber to linearize the frequency chirp is calculated to be approximately 7 cm, and the optimum prism separation is approximately 10 cm. With the pulse compressor optimized, pulse durations as short as 45 fsec were obtained, with average and peak powers in excess of 100 mW and 25 kW, respectively. Representative autocorrelation traces for these pulses are shown in Fig. 4.

In summary, we have demonstrated what is to our knowledge the first self-mode-locked Ti:Al_2O_3 laser that is capable of producing pulses with durations as short as 2.0 psec. We have also, for the first time to our knowledge, used intracavity dispersion compensation in a mode-locked Ti:Al_2O_3 laser to produce pulse durations as short as 60 fsec and peak powers of 90 kW. We believe that these are the shortest, highest-peak-power pulses that have been directly generated by a mode-locked Ti:Al_2O_3 laser to date. By using an extracavity fiber–prism compressor and utilizing high-dispersion ZnSe prisms, pulses as short as 45 fsec have been produced.

The overall funding of this research by the UK Science and Engineering Research Council is gratefully acknowledged. D. E. Spence acknowledges a research scholarship from the Department of Education for Northern Ireland.

References

1. J. T. Darrow and R. K. Jain, in *Digest of Meeting on Tunable Solid State Lasers* (Optical Society of America, Washington, D.C., 1989), paper FQ5.
2. G. B. Al'tshuler, V. B. Karasev, N. V. Kondratyuk, G. S. Kruglik, A. V. Okishev, G. A. Shirpko, V. S. Urbanovich, and A. P. Shkadarevich, Sov. Tech. Phys. Lett. **13**, 324 (1987).
3. R. Roy, P. A. Schulz, and A. Walter, Opt. Lett. **12**, 672 (1987).
4. P. A. Schulz, IEEE J. Quantum Electron. **24**, 1039 (1988).
5. J. D. Kafka, A. J. Alfrey, and T. Baer, in *Ultrafast Phenomena VI*, T. Yajima, K. Yoshihara, C. B. Harris, and S. Shionoya, eds. (Springer-Verlag, Berlin, 1988), p. 64.
6. N. Sarukura, Y. Ishida, H. Nakano, and Y. Yamamoto, Appl. Phys. Lett. **56**, 814 (1989).
7. P. A. Schulz, M. J. LaGasse, R. W. Schoenlein, and J. G. Fujimoto, in *Digest of Annual Meeting of the Optical Society of America* (Optical Society of America, Washington, D.C., 1988), paper MEE2.
8. P. M. W. French, J. A. R. Williams, and R. Taylor, Opt. Lett. **14**, 686 (1989).
9. W. Sibbett, in *Ultrafast Phenomena VII*, C. B. Harris, E. P. Ippen, G. A. Mourou, and A. H. Zewail, eds. (Springer-Verlag, Berlin, 1990), pp. 2–7.
10. J. Goodberlet, J. Wang, J. G. Fujimoto, and P. A. Schulz, Opt. Lett. **14**, 1125 (1989).
11. R. L. Fork, O. E. Martinez, and J. P. Gordon, Opt. Lett. **9**, 150 (1984).
12. J.-C. Diels, J. J. Fontaine, I. C. McMichael, and F. Simoni, Appl. Opt. **24**, 1270 (1985).

Femtosecond pulse generation by a dispersion-compensated, coupled-cavity, mode-locked Ti:sapphire laser

D. E. Spence and W. Sibbett

J. F. Allen Physics Research Laboratories, Department of Physics and Astronomy, University of St. Andrews, North Haugh, St. Andrews KY169SS, Scotland

Received December 5, 1990; revised manuscript received March 4, 1991

Results are presented that illustrate how the operation of a coupled-cavity mode-locked Ti:sapphire laser depends on some of the important operating parameters. In particular, it is shown how group-velocity dispersion plays a key role in determining the duration of the mode-locked pulses. By using dispersion compensation in both the main and the control cavities, transform-limited pulses have been generated that have durations as short as 90 fs with average and peak powers of 80 mW and 10 kW, respectively.

Titanium–sapphire ($Ti:Al_2O_3$) is now widely recognized to be an attractive gain medium for laser operation in the near-infrared spectral region. Its broad gain bandwidth means that in addition to its having a large tuning range it is especially well suited to ultrashort-pulse generation and amplification. $Ti:Al_2O_3$ lasers have been mode locked by a variety of techniques, including synchronous pumping,[1,2] acousto-optic mode locking,[3,4] passive mode locking,[5,6] injection seeding,[7] and coupled-cavity (also referred to as additive-pulse or interferential) mode locking,[8,9] in which the mode-locking process may be self-starting.[10]

Until recently, the shortest pulses reported for $Ti:Al_2O_3$ lasers had durations of 300 fs and were generated by using injection seeding techniques.[7] With a nonlinear external cavity, pulses as short as 800 fs were directly generated from an actively mode-locked, coupled-cavity laser,[8] and, with an extracavity diffraction-grating pair employed for dispersion compensation, the output pulse durations from a self-starting, coupled-cavity $Ti:Al_2O_3$ laser were compressed to 200 fs.[10] The use of an extracavity fiber–prism pulse compressor permitted 1.3-ps pulses generated by a dispersion-compensated, acousto-optically mode-locked $Ti:Al_2O_3$ laser to be compressed to 50 fs.[11] A recently reported study from our laboratory showed that pulses as short as 60 fs, having peak powers of more than 90 kW, can be directly produced by a self-mode-locked, dispersion-compensated $Ti:Al_2O_3$ laser.[12]

In this paper we present results for a coupled-cavity, mode-locked $Ti:Al_2O_3$ laser from which pulses with durations of 1.3 ps can be generated from the basic non-dispersion-compensated system. By implementation of an intracavity two-prism sequence for dispersion compensation[13] the pulse durations were reduced to 120 fs at average power levels of ~200 mW. A further reduction in pulse duration to 90 fs was achieved by incorporating a four-prism sequence within the control cavity. We also include experimental data that illustrate how the behavior of the laser depends on some of the primary operating parameters, such as the length of the fiber used in the control cavity and the fiber launch power. Additionally, the performance of the laser in a nonlinear Fabry–Perot (F–P) cavity configuration is compared with that for a nonlinear Michelson arrangement.[9,14]

The coupled-cavity, mode-locked $Ti:Al_2O_3$ laser, illustrated schematically in Fig. 1, was a modified Spectra-Physics Model 3900 system. The main laser cavity, consisting of mirrors M_0 to M_3, was extended to between 1.5 and 1.8 m, with the 20-mm-long, Brewster-angled $Ti:Al_2O_3$ gain medium placed in the center of the cavity. In the F–P cavity arrangement [Fig. 1(a)] plane output coupler M_0 had a transmission of ~5% over the 850–1000-nm spectral region, and spherical mirrors M_1 and M_2 (r = 10 cm) were highly reflecting over the 850–1000-nm range and highly transmitting for the 488–514-nm argon-ion laser pump wavelengths. The alternative, nonlinear Michelson, cavity configuration is illustrated in Fig. 1(b), where the beam splitter BS acted as the output coupler and had a transmission of ~3.5% over the 800–1000-nm region, and plane mirror M_5 was highly reflecting over the 750–950-nm range.

The pump laser was either a Spectra-Physics Model 2030 or Model 2040E argon-ion laser that operated on all lines in the visible at powers of as much as 15 W in a TEM_{00} mode. The pump beam passed through a periscope arrangement, which rotated the plane of polarization by 90°, and was focused into the $Ti:Al_2O_3$ gain medium by spherical mirror M_4, which had a radius of curvature of 22.8 cm. Prisms P_1 and P_2 were made from highly dispersive SF14 glass and were Brewster angled for minimum deviation at ~850 nm. They constituted the intracavity double-prism sequence for dispersion compensation, as shown in the inset of Fig. 1. The laser was tuned by means of the standard Spectra-Physics three-plate Lyot filter, a single-plate birefringent filter (BRF), or a variable-aperture slit placed between prism P_2 and mirror M_3.

An electronic stabilization loop controlled the movement of the mirror (mounted on piezoelectric translation stage PZT) in the control cavity such that interferometric stability between the two cavities could be maintained in the usual way.[15] The input signal for the electronics was usually the average power fed back into the laser from the external cavity, but the average output power from the

0740-3224/91/102053-08$05.00 © 1991 Optical Society of America

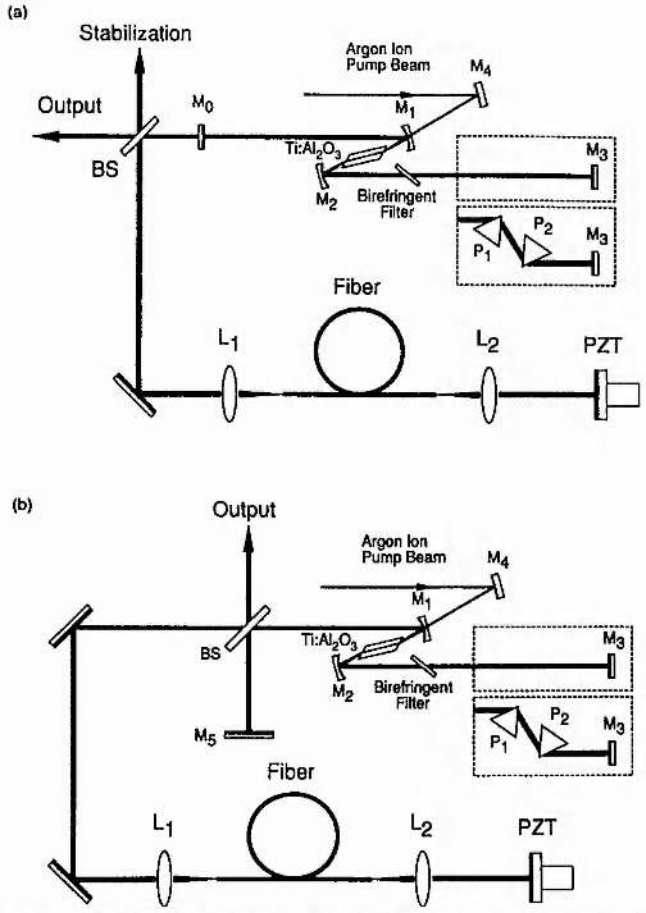

Fig. 1. Schematic diagram showing the nonlinear (a) F–P and (b) Michelson cavity configurations.

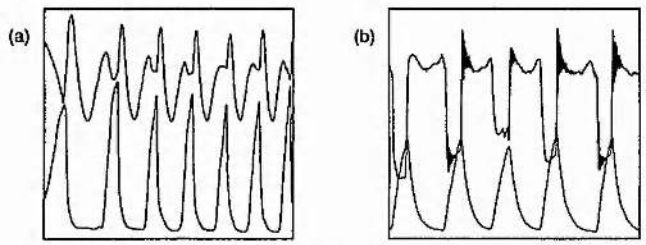

Fig. 2. Traces showing how (a) the average power and second-harmonic output (lower traces) and (b) the average power fed back from the coupled-cavity and second-harmonic output vary with the relative phase mismatch between the two cavities.

laser was occasionally used as the input signal. The monitored input signal was wavelength selected by using a diffraction grating and an aperture in front of the photodiode. The modulation on the signal returned from the fiber was larger than that on the average output from the laser, so the best stability for mode-locked operation was usually obtained by monitoring the signal returned from the external cavity. The traces in Fig. 2 illustrate how the average power fed back from the coupled cavity, the average output power of the laser, and the second-harmonic signal varied as the relative phase mismatch between the two cavities was adjusted by applying a linear voltage ramp to the piezoelectric translation stage.

In the F–P configuration an intensity component (70%) of the output from the main laser cavity was reflected by beam splitter BS and coupled into the single-mode control-cavity optical fiber (Andrew Corporation type 48280-1-P). Index-matching fluid was used between lenses L_1 and L_2 and the fiber ends to maximize the coupling efficiency between the two cavities and to avoid backreflections into the laser. Single-pass coupling efficiencies of 60–75% were achieved with this scheme. Interestingly, we found that it was not essential to use index-matching fluid, because when the coupling efficiency exceeded ~60% the back-reflection into the laser from the fiber ends could be less than a certain critical intensity level. To generate the shortest pulses, a second prism sequence consisting of four zinc selenide (ZnSe) prisms was placed in the control cavity between the beam splitter and lens L_1.

The basic non-dispersion-compensated laser generated pulses with durations as short as 1.3 ps (hyperbolic-secant-squared intensity profiles assumed) at a wavelength near 860 nm. In this case the tuning element was the Lyot filter that was supplied with the laser. The intensity and interferometric autocorrelation traces and the spectrum of a typical pulse are shown in Fig. 3. The loss of fringe visibility in the wings of the interferometric autocorrelation is characteristic of pulses with excess frequency chirp.[16] The duration–bandwidth product $\Delta\tau_p\Delta\nu = 1.0$, which is substantially greater than the transform limit of 0.32 for hyperbolic-secant-squared pulses, further

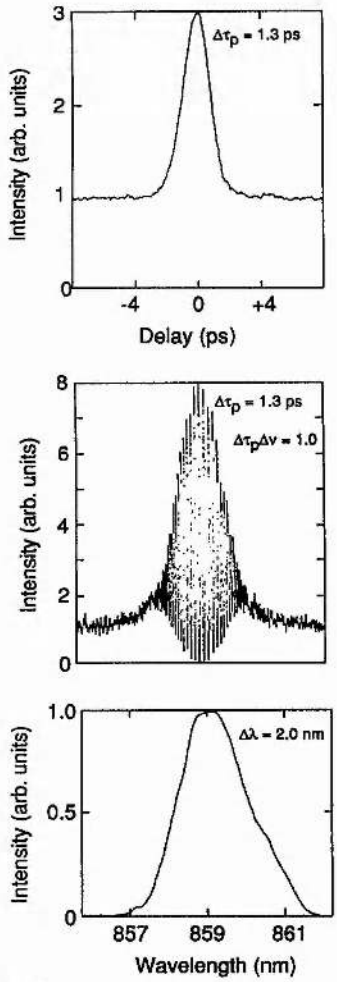

Fig. 3. Autocorrelation and spectral data for the basic non-dispersion-compensated laser.

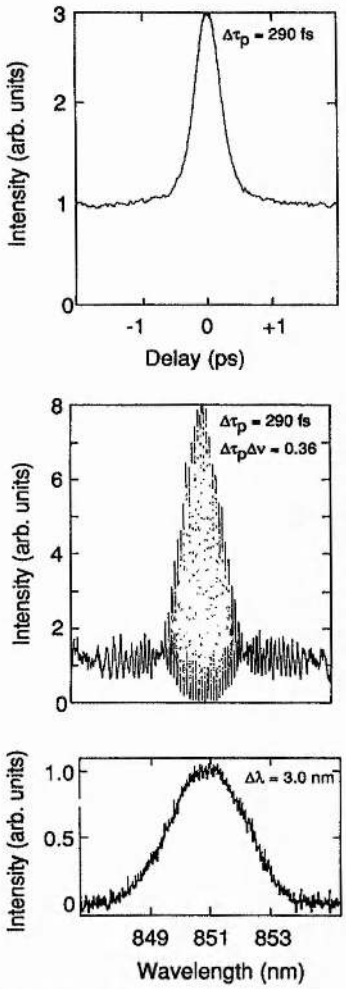

Fig. 4. Autocorrelation and spectral data for the basic non-dispersion-compensated laser with extracavity pulse compression, using a diffraction grating pair.

confirms the presence of this excess frequency chirp. These chirped pulses could be temporally compressed outside the laser resonator with either a diffraction-grating pair or a prism sequence employed to provide anomalous group-velocity dispersion (GVD). With this scheme the typical pulse durations of 2.3 ps were reduced to 290 fs, where duration–bandwidth products of ~0.36 were achieved for a grating separation of 30 mm. Representative autocorrelation and spectral data for these compressed pulses are shown in Fig. 4.

For a pump power of 6 W the average mode-locked output power was 110 mW, and the peak pulse powers exceeded 1 kW. In this case ~115 mW was launched into the 29-cm-long control-cavity fiber. With the diffraction-grating pair used for extracavity pulse compression, the average power was reduced to approximately 30 mW, but the peak pulse power was increased to more than 1.2 kW. The diffraction gratings used were optimized for a wavelength of 1.06 μm, and this explains their poor throughput efficiency at these shorter wavelengths. (Throughput efficiencies of more than 80% should be achievable with optimized gratings, which implies that the average and peak powers could be as high as 80 mW and 3.3 kW, respectively.) The tuning range of the mode-locked laser extended from 830 nm to ~960 nm; the limits of this range were primarily due to the properties of the control fiber and the reflectivity characteristics of the optics. Mode-locked operation was also demonstrated at wavelengths as short as 750 nm by substituting an appropriate set of optics and a control fiber. The performance in this wavelength range was similar to that in the 830–960-nm spectral region, for which the variation of pulse duration with wavelength is illustrated in Fig. 5.

The data in Fig. 6 show how the pulse duration varied with the power launched into the control-cavity fiber. (This launch power was altered by placing a variable neutral-density filter wheel at the input side of the fiber.) It can be seen from this graph that the pulse duration decreased as the fiber launch power was reduced until an optimum value was reached. Beyond this value any further decrease in power resulted in an increase in pulse duration until the self-starting operation could no longer be achieved. This behavior occurred because the phase shift of the pulses returned from the coupled cavity was dependent on the peak intensity in this cavity, and the shortest pulses were obtained when the phase shift was optimum for the particular operating conditions selected for the laser. This results from the fact that the degree of pulse shortening initially increases with the intensity-induced nonlinearity. If, however, this nonlinearity becomes too large the effectiveness of the pulse-shortening process may be compromised such that the laser may become unstable, as discussed later.

Various lengths of optical fibers ranging from 5 cm to 1.05 m were used in the control cavity. The variation of pulse duration as a function of the length of the fiber is

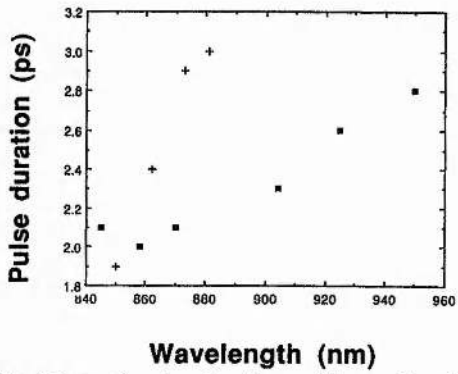

Fig. 5. Variation of pulse duration with wavelength for the non-dispersion-compensated laser. Filled squares, 29-cm fiber; pluses, 23-cm fiber.

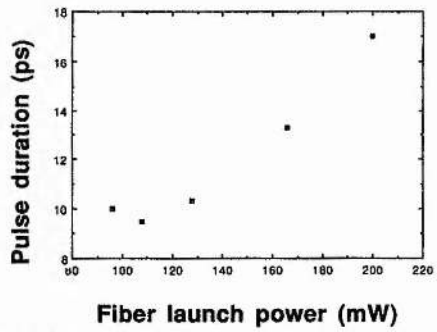

Fig. 6. Variation of pulse duration with the power launched into the external cavity for the non-dispersion-compensated laser.

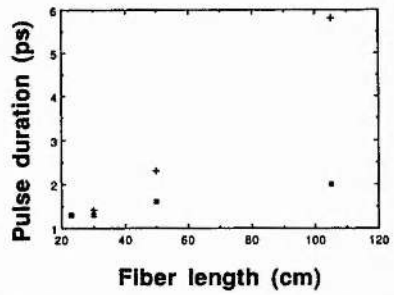

Fig. 7. Dependence of pulse duration on control fiber length for the non-dispersion-compensated laser. Filled squares, three-plate BRF; plus, 1.6-mm BRF.

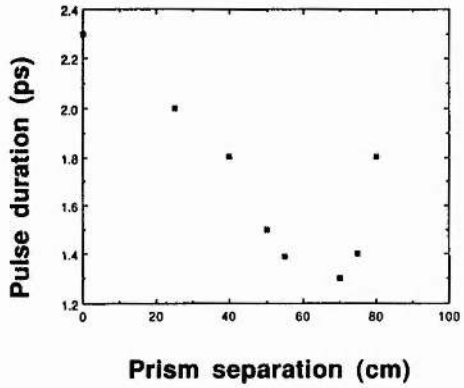

Fig. 8. Variation of pulse duration with the separation between the zinc selenide prism pairs in the external cavity.

shown in Fig. 7 for the laser with two thicknesses of BRF's. It can be seen from this figure that in both cases the pulse duration decreased linearly with decreasing fiber length. This can be explained in terms of the decrease in normal GVD and self-phase modulation (SPM) within the fiber in the spectral region of operation: As the fiber was shortened, the corresponding temporal broadening effects became less severe. It is also clear that the incorporation of a thinner BRF resulted in pulses with longer durations. This result is consistent with the thin BRF's less pronounced bandwidth restriction, which, in the presence of SPM and GVD, leads to an increased amount of excess frequency chirp, which results in pulses with longer durations.

The data in Fig. 7 imply that the shortest pulses were generated by minimizing the amount of dispersion in the control cavity. Shortening the fiber is not the ideal solution, as this also reduces the accessible optical nonlinearity, which in turn makes the self-starting process more difficult to establish. These results agree with the theoretical considerations suggested by Ippen *et al.*,[17] where it is predicted that self-starting can be achieved more easily with increased nonlinearity in the control cavity. Thus, in order to achieve minimum dispersion while retaining a suitable degree of control-cavity nonlinearity, we incorporated four ZnSe prisms, Brewster angled at ~850 nm, into the control cavity. This arrangement provided adjustable anomalous GVD, which compensated for the normal dispersion in the fiber. From Fig. 8 it can be seen how the pulse duration varied with the separation between the ZnSe prism pairs and hence with the total GVD in the control cavity. These results were taken for a 50-cm length of fiber and a 1.6-mm-thick BRF in the laser. For a pump power of 5 W the average output power was 70 mW, and the peak power was 0.7 kW, while the power launched into the fiber was 130 mW. The optimum prism separation was ~70 cm, and the minimum pulse duration achieved was 1.3 ps at a wavelength of 866 nm. Autocorrelation and spectral data for these pulses are included here as Fig. 9.

Although the pulse durations for this refined configuration were reduced by a factor of 1.8, it was evident from the interferometric autocorrelation traces and the associated duration–bandwidth products ($\Delta\tau_p\Delta\nu = 1.3$) that the pulses retained a significant amount of excess frequency chirp. This chirp could arise only within the main resonator and must therefore be primarily attributable to the normal dispersion and SPM in the Ti:Al_2O_3 gain medium itself.[9,18] In order to compensate for this dispersion, we placed two SF-14 glass prisms, having a separation of 35 cm, within the laser cavity as shown in the inset of Fig. 1. With this dispersion compensation in the main resonator only and 5.7 cm of fiber in the control cavity, the pulse durations were further reduced to 120 fs with a duration–bandwidth product of $\Delta\tau_p\Delta\nu = 0.32$. For a pump power of 7.5 W the average and the peak output powers

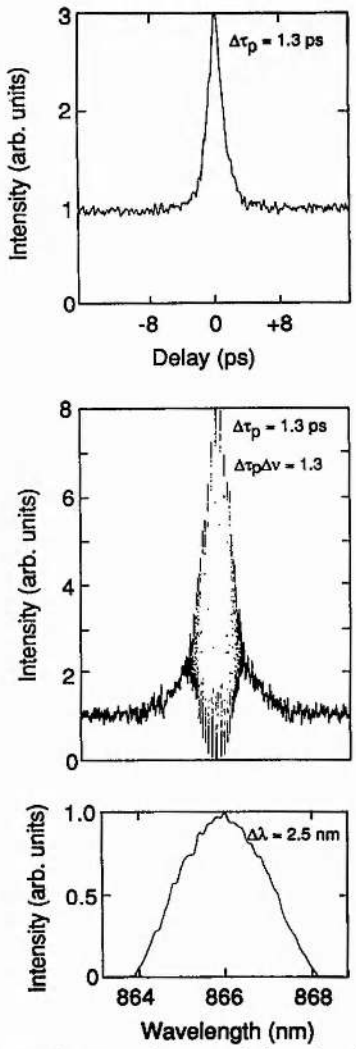

Fig. 9. Autocorrelation and spectral data for the mode-locked Ti:sapphire laser with dispersion compensation in the control cavity only.

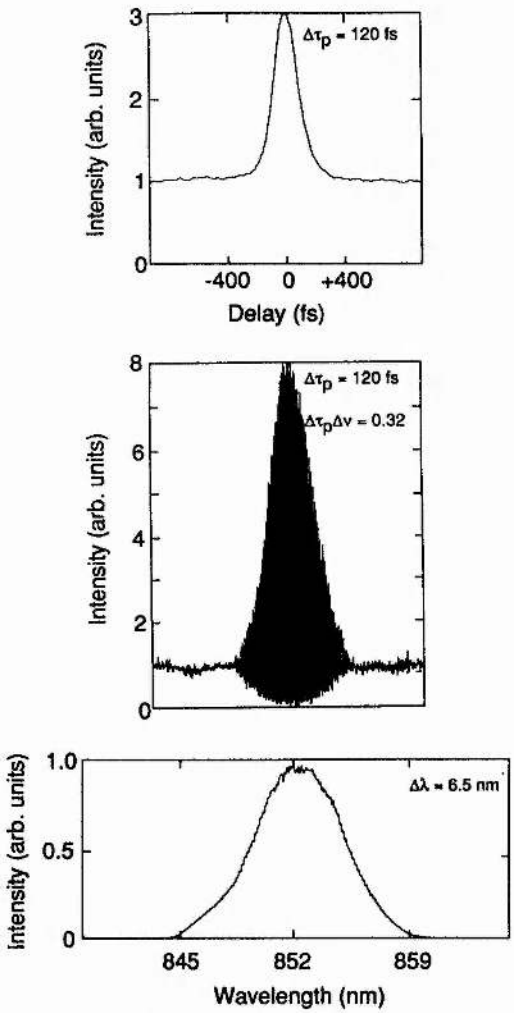

Fig. 10. Autocorrelation and spectral data for the mode-locked Ti:sapphire laser with dispersion compensation in the main cavity only.

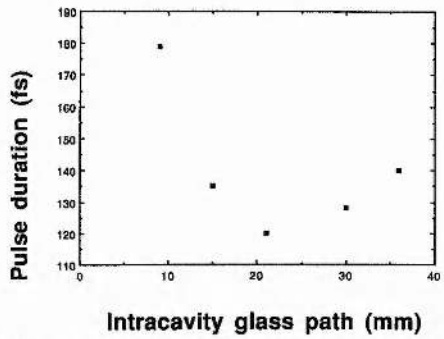

Fig. 11. Dependence of pulse duration on the total glass path within the main laser resonator for a constant prism separation of 35 cm.

were 200 mW and 20 kW, respectively, for a fiber launch power of 230 mW. The autocorrelation and spectral data for these pulses are shown in Fig. 10, and it is clear that they are essentially free from excess frequency chirp.

The variation of the pulse duration with the total path length of glass in the main laser cavity is shown in Fig. 11, from which it is evident that there was an optimum value at which the shortest pulses were generated. Although the pulse-broadening effects in the main cavity dominate those in the control cavity, it can be seen from Fig. 12 that the pulse durations still increase with the length of fiber used, so that the dispersion within the external cavity must still have a significant influence. Thus, in order to generate the shortest pulses, it was necessary to provide dispersion compensation in both cavities. With a 25-cm length of control fiber and with a prism separation of 35 cm in the main cavity and 14.5 cm in the control cavity, pulses as short as 90 fsec were generated with duration–

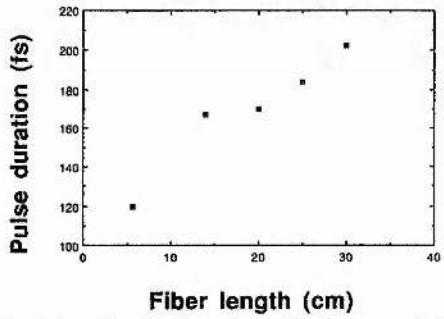

Fig. 12. Variation of pulse duration with the control-fiber length for dispersion compensation in the main laser resonator only.

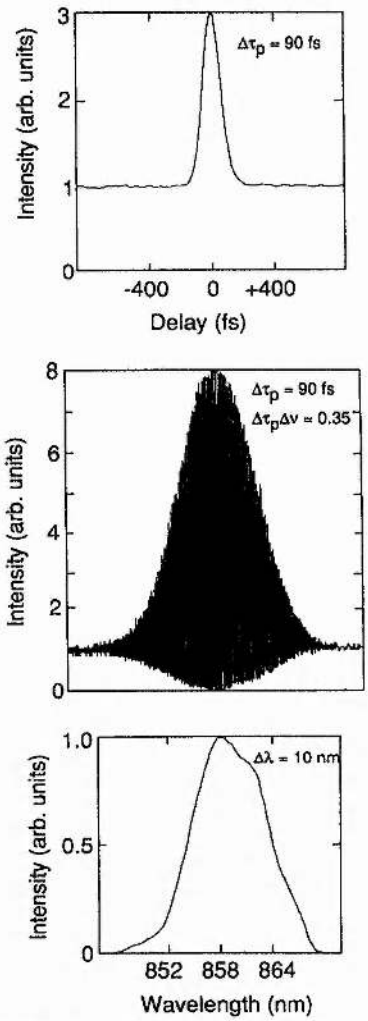

Fig. 13. Autocorrelation and spectral data for the mode-locked Ti:sapphire laser with dispersion compensation in both cavities.

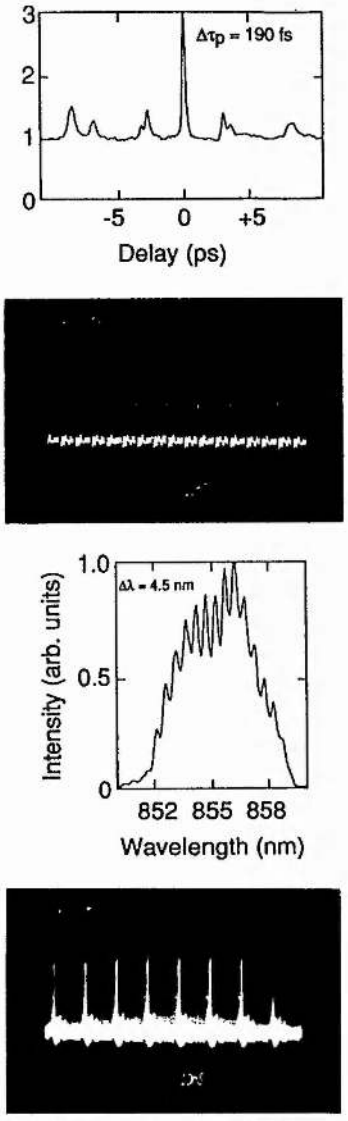

Fig. 14. Autocorrelation and associated spectral data of a multiple-pulsing state in the mode-locked Ti:sapphire laser when the subpulses are close to the main pulse. The oscillograms show multiple pulsing at twice the cavity frequency and a state where the timing of the subpulses is not fixed relative to the main pulse.

bandwidth products of 0.35. The intensity and interferometric autocorrelation traces and spectra associated with these shortest pulses are shown in Fig. 13. Under these conditions the GVD in both the main and the control cavities was anomalous, which was necessary in order to compensate for the frequency chirp resulting from SPM and normal GVD in the control fiber and the Ti:Al_2O_3 gain medium. These results were taken with a pump power of 8 W and a fiber launch power of 110 mW, which resulted in average and peak output powers of 80 mW and 10 kW, respectively.

In all cases there was a threshold fiber launch power below which self-starting did not occur. This threshold value decreased as the fiber length increased and also as the degree of dispersion compensation approached its optimum value. This behavior was to be expected, as in both cases the necessary nonlinearity for the self-starting operation could be achieved with lower average powers. A typical value of the threshold launch power for a 100-cm length of fiber was ~90 mW.

Although it was possible to find stable operating regimes within which good mode locking could be achieved, we also observed many other stable states in which some aspect of the mode-locked operation was compromised. The laser often showed a tendency toward multiple-pulse operation in which as many as six pulses were present within one cavity period. The subpulses occurred either close to the main pulse and equally spaced from it or at regular intervals during the cavity period. An intensity autocorrelation trace and associated spectrum for one such state with subpulses close to the main pulse are shown in Fig. 14 together with an oscillogram showing the pulse train for a state in which the subpulses are farther from the main pulse. In all cases these multiple-pulsing features were accompanied by a modulation on the spectrum, as shown in Fig. 14. The timing of the subpulses was generally not fixed relative to the main pulses, and they could often be seen to drift along between the main cavity pulses, taking anything from ~0.1 s to several seconds to do so.

Another common operating regime was characterized by the presence of relatively narrow spikes superimposed on the spectrum of the mode-locked laser, as illustrated in Fig. 15. These spikes could appear anywhere across the spectrum and sometimes were present at wavelengths well removed from the mode-locked spectrum when sufficient gain was available in these regions. Although these spike features were readily observed in the frequency domain, it was significant that the monitored mode-locked pulse train and autocorrelation traces offered no evidence of their existence. We believe that these features arise when the spectrum of the un-mode-locked laser breaks through the much broader mode-locked spectrum. When these spectral spikes were present it is most likely that the laser output consisted of either mode-locked pulses with broad, low-energy pedestals or a mode-locked pulse train that coexisted with a low-intensity cw beam. We have monitored several distinct states that were characterized by significantly different levels of second-harmonic intensity even though the pulse duration and the total average power from the laser remained essentially constant. This variation arose from the association of different average powers with the mode-locked portion of the output.

All of these effects were associated with a high level of peak pulse power in the fiber, which in turn corresponded to a greater nonlinear phase shift than was desirable for

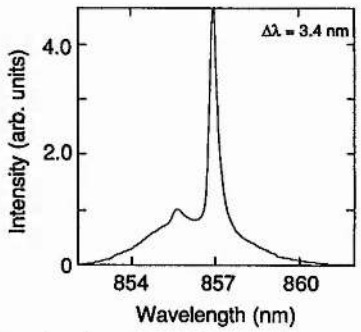

Fig. 15. Trace showing a typical cw laser spike breaking through the mode-locked spectrum of the laser.

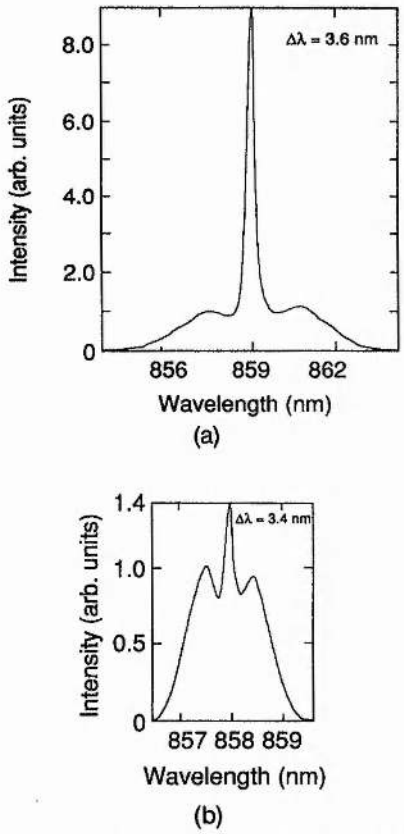

Fig. 16. Traces showing typical spectra returned from the control fiber. The main difference is in the relative intensity of the narrow spike.

mode locking. The laser seemed able to accommodate this peak power level either by multiple pulsing or by confining some of the energy into un-mode-locked radiation such that in each case there was a corresponding decrease in the peak pulse power. The spectrum of the pulses returned from the fiber is shown in Fig. 16. This type of spectrum was always observed when stable mode locking was achieved, but the intensity of the narrow spike did vary as shown.

The obvious way by which these undesirable effects could be avoided was to reduce the power launched into the fiber, but this made the self-starting conditions for mode locking more difficult to satisfy. Often the stable operating window for good mode locking seemed to lie at power levels that were below the threshold for self-starting, so that the laser would tend to exhibit some undesirable effects. It was difficult to identify the stable operating window precisely for a particular operating regime. In practice one had to achieve self-starting and then carefully adjust the pump power, the coupling efficiency, and the relative phase mismatch between the cavities, the wavelength, and the average power in the fiber until satisfactory stable mode locking was observed.

We have also used a coupled-cavity scheme with an acousto-optically mode-locked Ti:Al_2O_3 laser. With the laser already producing relatively short pulses (~100 ps), the pulse-shortening effects of the nonlinear external cavity could be utilized more easily than in the self-starting regime. The behavior of the laser in terms of pulse duration was similar to the self-starting case, although it was possible to operate with much lower intrafiber powers, so that the undesirable effects mentioned above could be more easily controlled. Further work is being carried out on various hybrid mode-locking schemes using acousto-optic modulation for the Ti:Al_2O_3 laser. At present it appears that the acousto-optic mode-locked coupled-cavity laser still represents a serious option for reliable ultrashort-pulse generation as compared with the purely passive self-starting laser.

The behavior of the mode-locked laser did not show any particular dependence on the length of the laser resonator provided that the two coupled-cavities were interferometrically matched. We observed mode locking with cavity lengths ranging from ~70 cm to more than 2 m. These limits were set merely by the practical constraints of the physical size of the laser and the space available on the optical table. In our studies we operated the laser with cavity lengths close to 1.7 m, as this provided the best compromise between size, stability, and high peak pulse powers. It was observed, however, that the stability and degree of mode locking was much better if both the main resonator and the coupled cavity had the same period rather than one being a multiple of the other. This was not surprising, because the latitude of stability decreases for the latter condition.

The stability of the laser for all the above assessments was good. With the stabilization electronics switched off, and depending on the conditions in the laboratory, mode-locked operation could be achieved for periods of a few milliseconds to several minutes. When the stabilization was switched on the laser would remain mode locked for periods of up to several hours. Under these conditions the laser mode locking was interrupted only by sudden physical shocks that the electronic control could not track or as a result of long-term variations in, for example, the coupling efficiency into the fiber.

The peak-to-peak amplitude fluctuations of the output of the laser were typically less than 10%. The major contributions to this noise were at frequencies of 50 and 300 Hz and could be traced directly to noise in the output of the pump laser. (The amplitude noise in the output of the Model 2040E was much better than that of the Model 2030.) When required, this noise could be reduced to less than 2% by placing an acousto-optic modulator

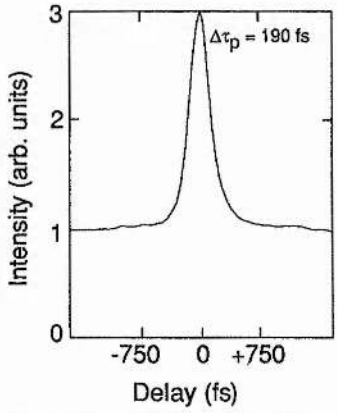

Fig. 17. Intensity autocorrelation data for pulses from the dispersion-compensated laser in the nonlinear Michelson cavity configuration.

(used as a noise suppressor) at the output of the pump laser to remove these amplitude fluctuations. However, thermal lensing in the modulator material meant that the usable pump power had to be kept at less than 6 W if pump beam degradation was to be avoided.

The mode-locked laser was also operated in the nonlinear Michelson cavity configuration illustrated in Fig. 1(b). In this arrangement the relative performance characteristics were similar to those reported for the color-center laser counterparts.[9] We observed that the pulse duration typically increased from 120 to 190 fs (see Fig. 17) and that the overall stability of the laser improved. This stability increase was not so dramatic as that previously observed for the KCl:Tl color-center laser because it was necessary in our Ti:Al_2O_3 laser configuration to make the cavity branch containing the nonlinear element twice the length of the arm containing the gain. The increase in stability was more dramatic when compared with that for the case in which the nonlinear cavity in the F–P arrangement was twice the length of the main cavity. In a configuration in which both arms of the Michelson cavity are the same length an even more dramatic increase in stability would be expected.

In summary, we have presented results that illustrate the various operating regimes of a self-starting, coupled-cavity, mode-locked Ti:Al_2O_3 laser. Our experimental results indicate how the operation of the laser depends on key operating parameters such as the length of optical fiber used in the control cavity and the power launched into the fiber. We have demonstrated that group-velocity dispersion plays an important role in determining the final pulse duration and have shown that, by proper control of this dispersion, transform-limited pulses as short as 90 fs can be generated. We believe that this is the first time that dispersion compensation has been used in both the main and the control cavities of a coupled-cavity mode-locked Ti:Al_2O_3 laser and that these are the shortest pulses yet produced from such a coupled-cavity laser configuration.

ACKNOWLEDGMENTS

The overall funding of this research by the U.K. Science and Engineering Research Council is gratefully acknowledged. D. E. Spence received a research scholarship from the Department of Education for Northern Ireland.

REFERENCES

1. J. T. Darrow and R. K. Jain, "Cw mode-locking of a room temperature solid-state laser," in *Tunable Solid State Lasers*, Vol. 20 of 1987 OSA Technical Digest Series (Optical Society of America, Washington, D.C., 1987), paper PD2.
2. G. B. Al'tshuler, V. B. Karasev, N. V. Kondratyuk, G. S. Kruglik, A. V. Okishev, G. A. Shirpko, V. S. Urbanovich, and A. P. Shkadarevich, "Generation of ultrashort pulses in a synchronously pumped Ti^{3+} laser," Sov. Tech. Phys. Lett. **13,** 324–325 (1987).
3. R. Roy, P. A. Schulz and A. Walter, "Acousto-optic modulator as an electronically selectable unidirectional device in a ring laser," Opt. Lett. **12,** 672–674 (1987).
4. J. D. Kafka, A. J. Alfrey, T. Baer, "Mode-locked continuous-wave titanium sapphire laser," in *Ultrafast Phenomena VI,* T. Yajima, K. Yoshihara, C. B. Harris, and S. Shionoya, eds., Vol. 48 of Springer Series in Chemical Physics (Springer-Verlag, Berlin, 1988), p. 64.
5. N. Sarukura, Y. Ishida, H. Nakano, and T. Yamamoto, "Cw passive mode locking of a Ti:sapphire laser," Appl. Phys. Lett. **56,** 814–815 (1989).
6. N. Sarukura, Y. Ishida, T. Yamamoto, and H. Nakano, "All solid-state cw passively mode-locked Ti:sapphire laser using a colored glass filter," Appl. Phys. Lett. **57,** 229–230 (1990).
7. P. A. Schulz, M. J. Lagasse, R. W. Schoenlein, and J. G. Fujimoto, "Femtosecond Ti:Al_2O_3 injection seeded laser," in *OSA Annual Meeting,* Vol. 11 of 1988 OSA Technical Digest Series (Optical Society of America, Washington, D.C., 1988), paper MEE2.
8. P. M. W. French, J. A. R. Williams, and R. Taylor, "Femtosecond pulse generation from a titanium-doped sapphire laser using nonlinear external feedback," Opt. Lett. **14,** 686–688 (1989).
9. W. Sibbett, "Hybrid and passive mode-locking techniques in coupled-cavity lasers," in *Ultrafast Phenomena VII,* C. B. Harris, E. P. Ippen, G. A. Mourou, and A. H. Zewail, eds., Vol. 53 of Springer Series in Chemical Physics, (Springer-Verlag, Berlin, 1990), pp. 2–7.
10. J. Goodberlet, J. Wang, J. G. Fujimoto, and P. A. Schulz, "Femtosecond passively mode-locked Ti:Al_2O_3 laser with a nonlinear external cavity," Opt. Lett. **14,** 1125–1127 (1989).
11. J. D. Kafka, M. L. Watts, D. L. Roach, M. S. Keirstead, H. W. Schaaf, and T. Baer, "Pulse compression of a mode-locked Ti:sapphire laser," in *Ultrafast Phenomena VII,* C. B. Harris, E. P. Ippen, G. A. Mourou, and A. H. Zewail, eds., Vol. 53 of Springer Series in Chemical Physics (Springer-Verlag, Berlin, 1990), pp. 66–68.
12. D. E. Spence, P. N. Kean, and W. Sibbett, "Sub-100 fs pulse generation from a self-mode-locked titanium-sapphire laser," *Conference on Lasers and Electro-Optics,* Vol. 7 of 1990 OSA Technical Digest Series (Optical Society of America, Washington, D.C., 1990), p. 619; "60-fsec pulse generation from a self-mode-locked Ti:sapphire laser," Opt. Lett. **16,** 42–44 (1991).
13. R. L. Fork, O. E. Martinez, and J. P. Gordon, "Negative dispersion using pairs of prisms," Opt. Lett. **9,** 150–152 (1984).
14. F. Ouellette and M. Piche, Passive mode locking with a nonlinear Michelson interferometer: transient and steady-state characteristics, Can. J. Phys. **66,** 903–913 (1988).
15. F. M. Mitschke and L. F. Mollenauer, "Stabilizing the soliton laser," IEEE J. Quantum Electron. **QE-22,** 2242–2250 (1986).
16. J.-C. Diels, J. J. Fontaine, I. C. McMichael, and F. Simoni, "Control and measurement of ultrashort pulse shapes (in amplitude and phase) with femtosecond accuracy," Appl. Opt. **24,** 1270–1282 (1985).
17. E. P. Ippen, L. Y. Liu, and H. A. Haus, "Self-starting conditions for additive-pulse mode-locked lasers," Opt. Lett. **15,** 183–185 (1990).
18. N. Sarukura, Y. Ishida, and H. Nakano, "Compression of intra-cavity chirped pulses from a cw passively mode-locked Ti:sapphire laser," Opt. Commun. **77,** 49–52 (1990).

Regeneratively initiated self-mode-locked Ti:sapphire laser

D. E. Spence, J. M. Evans, W. E. Sleat, and W. Sibbett

J. F. Allen Physics Research Laboratories, Department of Physics and Astronomy, University of St. Andrews, North Haugh, St. Andrews, KY16 9SS, Scotland

Received July 16, 1991

It is demonstrated that the incorporation of an acousto-optic modulator within the cavity of a self-mode-locked Ti:sapphire laser can lead to self-starting and stable generation of pulses that have durations of 60 fs when the acousto-optic device is driven regeneratively from the laser output. Data are also presented that show that the application of cavity-frequency locking techniques dramatically improves the phase noise characteristics of the mode-locked laser.

Ti:sapphire ($Ti:Al_2O_3$) is now widely recognized as an excellent solid-state material for laser operation in the near-infrared spectral region. Its broad gain bandwidth, extending from approximately 670 to 1100 nm, provides both a large tuning range and the ability to generate ultrashort pulses. Various mode-locking schemes have been employed in $Ti:Al_2O_3$ lasers whereby pulses having durations into the sub-100-fs regime have been produced. These include acousto-optic mode locking followed by pulse compression,[1] coupled-cavity or additive-pulse mode locking,[2] and self-mode-locking.[3]

Self-mode-locking has been demonstrated in a number of different configurations in which there are either no obvious mode-locking elements present in the cavity[3] or the final pulse duration is much shorter than that which might be expected.[4] At present the mode-locking mechanism is not fully understood, but it is clear that the χ_3 nonlinearity of the $Ti:Al_2O_3$ gain medium together with anomalous group-velocity dispersion provided by a prism pair plays an important role in the pulse-shortening process.

Although the mode-locking process is self-sustaining, it is not normally self-starting. This means that when initially switched on, the laser will usually oscillate in a cw, un-mode-locked manner, and some additional means of initiating the self-mode-locking process has to be utilized. In the originally reported research[3] this was achieved simply by tapping the table or one of the cavity mirror mounts, which resulted in intensity fluctuations that had durations sufficiently short to initiate the self-mode-locking process. Once initiated, the mode-locked pulse sequence could be retained for periods of as much as several hours depending on the degree of physical perturbation in the surrounding environment. This was not entirely satisfactory because the mode locking would cease at random and had then to be restarted manually. As a result, the laser was not an ideal pulse source for experiments requiring extended periods of stable operation.

Various active and passive schemes to initiate and stabilize the mode-locked output from the laser have been demonstrated. These include the use of saturable absorber dyes,[4] various types of coupled-cavity schemes,[5] and active cavity length modulation.[6] Although all these techniques are clearly applicable they can be unnecessarily complicated and/or may result in additional noise on the laser output. In the case of the saturable absorber dye, the especially attractive features of an all-solid-state system are unfortunately compromised.

In this Letter we describe how an acousto-optic modulator can be used to provide stable long-term operation of the self-mode-locked laser. This system is reliable, retains the advantages associated with all-solid-state systems, and is simple to set up and operate. We have also measured the phase noise of the laser, and experimental results are included to show how this can be significantly improved by employing cavity-frequency referencing techniques.

The self-mode-locked laser was based on a modified Spectra-Physics Model 3900 that has been described elsewhere[3] and for which the pump laser was a Spectra-Physics Model 2040E argon-ion system. This $Ti:Al_2O_3$ laser is capable of routinely generating pulses as short as 60 fs with average and peak powers of 600 mW and 100 kW, respectively, for a pump power of approximately 7 W.[3]

For initiation and stabilization purposes, an intracavity acousto-optic modulator (Newport Electro-Optics Model N12041-.85-LIT) was introduced close to the output coupler of an otherwise unchanged resonator. The modulator was driven, as is usually the case, at one half the cavity frequency (~43.0875 MHz). Initially the rf signal was derived from a signal generator (Marconi Model 2019) and amplified by using a rf amplifier to $\leq$400 mW before it was fed into the modulator. Under these conditions the laser would produce pulses having durations that ranged from sixty to several hundred picoseconds. However, when the cavity was properly aligned, the laser would spontaneously self-mode-lock and produce pulses having durations as short as 60 fs with no loss in average output power.

It was obvious that these femtosecond pulses had durations much shorter than those expected from active mode locking alone. It was also significant

0146-9592/91/221762-03$5.00/0 © 1991 Optical Society of America

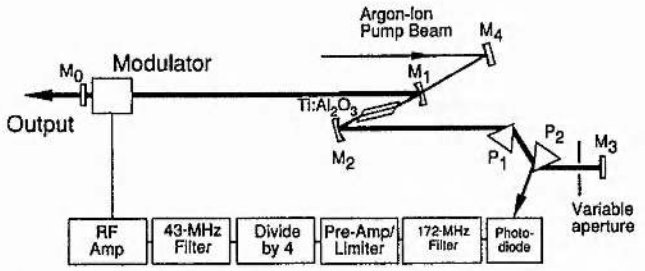

Fig. 1. Schematic diagram showing the laser cavity configuration and the modulator driver. M's, mirrors; P's, prisms.

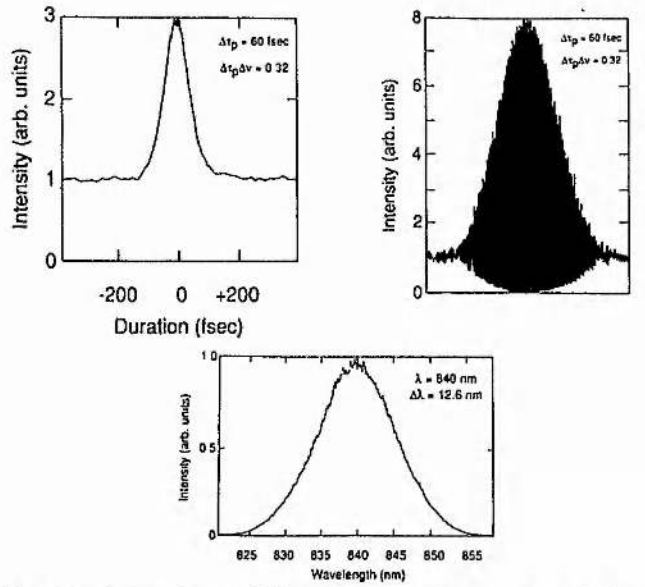

Fig. 2. Intensity and interferometric autocorrelation traces together with spectral data for the laser output.

that the pulse repetition rate was determined not by the modulator drive frequency, as expected for active mode locking and as observed when the pulse durations were in the picosecond regime, but by the cavity frequency. This was consistent with the passive nature of the pulse-shortening process.

Because the pulse repetition frequency was determined by the cavity frequency rather than the modulator drive frequency, stable operation demanded that these two frequencies be exactly matched. Our preferred practical approach was to derive the modulator drive signal from a frequency component of the output from the laser oscillator. In this way the drive frequency to the acousto-optic device was automatically matched to the cavity frequency. This type of scheme, which was first reported by Huggett[7] and termed regenerative mode locking, has been used in picosecond $Ti:Al_2O_3$ lasers,[8] but it should be stressed that in our case the modulation served only to initiate the self-mode-locking process by which the femtosecond pulses could ultimately be generated. In practice, the modulator was driven at a frequency midway between its resonances at a relatively low rf power ($\leq$400 mW) such that its influence on the pulse-shortening process was expected to be small once mode locking had been initiated.

The experimental arrangement for the laser with the intracavity modulator is illustrated schematically in Fig. 1. A small fraction of the laser output was directed onto a fast photodiode as shown in the figure. The second-harmonic component of the photodiode signal at ~172 MHz was filtered out with a bandwidth of ~5 MHz and then amplified by a preamplifier and a limiter. This signal was then passed through a divide-by-four circuit and filtered again at ~43 MHz. It was subsequently amplified to ~400 mW and supplied to the acousto-optic device. When the phase of this rf signal was suitably adjusted, the self-mode-locked operation started spontaneously. (An electronic delay line was included in the circuit for minor phase adjustments.) With this system, any initial fluctuations at the cavity frequency owing to mode beating were detected and amplified by the regenerative feedback process until the pulses had sufficiently short durations that the optical nonlinearities in the $Ti:Al_2O_3$ gain medium could dominate and lead to femtosecond pulse generation through the self-mode-locking mechanism.

In the self-mode-locked operation, the laser routinely generated pulses having durations of 60 fs and was wavelength tunable (using a variable-aperture slit located between prism P_2 and mirror M_3) over the 750–900-nm range. The extent of the tuning was limited only by the characteristics of the antireflection coating on the modulator. For a pump power of 7 W, the average output power of the laser was 600 mW, which corresponded to a peak pulse power of 100 kW. Representative data for the mode-locked laser output are shown in Fig. 2, where it is clearly evident that there was no degradation in the performance of the laser when an intracavity modulator was included. Significantly, the mode-locked operation was maintained continuously such that the influence of the modulator did not merely serve to start the self-mode-locked operation but also sustained it. Under these operating conditions the laser produced a beam that had a TEM_{00}-mode structure.

A phase-noise (or pulse timing jitter) characterization of the laser was also carried out. This was accomplished in the normal way by comparing the power spectrum sidebands of the fundamental and higher harmonics by using a spectrum analyzer (Hewlett Packard HP 71000 series) and fast photodiode (InGaAs avalanche photodiode or Telefunken BPW28).[9] The single-sideband phase-noise spectral density, determined from the fundamental and the 10th-harmonic signals, is shown in Fig. 3. This corresponds to pulse-timing jitter figures of 10.6 ps (50–500 Hz), 850 fs (500 Hz to 5 kHz), and 470 fs (5–50 kHz). It is apparent that most of the phase noise was present at frequencies within a few kilohertz of the carrier. In particular, the peaks at 50, 150, 300 Hz, etc. correspond to amplitude noise on the argon-ion pump laser, which accounts for the relatively high timing jitter in the 50–500-Hz region. No change in the measured phase noise was observed when the mode locker was switched off.

In an attempt to reduce the level of phase noise on

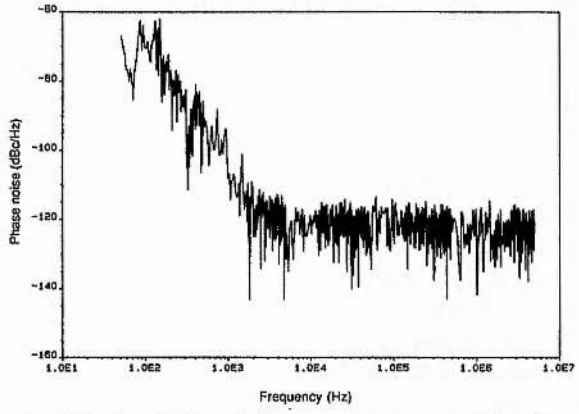

Fig. 3. Single-sideband phase-noise spectral density calculated using the fundamental and the 10th harmonic.

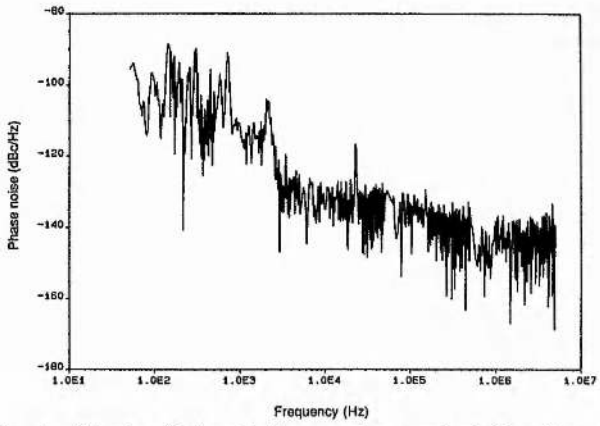

Fig. 4. Single-sideband phase-noise spectral density, calculated using the fundamental and the 20th harmonic, of the cavity-frequency-locked laser.

the mode-locked Ti:Al_2O_3 laser, the cavity frequency was locked[10] to an in-house-constructed ultralow phase-noise electronic crystal oscillator. Details of the locking electronics can be found in Ref. 11. The single-sideband phase-noise spectral density, calculated by using the fundamental and the 20th harmonic, for this improved system is shown in Fig. 4. (The additional peak near 2 kHz is due to a resonance that is attributable to the piezoelectric transducer.) These data correspond to pulse timing jitters of 640 fs (50–500 Hz), 460 fs (500 Hz to 5 kHz), and 170 fs (5–50 kHz), which represents a substantial improvement over those given above.

From the experimental data it is clear that most of the phase noise on the laser occurs at frequencies below approximately 3 kHz. This is characteristic of passively mode-locked systems. This phase noise is due mainly to environmental perturbations and to noise sources associated with the argon-ion power supply unit. Further improvements in timing jitter would require better isolation from the surrounding environment and, more importantly, a quieter pump source such as a frequency-doubled diode-pumped Nd:YAG system. In the region above approximately 5 kHz the recorded minimum noise level is limited to that of the measurement system. It is dependent mainly on the inherent noise associated with the type of photodiode used and on the optical power levels monitored. It is therefore not an accurate measure of the laser timing jitter at these frequencies.

In summary, we have described a self-mode-locked Ti:Al_2O_3 laser having supplementary regeneratively driven acousto-optic modulation. This has resulted in a self-starting, stable, all-solid-state source of sub-100-fs pulses in the 750–900-nm spectral region. By locking the cavity frequency to a high-quality crystal oscillator, the phase-noise characteristics of the laser have been significantly improved.

The overall funding of this research by the UK Science and Engineering Research Council is gratefully acknowledged. Research scholarships from the Department of Education for Northern Ireland (D. E. Spence) and the Science and Engineering Research Council (J. M. Evans) are also acknowledged.

References

1. J. D. Kafka, M. L. Watts, D. L. Roach, M. S. Keirstead, H. W. Schaaf, and T. Baer, *Ultrafast Phenomena VII*, Vol. 53 of Springer Series in Chemical Physics, C. B. Harris, E. P. Ippen, G. A. Mourou, and A. H. Zewail, eds. (Springer-Verlag, Berlin, 1990), p. 66.
2. D. E. Spence and W. Sibbett, J. Opt. Soc. Am. B **8,** 2053 (1991).
3. D. E. Spence, P. N. Kean, and W. Sibbett, in *Digest of Conference on Lasers and Electro-Optics* (Optical Society of America, Washington, D.C., 1990), paper CPDP10; Opt. Lett. **16,** 42 (1991).
4. Y. Ishida, N. Sarukura, and H. Nakano, in *Digest of Conference on Lasers and Electro-Optics* (Optical Society of America, Washington, D.C., 1991), paper JMB2.
5. G. W. 'tHooft, U. Keller, W. H. Knox, and J. E. Cunningham, in *Digest of Conference on Lasers and Electro-Optics* (Optical Society of America, Washington, D.C., 1991), paper JMA6.
6. L. Spinelli, B. Couillaud, N. Goldblatt, and D. K. Negus, in *Digest of Conference on Lasers and Electro-Optics* (Optical Society of America, Washington, D.C., 1991), CPDP7.
7. G. R. Huggett, Appl. Phys. Lett. **13,** 186 (1968).
8. J. D. Kafka, M. L. Watts, and T. Baer, in *Digest of Conference on Lasers and Electro-Optics* (Optical Society of America, Washington, D.C., 1991), paper JMB3.
9. D. von der Linde, Appl. Phys. B **39,** 201 (1986).
10. M. J. W. Rodwell, D. M. Bloom, and K. J. Weingarten, IEEE J. Quantum Electron. **25,** 817 (1989).
11. D. R. Walker, D. W. Crust, W. E. Sleat, and W. Sibbett, "Reduction of phase noise in passively mode-locked lasers," IEEE J. Quantum Electron. (to be published).